NAVAL POSTGRADUATE SCHOOL
Monterey, California

DISSERTATION

A THREE-DIMENSIONAL FLUTTER THEORY FOR ROTOR BLADES WITH TRAILING-EDGE FLAPS

by

Mark A. Couch

June 2003

Dissertation Supervisor and Advisor: E. Roberts Wood

Approved for public release; distribution is unlimited

THIS PAGE INTENTIONALLY LEFT BLANK

REPORT DOCUMENTATION PAGE			Form Approved OMB No. 0704-0188
Public reporting burden for this collection of information is estimated to average 1 hour per response, including the time for reviewing instruction, searching existing data sources, gathering and maintaining the data needed, and completing and reviewing the collection of information. Send comments regarding this burden estimate or any other aspect of this collection of information, including suggestions for reducing this burden, to Washington headquarters Services, Directorate for Information Operations and Reports, 1215 Jefferson Davis Highway, Suite 1204, Arlington, VA 22202-4302, and to the Office of Management and Budget, Paperwork Reduction Project (0704-0188) Washington DC 20503.			
1. AGENCY USE ONLY *(Leave blank)*	**2. REPORT DATE** June 2003	**3. REPORT TYPE AND DATES COVERED** Dissertation	
4. TITLE AND SUBTITLE: A Three-Dimensional Flutter Theory For Rotor Blades With Trailing-Edge Flaps			**5. FUNDING NUMBERS**
6. AUTHOR(S) Mark A. Couch			
7. PERFORMING ORGANIZATION NAME(S) AND ADDRESS(ES) Naval Postgraduate School Monterey, CA 93943-5000			**8. PERFORMING ORGANIZATION REPORT NUMBER**
9. SPONSORING / MONITORING AGENCY NAME(S) AND ADDRESS(ES) N/A			**10. SPONSORING / MONITORING AGENCY REPORT NUMBER**
11. SUPPLEMENTARY NOTES The views expressed in this thesis are those of the author and do not reflect the official policy or position of the Department of Defense or the U.S. Government.			
12a. DISTRIBUTION / AVAILABILITY STATEMENT Approved for public release; distribution is unlimited			**12b. DISTRIBUTION CODE** A

13. ABSTRACT ***(maximum 200 words)***

This dissertation develops the equations of motion for the structural and aerodynamic forces and moments of a rotor blade with a trailing-edge flap using eight degrees of freedom. Lagrange's equation is applied using normal modes to find the flutter frequency and speed similar to the classic fixed-wing method developed by Smilg and Wasserman. However, rotary-wing concerns are addressed including different freestream velocities along the blade (variation of reduced frequency along the span of the rotor blade) and the influence of previously shed vortices on the aerodynamic forces and moments (Loewy's returning wake). While Loewy [Ref. 49] did not explicitly state that his 2-D theory would apply to rotor blades with trailing-edge flaps, the manner in which the theory was developed allows it to be applied in this manner. Comparisons to classic 1DOF, 2DOF and 3DOF flutter theories are made to validate this theory in the limiting cases. Flutter analyses, including g-Ω plots, of an example rotor blade with five degrees of freedom are performed for various rigid body flap frequencies.

Classic methods of rotor blade design of ensuring freedom from flutter are to collocate the center of gravity (c.g.), elastic axis (e.a.), and aerodynamic center (a.c) at the 25% chord. With the development of rotor blades with trailing-edge flaps, it is shown that this current design practice is not valid when a trailing-edge flap is incorporated.

14. SUBJECT TERMS Flutter, Rotary Wing, Aeroelasticity. Trailing-edge Flaps, Unsteady Aerodynamics, Structural Dynamics, Holzer Method, Myklestad-Prohl Method, Rotor Blades, Vibrations			**15. NUMBER OF PAGES** 237
			16. PRICE CODE
17. SECURITY CLASSIFICATION OF REPORT Unclassified	**18. SECURITY CLASSIFICATION OF THIS PAGE** Unclassified	**19. SECURITY CLASSIFICATION OF ABSTRACT** Unclassified	**20. LIMITATION OF ABSTRACT** UL

NSN 7540-01-280-5500 Standard Form 298 (Rev. 2-89)
Prescribed by ANSI Std. 239-18

THIS PAGE INTENTIONALLY LEFT BLANK

Approved for public release; distribution is unlimited

A THREE-DIMENSIONAL FLUTTER THEORY FOR ROTOR BLADES WITH TRAILING-EDGE FLAPS

Mark A. Couch
Commander, United States Navy
B.S., Purdue University, 1984
M.S., Naval Postgraduate School, 1993

Submitted in partial fulfillment of the
requirements for the degree of

**DOCTOR OF PHILOSOPHY IN
AERONAUTICAL AND ASTRONAUTICAL ENGINEERING**

from the

**NAVAL POSTGRADUATE SCHOOL
June 2003**

Author: _____
Mark A. Couch

Approved by:

_____	_____
E. Roberts Wood Professor of Aeronautics and Astronautics Dissertation Supervisor	Max F. Platzer Distinguished Professor of Aeronautics and Astronautics
_____	_____
Donald A. Danielson Professor of Mathematics	Garth V. Hobson Professor of Aeronautics and Astronautics

_____
Russell W. Duren
Associate Professor of Aeronautics and Astronautics

Approved by: _____
Max F. Platzer, Chair, Department of Aeronautics and Astronautics

Approved by: _____
Carson K. Eoyang, Associate Provost for Academic Affairs

THIS PAGE INTENTIONALLY LEFT BLANK

ABSTRACT

This dissertation develops the equations of motion for the structural and aerodynamic forces and moments of a rotor blade with a trailing-edge flap using eight degrees of freedom. Lagrange's equation is applied using normal modes to find the flutter frequency and speed similar to the classic fixed-wing method developed by Smilg and Wasserman. However, rotary-wing concerns are addressed including different freestream velocities along the blade (variation of reduced frequency along the span of the rotor blade) and the influence of previously shed vortices on the aerodynamic forces and moments (Loewy's returning wake). While Loewy [Ref. 49] did not explicitly state that his 2-D theory would apply to rotor blades with trailing-edge flaps, the manner in which the theory was developed allows it to be applied in this manner. Comparisons to classic 1DOF, 2DOF and 3DOF flutter theories are made to validate this theory in the limiting cases. Flutter analyses, including g-Ω plots, of an example rotor blade with five degrees of freedom are performed for various rigid body flap frequencies.

Classic methods of rotor blade design of ensuring freedom from flutter are to collocate the center of gravity (c.g.), elastic axis (e.a.), and aerodynamic center (a.c) at the 25% chord. With the development of rotor blades with trailing-edge flaps, it is shown that this current design practice is not valid when a trailing-edge flap is incorporated.

THIS PAGE INTENTIONALLY LEFT BLANK

TABLE OF CONTENTS

LIST OF FIGURES

THIS PAGE INTENTIONALLY LEFT BLANK

LIST OF TABLES

THIS PAGE INTENTIONALLY LEFT BLANK

LIST OF SYMBOLS AND ABBREVIATIONS

$[\boldsymbol{A}_{n+1}]$	r.h.s. of transfer matrix for torsion or bending
$A_{h_0h_0} \rightarrow A_{\beta_1\beta_1}$	aerodynamic terms defined by equations (197) through (260)
$\overline{A}_{h_0h_0} \rightarrow \overline{A}_{\beta_1\beta_1}$	determinant elements of equation (280) defined by equations (281) through (344)
A_m	area enclosed by the median curve C_m
a	position of elastic axis non-dimensionalized by the semi-chord (b)
b	semi-chord length
c	position of trailing-edge flap hinge axis non-dimensionalized by the semi-chord (b)
C_n, C_{n+1}	local tension due to centrifugal force of blade section (Holzer and Myklestad-Prohl methods)
$C(k)$	Theodorsen's lift deficiency function
$C'(k)$	Loewy's lift deficiency function
$C'_N(k)$	finite wake lift deficiency function
C_m	the median curve of a thin-walled structure where the shear flow force acts tangent to the curve about the axis of rotation
C_{P_x}	Garrick's propulsive force coefficient
D	dissipation function
EI	bending structural stiffness
e	position of leading edge of trailing-edge flap non-dimensionalized by the semi-chord (b)
e_R	blade hinge offset, or effective hinge offset
$F(k)$	real part of Theodorsen's lift deficiency function
$F'(k)$	real part of Loewy's lift deficiency function
$F'_N(k)$	real part of finite wake lift deficiency function
$F_n + if_n$	aerodynamic lift force acting on the n^{th} blade element for a particular frequency component, $F_n \sin \omega_h t + f_n \cos \omega_h t$
F_0, F_1	rigid body and 1st blade torsional mode shapes, respectively
f_0, f_1, f_2, f_3	rigid body, 1st, 2nd, and 3rd bending mode shapes, respectively
f	$= \frac{\omega}{2\pi}$, frequency of oscillation in Hz
$G(k)$	imaginary part of Theodorsen's lift deficiency function
$G'(k)$	imaginary part of Loewy's lift deficiency function
$G'_N(k)$	imaginary part of finite wake lift deficiency function
G_n	flapwise aerodynamic damping constant for the n^{th} blade station

G_0, G_1	rigid body and 1st flap torsional mode shapes, respectively
G	shear modulus of elasticity
GJ	$= \dfrac{4A_m G}{\oint_{C_m} \dfrac{ds}{t(s)}}$, torsional structural stiffness, or torsional rigidity
$g_{h_0} \to g_{\beta_1}, g$	structural damping coefficients
$H_n^{(2)}(k)$	$= J_n(k) - iY_n(k)$, Hankel function of the second kind of order n, evaluated at k
h	displacement of an element of blade above the flapping plane
$\hat{h}$	$= \dfrac{2\pi v_i}{bQ\Omega} = \lambda r \dfrac{2\pi}{bQ}$, non-dimensional wake spacing
h_0, h_1, h_2, h_3	bending deflections due to rigid body, 1st, 2nd, and 3rd bending modes, respectively
$\bar{h}_0, \bar{h}_1, \bar{h}_2, \bar{h}_3$	amplitude of deflection for rigid body, 1st, 2nd, and 3rd bending modes (plunge motions), respectively
I_α	polar mass moment of inertia
$I_{\alpha_0}, I_{\alpha_1}$	generalized mass terms defined by equations (133) and (134)
I_β	mass moment of inertia of the flap about the flap hinge
I_{β_0}, I_{β_1}	generalize mass terms defined by equations (135) and (136)
$J_n(k)$	Bessel function of the first kind of order n, evaluated at k
k_a	polar radius of gyration of tensile stress carrying area about elastic axis
$k_{h_0} \to k_{\beta_1}$	potential energy coefficients
k_{m_1}	mass radius of gyration of blade section about chordwise axis
k_{m_2}	mass radius of gyration of blade section about axis perpendicular to chordwise axis
k_m	$= \sqrt{k_{m_1}^2 + k_{m_2}^2}$, mass radius of gyration of blade section about elastic axis
K_{root}	pitch control stiffness at root of blade
$[\boldsymbol{K_n}]$	l.h.s. of transfer matrix for torsion or bending
k	reduced frequency, $k = \dfrac{\omega b}{v}$ for fixed wing and $k = \dfrac{b\omega}{\Omega r} = \dfrac{mb}{r}$ for rotary wing
k_β	torsional spring constant (stiffness) of flap restraint about flap hinge
L'	lift force per unit span
L_h	aerodynamic lift coefficient due to bending oscillations of blade
L_α	aerodynamic lift coefficient due to torsional (pitch) oscillations of blade about ¼-chord

L_β	aerodynamic lift coefficient due to oscillations (deflections) of trailing-edge flap about its leading edge
L_z	aerodynamic lift coefficient due to translatory oscillations (deflections) of trailing-edge flap perpendicular to blade chord
$l_{n,n+1}$	length of segment between concentrated masses n and n+1
M	bending moment
M'	moment per unit span due to blade rotation about the 25% chord
M_{app}	applied moment
M_n, M_{n+1}	bending moment of blade section (Myklestad-Prohl method)
M_{root}	bending moment at blade root (Myklestad-Prohl method)
M_y	moment about y-axis
M_h	aerodynamic moment coefficient about blade ¼-chord due to bending oscillations of blade
M_α	aerodynamic moment coefficient about blade ¼-chord due to torsional (pitch) oscillations of blade about ¼-chord
M_β	aerodynamic moment coefficient about blade ¼-chord due to oscillations (deflections) of trailing-edge flap about its leading edge
M_z	aerodynamic moment coefficient about blade ¼-chord due to translatory oscillations (deflections) of trailing-edge flap perpendicular to blade chord
$M_0 \rightarrow M_3$	generalized mass terms defined by equations (129) through (132)
m	$= \frac{\omega}{\Omega}$, frequency ratio
$m(y), m_n$	mass of blade section
N_b	number of rotor blades
P	concentrated force
P_h	aerodynamic lift coefficient acting on trailing-edge flap due to bending oscillations of blade
P_α	aerodynamic lift coefficient acting on the trailing-edge flap due to torsional (pitch) oscillations of the blade about ¼-chord
P_β	aerodynamic lift coefficient acting on trailing-edge flap due to oscillations (deflections) of the trailing-edge flap about its leading edge
P_z	aerodynamic lift coefficient acting on trailing-edge flap due to translatory oscillations (deflections) of trailing-edge flap perpendicular to blade chord
$P_{\alpha_0\beta_0} \rightarrow P_{\alpha_1\beta_1}$	generalized mechanical terms defined by equations (153) through (156)
p	$= -\frac{1}{3}\left(\sqrt{1-c^2}\right)^3$, part of Theodorsen's T-functions

Q	number of blades
$Q'_{h_0} \rightarrow Q'_{\beta_1}$	generalized forces per unit length
$Q_{h_0} \rightarrow Q_{\beta_1}, Q_n$	generalized forces for rotor blade
q	blade number ($1 \rightarrow Q$)
q_n	degrees of freedom (displacements)
$\dot{q}_n$	first time derivatives of the degrees of freedom (velocities)
r	blade section radial distance from axis of rotation
S_n, S_{n+1}	shear force of blade section (Myklestad-Prohl method)
S_{root}	shear force at root of blade (Myklestad-Prohl method)
S_α	static mass moment of inertia (static unbalance) for rotor-flap combination
$S_{\alpha_{00}} \rightarrow S_{\alpha_{31}}$	generalized mechanical terms defined by equations (137) through (144)
S_β	static mass moment of inertia of flap about flap hinge
$S_{\beta_{00}} \rightarrow S_{\beta_{31}}$	generalized mechanical terms defined by equations (145) through (152)
T	kinetic energy
T'	moment per unit span due to flap rotation about the hinge
T_h	aerodynamic moment coefficient about leading edge of trailing-edge flap due to bending oscillations of blade
T_α	aerodynamic moment coefficient about leading edge of trailing-edge flap due to torsional (pitch) oscillations of blade about ¼-chord
T_β	aerodynamic moment coefficient about leading edge of trailing-edge flap due to oscillation (deflections) of trailing-edge flap about its leading edge
T_z	aerodynamic moment coefficient about leading edge of trailing-edge flap due to translatory oscillations of trailing-edge flap perpendicular to blade chord
T_n, T_{n+1}	torsional moment of blade section (Holzer method)
T_{root}	torsional moment at root of blade (Holzer method)
$T_1 \rightarrow T_{14}$	Theodorsen's T-functions
$[\boldsymbol{T}_{n+1}]$	complete transfer matrix for torsion or bending
$t(s)$	local thickness at the point where the shear stress is evaluated
U	potential energy
v	freestream velocity
v_i	induced velocity
$W(k, \hat{h}, m)$	Loewy's wake weighting function
$W_N(k, \hat{h}, m)$	finite wake weighting function

w	downwash velocity
$\boldsymbol{X_n}, \boldsymbol{X_{n+1}}$	state vector for torsion or bending
X_{shift}	horizontal shift of lead airfoil in a two-airfoil oscillating system
x	chordwise coordinate of displacement
$Y_n(k)$	Bessel function of the second kind of order n, evaluated at k
y	spanwise coordinate of displacement
z_n, z_{n+1}	deflection of out-of-plane bending (flapping) of blade section (Myklestad-Prohl method)
α	angle of rotation (pitch) for rotor blade
α_0, α_1	blade torsional deflections due to rigid body and 1st blade torsional modes, respectively
$\overline{\alpha}_0, \overline{\alpha}_1$	amplitude of rotation for rigid body and 1st blade torsional modes (pitch motions), respectively
β	angle of deflection for trailing-edge flap
β_0, β_1	flap torsional deflections due to rigid body and 1st flap torsional modes, respectively
$\overline{\beta}_0, \overline{\beta}_1$	amplitude of flap deflection for rigid body and 1st flap torsional modes, respectively
β_n, β_{n+1}	angle of out-of-plane bending (flapping) of blade section (Myklestad-Prohl method)
β_{root}	angle of out-of-plane bending (flapping) at root of blade (Myklestad-Prohl method)
ϕ, ϕ_n, ϕ_{n+1}	angle of twist of blade section (Holzer method)
ϕ_{root}	angle of twist at root of blade (Holzer method)
$\phi_1 \rightarrow \phi_{37}$	Küssner's ϕ-functions
Γ	total circulation around the airfoil
$\gamma, \gamma_a, \gamma_{nq}$	vorticity generated by airfoil
λ	inflow
λ_v	$= \frac{2\pi v}{\omega}$, wavelength of layers of shed vorticity
μ	mass per unit length
θ	$= \theta_0 + \theta_B$, local pitch angle due to time variation of root pitch angle and geometric twist of rotor blade
ρ	density of air
Ω	rotational velocity of rotor blades
Ω_0	normal rotational velocity of rotor blades (203 rpm for example rotor blade)
ω	frequency of oscillation (flutter frequency)
ω_h	natural frequency of oscillation in bending
ω_α	natural frequency of oscillation in torsion

ω_β	natural frequency of oscillation of flap (aileron)
ξ	chordwise coordinate
ψ_q	phase angle by which the notion of the q^{th} blade leads that of the reference blade

ACKNOWLEDGMENTS

I would like to give my sincere appreciation and heartfelt thanks to my advisor, Bob Wood, for his guidance, encouragement, and many hours of discussion that led to the completion of this project. I will always appreciate the friendship he and his wife, Cheri, gave, and I look forward to continuing my work with him in the future. I would like to thank my dissertation committee, composed of Max Platzer, Don Danielson, Garth Hobson and Russ Duren, for your support and friendship over the past several years. I would also like to thank Bob Ball for his mentorship as I took over teaching his Aircraft Combat Survivability course. While he cheered for me in my newfound successes with his course, he always reminded me that I needed to finish this dissertation in order to truly take over the course from him.

To the staff and faculty in the Department of Aeronautics and Astronautics, this has been an enjoyable four years, and it is sad that the department must soon close shop. You will be sorely missed, but not forgotten. I would like to thank my friends (and family) at Calvary Chapel Monterey Bay. They were there for us during our toughest times and greatest joys. May God continue to bless you and keep you always.

I would like to thank my daughters, Kelsey and Amy for putting up with Dad being a student once again. You both are becoming nice young ladies, and I appreciate your love and support. To my son, Joshua, words cannot express how much you have meant to the whole family. While you may never remember your time in Monterey, the meaning of your name says it all.

And lastly, I would like to give my deepest thanks to my lovely wife, Pam, for her encouragement, support, and love throughout our time in Monterey and over the past nineteen years of marriage. I know the Lord has blessed me by the gift of having you as my wife, and I know you will join me in praising God for finally completing this work.

THIS PAGE INTENTIONALLY LEFT BLANK

I. INTRODUCTION

A. AEROELASTICITY

Aeroelasticity has been defined as the study of the interaction between the aerodynamic forces and the elastic structure of a body in an airstream [Ref. 1]. This interaction may tend to become smaller over time (convergent) and produce a stable condition, or it may become larger over time (divergent) and possibly cause structural damage to the aircraft. If a body is infinitely stiff, aeroelastic problems would not exist since the body would not be capable of bending or twisting. In order to decrease the weight of an aircraft, flexible, light-weight structures are normally used in the design. The structural flexibility by itself is not an inherent problem for aircraft designers, but when coupled with large aerodynamic forces, aeroelastic phenomena may arise. These aeroelastic phenomena may cause additional structural deformations that may produce even larger aerodynamic forces, which makes the problem of aeroelasticity a concern.

In this research, the aircraft structure being considered is a helicopter rotor blade with a trailing-edge flap incorporated along a finite portion of the blade. A schematic of this type of rotor blade is shown in Figure 1 [Ref. 2]. The typical design of a rotor blade is that of a very flexible, high-aspect ratio wing with the stiffness of the rotor blade being increased somewhat by the large centrifugal force acting on it. The presence of this centrifugal force introduces additional dynamic forces into the aeroelastic phenomena described above and suggests that inertial forces should be included as a third element, and therefore creating a triangle of interaction among the aerodynamic, elastic and inertial forces. The aeroelastic triangle shown in Figure 2 from Bisplinghoff, Ashley and Halfman [Ref. 1] is the most comprehensive illustration of the interdisciplinary nature of aeroelasticity. The sides of the triangle represent some of the classic couplings that have grown into disciplines of their own. The interaction between elastic and inertial forces is referred to as the field of structural dynamics and encompasses mechanical vibrations. The interaction between aerodynamic and inertial forces is referred to as flight mechanics and encompasses dynamic stability. The interaction between aerodynamic and elastic forces is normally referred to as static aeroelasticity and encompasses load distribution,

torsional divergence, control effectiveness, control reversal, and static stability. However, it is the interaction between all three forces – aerodynamic, elastic and inertial – that is of concern for most rotary wing aeroelastic analyses. The three-way interaction of the forces is referred to as dynamic aeroelasticity and encompasses flutter, buffeting, transient dynamic response, and aeroelastic effects on dynamic stability.

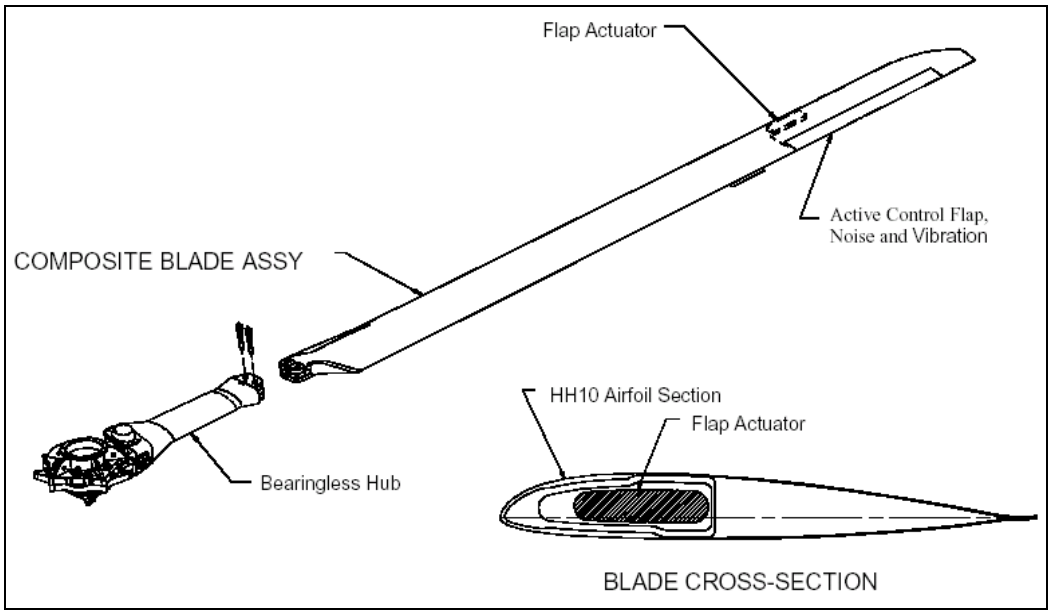

Figure 1. Rotor blade with trailing-edge flap (from Ref. 2).

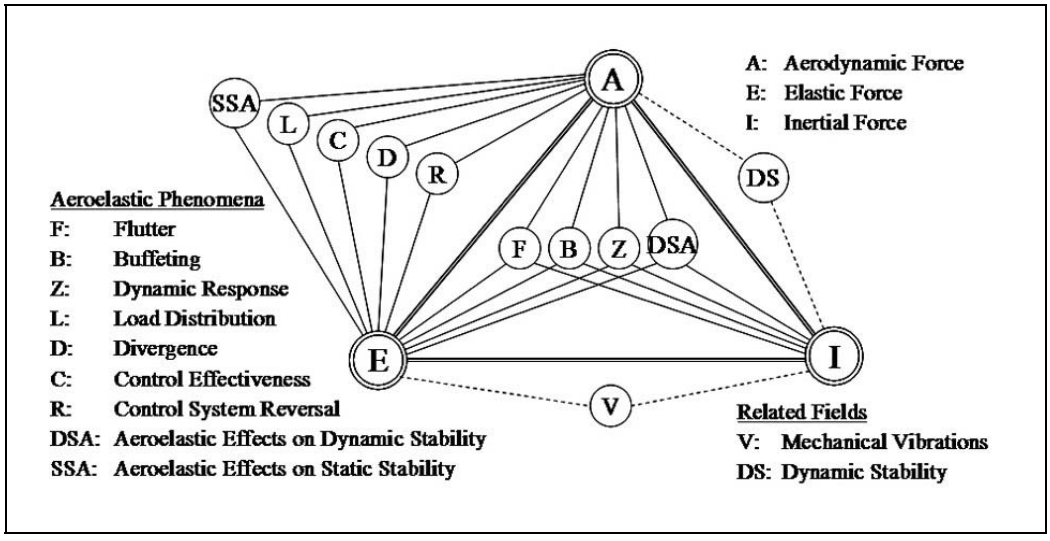

Figure 2. Aeroelastic triangle (from Ref. 1).

B. ROTARY WING AEROELASTICITY

1. Typical Rotor Blade Design

Flutter is normally defined as an aeroelastic, self-excited vibration, in which the external source of energy is the air stream. When flutter occurs, the air stream provides energy to the system more rapidly than it is dissipated by damping [Ref. 3]. The requirements for designing helicopter rotor blades to be free of flutter are contained in Federal Aviation Regulations under Aircraft Circular 27-1B for normal category rotorcraft [Ref. 4] and Aircraft Circular 29-2C for transport category rotorcraft [Ref. 5]. Section 629 of both circulars state that the rotorcraft must be free from flutter. Additionally, section 629A of AC 29-2C requires that

> *each aerodynamic surface of the rotorcraft must be free from divergence in addition to the requirement of freedom from flutter. The aeroelastic stability evaluations required by this regulation include flutter and divergence. Compliance with this regulatory requirement should be shown by analysis and/or flight test, supported by any other means found necessary by the Administrator. The aeroelastic evaluation of the rotorcraft should include an investigation of the significant elastic, inertia and aerodynamic forces on all aerodynamic surfaces (including rotor blades) and their supporting structure. The forces associated with the rotations and displacements of the plane of the rotors should be considered.*

The typical approach in designing rotor blades (without trailing-edge flaps) to be free from flutter can be summarized in a statement, from the 1960 Sikorsky Report No. 50131 for the Advanced Tactical Helicopter (A.T.H.) [Ref. 6]:

> *Main and tail rotor blades of the A.T.H. have been designed so that center of gravity, elastic axis, and aerodynamic center are coincident. Also, the control system for the main rotor is stiff with high internal damping. No main or tail rotor blade flutter has been experienced with earlier model helicopters possessing these design features.*
>
> *Main and tail rotor blades for the HSS-2, which are the same as those of the A.T.H., have been installed on Sikorsky whirl stands, and tested at maximum design-limit speeds. Main rotor blades were tested for power-on and power-off conditions. Tail rotor test conditions were power-on and power-off. Observation of blades during these tests indicated no flutter or divergence at maximum operating conditions.*

This design practice of collocating the center of gravity, elastic axis and aerodynamic center has the advantage of decoupling the aerodynamic, elastic and dynamic equations

of motion. While this assures freedom from flutter and other aeroelastic phenomena, it provides additional constraints on rotor blade design not normally followed in fixed-wing design. A rotor blade designed with the center of gravity, elastic axis and aerodynamic center coincident at the quarter-chord will be heavier than one free of that restriction. The added weight in the rotor blade may necessitate a larger power plant and a larger gearbox, and the rotor blade itself may be larger than needed in order to provide the necessary rotor thrust to achieve flight. Also, if strictly followed, this design constraint rules out use of a trailing-edge flap because the aerodynamic center will move when the flap angle is changed [Ref. 7 and 8], and the elastic axis and center of gravity may shift when a trailing-edge flap is incorporated.

2. Helicopter Vibration Reduction

The most recent use of trailing-edge flaps is to reduce the vibrations caused by the rotor system. Vibration reduction has long been a concern for helicopter designers. In 1957, the American Helicopter Society held a "Rotary Round Table" devoted to the subject of "How Can Helicopter Vibrations be Minimized?" with contributions from leading experts on the subject [Ref. 9]. Loewy [Ref. 10] cites a quote from Alexander Yakovlev, a famous Russian aircraft designer, detailing the persistent frustration in reducing helicopter vibrations. Loewy makes an additional argument referencing Bisplinghoff's aeroelastic triangle (Figure 2) that if the definition of dynamic response (Z) is expanded to include periodic phenomena, helicopter vibrations would fall into this category since the major source of fixed airframe vibrations is caused by the periodic aerodynamic response of the rotating blades. Bousman [Ref. 11] states, "The problems of loads and vibrations have always been part of the helicopter development and in this sense have been at the forefront of all efforts by dynamicists in the industry." The primary motivation for the dynamicist is to reduce the vibration levels during the helicopter's development phase.

Early efforts to control vibrations in the fixed airframe were normally accomplished with some type of vibration control device. These devices can be categorized as "Amplitude Reducers", "Force Attenuators", or "Source Alleviators" [Ref. 10]. Amplitude reducers act to reduce the effects of the response by either isolating part

of the helicopter from the fixed system by ensuring the natural frequency of the isolated system is low compared to the excitation frequency, or putting dynamic absorbers in the structure that produce an opposing force (damping) to the vibration in some particular direction. Both devices are passive and are tuned to reduce vibrations at normal operating rpm of the rotor, and they may not provide the necessary vibration reduction outside the normal operating range. Counter-rotating weights and oscillating, weighted hydraulic cylinders are active devices that can create inertial forces that oppose the vibrational forces and can be tuned to changes in rotor rpm.

Force attenuators are devices placed between the excitation and responding structure to reduce the transmitted vibratory force. The two primary force attenuators are rotor isolation systems and pendulum absorbers. The rotor isolation systems attenuate in-plane hub forces or pitching and rolling moments by using the inertia of the isolated rotor mass as a counter-force. These isolation systems are normally tuned to the operating rpm of the rotor. The pendulum absorbers have an advantage in that their natural frequencies are proportional to the rotor speed, and they are properly tuned regardless of rotor speed. However, pendulum absorbers can become de-tuned when oscillation amplitudes become too large. Sikorsky's H-60 uses "bifilar" pendulum absorbers to help reduce vibrations as shown in Figure 3 [Ref. 12].

Source alleviators are devices that reduce the vibrations at their source, the main rotor. Dynamic pendulum absorbers attached to the blades have been used with some success, but concerns about weight and aerodynamic drag have limited their use [Ref. 10].

a. Higher Harmonic Control

The most promising development in reducing helicopter vibrations at their source has been the implementation of higher harmonic control (HHC) [Ref. 13]. HHC is an active control concept that introduces control inputs into the non-rotating reference frame at the rotor hub in order to reduce the vibratory loads caused by the aerodynamic loads in the rotating reference frame of the hub. Higher harmonic blade pitch control is achieved by superimposing an N_b/rev input motion upon pilot cyclic and collective control inputs. The N_b/rev inputs in the non-rotating reference frame generate N_b/rev,

(N_b–1)/rev and (N_b+1)/rev inputs in the rotating reference frame, which correspond to the frequencies at which the primary vibrational loads are transmitted to the fuselage. Results from the OH-6A flight tests showed a reduction in vibration levels of up to 90% with HHC on. Additionally, the open loop data showed significant reductions in the main rotor shaft torque and engine power indicating that HHC may be providing performance improvements along with the vibration reduction [Ref. 13].

Rotary wing, unsteady aerodynamics for a thin, oscillating airfoil has been used to explain the mechanism behind the performance improvements seen on the OH-6A [Ref. 14 and 15], which provides a practical example of Loewy's premise that helicopter vibrations are a periodic dynamic response involving all three forces in the aeroelastic triangle. Wind tunnel tests on a scaled model of the Boeing Vertol CH-47D with HHC [Ref. 16] installed also showed both vibration reduction and performance improvement, but flight tests on the Sikorsky S-76A [Ref. 17 and 18] and the Aerospatiale S-349 Gazelle [Ref. 19] showed only vibration reduction. The reason for the lack of observed performance improvements can be explained by the larger freeplay in the flight control system that was apparent in the Sikorsky and Aerospatiale HHC designs due to the locations that the installed HHC components [Ref. 15].

b. Individual Blade Control

A logical progression from HHC, in which inputs are made in the fixed system at the hub, is to make inputs on the blades themselves in the rotating frame of reference. This type of control input is commonly referred to as individual blade control (IBC). There are three common approaches to implementing IBC on the rotor system [Ref. 20]. The first approach used is to oscillate each blade in pitch by changing the root pitch angle. This method is similar to HHC in that inputs are made to the entire blade. The primary difference is that HHC uses the rotor as a filter so that the rotating reference frame experiences the (N_b±1)/rev inputs while IBC can provide any input frequency to the rotating reference frame. The most recent use of this method was reported in the wind tunnel tests of a full-scale H-60 rotor blade in which the standard pitch links were replaced with hydraulic actuators to allow for the IBC inputs [Ref. 21]. The second approach uses embedded piezoelectric fibers to serve as actuators within a composite spar

that induce a distributed twisting moment along the span of the rotor. This approach is commonly called the active twist rotor (ATR). The first closed-loop wind tunnel tests were conducted as part of the NASA/Army/MIT/University of Michigan Active Twist Program demonstrating the ATR proof of concept, but to date it has not been implemented on a full-scale rotor [Ref. 22, 23, and 24]. The third approach incorporates a trailing-edge flap located along a finite segment of each rotor span, and inputs are made by oscillating the flap angle. The trailing edge flap is normally located along a portion of the blade that includes the point of the resultant aerodynamic force on the rotor blade. This research will focus only on the trailing edge flap when referring to IBC.

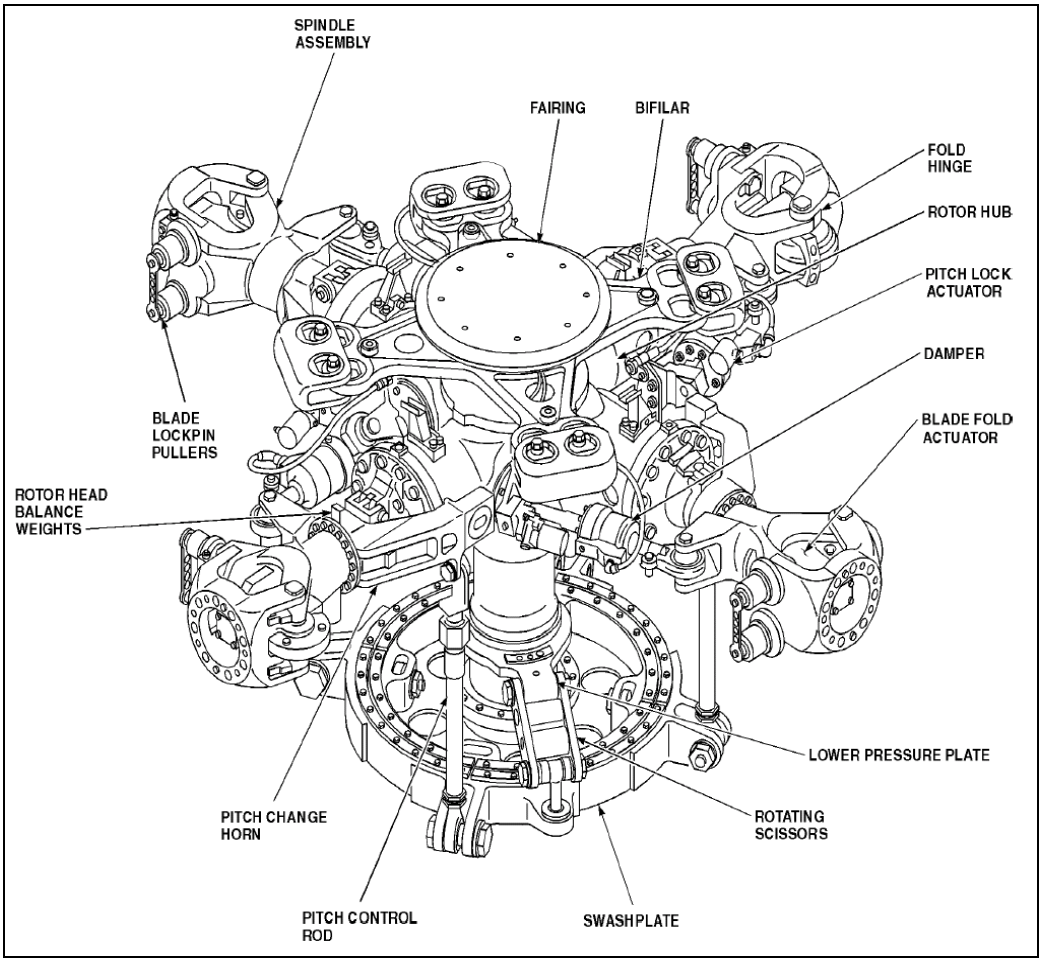

Figure 3. Sikorsky H-60 main rotor hub (from Ref. 12).

c. The Trailing-Edge Flap

The concept of incorporating a trailing-edge flap on a rotor blade is not new. The Kaman H-2 was a very successful helicopter that used a trailing-edge flap to provide cyclic and collective pitch control [Ref. 25] in all flight regimes. The most recent applications of the trailing-edge flap have focused on the vibration reduction potential through the use of smart materials as part of an IBC concept [Ref. 26]. Analytical studies have indicated that the use of trailing-edge flaps can produce vibration reduction levels equivalent to those seen by HHC but for much less power [Ref. 27 and 28]. Two full-scale active flap programs are currently underway: Boeing is working on a piezoelectric-stack actuated flap for the MD-900 Explorer [Ref. 2], and Eurocopter is working on a piezoelectric-stack actuator for the EC-135 [Ref. 29].

3. Dissertation Objective

The aeroelastic analyses for the trailing-edge flaps have been routinely performed using a computational code such as CAMRAD II, CAMRAD/JA, 2GCHAS, UMARC, and others [Ref. 2, 30, and 31]. While these codes are quite capable of predicting rotor vibrations, they all work predominantly in the time domain and require much effort to learn how to use them to the fullest extent of their capabilities. Time history plots are generated and analyzed in order to see if any instability, such as flutter, existed. The lack of a closed-form, frequency-domain solution for the aeroelastic analysis of rotor blades with trailing-edge flaps is very apparent in a review of the literature. The purpose of this dissertation is to develop the coupled aeroelastic equations of motion in order to perform a flutter analysis for rotor blades with trailing-edge flaps. This flutter analysis will be in the frequency domain and take into consideration bending and torsional mode shapes for the rotating blade, rigid body motion in pitch and flap, and the effects of rotary-wing unsteady aerodynamics. Comparisons will be made with classical fixed wing unsteady aerodynamics to determine the effects of layers of shed vorticity beneath the rotor blade on the flutter speed.

II. BACKGROUND

A. STRUCTURAL DYNAMICS

Since a helicopter rotor blade can be treated as a rotating flexible beam, the classic methods of determining the structural dynamics of a beam can be used. Yntema [Ref. 32] is a notable example in which beams of variable cross section, but linear with span, and different root end suspensions are analyzed in detail for an untwisted rotor blade in pure vertical (flapwise) bending. However, a rotor blade undergoes vertical, inplane (chordwise), and torsional (twisting) deformations as it rotates about the main rotor drive shaft, and a beam theory that includes motion in more than one plane is needed for use with a flutter theory. Wood and Hilzinger [Ref. 33] developed the fully coupled equations of motion for aeroelastic response of rotor blades that is based on the superposition of separate harmonics of blade force response, which result from response of the blade to individual harmonics of airloads. While this method is very robust, some assumptions will be made in regards to which coupled modes to use in order to develop a simplified flutter theory. This method is an extension of the work by Gerstenberger and Wood [Ref. 34] on the coupled equations of motion for flapwise and chordwise bending, which uses the method developed by Myklestad [Ref. 35] and Prohl [Ref. 36] for calculating natural frequencies and modes.

In the analysis to follow, the aerodynamic coupling due to blade inplane motion has been neglected since it is a higher order effect compared to the flapwise and torsional deformations. Therefore, only the natural frequencies of vertical bending and torsional twisting must be determined in order to perform a flutter analysis. To account for the change in structural properties along the blade, lumped-mass parameters will be developed so that the partial differential equations of motion can be replaced with a set of ordinary differential equations, which can then be written in transfer matrix format so that in iterative solution may be obtained. In each case, bending and twisting, the equations of motion account for the large centrifugal forces on the rotor blade.

1. Holzer Method for Uncoupled Torsional Natural Frequencies

The development of linearized, coupled, nonuniform, rotating blade equations for torsion are based on the work of Houbolt and Brooks [Ref. 37]. Hodges and Dowell [Ref. 38] expanded the work of Houbolt and Brooks to include nonlinear structural and inertial effects, however for this analysis only the linearized equations will be used. The differential equations developed by Houbolt and Brooks are derived from the strain-displacement equations, and for torsion only can be written as

$$\begin{aligned}
&\mu k_m^2 \frac{\partial^2 \phi(y,t)}{\partial t^2} - \frac{\partial}{\partial y}\left\{\left(GJ + Ck_a^2 + EB_1\left(\frac{\partial \theta}{\partial y}\right)^2\right)\frac{\partial \phi(y,t)}{\partial y}\right\} \\
&\quad + \Omega^2 \mu\left[\left(k_{m_2}^2 - k_{m_1}^2\right)\cos 2\theta + e_c e_0 \cos\theta\right]\phi(y,t) \\
&\quad = M_{app} = M_\theta + \frac{\partial}{\partial y}\left(Ck_a^2 \frac{\partial \theta}{\partial y}\right) - \Omega^2 \mu\left[\left(k_{m_2}^2 - k_{m_1}^2\right)\sin\theta\cos\theta + e_c e_0 \sin\theta\right]
\end{aligned} \tag{1}$$

where

μ = mass per unit length

$k_m = \sqrt{k_{m_1}^2 + k_{m_2}^2}$,

k_{m_1} = mass radius of gyration of the blade section about the chordwise axis,

k_{m_2} = mass radius of gyration of the blade section about an axis perpendicular to the chordwise axis through the elastic axis

$GJ = \dfrac{4A_m G}{\oint_{C_m} \dfrac{ds}{t(s)}}$ = torsional rigidity or torsional stiffness,

$C = \int_r^R m\Omega^2 y\, dy$, local tension due to centrifugal force,

k_a = polar radius of gyration of the tensile stress carrying area about the elastic axis,

E = Young's modulus of elasticity

$B_1 = \int_{\eta_{TE}}^{\eta_{LE}} t\eta^2\left[\eta^2 + \dfrac{t^2}{6} - k_a^2\right] d\eta$, section constant

t = chordwise thickness

η = chordwise position integration variable measured from trailing edge to leading edge

Ω = rotation velocity of the rotor blade,

e_c = distance between c.g. and elastic axis, positive when mass axis lies ahead of elastic axis

e_0 = distance at root between elastic axis and axis about which blade is rotating (pitch root axis), positive when elastic axis lies ahead of root pitch axis

θ = $\theta_0(t) + \theta_B(y)$ = local pitch angle due to the time variation of the root pitch angle and the geometric twist of the rotor blade,

M_θ = aerodynamic torque loading per unit length,

and M_{app} = the total applied moment.

It should be noted that the *GJ* term is not simply the product of the shear modulus (*G*) and the polar moment of inertia (*J*). In fact, Timoshenko and Goodier [Ref. 39] describe torsional rigidity as the factor by which the torque is divided to obtain the twist per unit length, or for a nonrotating beam

$$\frac{d\phi}{dy} = \frac{T}{GJ} \tag{2}$$

which is sometimes referred to as the St. Venant-type torsional stiffness. Since a rotor blade has a noncircular, thin-walled cross section, the *J* term is not the polar moment of inertia at all. Using the method developed by Timoshenko and Goodier with the nomenclature used by Craig [Ref. 40], the angle of twist for a thin-walled cross section can be written as

$$\phi(y) = \frac{T(s)\,y}{4A_m^2 G} \oint_{C_m} \frac{ds}{t(s)}, \tag{3}$$

where C_m is the median curve and $t(s)$ is the thickness of the cross section as a function of circumferential location (s). Taking the derivative of the angle of twist with respect to y, equation (3) becomes

$$\frac{d\phi}{dy} = \frac{T(s)}{4A_m^2 G} \oint_{C_m} \frac{ds}{t(s)}, \tag{4}$$

and thus by the definition of *GJ* in equation (2),

$$GJ = \frac{4A_m^2 G}{\oint_{C_m} \frac{ds}{t(s)}} \tag{5}$$

Equation (1) can be simplified by noting that the total applied moment can be set to zero in order to obtain the uncoupled torsional natural frequencies, or

$$M_{app} = 0\,. \tag{6}$$

Additionally, since the blade cross-sectional thickness is much less than the chord, the mass radii of gyration can be simplified as follows:

$$k_{m_2}^2 >> k_{m_1}^2 \Rightarrow k_m^2 \approx k_{m_2}^2\,. \tag{7}$$

If it is assumed that the pitch root axis is coincident with the elastic axis, then

$$e_0 = 0\,. \tag{8}$$

Applying equations (6) through (8) to equation (1) and noting that the mass moment of inertia, $I_\alpha = \mu k_m^2$, the result is

$$\frac{\partial}{\partial y}\left\{\left(GJ + Ck_a^2 + EB_1\left(\frac{\partial\theta}{\partial y}\right)^2\right)\frac{\partial\phi(y,t)}{\partial y}\right\} - I_\alpha\frac{\partial^2\phi(y,t)}{\partial t^2} - \left(I_\alpha\Omega^2\cos 2\theta\right)\phi(y,t) = 0\,. \tag{9}$$

Bielawa [Ref. 41] describes the first term (*GJ*) on the left side of equation (9) is the torsional stiffness term. The second term (Ck_a^2) is the tension-torsion term that tends to untwist a pre-twisted blade due to centrifugal force, and the third term, $EB_1\left(\partial\theta/\partial y\right)$, is the incremental torsional stiffening or the coiled spring effect. The fourth term (I_α) is the torsional inertia, and the fifth term ($I_\alpha\Omega^2\cos 2\theta$) in equation (9) is called the "tennis racket effect", or propeller moment, and also tends to untwist a pre-twisted blade. The untwisting effect terms essentially provide extra stiffening of the rotating blade as a function of the rotational velocity. The net effect will be an increase in the uncoupled torsional natural frequency. While the local pitch angle, θ, is a function of both time (the sinusoidal variation in pitch of the blade root) and radial position (blade pre-twist), a reasonable approximation can be made that the blade root pitch angle is constant, and that

the only variation along the span of the blade (pretwist) is needed, or $\theta = \theta(y)$ only. If the pretwist is restricted to linear twist only, the slope will be a constant, the partial derivative with respect to y will be zero, and equation (9) becomes

$$\frac{\partial}{\partial y}\left\{\left(GJ + Ck_a^2\right)\frac{\partial \phi(y,t)}{\partial y}\right\} - I_\alpha \frac{\partial^2 \phi(y,t)}{\partial t^2} - \left(I_\alpha \Omega^2 \cos 2\theta\right)\phi(y,t) = 0. \tag{10}$$

A solution to equation (10) can be obtained using the method of separation of variables in which it is assumed that

$$\phi(y,t) = Y(y)T(t). \tag{11}$$

The partial derivatives of equation (11) can be written as

$$\frac{\partial^2 \phi(y,t)}{\partial t^2} = Y(y)\frac{\partial^2 T}{\partial t^2} \tag{12}$$

and

$$\frac{\partial \phi(y,t)}{\partial y} = \frac{\partial Y(y)}{\partial y}T(t) \tag{13}$$

Allowing the beam to experience simple harmonic motion of the form of $T(t) = e^{i\omega_\alpha t}$, equations (12) and (13) can be substituted into equation (10) yielding

$$\frac{d}{dy}\left\{\left(GJ(y) + C(y)k_a^2(y)\right)\frac{d\phi(y)}{dy}\right\} = -I_\alpha \phi(y)\left(\omega_\alpha^2 - \Omega^2 \cos 2\theta\right), \tag{14}$$

where it is noted that $\phi(y) = Y(y)$. Equation (14) can be written as a set of two first order ordinary differential equations by noting that

$$\frac{d\phi}{dy} = \frac{T(y)}{GJ(y) + Ck_a^2(y)} \tag{15}$$

and

$$\frac{d}{dy}\left(T(y)\right) = -I_\alpha(y)\phi(y)\left(\omega_\alpha^2 - \Omega^2 \cos 2\theta\right) \tag{16}$$

In order to solve equation (14) or equations (15) and (16), two boundary conditions must be applied. The first boundary condition is that the torque at the tip must

be zero since the blade is free to rotate at that end. The second boundary condition is applied at the root end and is dependent on the type of restraint used on the rotor blade. For this research, three root end boundary conditions will be considered for the torsional deflection: articulated with no pitch restraint ($T_{root} = 0$), rigid hingeless ($\phi_{root} = 0$), and finite pitch control stiffness at the root ($K_{root}\phi_{root} - T_{root} = 0$). Since the boundary conditions are on opposite ends, the problem becomes one of trial and error to find the correct natural frequency, ω_α.

Since the torsional rigidity and torsional inertia can be complicated functions of y and may contain discontinuities, it is not always possible to solve equation (14) exactly. However, if the rotor blade is divided into a convenient number of segments with the mass of each segment divided by two and concentrated at each end of the segment, then a lumped-mass parameter system can be developed that would allow for reasonable approximations to the continuous beam. With the mass now concentrated at each end of the segment, a massless, flexible connection is made to approximate the continuous system as a discrete one. Figure 4 is the free body diagram for the single, rotating lumped-mass segment [Ref. 42], and the torque equation can be written as

$$T_n = T_{n+1} + I_{\alpha_n}\phi_n\left(\omega_\alpha^2 - \Omega^2\cos\theta_n\right). \tag{17}$$

Applying the fundamental theorem of calculus to equation (15) and rearranging the terms yields the incremental torsional deformation for a single segment,

$$\Delta\phi_{n,n+1} = \frac{T_{n+1}}{\left[\left(GJ\right)_{n+1} + \left(Ck_a^2\right)_{n+1}\right]} l_{n,n+1}, \tag{18}$$

where $l_{n,n+1}$ is the distance between concentrated masses n and n+1. The angle of twist of a single segment can now be written as

$$\phi_n = \phi_{n+1} - \Delta\phi_{n,n+1} = \phi_{n+1} - \frac{T_{n+1}}{\left[\left(GJ\right)_{n+1} + \left(Ck_a^2\right)_{n+1}\right]} l_{n,n+1}. \tag{19}$$

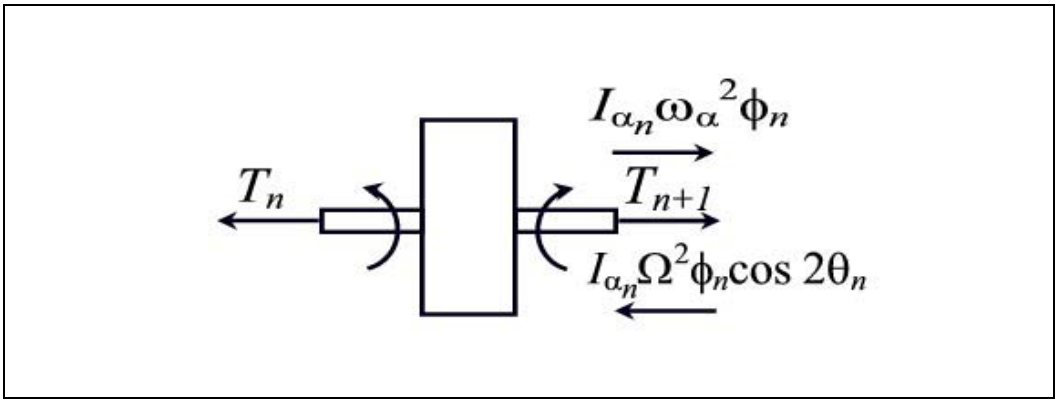

Figure 4. Torsional free body diagram for rotating lumped-mass segment.

Equations (18) and (19) can be written in transfer matrix form as

$$\begin{bmatrix} 1 & 0 \\ -I_{\alpha_n}\left(\omega_\alpha^2 - \Omega^2\cos\theta_n\right) & 1 \end{bmatrix}\begin{bmatrix}\phi \\ T\end{bmatrix}_n = \begin{bmatrix} 1 & -l_{n,n+1}\Big/\left[\left(GJ\right)_{n+1} + \left(Ck_a^2\right)_{n+1}\right] \\ 0 & 1 \end{bmatrix}\begin{bmatrix}\phi \\ T\end{bmatrix}_{n+1}. \quad (20)$$

The Holzer method [Ref. 3] is normally applied in the following manner after the rotor blade is divided into *N* segments. (The standard nomenclature is that *N* refers to the segment closest to the tip and 1 refers to the segment closest to the root.) First, assume a natural frequency, ω_α. Second, arbitrarily set the tip torsional deflection to 1 radian, or

$$\phi_N = 1. \quad (21)$$

This step will normalize the deflection curve so that the tip deflection will be 1 radian with the free end torsional moment set to zero. The third step is to find the torsional moment at segment *N*. Since $T_{tip} = 0$, it is easily seen from equation (17) that

$$T_N = I_{\alpha_N}\left(\omega_\alpha^2 - \Omega^2\cos\theta_n\right). \quad (22)$$

It may seem that equation (22) contradicts the boundary condition of zero torque at the tip, but it should be noted that the mass of the last element is concentrated at the tip and truly represents an average condition for that segment [Ref. 43]. The fourth step is to find the torsional deflection at segment *N*-1 using equation (19), which yields

$$\phi_{N-1} = 1 - \frac{T_N}{\left(GJ\right)_N}\Delta y_{n,n+1}. \quad (23)$$

The fifth step is to apply equation (17) again, which yields

$$T_{N-1} = T_N + I_{\alpha_{N-1}} \omega_\alpha^2. \tag{24}$$

The fourth and fifth steps can now be repeated for each segment in descending order until the torque and torsional deflection at the root are obtained. The solutions at the root can now be compared to the boundary condition at the root. If the boundary condition matches, the assumed frequency is a torsional natural frequency [Ref. 3]. If the boundary condition does not match, a new frequency is assumed, and the method continues in an iterative manner until the boundary conditions are met.

While the recursive application of equations (21) through (24) is not difficult, it is sometimes more convenient in programming to use equation (20) directly. Equation (20) can be written in the form

$$\left[\mathbf{K_n}\right]\mathbf{X_n} = \left[\mathbf{A_{n+1}}\right]\mathbf{X_{n+1}} \tag{25}$$

where

$$\mathbf{X_n} = \begin{bmatrix} \phi \\ T \end{bmatrix}_n,$$

$$\mathbf{X_{n+1}} = \begin{bmatrix} \phi \\ T \end{bmatrix}_{n+1},$$

and $\left[\mathbf{K_n}\right]$ and $\left[\mathbf{A_{n+1}}\right]$ are defined by the matrices in equation (20). Pre-multiplying equation (25) by $\left[\mathbf{K_n}\right]^{-1}$ yields

$$\mathbf{X_n} = \left[\mathbf{K_n}\right]^{-1}\left[\mathbf{A_{n+1}}\right]\mathbf{X_{n+1}} = \left[\mathbf{T_{n+1}}\right]\mathbf{X_{n+1}}. \tag{26}$$

The boundary conditions at the tip are given as

$$\mathbf{X}_{tip} = \begin{bmatrix} 1 \\ 0 \end{bmatrix}, \tag{27}$$

and the boundary condition at the root is given by

$$\mathbf{X}_{root} = \begin{bmatrix} \phi_{root} \\ 0 \end{bmatrix} \quad \text{for an articulated rotor}$$

$$\mathbf{X}_{root} = \begin{bmatrix} 0 \\ T_{root} \end{bmatrix} \quad \text{for a rigid hingeless rotor}$$

or (28)

$$\mathbf{X}_{root} = \begin{bmatrix} \phi_{root} \\ T_{root} \end{bmatrix} \quad \text{where } K_{root}\phi_{root} - T_{root} = 0$$

for a rotor with finite control stiffness.

Appendix B contains a MATLAB® function that calculates the torsional natural frequencies of a rotor blade using equations (26) through (28). This function works in conjunction with the rotor blade flutter program contained in Appendix A.

2. Myklestad-Prohl Method for Uncoupled Bending Natural Frequencies

An extension of the Holzer method can be applied to the uncoupled bending modes and frequencies of a beam [Ref. 44]. This method was developed independently by Myklestad [Ref. 35] and Prohl [Ref. 36] is essentially the same as the Holzer method in that a natural frequency must first be assumed, and then a recursive procedure is applied to see if the boundary conditions match the calculated root forces and moments. The frequency that causes the boundary conditions to match the calculated forces is a bending natural frequency. The main difference is that the flexural bending problem is a solution to a 4^{th} order differential equation instead of a 2^{nd} order equation as for the torsional problem. A solution to the 4^{th} order equation requires that four boundary conditions be specified, and as will be shown below, these boundary conditions vary depending on the type of restraint used on the rotor blade. Additionally, the centrifugal forces will be included throughout the analysis since they can be calculated in advance, and they have a significant effect on the calculated natural frequencies. Like the case for the torsional natural frequencies, the primary effect of the centrifugal forces will be to increase the bending natural frequencies over the nonrotating case.

The flapwise bending motion is the deflection of the rotor blade in a plane perpendicular to the plane of rotation. Let h be the displacement of an element of the blade above the flapping plane, and r the distance from the axis of rotation along the y axis as shown in Figure 5 [Ref. 43]. The blade element equilibrium equations are

$$dC + \mu \Omega^2 y \, dy = 0 \tag{29}$$

$$dS + \mu \, dy \frac{\partial^2 h(y,t)}{\partial t^2} = 0 \tag{30}$$

$$C \, dh(y,t) + S \, dy - dM = 0 \tag{31}$$

where C is the centrifugal tension in the blade, M is the bending moment, S is the local shear force, and μ is the mass per unit length. Since the centrifugal force is a function of y only, equation (29) can be integrated from the station, r, to the spanwise end of the blade, R, yielding

$$C = \int_r^R \mu \Omega^2 y \, dy \, . \tag{32}$$

From equation (30), the change in shear force along the spanwise direction of the rotor blade is given by

$$\frac{\partial S}{\partial y} = -\mu \frac{\partial^2 h(y,t)}{\partial t^2}, \tag{33}$$

and the change in the bending moment along the spanwise direction is given from equation (31) as

$$\frac{\partial M}{\partial y} = C \frac{\partial h(y,t)}{\partial y} + S \tag{34}$$

Differentiating equation (34) with respect to the spanwise dimension, and substituting equation (33) into the result yields

$$\frac{\partial^2 M}{\partial y^2} = \frac{\partial}{\partial y}\left(C \frac{\partial h(y,t)}{\partial y} \right) - \mu \frac{\partial^2 h(y,t)}{\partial t^2} \tag{35}$$

The standard beam bending equation for the moment is given as,

$$M = EI \frac{\partial^2 h(y,t)}{\partial y^2} \, . \tag{36}$$

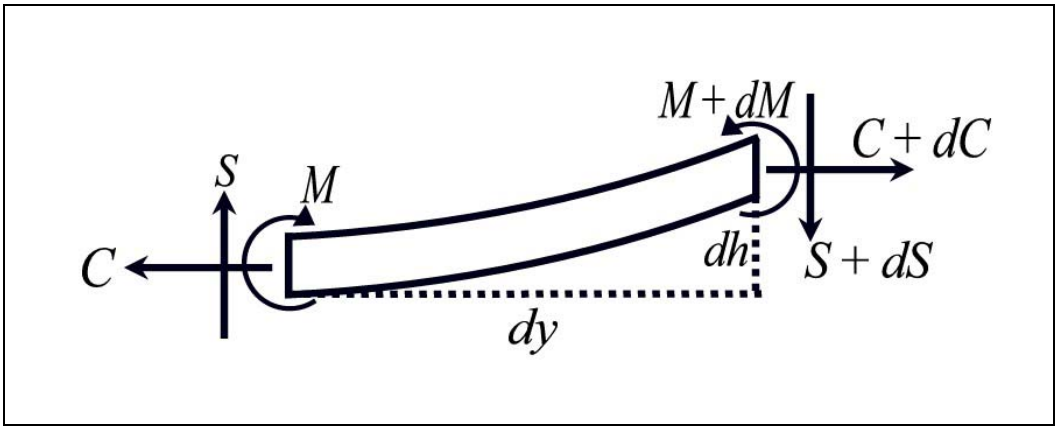

Figure 5. Flapwise forces on a blade element (from Ref. 41).

Substituting equation (36) into (35) yields

$$\frac{\partial^2}{\partial y^2}\left(EI\frac{\partial^2 h(y,t)}{\partial y^2}\right)-\frac{\partial}{\partial y}\left(C\frac{\partial h(y,t)}{\partial y}\right)+\mu\frac{\partial^2 h(y,t)}{\partial t^2}=0\,, \tag{37}$$

which is a modified Bernoulli-Euler equation. Equation (37) has been modified to the extent that centrifugal force has been included, which acts to stiffen the rotor blade as rotational velocity is increased.

A solution to equation (37) can also be obtained by using separation of variables. To find the uncoupled natural frequency, it will be assumed that the beam will experience simple harmonic motion of the form

$$h(y,t)=e^{i\omega_h t}h(y) \tag{38}$$

where ω_h is the natural frequency of oscillation in bending. Substitution of equation (38) into equation (37) yields

$$\frac{d^2}{dy^2}\left(EI(y)\frac{d^2 h(y)}{dy^2}\right)-\frac{d}{dy}\left(C(y)\frac{dh(y)}{dy}\right)-\mu\omega_h^2 h(y)=0 \tag{39}$$

Since equation (39) is a fourth order differential equation, four boundary conditions need to be specified – two tip end boundary conditions and two root end boundary conditions. The tip end boundary conditions are that the shear and the moment must vanish, or

$$S_{tip}=0 \qquad \text{and} \qquad M_{tip}=0. \tag{40}$$

The root end boundary conditions are dependent on the type of restraint used on the rotor blade. For this research, three root end boundary conditions will be considered for the bending deflection: articulated with no flap restraint ($y_{root} = 0$ and $M_{root} = 0$), rigid hingeless ($y_{root} = 0$ and $\beta_{root} = 0$), and flexible hingeless ($y_{root} = 0$ and $K_{root}\beta_{root} + M_{root} = 0$).

Obtaining a closed-form solution to equation (39) is normally not possible since the bending stiffness and the mass distribution can be complicated functions of the rotor span (y) and may contain discontinuities. In a manner similar to the Holzer method, the Myklestad-Prohl method divides the rotor blade into a convenient number of segments with the mass of each segment divided by two and concentrated at each end of the segment. This lumped-mass system allows equation (39) to be replaced by a set of four 1st order ordinary differential equations. Using the same nomenclature as in the Holzer method that the n^{th} segment is closer to the root and the $(n+1)^{th}$ segment is closer to the tip, a free body diagram of a lumped-mass blade element [Ref. 34] is shown in Figure 6 where ω_h is the bending frequency of oscillation, Ω is the rotational frequency of the rotor, G_n is the flapwise aerodynamic damping constant, and $F_n + if_n$ is the aerodynamic lift force acting on the blade element for a particular frequency.

Following the method of Gerstenberger and Wood [Ref. 34], the equilibrium of the in-plane forces can be written as

$$\sum F_y = 0 = C_{n+1} + m_n \Omega^2 r_n - C_n ,$$

or

$$C_n = C_{n+1} + m_n \Omega^2 r_n , \tag{41}$$

where m_n is the concentrated mass and r_n is the radial station at which this mass is located. It can be seen from equation (41) that the centrifugal forces at each segment are decoupled from the remainder of the solution and can be calculated prior to the iteration process. Using a summation instead of an integral, equation (41) can be written in a discrete form of equation (32) as

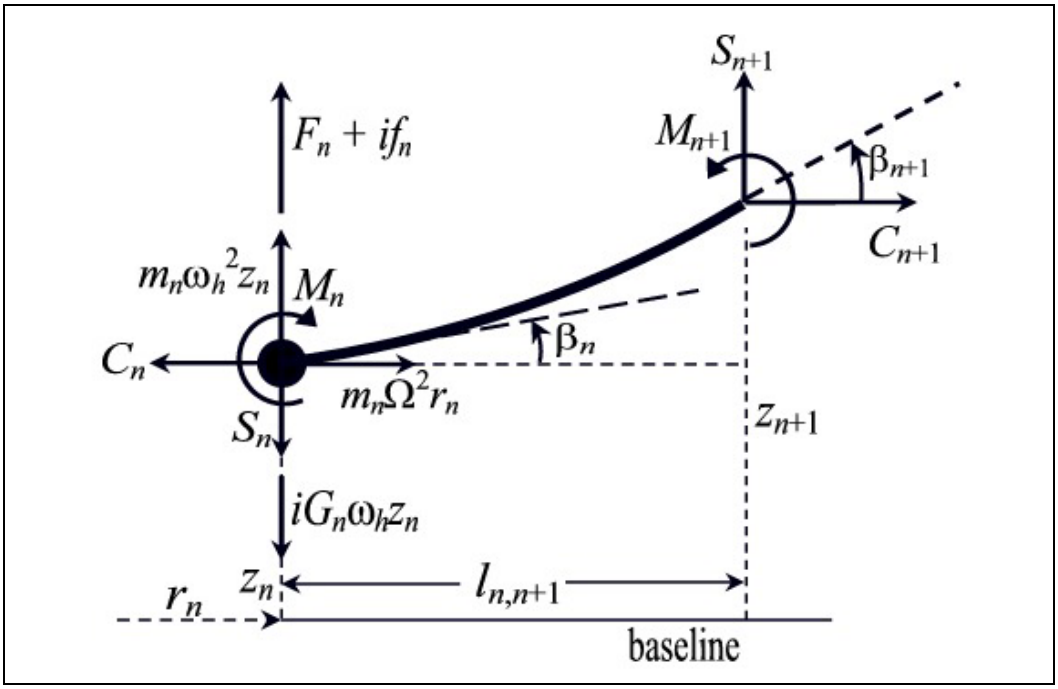

Figure 6. Free body diagram of a lumped-mass blade element (from Ref. 34).

$$C_n = \sum_{i=n}^{N} m_i \Omega^2 r_i \,. \tag{42}$$

Equilibrium of the out-of-plane forces can be written as

$$\sum F_z = 0 = S_{n+1} + m_n \omega_h^2 z_n - S_n - iG_n \omega_h z_n + F_n + if_n \,,$$

or

$$S_n - m_n \omega_h^2 z_n + iG_n \omega_h z_n - F_n - if_n = S_{n+1} \,. \tag{43}$$

At this point in the development of this flutter theory, only the uncoupled structural natural frequencies are needed, and the aerodynamic lift forces and damping can be dropped since they will be incorporated in a later section. Thus, equation (43) can be written as

$$S_n - m_n \omega_h^2 z_n = S_{n+1} \,. \tag{44}$$

And finally, equilibrium of the moments about the mass, m_n can be written as

$$+\circlearrowleft \sum M = 0 = M_{n+1} + l_{n,n+1} S_{n+1} - \left(z_{n+1} - z_n\right) C_{n+1} - M_n \,,$$

or

$$M_n - C_{n+1} z_n = M_{n+1} + l_{n.n+1} S_{n+1} - C_{n+1} z_{n+1}. \tag{45}$$

With the equilibrium equations given in equations (42), (44), and (45), it should be noted that the centrifugal force is decoupled from the shear and moment equations. In order to solve for the shear and moments, the force-deformation equations need to be written. Assuming that there on no discontinuities in the station length, $l_{n,n+1}$, the flapwise slope can be written as

$$\beta_n = \left(1 + \frac{l_{n,n+1}^2}{2(EI)_n} C_{n+1}\right)\beta_{n+1} - \left(\frac{l_{n,n+1}^2}{2(EI)_n}\right) S_{n+1} - \left(\frac{l_{n,n+1}}{(EI)_n}\right) M_{n+1}, \tag{46}$$

and the flapwise displacement can be written as

$$z_n + l_{n,n+1}\beta_n = z_{n+1} + \left(\frac{l_{n,n+1}^3}{3(EI)_n} C_{n+1}\right) - \left(\frac{l_{n,n+1}^3}{3(EI)_n}\right) S_{n+1} - \left(\frac{l_{n,n+1}^2}{2(EI)_n}\right) M_{n+1} \tag{47}$$

The in-plane equilibrium equations, (44) and (45), along with the force-deformation equations, (46) and (47), can be combined in transfer matrix format as follows

$$\begin{bmatrix} 1 & 0 & 0 & -m_n\omega_h^2 \\ 0 & 1 & 0 & -C_{n+1} \\ 0 & 0 & 1 & 0 \\ 0 & 0 & l_{n,n+1} & 1 \end{bmatrix} \begin{bmatrix} S \\ M \\ \beta \\ z \end{bmatrix}_n = \begin{bmatrix} 1 & 0 & 0 & 0 \\ l_{n,n+1} & 1 & 0 & -C_{n+1} \\ -\frac{l_{n,n+1}^2}{2(EI)_n} & -\frac{l_{n,n+1}}{(EI)_n} & 1 + \frac{l_{n,n+1}^2}{2(EI)_n} C_{n+1} & 0 \\ -\frac{l_{n,n+1}^3}{3(EI)_n} & -\frac{l_{n,n+1}^2}{2(EI)_n} & \frac{l_{n,n+1}^3}{3(EI)_n} C_{n+1} & 1 \end{bmatrix} \begin{bmatrix} S \\ M \\ \beta \\ z \end{bmatrix}_{n+1}. \tag{48}$$

Equation (48) can be written in the form

$$[\mathbf{K_n}]\mathbf{X_n} = [\mathbf{A_{n+1}}]\mathbf{X_{n+1}} \tag{49}$$

where

$$\mathbf{X_n} = \begin{bmatrix} S \\ M \\ \beta \\ z \end{bmatrix}_n, \qquad \mathbf{X_{n+1}} = \begin{bmatrix} S \\ M \\ \beta \\ z \end{bmatrix}_{n+1},$$

and $[\mathbf{K_n}]$ and $[\mathbf{A_{n+1}}]$ are defined by the matrices in equation (48). Pre-multiplying equation (49) by $[\mathbf{K_n}]^{-1}$ yields

$$\mathbf{X_n} = [\mathbf{K_n}]^{-1}[\mathbf{A_{n+1}}]\mathbf{X_{n+1}} = [\mathbf{T_{n+1}}]\mathbf{X_{n+1}}, \tag{50}$$

which can be applied recursively for each blade segment. By arbitrarily setting the deflection equal to one, the boundary conditions at the tip are given as

$$\mathbf{X}_{tip} = \begin{bmatrix} 0 \\ 0 \\ \beta_{tip} \\ 1 \end{bmatrix} \tag{51}$$

The boundary conditions at the root are dependent on the type of restraint used for the rotor blade, and are summarized as follows:

$$\mathbf{X}_{root} = \begin{bmatrix} S_{root} \\ 0 \\ \beta_{root} \\ 0 \end{bmatrix} \quad \text{for an articulated rotor}$$

$$\mathbf{X}_{root} = \begin{bmatrix} S_{root} \\ M_{root} \\ 0 \\ 0 \end{bmatrix} \quad \text{for a rigid hingeless rotor} \tag{52}$$

or

$$\mathbf{X}_{root} = \begin{bmatrix} S_{root} \\ M_{root} \\ \beta_{root} \\ 0 \end{bmatrix} \quad \text{where } K_{root}\beta_{root} + M_{root} = 0$$
for a rotor with a flexible hingeless restraint.

In order to solve equation (48) for the entire blade, equation (50) must be applied recursively from the tip to the root, or

$$\mathbf{X_1} = [\mathbf{T_2}][\mathbf{T_3}]\cdots[\mathbf{T_N}]\mathbf{X_N} \tag{53}$$

By letting

$$[\mathbf{T_2}][\mathbf{T_3}]\cdots[\mathbf{T_N}] = \mathbf{F_N}$$

where

$$\mathbf{F_N} = \begin{bmatrix} a_S & b_S & c_S & d_S \\ a_M & b_M & c_M & d_M \\ a_\beta & b_\beta & c_\beta & d_\beta \\ a_z & b_z & c_z & d_z \end{bmatrix} \tag{54}$$

Just as in the Holzer method, a frequency must first be assumed, and if that frequency satisfies the boundary conditions, the assumed frequency is a bending natural frequency. If the assumed frequency does not satisfy the boundary conditions, a new frequency is assumed, and the method continues in an iterative manner. Since S_1, M_1, and β_1 are not know in advance for the given root boundary conditions, the conditions for which equation (53) must be solved are:

(1) For an articulated rotor,

$$\begin{bmatrix} S_1 \\ 0 \\ \beta_1 \\ 0 \end{bmatrix} = \begin{bmatrix} a_S & b_S & c_S & d_S \\ a_M & b_M & c_M & d_M \\ a_\beta & b_\beta & c_\beta & d_\beta \\ a_z & b_z & c_z & d_z \end{bmatrix} \begin{bmatrix} 0 \\ 0 \\ \beta_N \\ 1 \end{bmatrix} \tag{55}$$

Equation (55) can be reduced to

$$\begin{bmatrix} 0 \\ 0 \end{bmatrix} = \begin{bmatrix} c_M & d_M \\ c_z & d_z \end{bmatrix} \begin{bmatrix} \beta_N \\ 1 \end{bmatrix}, \tag{56}$$

and since equation (56) is an homogenous equation, a solution exists only when the determinant goes to zero, or

$$\begin{vmatrix} c_M & d_M \\ c_z & d_z \end{vmatrix} = 0\,. \tag{57}$$

(2) Similarly for a rigid hingeless rotor,

$$\begin{bmatrix} S_1 \\ M_1 \\ 0 \\ 0 \end{bmatrix} = \begin{bmatrix} a_S & b_S & c_S & d_S \\ a_M & b_M & c_M & d_M \\ a_\beta & b_\beta & c_\beta & d_\beta \\ a_z & b_z & c_z & d_z \end{bmatrix} \begin{bmatrix} 0 \\ 0 \\ \beta_N \\ 1 \end{bmatrix}$$

which reduces to

$$\begin{bmatrix} 0 \\ 0 \end{bmatrix} = \begin{bmatrix} c_\beta & d_\beta \\ c_z & d_z \end{bmatrix} \begin{bmatrix} \beta_N \\ 1 \end{bmatrix},$$

and is satisfied only when

$$\begin{vmatrix} c_\beta & d_\beta \\ c_z & d_z \end{vmatrix} = 0 . \tag{58}$$

(3) Finally, for a flexible hingeless rotor

$$\begin{bmatrix} S_1 \\ M_1 \\ \beta_1 \\ 0 \end{bmatrix} = \begin{bmatrix} a_S & b_S & c_S & d_S \\ a_M & b_M & c_M & d_M \\ a_\beta & b_\beta & c_\beta & d_\beta \\ a_z & b_z & c_z & d_z \end{bmatrix} \begin{bmatrix} 0 \\ 0 \\ \beta_N \\ 1 \end{bmatrix}$$

which with the additional constraint of $K_{root}\beta_1 + M_1 = 0$ reduces to

$$\begin{bmatrix} 0 \\ 0 \end{bmatrix} = \begin{bmatrix} K_{root}c_\beta + c_M & K_{root}d_\beta + d_M \\ c_z & d_z \end{bmatrix} \begin{bmatrix} \beta_N \\ 1 \end{bmatrix},$$

and is satisfied only when

$$\begin{vmatrix} K_{root}c_\beta + c_M & K_{root}d_\beta + d_M \\ c_z & d_z \end{vmatrix} = 0 . \tag{59}$$

Equations (57), (58), and (59) are the boundary conditions that must be satisfied to find the bending natural frequencies for the given rotor restraint. Appendix C contains a MATLAB® function that calculates the bending natural frequencies. This function works in conjunction with the rotor blade flutter program contained in Appendix A.

B. AERODYNAMIC FORCES AND MOMENTS

1. Thin Airfoil Theory

Any general oscillating motion of an aircraft structure can be expressed in terms of translation from and/or rotation about some reference axis, assuming the displacements from equilibrium are small relative to the dimensions of the structure. If that structure contains a portion that is free to rotate about some hinge axis, the general displacement of an element of mass can be expressed in terms of translation from a reference axis, rotation about a reference axis, and rotation about the hinge axis. In the discussion that follows, the structure under consideration is a helicopter rotor blade that has a trailing-edge flap incorporated at the trailing edge as shown in Figure 7. The reference axis for translation will be the elastic axis of the undisturbed rotor blade, and the reference axis for blade rotation will also be the elastic axis.

Applying thin airfoil theory, the geometry of the helicopter rotor blade under consideration can be simplified to the two-dimensional representation shown in Figure 8. For the case of an inviscid, incompressible fluid, Smilg and Wasserman [Ref. 45] showed that the forces and moments per unit span on the airfoil are given as follows:

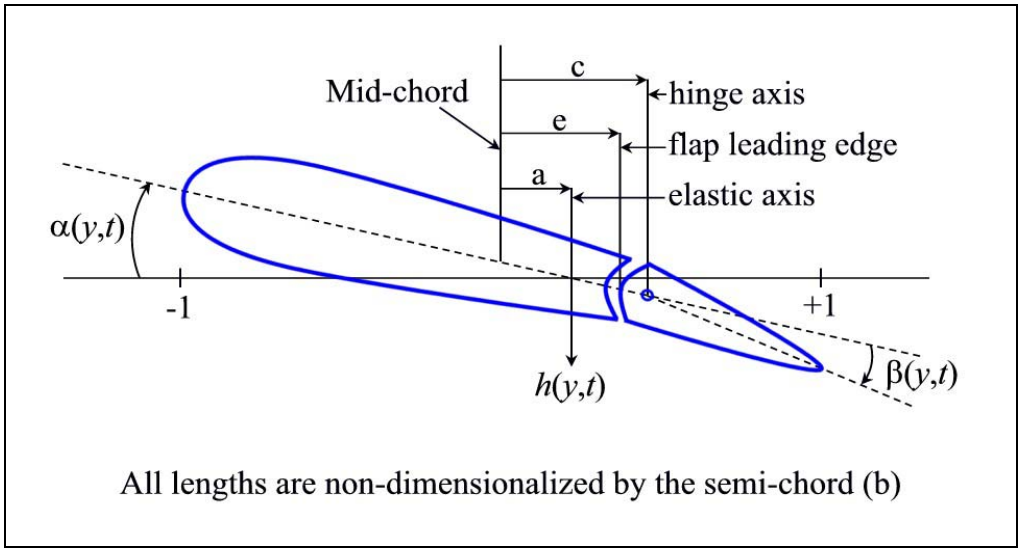

Figure 7. Schematic of rotor blade with trailing-edge flap.

(1) Wing lift force per unit span:

$$L' = \pi\rho b^3\omega^2 \left\{ L_h \frac{h}{b} + \left[L_\alpha - \left(\frac{1}{2} + a\right) L_h \right] \alpha + \left[L_\beta - (c-e) L_z \right] \beta \right\} \tag{60}$$

(2) Moment per unit span due to blade rotation about the wing quarter-chord:

$$\begin{aligned} M' = \pi\rho b^4\omega^2 \Bigg\{ & \left[M_h - \left(\frac{1}{2} + a\right) L_h \right] \frac{h}{b} \\ & + \left[M_\alpha - \left(\frac{1}{2} + a\right)\left(L_\alpha + M_h\right) + \left(\frac{1}{2} + a\right)^2 L_h \right] \alpha \\ & + \left[M_\beta - \left(\frac{1}{2} + a\right) L_\beta - (c-e)\left(M_z - \left(\frac{1}{2} + a\right) L_z \right) \right] \beta \Bigg\} \end{aligned} \tag{61}$$

(3) Moment per unit span due to flap rotation about the hinge:

$$\begin{aligned} T' = \pi\rho b^4\omega^2 \Bigg\{ & \left[T_h - (c-e) P_h \right] \frac{h}{b} \\ & + \left[T_\alpha - (c-e) P_\alpha - \left(\frac{1}{2} + a\right)\left(T_h - (c-e) P_h \right) \right] \alpha \\ & + \left[T_\beta - (c-e)\left(P_\beta + T_z \right) + (c-e)^2 P_z \right] \beta \Bigg\} \end{aligned} \tag{62}$$

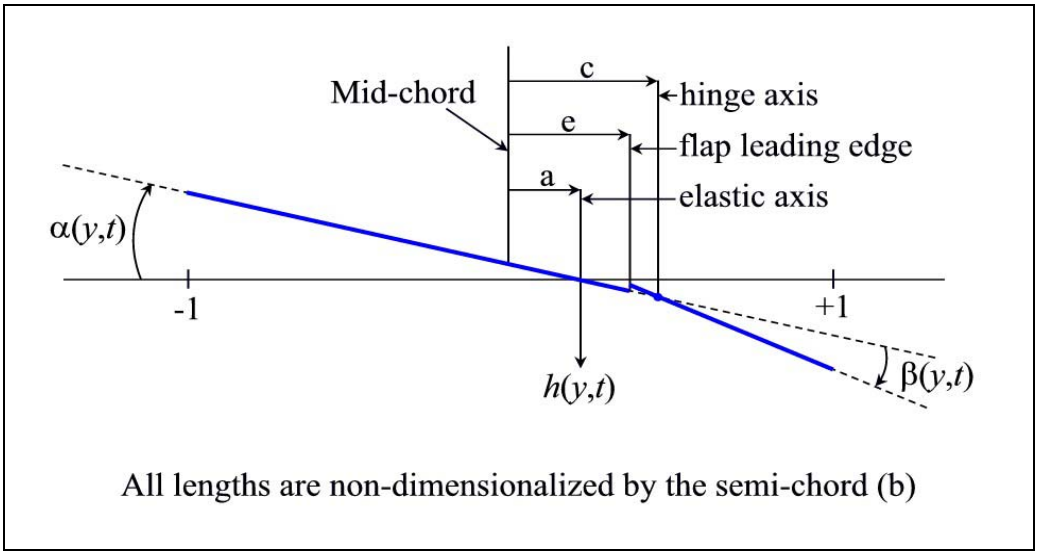

Figure 8. Two-dimensional schematic of rotor blade with trailing-edge flap.

where b is the semi-chord, k is the reduced frequency, the dimensions for a, c and e are given in Figure 8, and the L, M, T and P terms are listed below [Ref. 3 and 45].

$$L_h = 1 - \frac{2i}{k} C(k) \tag{63}$$

$$L_\alpha = \frac{1}{2} - \frac{i}{k}\left[1 + 2C(k)\right] - \frac{2}{k^2} C(k) \tag{64}$$

$$L_\beta = -\frac{T_1}{\pi} + \frac{i}{\pi k}\left[T_4 - T_{11} C(k)\right] - \frac{2}{k^2}\left(\frac{T_{10}}{\pi}\right) C(k) \tag{65}$$

$$L_z = -\frac{2i}{k}\left(\frac{\phi_1}{\pi}\right) C(k) + \frac{\phi_3}{\pi} \tag{66}$$

$$M_h = \frac{1}{2} \tag{67}$$

$$M_\alpha = \frac{3}{8} - \frac{i}{k} \tag{68}$$

$$M_\beta = -\frac{T_7}{\pi} - \left(e + \frac{1}{2}\right)\frac{T_1}{\pi} + \frac{i}{k}\left(\frac{2p + T_4}{\pi}\right) - \frac{1}{k^2}\left(\frac{T_4 + T_{10}}{\pi}\right) \tag{69}$$

$$M_z = -\frac{i}{k}\left(\frac{\phi_5}{\pi}\right) + \frac{1}{4}\left(\frac{\phi_6}{\pi}\right) \tag{70}$$

$$T_h = -\frac{T_1}{\pi} - \frac{i}{k}\left(\frac{T_{12}}{\pi}\right) C(k) \tag{71}$$

$$T_\alpha = -\frac{1}{\pi}\left[T_7 + \left(e + \frac{1}{2}\right) T_1\right] - \frac{i}{k}\left[\left(\frac{2p - 2T_1 - T_4}{2\pi}\right) + \frac{T_{12}}{\pi} C(k)\right] - \frac{1}{k^2}\left(\frac{T_{12}}{\pi}\right) C(k) \tag{72}$$

$$T_\beta = -\left(\frac{T_3}{\pi^2}\right) + \frac{i}{k}\left(\frac{T_4 T_{11} - T_{11} T_{12} C(k)}{2\pi^2}\right) - \frac{1}{k^2}\left(\frac{T_5 - T_4 T_{10} + T_{10} T_{12} C(k)}{\pi^2}\right) \tag{73}$$

$$T_z = -\frac{i}{k}\left(\frac{\phi_1 \phi_8 C(k) + \phi_{10}}{\pi^2}\right) + \frac{1}{2}\left(\frac{\phi_{37}}{\pi^2}\right) \tag{74}$$

$$P_h = -\frac{2i}{k}\left(\frac{\phi_{31}C(k)}{\pi}\right)+\frac{\phi_3}{\pi} \tag{75}$$

$$P_\alpha = -2\left[\frac{1}{k^2}+\frac{i}{k}\right]\left(\frac{\phi_{31}C(k)}{\pi}\right)-\frac{i}{k}\left(\frac{\phi_{32}}{\pi}\right)+\frac{\phi_6}{4\pi} \tag{76}$$

$$P_\beta = -\frac{2}{\pi}\left[\frac{\phi_1}{k^2}+\frac{i\phi_2}{2k}\right]\left(\frac{\phi_{31}C(k)}{\pi}\right)-\frac{\phi_{35}}{k^2\pi^2}-\frac{i}{k}\left(\frac{\phi_{36}}{\pi^2}\right)+\frac{\phi_{37}}{2\pi^2} \tag{77}$$

$$P_z = -\frac{2i}{k}\left(\frac{\phi_1\phi_{31}}{\pi^2}\right)C(k)-\frac{i}{k}\left(\frac{\phi_{35}}{\pi^2}\right)+\left(\frac{\phi_{17}}{\pi^2}\right) \tag{78}$$

Theodorsen's *T*-functions and Küssner's ϕ-functions given in equations (63) through (78) are functions of geometry only and are defined in Appendix F [Ref. 3, 46, and 47].

2. The Lift Deficiency Functions

a. Theodorsen's Lift Deficiency Function

The term $C(k)$ given in equations (63) through (78) is the lift deficiency function. In fixed-wing and some rotary-wing analyses Theodorsen's lift deficiency function is used [Ref. 3 and 46] and is defined by

$$C(k) = \frac{H_1^{(2)}(k)}{H_1^{(2)}(k)+iH_0^{(2)}(k)}, \tag{79}$$

where $H_n^{(2)}(k) = J_n(k) - iY_n(k)$ is a Hankel function of the second kind of order n, and k is the reduced frequency defined by

$$k = \frac{\omega b}{v}. \tag{80}$$

Theodorsen's lift deficiency function was originally developed for fixed-wing aircraft using potential flow theory and derived from the equations of motion for a 2-D harmonically oscillating airfoil in an inviscid, incompressible flow subjected to small disturbances. Theodorsen's lift deficiency function is normally written in terms of its real and imaginary parts, or

$$C(k) = F(k) + iG(k). \tag{81}$$

A typical plot of the real and imaginary parts is shown in Figure 9 as a function of $1/k$. Since the behavior of the functions $F(k)$ and $G(k)$ as k approaches zero and infinity is not easily seen, a semi-logarithmic plot of Theodorsen's lift deficiency function can be made and is shown in Figure 10 [Ref. 15 and 48]. This semi-logarithmic plot looks similar to a Bode plot of the complex lift deficiency function, $C(k)$, where $F(k)$ is the predominant magnitude term and $G(k)$ is the term that influences the phase angle. Superimposed on the plots in Figure 10 are the values for $G(k)$ for selected helicopters at their N_b/rev-reduced frequencies, where N_b/rev is the blade passage frequency for the given helicopter. That is, N_b/rev frequency is the product of the number of blades, N_b, times the rotor rotational speed, Ω. It should be noted that for the helicopters studied, all have their N_b/rev reduced frequencies in a range where $G(k)$ is noticeably non-zero, thus producing a natural phase relationship in the unsteady lift term of a rotor blade [Ref. 15].

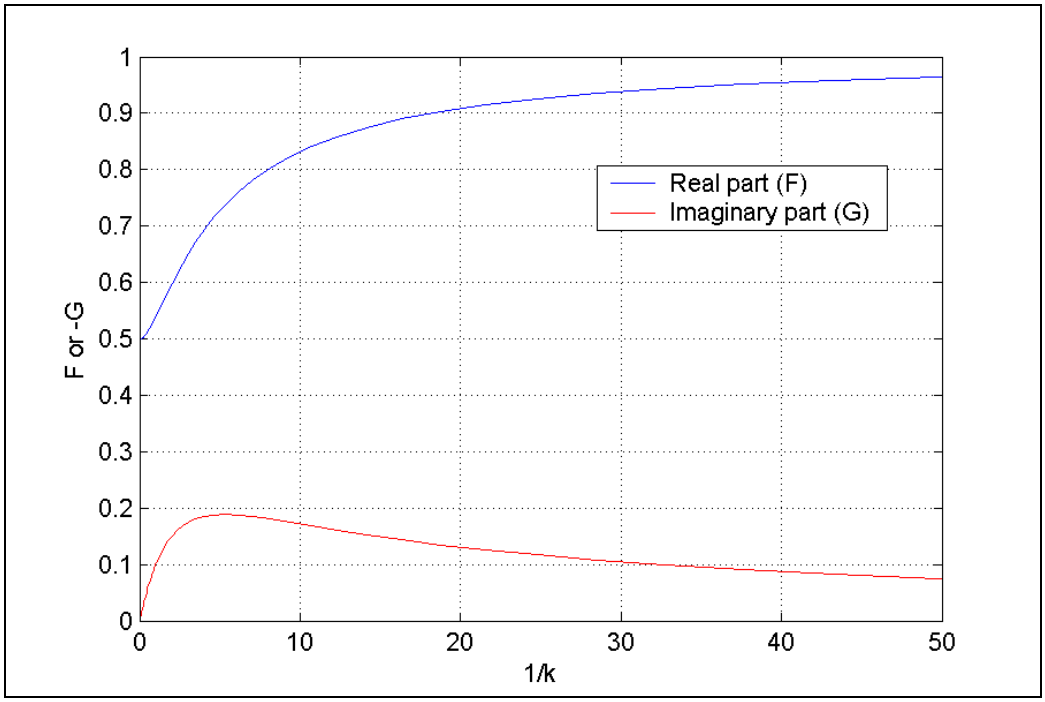

Figure 9. Conventional plot of Theodorsen's lift deficiency function.

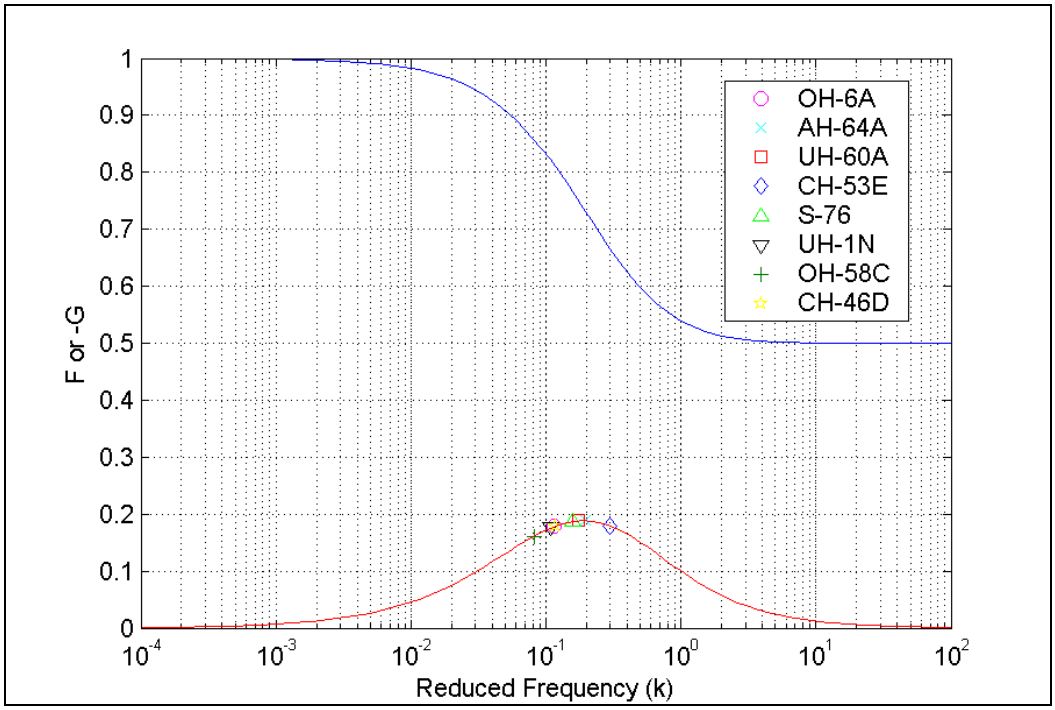

Figure 10. Semi-logarithmic plot of Theodorsen's lift deficiency function with N_b/rev reduced frequencies (from Ref. 15).

b. Loewy's Lift Deficiency Function

Helicopter unsteady aerodynamics are more complex than its fixed-wing counterpart. Vorticity is shed by blades on previous revolutions that must be accounted for since it will influence the lift and moments on the blade. Loewy [Ref. 49] explored this issue and looked at two cases: high inflow and low inflow. The high inflow case is shown in Figure 11a, and represents a case where the downwash generated by the rotor is of the same order of magnitude as the tip speed velocity. Practical examples would be lift fan designs in which the mass flow rate can be near 3000 lb_m/s or about 350 ft/s [Ref. 50]. It would be difficult in this case to determine the effects of the shed vorticity since it would be expected that all shed vorticity beyond a small fraction of a revolution would be too far below the reference blade to have a significant effect. In the low inflow case, shown in Figure 11b, layers of shed vorticity tend to remain essentially planar and remain close to the reference blade, and thus can have a significant effect on the aerodynamics of the rotor blade. In this case, the downwash generated by the rotor is at least an order of magnitude less than the tip speed velocity. Most conventional helicopters fall into this

category, including larger H-53E and V-22 aircraft with downwash velocities of 55-65 ft/s. Therefore, Loewy developed his theory for the case of low inflow since it could be applied to most conventional helicopters.

Loewy's lift deficiency function for the rotary-wing case in a hover is analogous to Theodorsen's, but the manner in which it was developed differs. Loewy used the Biot-Savart law instead of potential flow theory to account for the layers of shed vorticity beneath the reference rotor blade caused by the reference blade and other blades in previous revolutions. Figure 12 is a schematic of Loewy's two-dimensional model that was used to determine the effects of previously shed wakes on the lift deficiency function. Loewy assumed that there were an infinite number of wakes beneath the reference blade and applied the Biot-Savart law to each layer of shed vorticity to add together the effects on the differential downwash equation. Two indices are used to account for the vorticity shed by a given wake: n, which indicates the revolution number of the reference blade and q, which indicates the blade whose wake it is. The induced velocity or downwash resulting from an element of vorticity is obtained by,

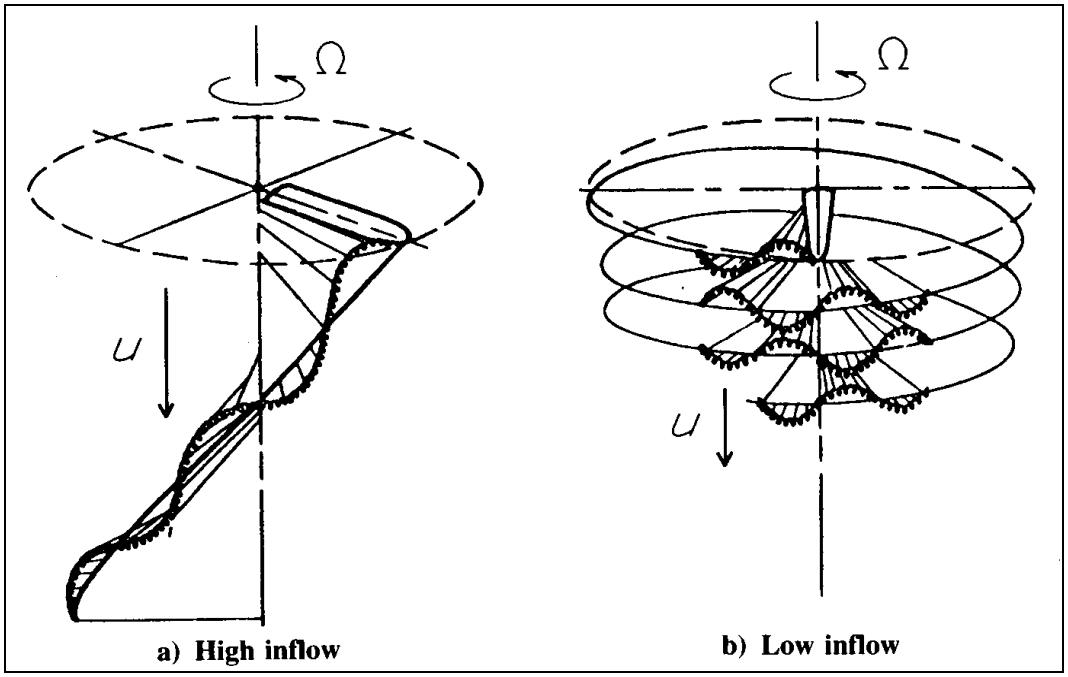

Figure 11. Loewy's inflow models (from Ref. 41 and 49)

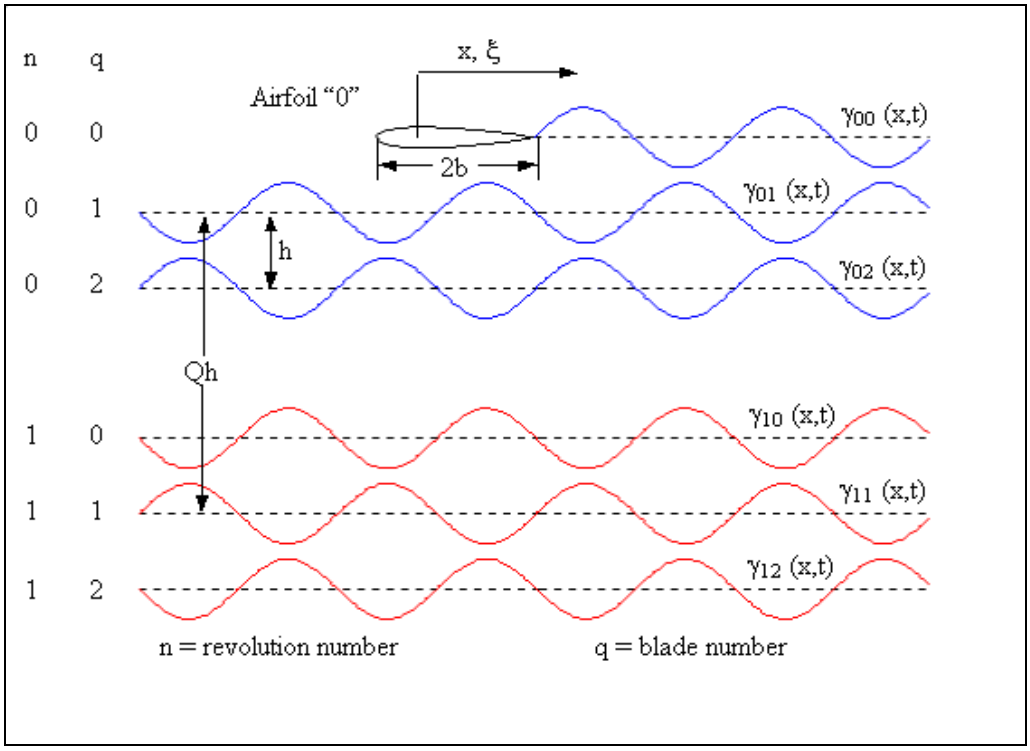

Figure 12. Loewy's aerodynamic model for multi-blade rotor system (from Ref. 49).

$$dw(x) = \frac{1}{2\pi}\left(\frac{\gamma_{nq}(x-\xi)d\xi}{(x-\xi)^2 + (nQ+q)^2\hat{h}^2}\right), \tag{82}$$

where γ_{nq} is the vorticity, Q is the number of rotor blades, and $\hat{h}$ is the non-dimensional wake spacing defined by

$$\hat{h} = \frac{2\pi v_i}{bQ\Omega} = \lambda r \frac{2\pi}{bQ}, \tag{83}$$

Writing the integrals involving the bound vorticity and the vorticity in the wake of the reference airfoil separately from the rows of vorticity below the plane of the rotor yield

$$w(x) = -\frac{1}{2\pi}\left[\int_{-1}^{1}\frac{\gamma_a(\xi)d\xi}{x-\xi} + \int_{1}^{\infty}\frac{\gamma_{00}(\xi)d\xi}{x-\xi} + \sum_{q=1}^{Q-1}\sum_{n=0}^{\infty}\int_{-\infty}^{\infty}\frac{\gamma_{nq}(\xi)(x-\xi)d\xi}{(x-\xi)^2 + (nQ+q)^2\hat{h}^2} + \sum_{n=1}^{\infty}\int_{-\infty}^{\infty}\frac{\gamma_{n0}(\xi)(x-\xi)d\xi}{(x-\xi)^2 + n^2Q^2\hat{h}^2}\right]. \tag{84}$$

The first integral represents the effects of the freestream on the airfoil (non-circulatory terms). The second integral represents the downwash velocity created by the vorticity generated by the reference wake (circulatory term). The third and fourth integral represent the downwash velocity created by the vorticity generated by previous blades or in previous revolutions (circulatory terms). The main difference between Loewy and Theodorsen is the terms which account for the vorticity generated by the reference blade and subsequent blades in previous revolutions.

It should be noted that no mention has been made of whether the blade does or does not have a flap incorporated. In fact, by using the Biot-Savart law and being concerned only with the vorticity generated (bound, wake of reference blade, or previously shed wake), it becomes unnecessary to state the exact configuration of the airfoil. *Thus, while Loewy* [*Ref. 49*] *did not explicitly state that his 2-D theory would apply to rotor blades with trailing-edge flaps, the manner in which the theory was developed allows it to be applied to this rotor blade configuration.* Loewy's theory will now be developed.

The vorticity shed by the q^{th} blade in the n^{th} revolution is given by

$$\gamma_{nq} = ik\Gamma e^{i\left(\psi_q - k\xi - 2\pi mq/Q - 2\pi mn\right)} \tag{85}$$

where Γ is the total circulation around the airfoil, ψ_q is the phase angle by which the motion of the q^{th} blade leads that of the reference blade, m is the ratio of oscillatory frequency to rotational frequency, and k is the reduced frequency. The variables m and k are defined as

$$m = \frac{\omega}{\Omega} \tag{86}$$

$$k = \frac{\omega b}{\Omega r} = \frac{mb}{r} \tag{87}$$

Substituting the vorticity expression from equation (85) into the integral downwash equation (84) yields

$$w(x) = -\frac{1}{2\pi}\left[\int_{-1}^{1}\frac{\gamma_a(\xi)\,d\xi}{x-\xi} - ik\Gamma\int_{1}^{\infty}\frac{e^{-ik\xi}\,d\xi}{x-\xi}\right.$$
$$-ik\Gamma\sum_{q=1}^{Q-1}e^{-i\left(2\pi mq/Q-\psi_q\right)}\sum_{n=0}^{\infty}e^{-i2\pi mn}\int_{-\infty}^{\infty}\frac{e^{-ik\xi}\left(x-\xi\right)d\xi}{\left(x-\xi\right)^2+\left(nQ+q\right)^2\hat{h}^2} \tag{88}$$
$$\left.-ik\Gamma\sum_{n=1}^{\infty}e^{-i2\pi mn}\int_{-\infty}^{\infty}\frac{e^{-ik\xi}\left(x-\xi\right)d\xi}{\left(x-\xi\right)^2+n^2Q^2\hat{h}^2}\right].$$

The last two integrals in equation (88) have the form

$$\int_{-\infty}^{\infty}\frac{e^{-ik\xi}\left(x-\xi\right)d\xi}{\left(x-\xi\right)^2+A^2} = i\pi e^{-k(ix+A)} \tag{89}$$

Substituting equation (89) into equation (88) and noting that the summations over *n* are convergent geometric series yields

$$w(x) = -\frac{1}{2\pi}\left[\int_{-1}^{1}\frac{\gamma_a(\xi)\,d\xi}{\left(x-\xi\right)} - ik\Gamma\int_{1}^{\infty}\frac{e^{-ik\xi}\,d\xi}{\left(x-\xi\right)} + \pi k\Gamma e^{-ikx}W(k,\hat{h},m)\right], \tag{90}$$

where $W\left(k,\hat{h},m\right)$ is defined as:

$$W\left(k,\hat{h},m\right) = \frac{1+\sum_{q=1}^{Q-1}\left(e^{k\hat{h}Q}e^{i2\pi m}\right)^{(Q-q)/Q}e^{i\psi_q}}{e^{k\hat{h}Q}e^{i2\pi m}-1}. \tag{91}$$

It should be noticed that the term *m* (the ratio of oscillatory frequency to rotational frequency) always occurs as $e^{i2\pi m}$, which makes *m* periodic. Therefore, the frequency ratio can be divided into two parts: an integer portion, representing the periodicity, and a noninteger portion, representing the phase relationship between the sinusoidal frequency of oscillation of the rotor blade and the rotational frequency of the rotor [Ref. 49]. In other words, oscillatory frequencies that are integer multiples of the rotational velocity (1P, 2P, (N_b – 1)P, etc.) correspond to *m* = integer, and the oscillatory frequencies which are noninteger multiples of the rotational frequency correspond to the phase relationship. Because of this periodicity, only the range $0 \le m < 1$ needs to be considered.

The form of the downwash equation in equation (90) can be solved by applying Söhngen's inversion formula [Ref. 51], which shows that an equation in the form

$$g(x) = \frac{1}{2\pi}\int_{-1}^{1} \frac{f(\xi)\,d\xi}{x-\xi} \tag{92}$$

has a solution of

$$f(x) = -\frac{2}{\pi}\sqrt{\frac{1-x}{1+x}}\int_{-1}^{1}\sqrt{\frac{1+\xi}{1-\xi}}\,\frac{g(\xi)\,d\xi}{x-\xi}. \tag{93}$$

Satisfying the condition $f(1)$ = finite is the same as employing the Kutta condition. The bound vorticity becomes

$$\begin{aligned}\gamma_a(x) = \frac{2}{\pi}\sqrt{\frac{1-x}{1+x}}\Bigg[&\int_{-1}^{1}\sqrt{\frac{1+\xi}{1-\xi}}\,\frac{w(\xi)\,d\xi}{x-\xi} \\ &-\frac{ik\Gamma}{2\pi}\int_{-1}^{1}\sqrt{\frac{1+\xi}{1-\xi}}\left(\frac{1}{x-\xi}\right)\int_{1}^{\infty}\frac{e^{-ik\eta}\,d\eta}{\xi-\eta}\,d\xi \\ &+\frac{k\Gamma}{2}W(k,\hat{h},m)\int_{-1}^{1}\sqrt{\frac{1+\xi}{1-\xi}}\,\frac{e^{-ik\xi}\,d\xi}{x-\xi}\Bigg].\end{aligned} \tag{94}$$

Evaluating the circulation over the entire airfoil yields

$$\Gamma = e^{ik}\int_{-1}^{1}\gamma_a(x)\,dx = \frac{2\displaystyle\int_{-1}^{1}\sqrt{\frac{1+\xi}{1-\xi}}\,w(\xi)\,d\xi}{i\pi k\left[\frac{1}{2}\left(H_1^{(2)}+iH_0^{(2)}\right)+\left(J_1+iJ_0\right)W(k,\hat{h},m)\right]}, \tag{95}$$

where the Hankel and Bessel functions are evaluated at reduced frequency (k).

Since the airfoil can be thought of as a vortex sheet, the generalized Bernoulli equation becomes

$$\Delta p(x) = -\rho\left[v\gamma_a(x,t) + b\frac{\partial}{\partial t}\int_{-1}^{x} \gamma_a(\xi,t)\, d\xi \right]. \tag{96}$$

If simple harmonic motion is assumed,

$$\frac{\partial}{\partial t}\gamma_a = i\omega\gamma_a, \tag{97}$$

and equation (96) becomes

$$\Delta p(x) = -\rho\left[v\gamma_a(x,t) + i\omega b\int_{-1}^{x} \gamma_a(\xi,t)\, d\xi \right]. \tag{98}$$

Substituting the bound vorticity equation (94) and the airfoil circulation equation (95) into equation (96) yield

$$\begin{aligned} -\frac{\Delta p(x)}{\rho\Omega r} = {} & \frac{\frac{2i}{\pi}\left[H_0^{(2)} + 2J_0 W(k,\hat{h},m) \right]}{H_1^{(2)} + iH_0^{(2)} + 2\left(J_1 + iJ_0\right)W(k,\hat{h},m)} \int_{-1}^{1} \sqrt{\frac{1-x}{1+x}}\sqrt{\frac{1+\xi}{1-\xi}}\, w(\xi)\, d\xi \\ & + \frac{2}{\pi}\int_{-1}^{1}\left[\sqrt{\frac{1-x}{1+x}}\sqrt{\frac{1+\xi}{1-\xi}}\left(\frac{1}{x-\xi}\right) - \frac{ik}{2}\log\left(\frac{1-x\xi-\sqrt{1-x^2}\sqrt{1-\xi^2}}{1-x\xi+\sqrt{1-x^2}\sqrt{1-\xi^2}} \right) \right] w(\xi)\, d\xi. \end{aligned} \tag{99}$$

The pressure distribution in equation (99) has the same form as Theodorsen [Ref. 46] if the factor multiplying the first integral is written as

$$\frac{2}{\pi}\left[1 - C'(k,\hat{h},m) \right],$$

where $C'(k,\hat{h},m)$ is Loewy's lift deficiency function. Solving for $C'(k,\hat{h},m)$ yields

$$C'\left(k,\hat{h},m\right) = \frac{H_1^{(2)} + 2J_1 W\left(k,\hat{h},m\right)}{H_1^{(2)} + iH_0^{(2)} + 2\left(J_1 + iJ_0\right)W\left(k,\hat{h},m\right)}. \tag{100}$$

Since $C'(k,\hat{h},m)$ is not a function of the chordwise location along the airfoil (x), the integration of the pressure distribution in equation (99) across the airfoil will yield

equations of motion given in equations (60), (61), and (62) except $C(k)$ will be replaced by $C'(k,\hat{h},m)$. It can be shown that as $W(k,\hat{h},m)$ approaches zero, $C'(k,\hat{h},m)=C(k)$, which corresponds to an infinite wake spacing $\left(\hat{h}\to\infty\right)$.

Since the wake weighting function is periodic, Loewy showed that the wake weighting function for a multi-blade rotor can be expressed by that of a single-blade rotor with modified values of $\hat{h}$ and m that yield the same value of W. For a single-blade rotor, the wake weighting function becomes

$$W(k,\hat{h},m)=\frac{1}{e^{k\hat{h}}e^{i2\pi m}-1}, \tag{101}$$

where $\hat{h}$ and m are now the modified values of the wake spacing and frequency ratio.

Loewy's lift deficiency function can also be written in terms of its real and imaginary parts as

$$C'\left(k,\hat{h},m\right)=F'\left(k,\hat{h},m\right)+iG'\left(k,\hat{h},m\right). \tag{102}$$

Semi-logarithmic plots of Loewy's lift deficiency function are shown in Figure 13 through Figure 16 for m = 0, 0.25, 0.5 and 0.75 respectively.

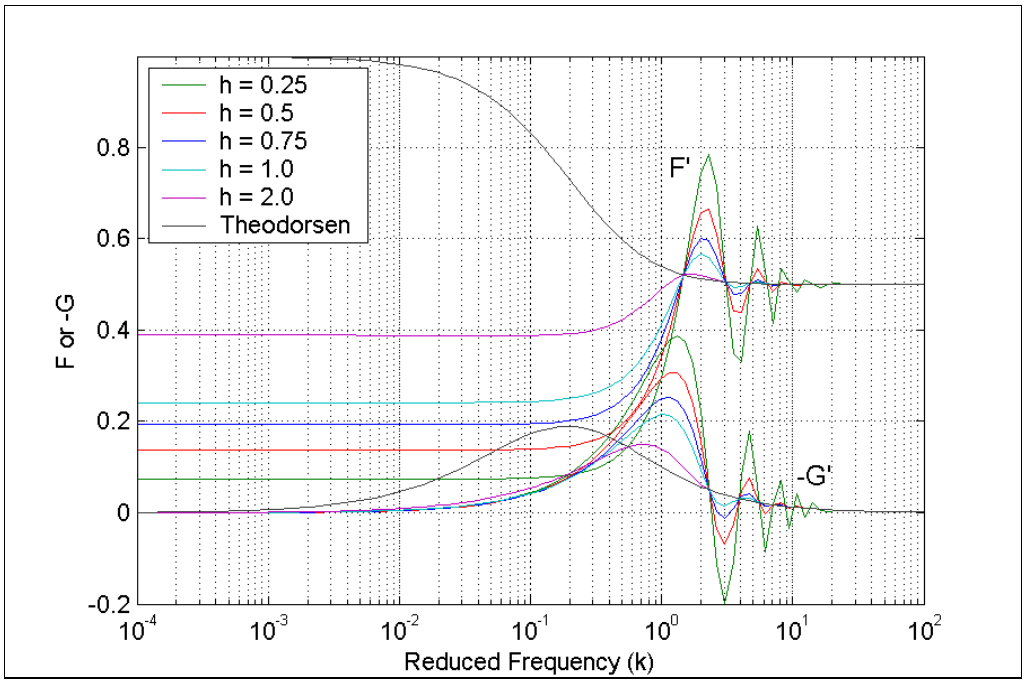

Figure 13. Loewy's lift deficiency function (m = 0).

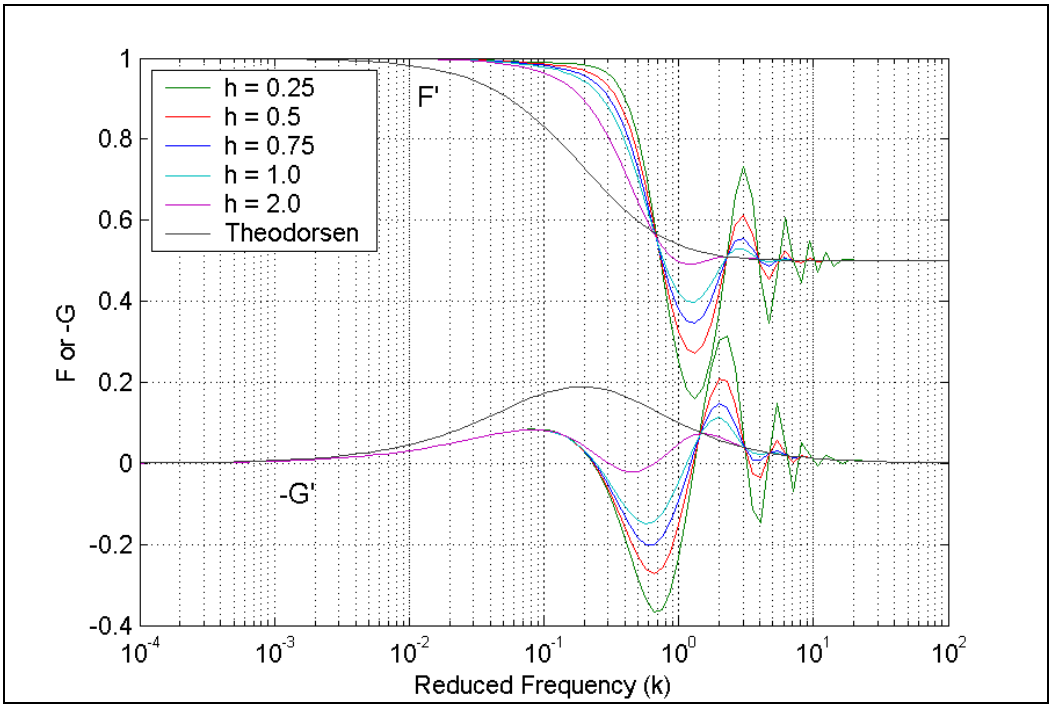

Figure 14. Loewy's lift deficiency function (*m* = 0.25).

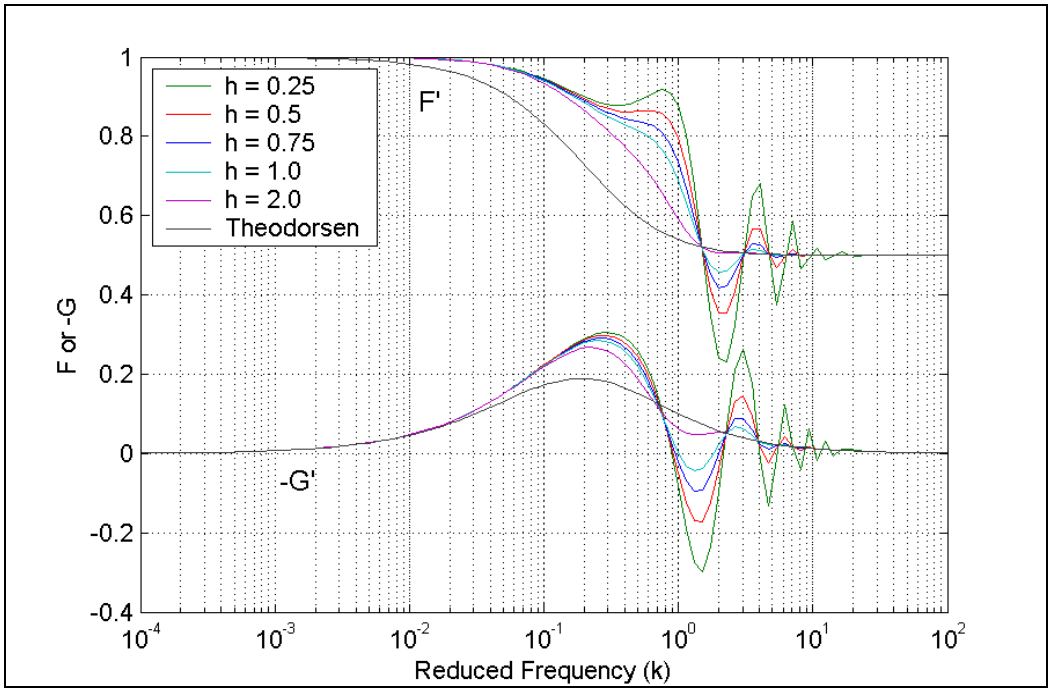

Figure 15. Loewy's lift deficiency function (*m* = 0.5).

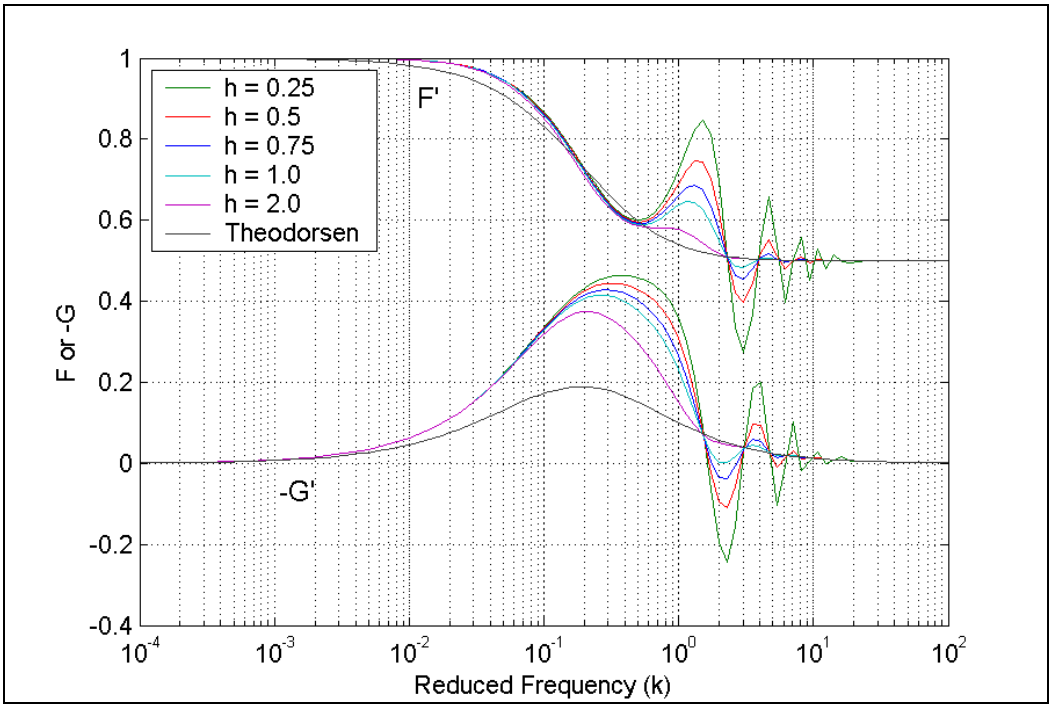

Figure 16. Loewy's lift deficiency function (*m* = 0.75).

c. Finite Wake Lift Deficiency Function

It can be seen in Figure 13 (m = 0) that the real part of Loewy's lift deficiency function does not converge towards Theodorsen's solution as $k \to 0$. This nonconvergence is particularly evident as $\hat{h} \to 0$. In fact when $\hat{h} = 0$ and m = 0, a singularity can be seen in the wake weighting function. The source of this singularity is found in the development of equation (90), in which the solution to the integrals associated with the wakes that were previously shed have the form of

$$\int_{-\infty}^{\infty} \frac{e^{-ik\xi}(x-\xi)d\xi}{(x-\xi)^2 + A^2} = i\pi e^{-k(ix+A)}.$$

The third term in equation (88) becomes

$$\begin{aligned} &-ik\Gamma\sum_{q=1}^{Q-1}e^{i\left(\psi_q-2\pi mq/Q\right)}\sum_{n=0}^{\infty}e^{-i2\pi mn}\int_{-\infty}^{\infty}\frac{e^{-ik\xi}\left(x-\xi\right)}{\left(x-\xi\right)^2+\left(nQ+q\right)^2\hat{h}^2}d\xi \\ &=\pi k\Gamma e^{-ikx}\sum_{q=1}^{Q-1}e^{i\psi_q-\left(q/Q\right)\left[2\pi mi+kQ\hat{h}\right]}\sum_{n=0}^{\infty}e^{-n\left(i2\pi m+kQ\hat{h}\right)}. \end{aligned} \tag{103}$$

Since $kQ\hat{h}$ is always positive, the summation over *n* is a convergent geometric series of the form

$$\sum_{n=0}^{\infty}\lambda^n=\frac{1}{1-\lambda}$$

in which

$$\lambda^n=e^{-n\left(i2\pi m+kQ\hat{h}\right)}=\left(e^{-\left(i2\pi m+kQ\hat{h}\right)}\right)^n$$

with the restriction that $\left|\lambda\right|<1$. Thus,

$$\sum_{n=0}^{\infty}\left(e^{-\left(i2\pi m+kQ\hat{h}\right)}\right)^n=\frac{1}{1-e^{-\left(i2\pi m+kQ\hat{h}\right)}},$$

and equation (103) becomes

$$\begin{aligned} &-ik\Gamma\sum_{q=1}^{Q-1}e^{i\left(\psi_q-2\pi mq/Q\right)}\sum_{n=0}^{\infty}e^{-i2\pi mn}\int_{-\infty}^{\infty}\frac{e^{-ik\xi}\left(x-\xi\right)}{\left(x-\xi\right)^2+\left(nQ+q\right)^2\hat{h}^2}d\xi \\ &=\pi k\Gamma e^{-ikx}\frac{\displaystyle\sum_{q=1}^{Q-1}e^{i\psi_q-\left(q/Q\right)\left[2\pi mi+kQ\hat{h}\right]}}{1-e^{-\left(i2\pi m+kQ\hat{h}\right)}} \end{aligned} \tag{104}$$

Similarly, the fourth term of equation (88) can be written as

$$-ik\Gamma\sum_{n=0}^{\infty}e^{-i2\pi mn}\int_{-\infty}^{\infty}\frac{e^{-ik\xi}\left(x-\xi\right)}{\left(x-\xi\right)^2+n^2Q^2\hat{h}^2}d\xi=\pi k\Gamma e^{-ikx}\frac{e^{-\left(i2\pi m+kQ\hat{h}\right)}}{1-e^{-\left(i2\pi m+kQ\hat{h}\right)}} \tag{105}$$

by noting that

$$\sum_{n=1}^{\infty}\left(e^{-\left(i2\pi m+kQ\hat{h}\right)}\right)^{n}=\sum_{n=0}^{\infty}\left(e^{-\left(i2\pi m+kQ\hat{h}\right)}\right)^{n}-1.$$

Combining equations (104) and (105) yields

$$\pi k\Gamma e^{-ikx}\frac{1+\sum_{q=1}^{Q-1}\left(e^{k\hat{h}Q}e^{i2\pi m}\right)^{(Q-q)/Q}e^{i\psi_q}}{e^{k\hat{h}Q}e^{i2\pi m}-1}=\pi k\Gamma e^{-ikx}W\left(k,\hat{h},m\right)$$

where $W(k,\hat{h},m)$ is defined by equation (91) as

$$W\left(k,\hat{h},m\right)=\frac{1+\sum_{q=1}^{Q-1}\left(e^{k\hat{h}Q}e^{i2\pi m}\right)^{(Q-q)/Q}e^{i\psi_q}}{e^{k\hat{h}Q}e^{i2\pi m}-1}.$$

The requirement for the convergence of both geometric series given in equations (103) and (105) is that

$$\left|e^{-\left(i2\pi m+kQ\hat{h}\right)}\right|<1. \tag{106}$$

Since Q is always positive and nonzero, when m = 0, if the product $k\hat{h}\to 0$, then a singularity will exist since equation (106) will not be satisfied. While the mathematical singularity can be identified, its physical significance is still unclear [Ref. 49]. The assumptions of thin airfoil theory in which both the airfoil and wakes have zero thickness, and that if $\hat{h}=0,$ the wakes have no displacement from the plane of the rotor blade are unrealistic when all are assumed at the same time.

The problem of convergence as $k\hat{h}\to 0$ when m = 0 can be avoided by using only a finite number of wakes beneath the reference airfoil. If the number of wakes (N) is made sufficiently large, then the infinite geometric series can be approximated by a finite geometric series [Ref. 48]. The development of the finite wake lift deficiency function is identical to that of Loewy, except the infinite series in equation (84) is replaced by a finite series in the form of

$$w(x) = -\frac{1}{2\pi}\left[\int_{-1}^{1}\frac{\gamma_a(\xi)\,d\xi}{x-\xi} - ik\Gamma\int_{1}^{\infty}\frac{e^{-ik\xi}\,d\xi}{x-\xi}\right.$$
$$-ik\Gamma\sum_{q=1}^{Q-1}e^{-i\left(2\pi mq/Q-\psi_q\right)}\sum_{n=0}^{N}e^{-i2\pi mn}\int_{-\infty}^{\infty}\frac{e^{-ik\xi}\left(x-\xi\right)d\xi}{\left(x-\xi\right)^2+\left(nQ+q\right)^2\hat{h}^2} \tag{107}$$
$$\left.-ik\Gamma\sum_{n=1}^{N}e^{-i2\pi mn}\int_{-\infty}^{\infty}\frac{e^{-ik\xi}\left(x-\xi\right)d\xi}{\left(x-\xi\right)^2+n^2Q^2\hat{h}^2}\right].$$

Using equation (89) to solve the last to integrals in equation (107) yields

$$w(x) = -\frac{1}{2\pi}\left[\int_{-1}^{1}\frac{\gamma_a(\xi)\,d\xi}{\left(x-\xi\right)} - ik\Gamma\int_{1}^{\infty}\frac{e^{-ik\xi}\,d\xi}{\left(x-\xi\right)}\right.$$
$$\left.+\pi k\Gamma e^{-ikx}\left(\sum_{q=1}^{Q-1}e^{-i\left(2\pi q/Q-\psi_q\right)}\sum_{n=0}^{N}e^{-i2\pi mn}e^{-k\left(nQ+q\right)h}+\sum_{n=1}^{N}e^{-i2\pi mn}e^{-nQkh}\right)\right]. \tag{108}$$

where the term in parentheses is the finite wake weighting function defined by

$$W_N(k,h,m) = \sum_{q=1}^{Q-1}e^{-i\left(2\pi q/Q-\psi_q\right)}\sum_{n=0}^{N}e^{-i2\pi mn}e^{-k\left(nQ+q\right)h}+\sum_{n=1}^{N}e^{-i2\pi mn}e^{-nQkh}\,. \tag{109}$$

and the requirement for convergence given in equation (106) is no longer needed.

A modified-Loewy, or finite-wake lift deficiency function [Ref. 48] can be written as

$$C'_N\left(k,\hat{h},m\right) = \frac{H_1^{(2)}\left(k\right)+2J_1\left(k\right)W_N\left(k,\hat{h},m\right)}{H_1^{(2)}\left(k\right)+iH_0^{(2)}\left(k\right)+2\left(J_1+iJ_0\right)W_N\left(k,\hat{h},m\right)}\,. \tag{110}$$

For a single-blade rotor, the wake weighting function becomes

$$W_N(k,\hat{h},m) = \sum_{n=1}^{N}e^{-i2\pi mn}e^{-nk\hat{h}}\,, \tag{111}$$

and for the case of a single wake, the wake weighting function becomes

$$W_1 = e^{-\left(i2\pi m+kh\right)}\,. \tag{112}$$

The finite wake lift deficiency function can also be written in terms of its real and imaginary parts as

$$C'_N\left(k,\hat{h},m\right)=F'_N\left(k,\hat{h},m\right)+iG'_N\left(k,\hat{h},m\right). \tag{113}$$

A semi-logarithmic plot of the finite wake lift deficiency function with $N = 100$ for $m = 0$ is shown in Figure 17. This figure shows that the singularity introduced by Loewy has essentially been eliminated, and the results tend to converge towards Theodorsen's solution as $k \to 0$. It is also interesting to look at the lift deficiency function when only a single wake is present below the reference airfoil. Semi-logarithmic plots of the single wake lift deficiency function are shown in Figure 18 through Figure 21 for $m = 0$, 0.25, 0.5 and 0.75 respectively. Note that in Figure 20, the real part of the lift deficiency function is greater that 1.0. This figure is a great illustration of the use of the Biot-Savart law, in that a single layer of vorticity below the rotor blade can increase the lift of the blade if the phase difference between the trailing vortex from the reference blade and the single layer of vorticity is 180°. This efficient alignment of layers of vorticity is depicted in Figure 22.

The limitations of both the Loewy and finite-wake lift deficiency function are that it is restricted to a helicopter in hover with low inflow velocity, and secondary effects such as radial velocity and other three-dimensional effects are neglected. As can be seen in Figure 13 through Figure 21, the effect of layers of vorticity beneath the rotor can have a significant effect on the lift deficiency function with the introduction of frequency ratio and wake spacing as additional parameters. The effect of wake spacing can better illustrated by Figure 23, in which the real and imaginary parts of Loewy's and the single wake lift deficiency functions are plotted against wake spacing for $k = 0.2$ and $m = 0.25$ and 0.5. It can be seen that when $\hat{h} > 20$, which corresponds to high inflow, the effects of any shed layer of vorticity is negligible, and $C'\left(k,\hat{h},m\right)$ and $C'_N\left(k,\hat{h},m\right) \to C\left(k\right)$. Because of effects of the wake are incorporated into the lift deficiency function, the equations of motion for the aerodynamic forces and moments given in equations (60), (61) and (62) are the same. The only difference in the force and

moment equations would be the choice of lift deficiency function. In order to examine the effect on the flutter solution, all three lift deficiency functions will be used in the flutter analysis.

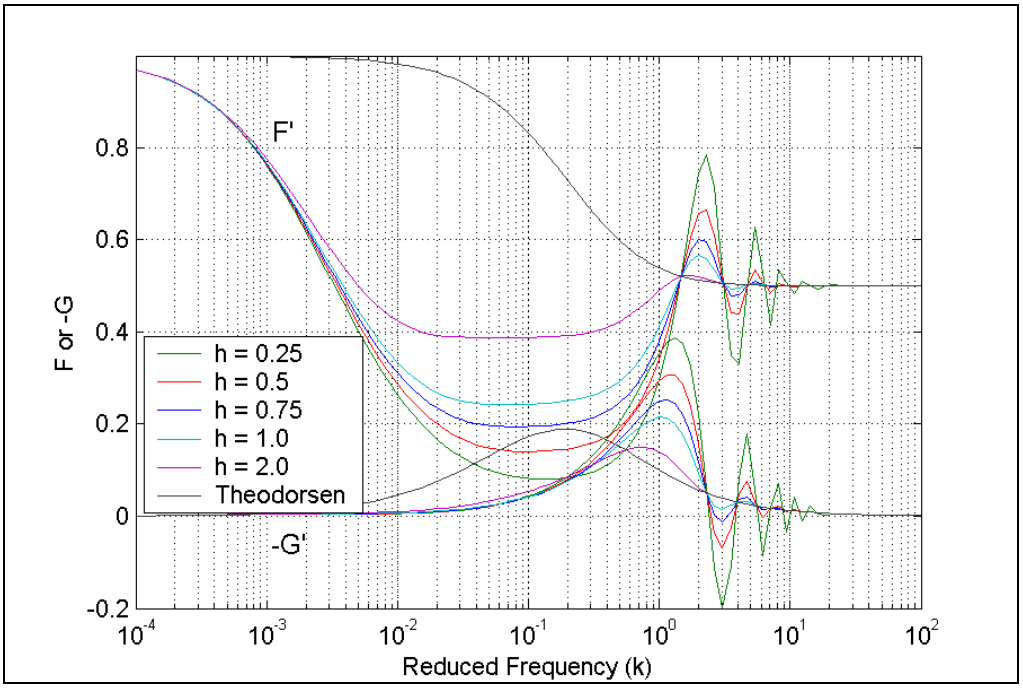

Figure 17. Finite wake estimate to Loewy's lift deficiency function (*m* = 0).

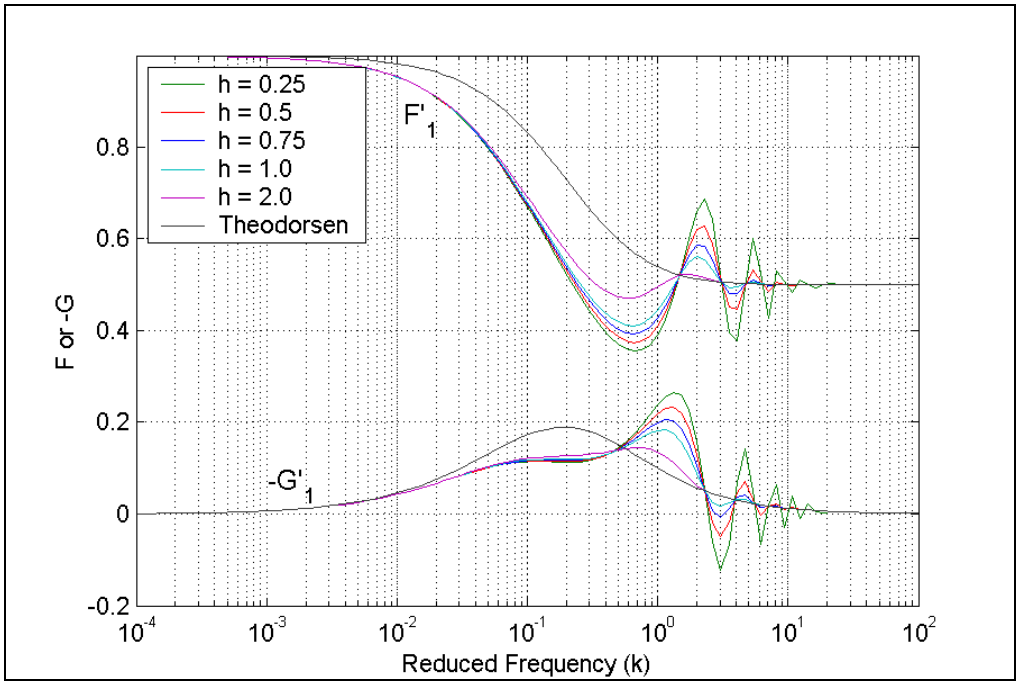

Figure 18. Single wake lift deficiency function (*m* = 0).

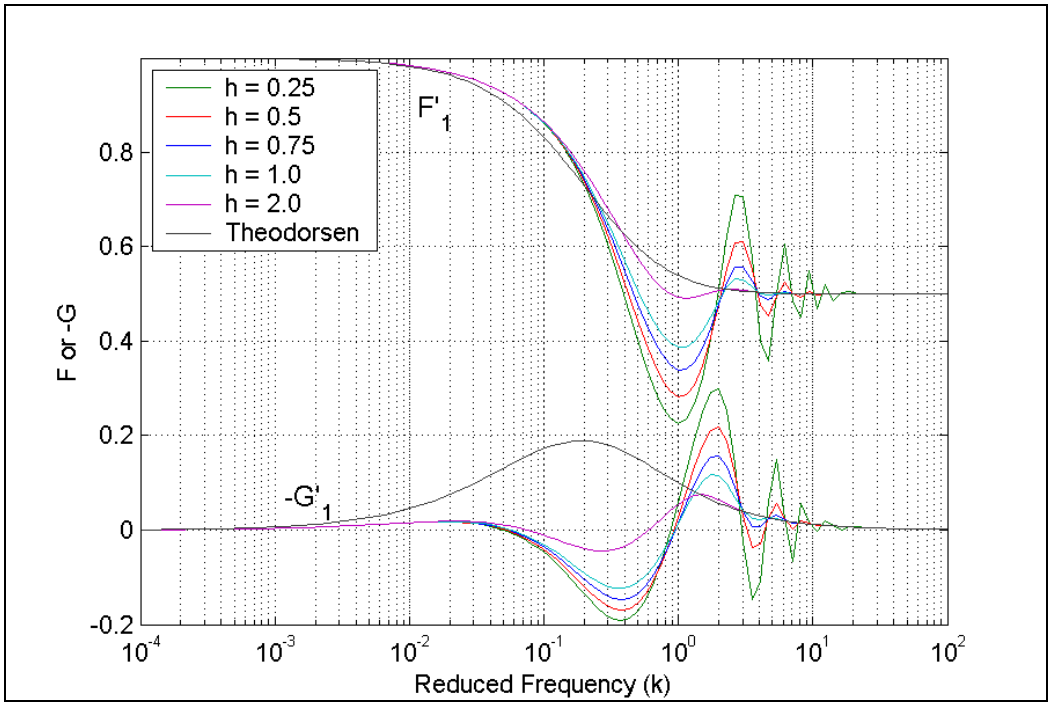

Figure 19. Single wake lift deficiency function (*m* = 0.25).

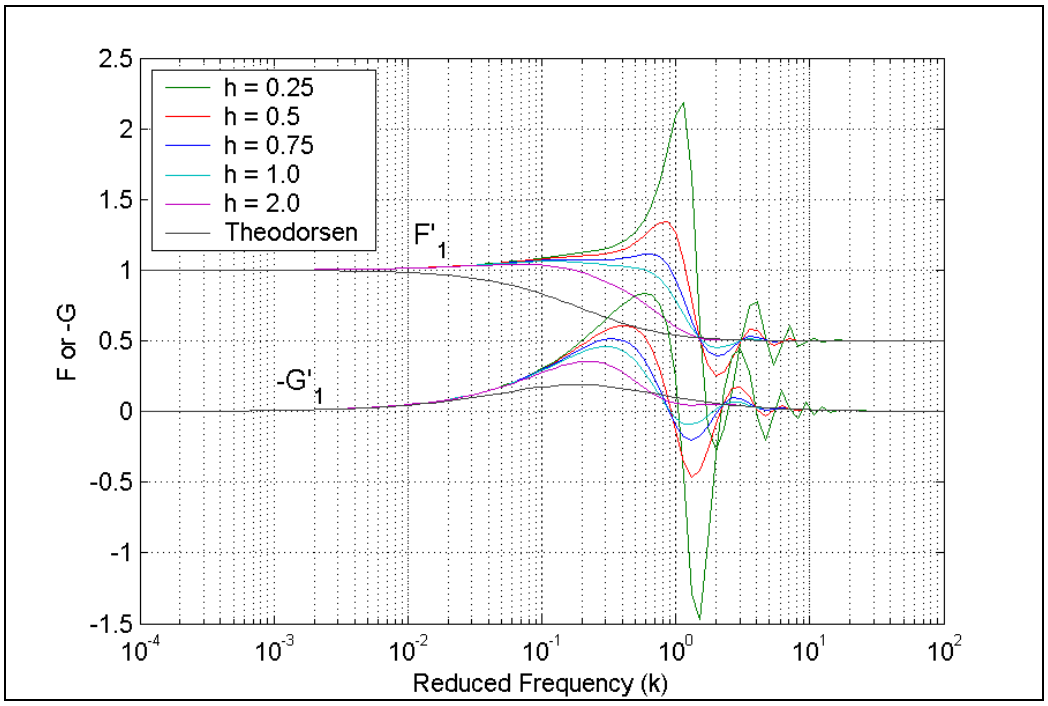

Figure 20. Single wake lift deficiency function (*m* = 0.5).

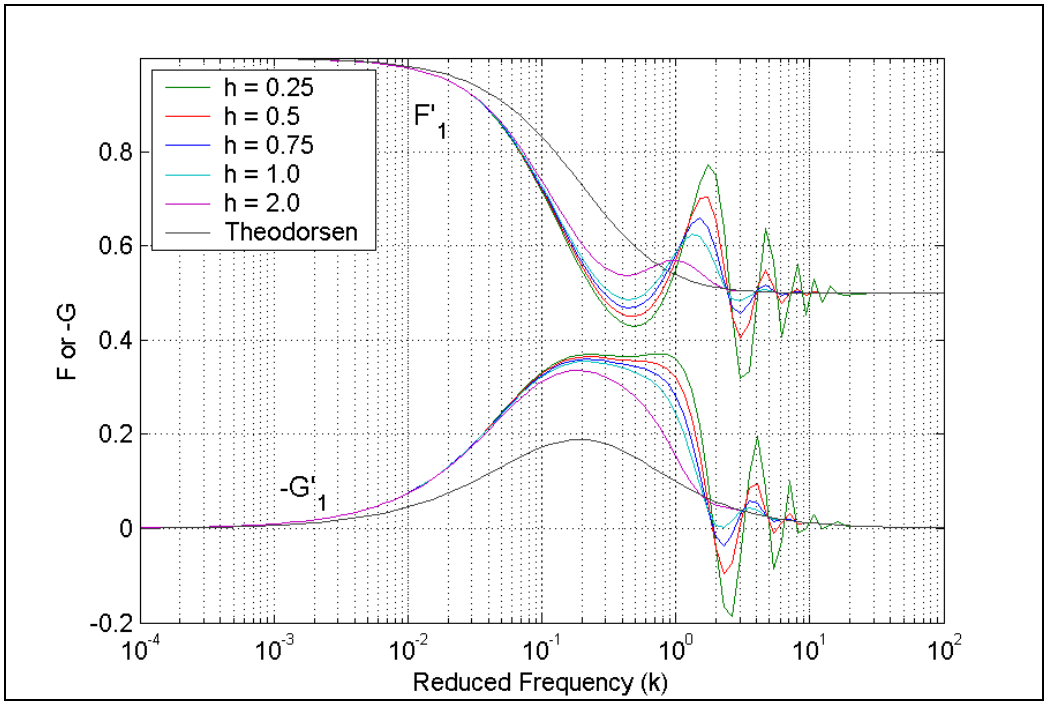

Figure 21. Single wake lift deficiency function (*m* = 0.75).

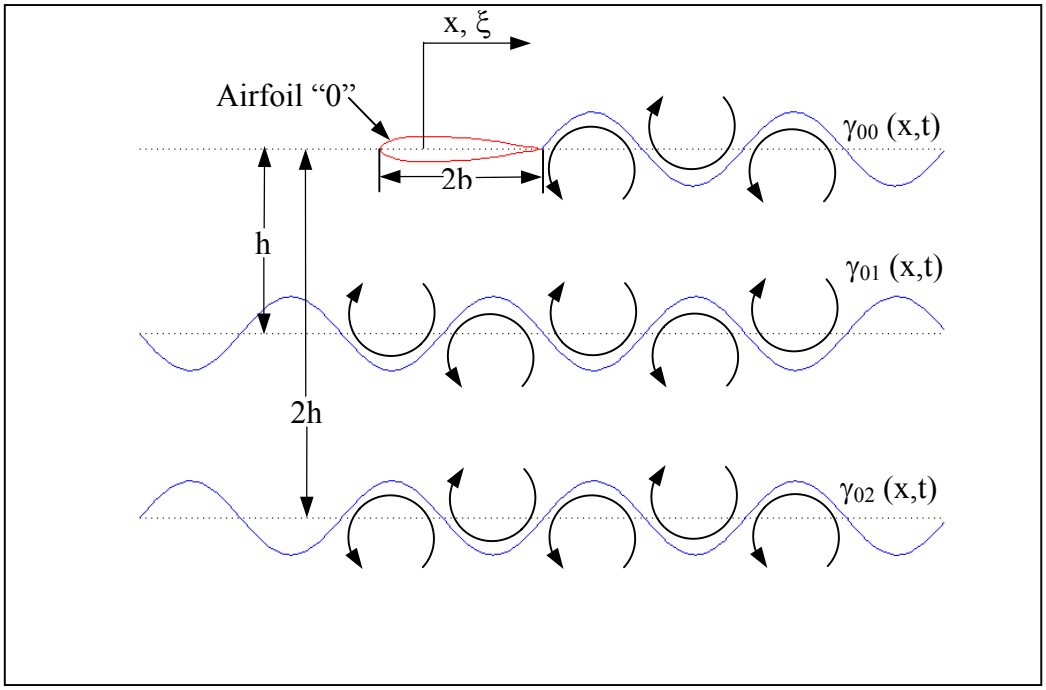

Figure 22. Vortex interaction when wakes are 180° out of phase (*m* = 0.5) (from Ref. 15 and 48).

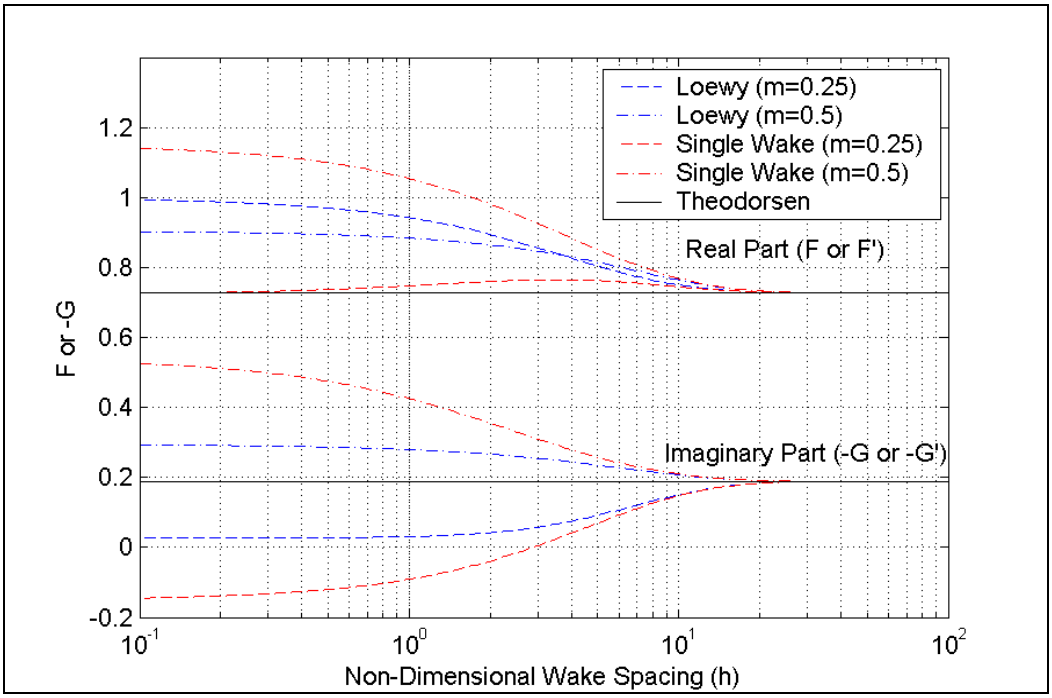

Figure 23. Effect of wake spacing on Loewy's and finite wake lift deficiency functions (k = 0.2).

III. 3-D ROTOR BLADE FLUTTER THEORY

A. THE FLUTTER EQUATION

The basic approach to the three-dimensional rotor blade flutter problem is similar to that developed by Scanlan and Rosenbaum [Ref. 3] for a fixed-wing aircraft and Daughaday, DuWaldt, and Gates [Ref. 52] for rotary-wing aircraft. Lagrange's equation is applied using the aerodynamic forces and moments given by two-dimensional strip theory for an incompressible flow, but with a modified lift deficiency function, such as Loewy's or the finite-wake model. The problem will be three-dimensional only to the extent that the blade sectional variations of mass, geometry and freestream velocity ($v = \Omega r$) are taken into account. There is an assumption that the aerodynamic forces and moments do not change the uncoupled modes shapes.

The robustness of the Lagrange approach can best be summarized by Lagrange himself in *Mechanique Analytique* [Ref. 53],

> *The methods which I present here do not require either constructions or reasonings of geometrical or mechanical nature, but only those algebraic operations proceeding after a regular and uniform plan. Those who love the Analysis, will see with pleasure Mechanics made a branch of it and will be grateful to me for having thus extended its domain.*
>
> - J. L. Lagrange, 1788

Lagrange's equation for a conservative system is given as:

$$\frac{d}{dt}\left(\frac{\partial T}{\partial \dot{q}_n}\right) - \frac{\partial T}{\partial q_n} + \frac{\partial U}{\partial q_n} + \frac{\partial D}{\partial \dot{q}_n} = Q_n \tag{114}$$

where $T \equiv$ kinetic energy, $U \equiv$ potential energy, $D \equiv$ dissipation function, and $Q_n \equiv$ generalized internal forces. The q_n terms are the degrees of freedom (displacements) and the $\dot{q}_n$ represent the first time derivatives of the degrees of freedom (velocities).

1. Superposition of Normal modes

With the aerodynamic forces defined, the bending deflection of the elastic axis at station y when the rotor blade is vibrating in the n^{th} uncoupled vertical bending mode may be defined as

$$h(y,t) = \sum_{n=1}^{N} f_n(y) h_n(t) \tag{115}$$

where $f_n(y)$ is the characteristic function (mode shape) for the rotor blade, and the quantities $h_n(t)$ are normal coordinates that can be considered as weighting functions for each mode that contributes to the deflection. The eigenvector functions $f_n(y)$ possess the property of orthogonality since they can be shown to reduce the kinetic and potential energy expressions to sums of squares of the coordinates with no cross product terms [Ref. 3]. The rotational deflection of the rotor blade about the elastic axis can be written in terms of the blade torsion modes as

$$\alpha(y,t) = \sum_{n=1}^{N} F_n(y) \alpha_n(t) \tag{116}$$

where $F_n(y)$ is the characteristic function of the n^{th} uncoupled torsional mode of the rotor blade, and $\alpha_n(t)$ is the corresponding normal coordinate. The rotational deflection of the flap about the hinge line can be written in terms of flap torsion modes as

$$\beta(y,t) = \sum_{n=1}^{N} G_n(y) \beta_n(t) \tag{117}$$

where $G_n(y)$ is the characteristic function of the n^{th} uncoupled torsional mode of the flap, and $\beta_n(t)$ is the corresponding normal coordinate. The generalized normal coordinates are in the form

$$h_n(t) = \bar{h}_n e^{i(\omega t + \phi_n)}$$

$$\alpha_n(t) = \bar{\alpha}_n e^{i(\omega t + \theta_n)}$$

$$\beta_n(t) = \bar{\beta}_n e^{i(\omega t + \delta_n)}$$

where ϕ_n, θ_n and δ_n are the phase angles relationships. The bending, blade torsional, and flap torsional deflections given in equations (115), (116) and (117) can be written as

$$h(y,t) = h_0(t) f_0(y) + h_1(t) f_1(y) + h_2(t) f_2(y) + \ldots \tag{118}$$

$$\alpha(y,t) = \alpha_0(t) F_0(y) + \alpha_1(t) F_1(y) + \alpha_2(t) F_2(y) + \ldots \tag{119}$$

$$\beta(y,t) = \beta_0(t) G_0(y) + \beta_1(t) G_1(y) + \beta_2(t) G_2(y) + \ldots \tag{120}$$

where

$$f_0(y) = \begin{Bmatrix} \frac{y}{R} \text{ for an articulated rotor} \\ 0 \text{ for a hingless rotor} \end{Bmatrix}$$

$f_1(y) =$ 1st vertical bending mode

$f_2(y) =$ 2nd vertical bending mode

$$F_0(y) = \begin{Bmatrix} 1 \text{ for blade rigid body motion} \\ 0 \text{ otherwise} \end{Bmatrix}$$

$F_1(y) =$ 1st blade-torsional mode

$F_2(y) =$ 2nd blade-torsional mode

$$G_0(y) = \begin{Bmatrix} 1 \text{ for trailing-edge flap rigid body motion} \\ 0 \text{ otherwise} \end{Bmatrix}$$

$G_1(y) =$ 1st trailing-edge flap-torsional mode

$G_2(y) =$ 2nd trailing-edge flap-torsional mode

Lagrange's equation can be written in matrix format as

$$\left[\bar{M}\right]\{\ddot{q}\} + \left[\bar{K}\right]\{q\} + \left[\bar{D}\right]\{\dot{q}\} = \left[\bar{Q}\right]. \tag{121}$$

where $\{q\}$ is the vector of generalized coordinates, $\left[\bar{M}\right]$ is the mass matrix, $\left[\bar{K}\right]$ is the stiffness matrix, $\left[\bar{D}\right]$ is the dissipation matrix, and $\left[\bar{Q}\right]$ is the generalized force matrix defined by

$$\left[\bar{Q}\right] = \frac{\partial W}{\partial q} = \frac{\partial W_{int}}{\partial q} + \frac{\partial W_{ext}}{\partial q}$$

in which W is the total work done on the system and can be divided into an internal component and an external component. For a conservative system, $W_{ext} \equiv 0$ since there

would be no external forces acting on the system. If simple harmonic motion is assumed, equation (121) becomes

$$-\omega^2\left[\bar{M}\right]\{q\}+\left[\bar{K}\right]\{q\}+i\omega\left[\bar{D}\right]\{q\}=\left[\bar{Q}\right] \tag{122}$$

For structural dynamics, the generalized internal forces will be set to zero. For unsteady aerodynamics, it will be shown that the generalized force matrix can be written as the product of an aerodynamic matrix and the generalized coordinates, and equation (122) can be written as

$$\omega^2\left[\bar{M}\right]\{q\}-\left[\bar{K}\right]\{q\}-i\omega\left[\bar{D}\right]\{q\}+\left[\bar{A}\right]\{q\}=0\,. \tag{123}$$

Note that in equation (123), all forces are functions of displacements and rotations and their respective derivatives, and there are no external forces applied to the system. Thus, a solution to equation (123) would involve an eigenvalue problem and would be the complementary, or transient solution to equation (121). A particular, or steady state solution would be required to find the response of the blade to externally applied forces.

Since this dissertation focuses on the flutter solution which solves for the coupled natural frequencies of vibration, it is assumed that the system responds in simple harmonic motion and that there are no externally applied forces, and thus, equation (123) can be used. The rigid body motions are functions of the generalized displacements and their respective derivatives. If these displacements (or velocities) were set to a specific value, such as setting the flap input amplitude to ±3°, then the rigid body motions must be taken as an externally applied force. A steady state or particular solution could be obtained by putting this on the right side in the form $F\sin\omega t$ and premultiplying it by the inverse of the dynamic system equations on the left hand side. However, if the displacements are not set to a specific value, the displacements are eigenvectors that are relative to each other. Simple harmonic motion is assumed so that a flutter solution may be obtained. For rigid body flapping of the blade (bending motion), the uncoupled natural frequency is given by

$$\omega_{h_0}=\Omega\sqrt{1+\frac{e_R S_b}{I_b}} \tag{124}$$

where e_R is the hinge offset, S_b is the static flapping moment of the blade, and I_b is the mass flapping moment of inertia of the blade [Ref. 54]. For typical hinge offsets, $\omega_{h_0} \approx 1.02\Omega$ to 1.04Ω. For rigid body blade torsion motion, the free pitch motion is given by

$$\omega_{\alpha_0} \approx \Omega \tag{125}$$

for most pitch hinge offsets [Ref. 55]. For rigid body trailing-edge flap motion, the free deflection motion can be written as

$$\omega_{\beta_0} = \sqrt{\frac{k_\beta}{I_\beta}} \tag{126}$$

where k_β is the torsional stiffness and I_β is the mass moment of inertia of the trailing-edge flap [Ref. 1]. Since the torsional stiffness of the trailing-edge flap can be varied, it can be tuned such that the flap rigid body uncoupled natural frequency is equal to the flap input frequency. In this dissertation, the flap uncoupled natural frequencies will be restricted to integer multiples of the rotational velocity in order to study the effects of inputs corresponding to higher harmonic control and the natural filtering of frequencies provided by the rotor. Table 1 contains a list of the corresponding flap uncoupled natural frequencies to integer multiples of rpm.

Table 1. List of Flap Uncoupled Natural Frequencies

ω_{β_0} as Integer Multiple of Rotational Speed	ω_{β_0} (rad/s)
0P $\Rightarrow$ infinite stiffness	Extremely high
1P	21.26
2P	42.52
3P	63.77
4P	85.03
5P	106.29
6P	127.55
7P	148.81

Using this method to account for rigid body motion allows the generalized force terms in equation (114) to contain only the aerodynamic forcing functions. With this type of approach, there is an inherent assumption that the aerodynamic forces and

moments defined by equations (60) through (62) are the same for both the tuned natural frequencies and the rigid body forced response equivalent system. Therefore, with the method of tuned natural frequencies, the bound vorticity defined by equation (94) is assumed to contain the vorticity due to the motion of the trailing-edge flap as well as the blade bending and torsional modes.

The number of degrees of freedom that one should consider in equations (118) through (120) depends on the particular design of the rotor blade and its corresponding structural properties. At a minimum for an articulated rotor blade with a trailing-edge flap, at least five degrees of freedom (5DOF) need to be considered – three rigid-body motions (h_0, α_0 and β_0), the first bending mode (h_1) and the first blade-torsional mode (α_1). A hingeless rotor requires at least three degrees of freedom (3DOF) – the first blade bending mode (h_1), the first blade-torsional mode (α_1), and rigid-body motion for the trailing-edge flap (β_0). Scanlan and Rosenbaum [Ref. 3] recommend that in general, if the frequency of the corresponding mode is less than 1.2 times that of the 1st blade torsional mode, then the mode shape should be considered. In most helicopter rotor blades the second and sometimes the third bending modes normally meet the conditions set by Scanlan and Rosenbaum. Additionally, to illustrate the potential coupling between the various modes, the first flap torsional mode will be included. Thus, an eight degree of freedom (8DOF) case will be developed with three rigid body modes (h_0, α_0 and β_0), three bending modes (h_1, h_2 and h_3), one blade torsional mode (α_1), and one flap torsional mode (β_1) to cover the majority of cases possible. A reduction or increase in the degrees of freedom can be made when warranted by rotor design (articulated or hingeless) and/or application of the uncoupled natural frequency criterion set by Scanlan and Rosenbaum.

2. Kinetic Energy Equation

Letting y be the variable along the spanwise direction of the rotor blade as shown in Figure 24. At station y, the motion will be assumed to be a downward deflection of the elastic axis, a clockwise rotation of the blade about the elastic axis, and a clockwise rotation of the flap about the flap hinge as shown in Figure 7 and Figure 8. The following sectional properties are defined as:

$m(y)$ = mass per unit length of rotor-flap combination

$I_\alpha(y)$ = mass moment of inertia per unit length of rotor-flap combination about the elastic axis

$I_\beta(y)$ = mass moment of inertia per unit length of the trailing-edge flap about the flap hinge

$S_\alpha(y)$ = static mass moment of inertia (static unbalance) per unit length of rotor-flap combination about the elastic axis

$S_\beta(y)$ = static mass moment of inertia per unit length of flap about flap hinge

b = semi-chord at station y

$(c-a)b$ = distance between elastic axis and flap hinge

If the rotor blade is moving with velocities $\dot{h}(y)$, $\dot{\alpha}(y)$, and $\dot{\beta}(y)$, the kinetic energy per unit length is given as:

$$dT(y)=\frac{1}{2}m(y)\left(\dot{h}(y)\right)^2+\frac{1}{2}I_\alpha(y)\left(\dot{\alpha}(y)\right)^2+\frac{1}{2}I_\beta(y)\left(\dot{\beta}(y)\right)^2+S_\alpha(y)\dot{h}(y)\dot{\alpha}(y) \\ +S_\beta(y)\dot{h}(y)\dot{\beta}(y)+\left[S_\beta(y)(c-a)b+I_\beta(y)\right]\dot{\alpha}(y)\dot{\beta}(y) \quad (127)$$

Substituting equations (118), (119) and (120) into equation (127) and integrating along the spanwise dimension from the hinge offset (e_R) to the rotor radius (R) when no flap term (β) is present and from r_1 to r_2 when a flap term is present yields,

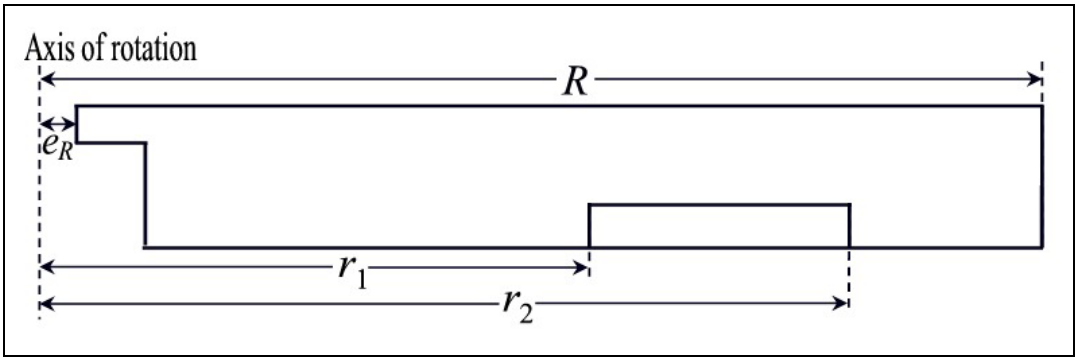

Figure 24. Rotor blade spanwise dimensions.

$$
\begin{aligned}
T = {} & \frac{1}{2}\dot{h}_0^2\int_{e_R}^{R} m(y)\left(f_0(y)\right)^2 dy + \frac{1}{2}\dot{h}_1^2\int_{e_R}^{R} m(y)\left(f_1(y)\right)^2 dy \\
& + \frac{1}{2}\dot{h}_2^2\int_{e_R}^{R} m(y)\left(f_2(y)\right)^2 dy + \frac{1}{2}\dot{h}_3^2\int_{e_R}^{R} m(y)\left(f_3(y)\right)^2 dy \\
& + \frac{1}{2}\dot{\alpha}_0^2\int_{e_R}^{R} I_\alpha(y)\left(F_0(y)\right)^2 dy + \frac{1}{2}\dot{\alpha}_1^2\int_{e_R}^{R} I_\alpha(y)\left(F_1(y)\right)^2 dy \\
& + \frac{1}{2}\dot{\beta}_0^2\int_{r_1}^{r_2} I_\beta(y)\left(G_0(y)\right)^2 dy + \frac{1}{2}\dot{\beta}_1^2\int_{r_1}^{r_2} I_\alpha(y)\left(G_1(y)\right)^2 dy \\
& + \dot{h}_0\dot{\alpha}_0\int_{e_R}^{R} S_\alpha(y) f_0(y) F_0(y) dy + \dot{h}_1\dot{\alpha}_0\int_{e_R}^{R} S_\alpha(y) f_1(y) F_0(y) dy \\
& + \dot{h}_2\dot{\alpha}_0\int_{e_R}^{R} S_\alpha(y) f_2(y) F_0(y) dy + \dot{h}_3\dot{\alpha}_0\int_{e_R}^{R} S_\alpha(y) f_3(y) F_0(y) dy \\
& + \dot{h}_0\dot{\alpha}_1\int_{e_R}^{R} S_\alpha(y) f_0(y) F_1(y) dy + \dot{h}_1\dot{\alpha}_1\int_{e_R}^{R} S_\alpha(y) f_1(y) F_1(y) dy \\
& + \dot{h}_2\dot{\alpha}_1\int_{e_R}^{R} S_\alpha(y) f_2(y) F_1(y) dy + \dot{h}_3\dot{\alpha}_1\int_{e_R}^{R} S_\alpha(y) f_3(y) F_1(y) dy \\
& + \dot{h}_0\dot{\beta}_0\int_{r_1}^{r_2} S_\beta(y) f_0(y) G_0(y) dy + \dot{h}_1\dot{\beta}_0\int_{r_1}^{r_2} S_\beta(y) f_1(y) G_0(y) dy \\
& + \dot{h}_2\dot{\beta}_0\int_{r_1}^{r_2} S_\beta(y) f_2(y) G_0(y) dy + \dot{h}_3\dot{\beta}_0\int_{r_1}^{r_2} S_\alpha(y) f_3(y) G_0(y) dy \\
& + \dot{h}_0\dot{\beta}_1\int_{r_1}^{r_2} S_\beta(y) f_0(y) G_1(y) dy + \dot{h}_1\dot{\beta}_1\int_{r_1}^{r_2} S_\beta(y) f_1(y) G_1(y) dy \\
& + \dot{h}_2\dot{\beta}_1\int_{r_1}^{r_2} S_\beta(y) f_1(y) G_0(y) dy + \dot{h}_3\dot{\beta}_1\int_{r_1}^{r_2} S_\alpha(y) f_3(y) G_1(y) dy \\
& + \dot{\alpha}_0\dot{\beta}_0\int_{r_1}^{r_2} \left[S_\beta(y)(c-a)b + I_\beta(y)\right] F_0(y) G_0(y) dy \\
& + \dot{\alpha}_1\dot{\beta}_0\int_{r_1}^{r_2} \left[S_\beta(y)(c-a)b + I_\beta(y)\right] F_1(y) G_0(y) dy \\
& + \dot{\alpha}_0\dot{\beta}_1\int_{r_1}^{r_2} \left[S_\beta(y)(c-a)b + I_\beta(y)\right] F_0(y) G_1(y) dy \\
& + \dot{\alpha}_1\dot{\beta}_1\int_{r_1}^{r_2} \left[S_\beta(y)(c-a)b + I_\beta(y)\right] F_1(y) G_1(y) dy. \qquad (128)
\end{aligned}
$$

The generalized masses, static unbalance and mechanical coupling terms are defined by the following quantities:

$$M_0 = \int_{e_R}^{R} m(y)\left[f_0(y)\right]^2 dy \tag{129}$$

$$M_1 = \int_{e_R}^{R} m(y)\left[f_1(y)\right]^2 dy \tag{130}$$

$$M_2 = \int_{e_R}^{R} m(y)\left[f_2(y)\right]^2 dy \tag{131}$$

$$M_3 = \int_{e_R}^{R} m(y)\left[f_3(y)\right]^2 dy \tag{132}$$

$$I_{\alpha_0} = \int_{e_R}^{R} I_\alpha(y)\left[F_0(y)\right]^2 dy \tag{133}$$

$$I_{\alpha_1} = \int_{e_R}^{R} I_\alpha(y)\left[F_1(y)\right]^2 dy \tag{134}$$

$$I_{\beta_0} = \int_{r_1}^{r_2} I_\beta(y)\left[G_0(y)\right]^2 dy \tag{135}$$

$$I_{\beta_1} = \int_{r_1}^{r_2} I_\beta(y)\left[G_1(y)\right]^2 dy \tag{136}$$

$$S_{\alpha_{00}} = \int_{e_R}^{R} S_\alpha(y) f_0(y) F_0(y) dy \tag{137}$$

$$S_{\alpha_{10}} = \int_{e_R}^{R} S_\alpha(y) f_1(y) F_0(y) dy \tag{138}$$

$$S_{\alpha_{20}} = \int_{e_R}^{R} S_\alpha(y) f_2(y) F_0(y) dy \tag{139}$$

$$S_{\alpha_{30}} = \int_{e_R}^{R} S_\alpha(y) f_3(y) F_0(y) dy \tag{140}$$

$$S_{\alpha_{01}} = \int_{e_R}^{R} S_{\alpha}(y) f_0(y) F_1(y) dy \tag{141}$$

$$S_{\alpha_{11}} = \int_{e_R}^{R} S_{\alpha}(y) f_1(y) F_1(y) dy \tag{142}$$

$$S_{\alpha_{21}} = \int_{e_R}^{R} S_{\alpha}(y) f_2(y) F_1(y) dy \tag{143}$$

$$S_{\alpha_{31}} = \int_{e_R}^{R} S_{\alpha}(y) f_3(y) F_1(y) dy \tag{144}$$

$$S_{\beta_{00}} = \int_{r_1}^{r_2} S_{\beta}(y) f_0(y) G_0(y) dy \tag{145}$$

$$S_{\beta_{10}} = \int_{r_1}^{r_2} S_{\beta}(y) f_1(y) G_0(y) dy \tag{146}$$

$$S_{\beta_{20}} = \int_{r_1}^{r_2} S_{\beta}(y) f_2(y) G_0(y) dy \tag{147}$$

$$S_{\beta_{30}} = \int_{r_1}^{r_2} S_{\beta}(y) f_3(y) G_0(y) dy \tag{148}$$

$$S_{\beta_{01}} = \int_{r_1}^{r_2} S_{\beta}(y) f_0(y) G_1(y) dy \tag{149}$$

$$S_{\beta_{11}} = \int_{r_1}^{r_2} S_{\beta}(y) f_1(y) G_1(y) dy \tag{150}$$

$$S_{\beta_{21}} = \int_{r_1}^{r_2} S_{\beta}(y) f_2(y) G_1(y) dy \tag{151}$$

$$S_{\beta_{31}} = \int_{r_1}^{r_2} S_{\beta}(y) f_3(y) G_1(y) dy \tag{152}$$

$$P_{\alpha_0\beta_0} = \int_{r_1}^{r_2} \left[S_{\beta}(y)(c-a)b + I_{\beta}(y) \right] F_0(y) G_0(y) dy \tag{153}$$

$$P_{\alpha_1\beta_0} = \int_{r_1}^{r_2} \left[S_\beta(y)(c-a)b + I_\beta(y) \right] F_1(y) G_0(y)\, dy \tag{154}$$

$$P_{\alpha_0\beta_1} = \int_{r_1}^{r_2} \left[S_\beta(y)(c-a)b + I_\beta(y) \right] F_0(y) G_1(y)\, dy \tag{155}$$

$$\text{and } P_{\alpha_1\beta_1} = \int_{r_1}^{r_2} \left[S_\beta(y)(c-a)b + I_\beta(y) \right] F_1(y) G_1(y)\, dy \tag{156}$$

Substituting equations (129) through (156) into equation (128) yields

$$\begin{aligned} T = {} & \frac{1}{2}M_0\dot{h}_0^2 + \frac{1}{2}M_1\dot{h}_1^2 + \frac{1}{2}M_2\dot{h}_2^2 + \frac{1}{2}M_3\dot{h}_3^2 + \frac{1}{2}I_{\alpha_0}\dot{\alpha}_0^2 + \frac{1}{2}I_{\alpha_1}\dot{\alpha}_1^2 + \frac{1}{2}I_{\beta_0}\dot{\beta}_0^2 + \frac{1}{2}I_{\beta_1}\dot{\beta}_1^2 \\ & + S_{\alpha_{00}}\dot{h}_0\dot{\alpha}_0 + S_{\alpha_{10}}\dot{h}_1\dot{\alpha}_0 + S_{\alpha_{20}}\dot{h}_2\dot{\alpha}_0 + S_{\alpha_{30}}\dot{h}_3\dot{\alpha}_0 + S_{\alpha_{01}}\dot{h}_0\dot{\alpha}_1 + S_{\alpha_{11}}\dot{h}_1\dot{\alpha}_1 + S_{\alpha_{21}}\dot{h}_2\dot{\alpha}_1 + S_{\alpha_{31}}\dot{h}_2\dot{\alpha}_1 \\ & + S_{\beta_{00}}\dot{h}_0\dot{\beta}_0 + S_{\beta_{10}}\dot{h}_1\dot{\beta}_0 + S_{\beta_{20}}\dot{h}_2\dot{\beta}_0 + S_{\beta_{30}}\dot{h}_3\dot{\alpha}_0 + S_{\beta_{01}}\dot{h}_0\dot{\beta}_1 + S_{\beta_{11}}\dot{h}_1\dot{\beta}_1 + S_{\beta_{21}}\dot{h}_2\dot{\beta}_1 + S_{\beta_{31}}\dot{h}_3\dot{\alpha}_1 \\ & + P_{\alpha_0\beta_0}\dot{\alpha}_0\dot{\beta}_0 + P_{\alpha_1\beta_0}\dot{\alpha}_1\dot{\beta}_0 + P_{\alpha_0\beta_1}\dot{\alpha}_0\dot{\beta}_1 + P_{\alpha_1\beta_1}\dot{\alpha}_1\dot{\beta}_1. \end{aligned} \tag{157}$$

3. Potential Energy Equation

The potential energy stored in the system, when the system is deflected, is the strain energy of bending, blade-torsion, flap-torsion, and control system strain due to bending, blade-torsion and flap-torsion. The total strain energy can be written as

$$\begin{aligned} U = {} & \frac{1}{2}\int_{e_R}^{R} EI(y)\left\{\frac{\partial^2}{\partial y^2}\left[h_0 f_0(y)\right]\right\}^2 dy + \frac{1}{2}\int_{e_R}^{R} EI(y)\left\{\frac{\partial^2}{\partial y^2}\left[h_1 f_1(y)\right]\right\}^2 dy \\ & + \frac{1}{2}\int_{e_R}^{R} EI(y)\left\{\frac{\partial^2}{\partial y^2}\left[h_2 f_2(y)\right]\right\}^2 dy + \frac{1}{2}\int_{e_R}^{R} EI(y)\left\{\frac{\partial^2}{\partial y^2}\left[h_3 f_3(y)\right]\right\}^2 dy \\ & + \frac{1}{2}\int_{e_R}^{R} GJ_\alpha(y)\left\{\frac{\partial}{\partial y}\left[\alpha_0 F_0(y)\right]\right\}^2 dy + \frac{1}{2}\int_{e_R}^{R} GJ_\alpha(y)\left\{\frac{\partial}{\partial y}\left[\alpha_1 F_1(y)\right]\right\}^2 dy \\ & + \frac{1}{2}\int_{r_1}^{r_2} GJ_\beta(y)\left\{\frac{\partial}{\partial y}\left[\beta_0 G_0(y)\right]\right\}^2 dy + \frac{1}{2}\int_{r_1}^{r_2} GJ_\beta(y)\left\{\frac{\partial}{\partial y}\left[\beta_1 G_1(y)\right]\right\}^2 dy. \end{aligned} \tag{158}$$

The first and second partial derivatives of the mode shapes in equation (158) are not normally easy to calculate – the exception being for the case of a uniform rotor blade with linear twist. Additionally, the first and second derivatives of $F_0(y)$ and $G_0(y)$ are zero since these terms are either 0 or 1. Therefore, simplified expressions for the terms in the potential need to be found. Defining the following quantities:

$$k_{h_0} = \int_{e_R}^{R} EI(y)\left\{\frac{\partial^2}{\partial y^2}\left[f_0(y)\right]\right\}^2 dy$$

$$k_{h_1} = \int_{e_R}^{R} EI(y)\left\{\frac{\partial^2}{\partial y^2}\left[f_1(y)\right]\right\}^2 dy$$

$$k_{h_2} = \int_{e_R}^{R} EI(y)\left\{\frac{\partial^2}{\partial y^2}\left[f_2(y)\right]\right\}^2 dy$$

$$k_{h_3} = \int_{e_R}^{R} EI(y)\left\{\frac{\partial^2}{\partial y^2}\left[f_3(y)\right]\right\}^2 dy$$

$$k_{\alpha_0} = \int_{e_R}^{R} GJ_\alpha(y)\left\{\frac{\partial}{\partial y}\left[F_0(y)\right]\right\}^2 dy$$

$$k_{\alpha_1} = \int_{e_R}^{R} GJ_\alpha(y)\left\{\frac{\partial}{\partial y}\left[F_1(y)\right]\right\}^2 dy$$

$$k_{\beta_0} = \int_{r_1}^{r_2} GJ_\beta(y)\left\{\frac{\partial}{\partial y}\left[G_0(y)\right]\right\}^2 dy$$

$$\text{and } k_{\beta_1} = \int_{r_1}^{r_2} GJ_\beta(y)\left\{\frac{\partial}{\partial y}\left[G_1(y)\right]\right\}^2 dy,$$

then equation (158) becomes

$$U = \frac{1}{2}k_{h_0}h_0^2 + \frac{1}{2}k_{h_1}h_1^2 + \frac{1}{2}k_{h_2}h_2^2 + \frac{1}{2}k_{h_3}h_3^2 + \frac{1}{2}k_{\alpha_0}\alpha_0^2 + \frac{1}{2}k_{\alpha_1}\alpha_1^2 + \frac{1}{2}k_{\beta_0}\beta_0^2 + \frac{1}{2}k_{\beta_1}\beta_1^2 \quad (159)$$

In order to determine the values of k_i in equation (159), it will be assumed that the rotor blade is oscillating in simple harmonic motion in a vacuum (no dissipation, or damping terms), but it will be restrained so that the oscillation occurs in only one degree of freedom at a time. Therefore, the static moments of inertia are, by definition, zero. The eight conditions to be analyzed are:

(1) $h_0 = \bar{h}_0 e^{i\omega_{h_1} t}$, with $h_1 = h_2 = h_3 = \alpha_0 = \alpha_1 = \beta_0 = \beta_1 = 0$

(2) $h_1 = \bar{h}_1 e^{i\omega_{h_1} t}$, with $h_0 = h_2 = h_3 = \alpha_0 = \alpha_1 = \beta_0 = \beta_1 = 0$

(3) $h_2 = \bar{h}_2 e^{i\omega_{h_2} t}$, with $h_0 = h_1 = h_3 = \alpha_0 = \alpha_1 = \beta_0 = \beta_1 = 0$

(4) $h_3 = \bar{h}_3 e^{i\omega_{h_3} t}$, with $h_0 = h_1 = h_2 = \alpha_0 = \alpha_1 = \beta_0 = \beta_1 = 0$

(5) $\alpha_0 = \bar{\alpha}_0 e^{i\omega_{\alpha_0} t}$, with $h_0 = h_1 = h_2 = h_3 = \alpha_1 = \beta_0 = \beta_1 = 0$

(6) $\alpha_1 = \bar{\alpha}_1 e^{i\omega_{\alpha_1} t}$, with $h_0 = h_1 = h_2 = h_3 = \alpha_0 = \beta_0 = \beta_1 = 0$

(7) $\beta_0 = \bar{\beta}_0 e^{i\omega_{\beta_0} t}$, with $h_0 = h_1 = h_2 = h_3 = \alpha_0 = \alpha_1 = \beta_1 = 0$

(8) $\beta_1 = \bar{\beta}_1 e^{i\omega_{\beta_1} t}$, with $h_0 = h_1 = h_2 = \alpha_0 = \alpha_1 = \beta_0 = 0$

For condition (1), Lagrange's equation of motion reduces to

$$\frac{d}{dt}\left(\frac{\partial T}{\partial \dot{h}_0}\right) + \frac{\partial U}{\partial h_0} = 0$$

$$\frac{d}{dt}\left(M_0 \dot{h}_0\right) + k_{h_0} h_0 = 0$$

$$\text{or } M_0 \ddot{h}_0 + k_{h_0} h_0 = 0$$

Taking the 2nd time derivative of h_0 yields $\ddot{h}_0 = -\omega_{h_0}^2 \bar{h}_0 e^{i\omega_{h_0} t} = -\omega_{h_0}^2 h_0$, and thus

$$\left(-M_0 \omega_{h_0}^2 + k_{h_0}\right) h_0 = 0$$

At this point, it is assumed that h_0 is non-zero, and the term in parentheses must be equal to zero, or

$$k_{h_0} = M_0 \omega_{h_0}^2 \tag{160}$$

Similarly, for conditions (2) through (8), the values of the potential energy coefficients can be expressed in terms of the uncoupled natural frequencies as:

$$k_{h_1} = M_1 \omega_{h_1}^2 \tag{161}$$

$$k_{h_2} = M_2 \omega_{h_2}^2 \tag{162}$$

$$k_{h_3} = M_3 \omega_{h_3}^2 \tag{163}$$

$$k_{\alpha_0} = I_{\alpha_0} \omega_{\alpha_0}^2 \tag{164}$$

$$k_{\alpha_1} = I_{\alpha_1} \omega_{\alpha_1}^2 \tag{165}$$

$$k_{\beta_0} = I_{\beta_0} \omega_{\beta_0}^2 \tag{166}$$

$$k_{\beta_1} = I_{\beta_1}\omega_{\beta_1}^2 \tag{167}$$

Substituting equations (160) through (167) in equation (159) yields

$$\begin{aligned} U = {} & \frac{1}{2}M_0\omega_{h_0}^2 h_0^2 + \frac{1}{2}M_1\omega_{h_1}^2 h_1^2 + \frac{1}{2}M_2\omega_{h_2}^2 h_2^2 + \frac{1}{2}M_3\omega_{h_3}^2 h_3^2 \\ & + \frac{1}{2}I_{\alpha_0}\omega_{\alpha_0}^2\alpha_0^2 + \frac{1}{2}I_{\alpha_1}\omega_{\alpha_1}^2\alpha_1^2 + \frac{1}{2}I_{\beta_0}\omega_{\beta_0}^2\beta_0^2 + \frac{1}{2}I_{\beta_1}\omega_{\beta_1}^2\beta_1^2 \end{aligned} \tag{168}$$

4. Structural Damping – Dissipation Function

Damping can be represented as a force of magnitude proportional to the elastic restoring force and in phase with the velocity of oscillation. Therefore, a dissipation function can be defined as

$$\begin{aligned} D = {} & \frac{M_0 g_{h_0}\omega_{h_0}^2\dot{h}_0^2}{2\omega} + \frac{M_1 g_{h_1}\omega_{h_1}^2\dot{h}_1^2}{2\omega} + \frac{M_2 g_{h_2}\omega_{h_2}^2\dot{h}_2^2}{2\omega} + \frac{M_3 g_{h_3}\omega_{h_3}^2\dot{h}_3^2}{2\omega} \\ & + \frac{I_{\alpha_0} g_{\alpha_0}\omega_{\alpha_0}^2\dot{\alpha}_0^2}{2\omega} + \frac{I_{\alpha_1} g_{\alpha_1}\omega_{\alpha_1}^2\dot{\alpha}_1^2}{2\omega} + \frac{I_{\beta_0} g_{\beta_0}\omega_{\beta_0}^2\dot{\beta}_0^2}{2\omega} + \frac{I_{\beta_1} g_{\beta_1}\omega_{\beta_1}^2\dot{\beta}_1^2}{2\omega} \end{aligned} \tag{169}$$

where ω is the flutter frequency and the M and I terms are defined by equations (129) through (136).

5. Generalized Forces

The oscillatory aerodynamic lift and moment equations per unit length are given in equations (60), (61) and (62). By substituting the expressions for the deflections given in equations (118), (119) and (120) into equations (60), (61) and (62), the results are

$$\begin{aligned} L' = \pi\rho b^3\omega^2 \Bigg\{ & L_h\left(\frac{h_0 f_0(y) + h_1 f_1(y) + h_2 f_2(y) + h_3 f_3(y)}{b}\right) \\ & + \left[L_\alpha - \left(\frac{1}{2}+a\right)L_h\right]\left[\alpha_0 F_0(y) + \alpha_1 F_1(y)\right] \\ & + \left[L_\beta - (c-e)L_z\right]\left[\beta_0 G_0(y) + \beta_1 G_1(y)\right]\Bigg\} \end{aligned} \tag{170}$$

$$M' = \pi\rho b^4\omega^2 \left\{ \left[M_h - \left(\frac{1}{2}+a\right)L_h \right] \left[\frac{h_0 f_0(y) + h_1 f_1(y) + h_2 f_2(y) + h_3 f_3(y)}{b} \right] \right.$$
$$+ \left[M_\alpha - \left(\frac{1}{2}+a\right)\left(L_\alpha + M_h\right) + \left(\frac{1}{2}+a\right)^2 L_h \right] \left[\alpha_0 F_0(y) + \alpha_1 F_1(y) \right] \qquad (171)$$
$$\left. + \left[M_\beta - \left(\frac{1}{2}+a\right)L_\beta - (c-e)\left(M_z - \left(\frac{1}{2}+a\right)L_z \right) \right] \left[\beta_0 G_0(y) + \beta_1 G_1(y) \right] \right\}$$

$$T' = \pi\rho b^4\omega^2 \left\{ \left[T_h - (c-e)P_h \right] \left[\frac{h_0 f_0(y) + h_1 f_1(y) + h_2 f_2(y) + h_3 f_3(y)}{b} \right] \right.$$
$$+ \left[T_\alpha - (c-e)P_\alpha - \left(\frac{1}{2}+a\right)\left(T_h - (c-e)P_h\right) \right] \left[\alpha_0 F_0(y) + \alpha_1 F_1(y) \right] \qquad (172)$$
$$\left. + \left[T_\beta - (c-e)\left(P_\beta + T_z\right) + (c-e)^2 P_z \right] \left[\beta_0 G_0(y) + \beta_1 G_1(y) \right] \right\}$$

The generalized force in the h_0 degree of freedom, Q_{h_0}, is determined from the virtual work done by displacing the rotor blade from h_0 to $(h_0 + \delta h_0)$, while holding all other degrees of freedom constant. This displacement is a result of the aerodynamic forces and moments acting on the rotor blade and any control forces that displace the rotor blade, or

$$\delta W = L'\delta h_0 = L'\left(\delta h_0 f_0(y) + \delta h_1 f_1(y) + \delta h_2 f_2(y) + \delta h_3 f_3(y)\right)$$

Thus,

$$Q'_{h_0} = \frac{\delta W}{\delta h_0} = L' f_0(y) \qquad (173)$$

$$Q'_{h_1} = \frac{\delta W}{\delta h_1} = L' f_1(y) \qquad (174)$$

$$Q'_{h_2} = \frac{\delta W}{\delta h_2} = L' f_2(y) \qquad (175)$$

$$Q'_{h_3} = \frac{\delta W}{\delta h_3} = L' f_3(y) \qquad (176)$$

Similarly,

$$Q'_{\alpha_0} = M'F_0(y) \tag{177}$$

$$Q'_{\alpha_1} = M'F_1(y) \tag{178}$$

$$Q'_{\beta_0} = M'G_0(y) \tag{179}$$

$$Q'_{\beta_1} = M'G_1(y) \tag{180}$$

To find the generalized forces for the entire rotor blade, the section generalized forces given in equations (173) through (180) are integrated along the span of the rotor blade from e_R to R for blade bending and torsion modes and from r_1 to r_2 for flap-torsion modes, resulting in

$$Q_{h_0} = \int_{e_R}^{R} L'f_0(y)\,dy \tag{181}$$

$$Q_{h_1} = \int_{e_R}^{R} L'f_1(y)\,dy \tag{182}$$

$$Q_{h_2} = \int_{e_R}^{R} L'f_2(y)\,dy \tag{183}$$

$$Q_{h_3} = \int_{e_R}^{R} L'f_3(y)\,dy \tag{184}$$

$$Q_{\alpha_0} = \int_{e_R}^{R} M'F_0(y)\,dy \tag{185}$$

$$Q_{\alpha_1} = \int_{e_R}^{R} M'F_1(y)\,dy \tag{186}$$

$$Q_{\beta_0} = \int_{r_1}^{r_2} T'G_0(y)\,dy \tag{187}$$

$$Q_{\beta_1} = \int_{r_1}^{r_2} T'G_1(y)\,dy\,. \tag{188}$$

Substituting equations (170), (171) and (172) into equations (181) through (188) yield

$$Q_{h_0} = \pi\rho\omega^2 \left(A_{h_0h_0} h_0 + A_{h_0h_1} h_1 + A_{h_0h_2} h_2 + A_{h_0h_3} h_3 + A_{h_0\alpha_0} \alpha_0 + A_{h_0\alpha_1} \alpha_1 + A_{h_0\beta_0} \beta_0 + A_{h_0\beta_1} \beta_1 \right) \tag{189}$$

$$Q_{h_1} = \pi\rho\omega^2 \left(A_{h_1h_0} h_0 + A_{h_1h_1} h_1 + A_{h_1h_2} h_2 + A_{h_1h_3} h_3 + A_{h_1\alpha_0} \alpha_0 + A_{h_1\alpha_1} \alpha_1 + A_{h_1\beta_0} \beta_0 + A_{h_1\beta_1} \beta_1 \right) \tag{190}$$

$$Q_{h_2} = \pi\rho\omega^2 \left(A_{h_2h_0} h_0 + A_{h_2h_1} h_1 + A_{h_2h_2} h_2 + A_{h_2h_3} h_3 + A_{h_2\alpha_0} \alpha_0 + A_{h_2\alpha_1} \alpha_1 + A_{h_2\beta_0} \beta_0 + A_{h_2\beta_1} \beta_1 \right) \tag{191}$$

$$Q_{h_3} = \pi\rho\omega^2 \left(A_{h_3h_0} h_0 + A_{h_3h_1} h_1 + A_{h_3h_2} h_2 + A_{h_3h_3} h_3 + A_{h_3\alpha_0} \alpha_0 + A_{h_3\alpha_1} \alpha_1 + A_{h_3\beta_0} \beta_0 + A_{h_3\beta_1} \beta_1 \right) \tag{192}$$

$$Q_{\alpha_0} = \pi\rho\omega^2 \left(A_{\alpha_0h_0} h_0 + A_{\alpha_0h_1} h_1 + A_{\alpha_0h_2} h_2 + A_{\alpha_0h_3} h_3 + A_{\alpha_0\alpha_0} \alpha_0 + A_{\alpha_0\alpha_1} \alpha_1 + A_{\alpha_0\beta_0} \beta_0 + A_{\alpha_0\beta_1} \beta_1 \right) \tag{193}$$

$$Q_{\alpha_1} = \pi\rho\omega^2 \left(A_{\alpha_1h_0} h_0 + A_{\alpha_1h_1} h_1 + A_{\alpha_1h_2} h_2 + A_{\alpha_1h_3} h_3 + A_{\alpha_1\alpha_0} \alpha_0 + A_{\alpha_1\alpha_1} \alpha_1 + A_{\alpha_1\beta_0} \beta_0 + A_{\alpha_1\beta_1} \beta_1 \right) \tag{194}$$

$$Q_{\beta_0} = \pi\rho\omega^2 \left(A_{\beta_0h_0} h_0 + A_{\beta_0h_1} h_1 + A_{\beta_0h_2} h_2 + A_{\beta_0h_3} h_3 + A_{\beta_0\alpha_0} \alpha_0 + A_{\beta_0\alpha_1} \alpha_1 + A_{\beta_0\beta_0} \beta_0 + A_{\beta_0\beta_1} \beta_1 \right) \tag{195}$$

and

$$Q_{\beta_1} = \pi\rho\omega^2 \left(A_{\beta_1h_0} h_0 + A_{\beta_1h_1} h_1 + A_{\beta_1h_2} h_2 + A_{\beta_1h_3} h_3 + A_{\beta_1\alpha_0} \alpha_0 + A_{\beta_1\alpha_1} \alpha_1 + A_{\beta_1\beta_0} \beta_0 + A_{\beta_1\beta_1} \beta_1 \right) \tag{196}$$

where the expressions for aerodynamic terms that couple the modes together and incorporate a lift deficiency function are given as

$$A_{h_0h_0} = \int_{e_R}^{R} b^2 \left[f_0(y) \right]^2 L_h dy \tag{197}$$

$$A_{h_0h_1} = \int_{e_R}^{R} b^2 f_0(y) f_1(y) L_h dy \tag{198}$$

$$A_{h_0h_2} = \int_{e_R}^{R} b^2 f_0(y) f_2(y) L_h dy \tag{199}$$

$$A_{h_0h_3} = \int_{e_R}^{R} b^2 f_0(y) f_3(y) L_h dy \tag{200}$$

$$A_{h_0\alpha_0} = \int_{e_R}^{R} b^3 f_0(y) F_0(y) \left[L_\alpha - \left(\frac{1}{2} + a \right) L_h \right] dy \tag{201}$$

$$A_{h_0\alpha_1} = \int_{e_R}^{R} b^3 f_0(y) F_1(y) \left[L_\alpha - \left(\frac{1}{2} + a \right) L_h \right] dy \tag{202}$$

$$A_{h_0\beta_0} = \int_{r_1}^{r_2} b^3 f_0(y) G_0(y) \left[L_\beta - (c-e) L_z \right] dy \tag{203}$$

$$A_{h_0\beta_1} = \int_{r_1}^{r_2} b^3 f_0(y) G_1(y) \left[L_\beta - (c-e) L_z \right] dy \tag{204}$$

$$A_{h_1h_0} = \int_{e_R}^{R} b^2 f_1(y) f_0(y) L_h dy = A_{h_0h_1} \tag{205}$$

$$A_{h_1h_1} = \int_{e_R}^{R} b^2 \left[f_1(y) \right]^2 L_h dy \tag{206}$$

$$A_{h_1h_2} = \int_{e_R}^{R} b^2 f_1(y) f_2(y) L_h dy \tag{207}$$

$$A_{h_1h_3} = \int_{e_R}^{R} b^2 f_1(y) f_3(y) L_h dy \tag{208}$$

$$A_{h_1\alpha_0} = \int_{e_R}^{R} b^3 f_1(y) F_0(y) \left[L_\alpha - \left(\frac{1}{2} + a \right) L_h \right] dy \tag{209}$$

$$A_{h_1\alpha_1} = \int_{e_R}^{R} b^3 f_1(y) F_1(y) \left[L_\alpha - \left(\frac{1}{2} + a \right) L_h \right] dy \tag{210}$$

$$A_{h_1\beta_0} = \int_{r_1}^{r_2} b^3 f_1(y) G_0(y) \left[L_\beta - (c-e) L_z \right] dy \tag{211}$$

$$A_{h_1\beta_1} = \int_{r_1}^{r_2} b^3 f_1(y) G_1(y) \left[L_\beta - (c-e) L_z \right] dy \tag{212}$$

$$A_{h_2h_0} = \int_{e_R}^{R} b^2 f_2(y) f_0(y) L_h dy = A_{h_0h_2} \tag{213}$$

$$A_{h_2h_1} = \int_{e_R}^{R} b^2 f_2(y) f_1(y) L_h dy = A_{h_1h_2} \tag{214}$$

$$A_{h_2h_2} = \int_{e_R}^{R} b^2 \left[f_2(y) \right]^2 L_h dy \tag{215}$$

$$A_{h_2h_3} = \int_{e_R}^{R} b^2 f_2(y) f_3(y) L_h dy \tag{216}$$

$$A_{h_2\alpha_0} = \int_{e_R}^{R} b^3 f_2(y) F_0(y) \left[L_\alpha - \left(\frac{1}{2} + a \right) L_h \right] dy \tag{217}$$

$$A_{h_2\alpha_1} = \int_{e_R}^{R} b^3 f_2(y) F_1(y) \left[L_\alpha - \left(\frac{1}{2} + a \right) L_h \right] dy \tag{218}$$

$$A_{h_2\beta_0} = \int_{r_1}^{r_2} b^3 f_2(y) G_0(y) \left[L_\beta - (c-e) L_z \right] dy \tag{219}$$

$$A_{h_2\beta_1} = \int_{r_1}^{r_2} b^3 f_2(y) G_1(y) \left[L_\beta - (c-e) L_z \right] dy \tag{220}$$

$$A_{h_3h_0} = \int_{e_R}^{R} b^2 f_3(y) f_0(y) L_h dy = A_{h_0h_3} \tag{221}$$

$$A_{h_3h_1} = \int_{e_R}^{R} b^2 f_3(y) f_1(y) L_h dy = A_{h_1h_3} \tag{222}$$

$$A_{h_3h_2} = \int_{e_R}^{R} b^2 f_3(y) f_2(y) L_h dy = A_{h_2h_3} \tag{223}$$

$$A_{h_3h_3} = \int_{e_R}^{R} b^2 \left[f_3(y) \right]^2 L_h dy \tag{224}$$

$$A_{h_3\alpha_0} = \int_{e_R}^{R} b^3 f_3(y) F_0(y) \left[L_\alpha - \left(\frac{1}{2} + a \right) L_h \right] dy \tag{225}$$

$$A_{h_3\alpha_1} = \int_{e_R}^{R} b^3 f_3(y) F_1(y) \left[L_\alpha - \left(\frac{1}{2} + a \right) L_h \right] dy \tag{226}$$

$$A_{h_3\beta_0} = \int_{r_1}^{r_2} b^3 f_3(y) G_0(y) \left[L_\beta - (c-e) L_z \right] dy \tag{227}$$

$$A_{h_3\beta_1} = \int_{r_1}^{r_2} b^3 f_3(y) G_1(y) \left[L_\beta - (c-e) L_z \right] dy \tag{228}$$

$$A_{\alpha_0 h_0} = \int_{e_R}^{R} b^3 F_0(y) f_0(y) \left[M_h - \left(\frac{1}{2} + a \right) L_h \right] dy \tag{229}$$

$$A_{\alpha_0 h_1} = \int_{e_R}^{R} b^3 F_0(y) f_1(y) \left[M_h - \left(\frac{1}{2} + a \right) L_h \right] dy \tag{230}$$

$$A_{\alpha_0 h_2} = \int_{e_R}^{R} b^3 F_0(y) f_2(y) \left[M_h - \left(\frac{1}{2} + a \right) L_h \right] dy \tag{231}$$

$$A_{\alpha_0 h_3} = \int_{e_R}^{R} b^3 F_0(y) f_3(y) \left[M_h - \left(\frac{1}{2} + a \right) L_h \right] dy \tag{232}$$

$$A_{\alpha_0\alpha_0} = \int_{e_R}^{R} b^4 \left[F_0(y) \right]^2 \left[M_\alpha - \left(\frac{1}{2} + a \right) (L_\alpha + M_h) + \left(\frac{1}{2} + a \right)^2 L_h \right] dy \tag{233}$$

$$A_{\alpha_0\alpha_1} = \int_{e_R}^{R} b^4 F_0(y) F_1(y) \left[M_\alpha - \left(\frac{1}{2} + a \right) (L_\alpha + M_h) + \left(\frac{1}{2} + a \right)^2 L_h \right] dy \tag{234}$$

$$A_{\alpha_0\beta_0} = \int_{r_1}^{r_2} b^4 F_0(y) G_0(y) \left[M_\beta - \left(\frac{1}{2} + a \right) L_\beta - (c-e) M_z + (c-e) \left(\frac{1}{2} + a \right) L_z \right] dy \tag{235}$$

$$A_{\alpha_0\beta_1} = \int_{r_1}^{r_2} b^4 F_0(y) G_1(y) \left[M_\beta - \left(\frac{1}{2} + a \right) L_\beta - (c-e) M_z + (c-e) \left(\frac{1}{2} + a \right) L_z \right] dy \tag{236}$$

$$A_{\alpha_1 h_0} = \int_{e_R}^{R} b^3 F_1(y) f_0(y) \left[M_h - \left(\frac{1}{2} + a \right) L_h \right] dy \tag{237}$$

$$A_{\alpha_1 h_1} = \int_{e_R}^{R} b^3 F_1(y) f_1(y) \left[M_h - \left(\frac{1}{2} + a \right) L_h \right] dy \tag{238}$$

$$A_{\alpha_1 h_2} = \int_{e_R}^{R} b^3 F_1(y) f_2(y) \left[M_h - \left(\frac{1}{2} + a \right) L_h \right] dy \tag{239}$$

$$A_{\alpha_1 h_3} = \int_{e_R}^{R} b^3 F_1(y) f_3(y) \left[M_h - \left(\frac{1}{2} + a \right) L_h \right] dy \tag{240}$$

$$A_{\alpha_1 \alpha_0} = \int_{e_R}^{R} b^4 F_1(y) F_0(y) \left[M_\alpha - \left(\frac{1}{2} + a \right) (L_\alpha + M_h) + \left(\frac{1}{2} + a \right)^2 L_h \right] dy = A_{\alpha_0 \alpha_1} \tag{241}$$

$$A_{\alpha_1 \alpha_1} = \int_{e_R}^{R} b^4 \left[F_1(y) \right]^2 \left[M_\alpha - \left(\frac{1}{2} + a \right) (L_\alpha + M_h) + \left(\frac{1}{2} + a \right)^2 L_h \right] dy \tag{242}$$

$$A_{\alpha_1 \beta_0} = \int_{r_1}^{r_2} b^4 F_1(y) G_0(y) \left[M_\beta - \left(\frac{1}{2} + a \right) L_\beta - (c-e) M_z + (c-e) \left(\frac{1}{2} + a \right) L_z \right] dy \tag{243}$$

$$A_{\alpha_1 \beta_1} = \int_{r_1}^{r_2} b^4 F_1(y) G_1(y) \left[M_\beta - \left(\frac{1}{2} + a \right) L_\beta - (c-e) M_z + (c-e) \left(\frac{1}{2} + a \right) L_z \right] dy \tag{244}$$

$$A_{\beta_0 h_0} = \int_{r_1}^{r_2} b^3 G_0(y) f_0(y) \left[T_h - (c-e) P_h \right] dy \tag{245}$$

$$A_{\beta_0 h_1} = \int_{r_1}^{r_2} b^3 G_0(y) f_1(y) \left[T_h - (c-e) P_h \right] dy \tag{246}$$

$$A_{\beta_0 h_2} = \int_{r_1}^{r_2} b^3 G_0(y) f_2(y) \left[T_h - (c-e) P_h \right] dy \tag{247}$$

$$A_{\beta_0 h_3} = \int_{r_1}^{r_2} b^3 G_0(y) f_3(y) \left[T_h - (c-e) P_h \right] dy \tag{248}$$

$$A_{\beta_0 \alpha_0} = \int_{r_1}^{r_2} b^4 G_0(y) F_0(y) \left[T_\alpha - (c-e) P_\alpha + \left(\frac{1}{2} + a \right) T_h + \left(\frac{1}{2} + a \right) (c-e) P_h \right] dy \tag{249}$$

$$A_{\beta_0 \alpha_1} = \int_{r_1}^{r_2} b^4 G_0(y) F_1(y) \left[T_\alpha - (c-e) P_\alpha + \left(\frac{1}{2} + a \right) T_h + \left(\frac{1}{2} + a \right) (c-e) P_h \right] dy \tag{250}$$

$$A_{\beta_0\beta_0} = \int_{r_1}^{r_2} b^4 \left[G_0(y) \right]^2 \left[T_\beta - (c-e)\left(P_\beta + T_z \right) + (c-e)^2 P_z \right] dy \tag{251}$$

$$A_{\beta_0\beta_1} = \int_{r_1}^{r_2} b^4 G_0(y) G_1(y) \left[T_\beta - (c-e)\left(P_\beta + T_z \right) + (c-e)^2 P_z \right] dy \tag{252}$$

$$A_{\beta_1 h_0} = \int_{r_1}^{r_2} b^3 G_1(y) f_0(y) \left[T_h - (c-e) P_h \right] dy \tag{253}$$

$$A_{\beta_1 h_1} = \int_{r_1}^{r_2} b^3 G_1(y) f_1(y) \left[T_h - (c-e) P_h \right] dy \tag{254}$$

$$A_{\beta_1 h_2} = \int_{r_1}^{r_2} b^3 G_1(y) f_2(y) \left[T_h - (c-e) P_h \right] dy \tag{255}$$

$$A_{\beta_1 h_3} = \int_{r_1}^{r_2} b^3 G_1(y) f_3(y) \left[T_h - (c-e) P_h \right] dy \tag{256}$$

$$A_{\beta_1\alpha_0} = \int_{r_1}^{r_2} b^4 G_1(y) F_0(y) \left[T_\alpha - (c-e) P_\alpha + \left(\frac{1}{2} + a \right) T_h + \left(\frac{1}{2} + a \right)(c-e) P_h \right] dy \tag{257}$$

$$A_{\beta_1\alpha_1} = \int_{r_1}^{r_2} b^4 G_1(y) F_1(y) \left[T_\alpha - (c-e) P_\alpha + \left(\frac{1}{2} + a \right) T_h + \left(\frac{1}{2} + a \right)(c-e) P_h \right] dy \tag{258}$$

$$A_{\beta_1\beta_0} = \int_{r_1}^{r_2} b^4 G_1(y) G_0(y) \left[T_\beta - (c-e)\left(P_\beta + T_z \right) + (c-e)^2 P_z \right] dy = A_{\beta_0\beta_1} \tag{259}$$

$$A_{\beta_1\beta_1} = \int_{r_1}^{r_2} b^4 \left[G_1(y) \right]^2 \left[T_\beta - (c-e)\left(P_\beta + T_z \right) + (c-e)^2 P_z \right] dy \tag{260}$$

6. Lagrange's Equations of Motion

Now that all the terms in Lagrange's equation have been developed, it will first be noted that the kinetic energy equation is only a function of the derivative of the generalized displacement ($\dot{h}_0, \dot{h}_1, \dot{h}_2, \dot{h}_3, \dot{\alpha}_o, \dot{\alpha}_1, \dot{\beta}_0$ or $\dot{\beta}_1$), or the velocity. Thus, Lagrange's equation reduces to

$$\frac{d}{dt}\left(\frac{\partial T}{\partial \dot{q}_n} \right) + \frac{\partial U}{\partial q_n} + \frac{\partial D}{\partial \dot{q}_n} = Q_n \,. \tag{261}$$

Applying equation (261) to the 8DOF yields the following equations

$$M_0\ddot{h}_0 + S_{\alpha_{00}}\ddot{\alpha}_0 + S_{\alpha_{01}}\ddot{\alpha}_1 + S_{\beta_{00}}\ddot{\beta}_0 + S_{\beta_{01}}\ddot{\beta}_1 + M_0\omega_{h_0}^2 h_0 + \frac{M_0\omega_{h_0}^2 g_{h_0}}{\omega}\dot{h}_0 = Q_{h_0} \tag{262}$$

$$M_1\ddot{h}_1 + S_{\alpha_{10}}\ddot{\alpha}_0 + S_{\alpha_{11}}\ddot{\alpha}_1 + S_{\beta_{10}}\ddot{\beta}_0 + S_{\beta_{11}}\ddot{\beta}_1 + M_1\omega_{h_1}^2 h_1 + \frac{M_1\omega_{h_1}^2 g_{h_1}}{\omega}\dot{h}_1 = Q_{h_1} \tag{263}$$

$$M_2\ddot{h}_2 + S_{\alpha_{20}}\ddot{\alpha}_0 + S_{\alpha_{21}}\ddot{\alpha}_1 + S_{\beta_{20}}\ddot{\beta}_0 + S_{\beta_{21}}\ddot{\beta}_1 + M_2\omega_{h_2}^2 h_2 + \frac{M_2\omega_{h_2}^2 g_{h_2}}{\omega}\dot{h}_2 = Q_{h_2} \tag{264}$$

$$M_3\ddot{h}_3 + S_{\alpha_{30}}\ddot{\alpha}_0 + S_{\alpha_{31}}\ddot{\alpha}_1 + S_{\beta_{30}}\ddot{\beta}_0 + S_{\beta_{31}}\ddot{\beta}_1 + M_3\omega_{h_3}^2 h_3 + \frac{M_3\omega_{h_3}^2 g_{h_3}}{\omega}\dot{h}_3 = Q_{h_3} \tag{265}$$

$$\begin{aligned} &I_{\alpha_0}\ddot{\alpha}_0 + S_{\alpha_{00}}\ddot{h}_0 + S_{\alpha_{10}}\ddot{h}_1 + S_{\alpha_{20}}\ddot{h}_2 + S_{\alpha_{30}}\ddot{h}_3 \\ &\quad + P_{\alpha_0\beta_0}\ddot{\beta}_0 + P_{\alpha_0\beta_1}\ddot{\beta}_1 + I_{\alpha_0}\omega_{\alpha_0}^2\alpha_0 + \frac{I_{\alpha_0}\omega_{\alpha_0}^2 g_{\alpha_0}}{\omega}\dot{\alpha}_0 = Q_{\alpha_0} \end{aligned} \tag{266}$$

$$\begin{aligned} &I_{\alpha_1}\ddot{\alpha}_1 + S_{\alpha_{01}}\ddot{h}_0 + S_{\alpha_{11}}\ddot{h}_1 + S_{\alpha_{21}}\ddot{h}_2 + S_{\alpha_{31}}\ddot{h}_3 \\ &\quad + P_{\alpha_1\beta_0}\ddot{\beta}_0 + P_{\alpha_1\beta_1}\ddot{\beta}_1 + I_{\alpha_1}\omega_{\alpha_1}^2\alpha_1 + \frac{I_{\alpha_1}\omega_{\alpha_1}^2 g_{\alpha_1}}{\omega}\dot{\alpha}_1 = Q_{\alpha_1} \end{aligned} \tag{267}$$

$$\begin{aligned} &I_{\beta_0}\ddot{\beta}_0 + S_{\beta_{00}}\ddot{h}_0 + S_{\beta_{10}}\ddot{h}_1 + S_{\beta_{20}}\ddot{h}_2 + S_{\beta_{30}}\ddot{h}_3 \\ &\quad + P_{\alpha_0\beta_0}\ddot{\alpha}_0 + P_{\alpha_1\beta_0}\ddot{\alpha}_1 + I_{\beta_0}\omega_{\beta_0}^2\beta_0 + \frac{I_{\beta_0}\omega_{\beta_0}^2 g_{\beta_0}}{\omega}\dot{\beta}_0 = Q_{\beta_0} \end{aligned} \tag{268}$$

$$\begin{aligned} &I_{\beta_1}\ddot{\beta}_1 + S_{\beta_{01}}\ddot{h}_0 + S_{\beta_{11}}\ddot{h}_1 + S_{\beta_{21}}\ddot{h}_2 + S_{\beta_{31}}\ddot{h}_3 \\ &\quad + P_{\alpha_0\beta_1}\ddot{\alpha}_0 + P_{\alpha_1\beta_1}\ddot{\alpha}_1 + I_{\beta_1}\omega_{\beta_1}^2\beta_1 + \frac{I_{\beta_1}\omega_{\beta_1}^2 g_{\beta_1}}{\omega}\dot{\beta}_1 = Q_{\beta_1} \end{aligned} \tag{269}$$

If simple harmonic motion is assumed, that is: $\ddot{h}_n = -\omega^2 h_n$, $\dot{h}_n = i\omega h_n$, $\ddot{\alpha}_n = -\omega^2\alpha_n$, $\dot{\alpha}_n = i\omega\alpha_n$, $\ddot{\beta}_n = -\omega^2\beta_n$, and $\dot{\beta}_n = i\omega\beta_n$, and the expressions for Q_{h_n}, Q_{α_n}, and Q_{β_n} given in equations (189) through (196) are substituted into equations (262) through (269), the results are:

$$\left[\pi\rho A_{h_0h_0}+M_0-M_0\left(1+ig_{h_0}\right)\left(\frac{\omega_{h_0}}{\omega}\right)^2\right]h_0+\left(\pi\rho A_{h_0h_1}\right)h_1+\left(\pi\rho A_{h_0h_2}\right)h_2$$
$$+\left(\pi\rho A_{h_0h_3}\right)h_3+\left(\pi\rho A_{h_0\alpha_0}+S_{\alpha_{00}}\right)\alpha_0+\left(\pi\rho A_{h_0\alpha_1}+S_{\alpha_{01}}\right)\alpha_1 \qquad (270)$$
$$+\left(\pi\rho A_{h_0\beta_0}+S_{\beta_{00}}\right)\beta_0+\left(\pi\rho A_{h_0\beta_1}+S_{\beta_{01}}\right)\beta_1=0$$

$$\left(\pi\rho A_{h_1h_0}\right)h_0+\left[\pi\rho A_{h_1h_1}+M_1-M_1\left(1+ig_{h_1}\right)\left(\frac{\omega_{h_1}}{\omega}\right)^2\right]h_1+\left(\pi\rho A_{h_1h_2}\right)h_2$$
$$+\left(\pi\rho A_{h_1h_3}\right)h_3+\left(\pi\rho A_{h_1\alpha_0}+S_{\alpha_{10}}\right)\alpha_0+\left(\pi\rho A_{h_1\alpha_1}+S_{\alpha_{11}}\right)\alpha_1 \qquad (271)$$
$$+\left(\pi\rho A_{h_1\beta_0}+S_{\beta_{10}}\right)\beta_0+\left(\pi\rho A_{h_1\beta_1}+S_{\beta_{11}}\right)\beta_1=0$$

$$\left(\pi\rho A_{h_2h_0}\right)h_0+\left(\pi\rho A_{h_2h_1}\right)h_1+\left[\pi\rho A_{h_2h_2}+M_2-M_2\left(1+ig_{h_2}\right)\left(\frac{\omega_{h_2}}{\omega}\right)^2\right]h_2$$
$$+\left(\pi\rho A_{h_2h_3}\right)h_3+\left(\pi\rho A_{h_2\alpha_0}+S_{\alpha_{20}}\right)\alpha_0+\left(\pi\rho A_{h_2\alpha_1}+S_{\alpha_{21}}\right)\alpha_1 \qquad (272)$$
$$+\left(\pi\rho A_{h_2\beta_0}+S_{\beta_{20}}\right)\beta_0+\left(\pi\rho A_{h_2\beta_1}+S_{\beta_{21}}\right)\beta_1=0$$

$$\left(\pi\rho A_{h_3h_0}\right)h_0+\left(\pi\rho A_{h_3h_1}\right)h_1+\left(\pi\rho A_{h_3h_2}\right)h_2$$
$$+\left[\pi\rho A_{h_3h_3}+M_3-M_3\left(1+ig_{h_3}\right)\left(\frac{\omega_{h_3}}{\omega}\right)^2\right]h_3+\left(\pi\rho A_{h_3\alpha_0}+S_{\alpha_{30}}\right)\alpha_0 \qquad (273)$$
$$+\left(\pi\rho A_{h_3\alpha_1}+S_{\alpha_{31}}\right)\alpha_1+\left(\pi\rho A_{h_3\beta_0}+S_{\beta_{30}}\right)\beta_0+\left(\pi\rho A_{h_3\beta_1}+S_{\beta_{31}}\right)\beta_1=0$$

$$\left(\pi\rho A_{\alpha_0h_0}+S_{\alpha_{00}}\right)h_0+\left(\pi\rho A_{\alpha_0h_1}+S_{\alpha_{10}}\right)h_1+\left(\pi\rho A_{\alpha_0h_2}+S_{\alpha_{20}}\right)h_2$$
$$+\left(\pi\rho A_{\alpha_0h_3}+S_{\alpha_{30}}\right)h_3+\left[\pi\rho A_{\alpha_0\alpha_0}+I_{\alpha_0}-I_{\alpha_0}\left(1+ig_{\alpha_0}\right)\left(\frac{\omega_{\alpha_0}}{\omega}\right)^2\right]\alpha_0 \qquad (274)$$
$$+\pi\rho A_{\alpha_0\alpha_1}\alpha_1+\left(\pi\rho A_{\alpha_0\beta_0}+P_{\alpha_0\beta_0}\right)\beta_0+\left(\pi\rho A_{\alpha_0\beta_1}+P_{\alpha_0\beta_1}\right)\beta_1=0$$

$$\left(\pi\rho A_{\alpha_1h_0}+S_{\alpha_{01}}\right)h_0+\left(\pi\rho A_{\alpha_1h_1}+S_{\alpha_{11}}\right)h_1+\left(\pi\rho A_{\alpha_1h_2}+S_{\alpha_{21}}\right)h_2$$
$$+\left(\pi\rho A_{\alpha_1h_3}+S_{\alpha_{31}}\right)h_3+\pi\rho A_{\alpha_1\alpha_0}\alpha_0+\left[\pi\rho A_{\alpha_1\alpha_1}+I_{\alpha_1}-I_{\alpha_1}\left(1+ig_{\alpha_1}\right)\left(\frac{\omega_{\alpha_1}}{\omega}\right)^2\right]\alpha_1 \qquad (275)$$
$$+\left(\pi\rho A_{\alpha_1\beta_0}+P_{\alpha_1\beta_0}\right)\beta_0+\left(\pi\rho A_{\alpha_1\beta_1}+P_{\alpha_1\beta_1}\right)\beta_1=0$$

$$\left(\pi\rho A_{\beta_0 h_0} + S_{\beta_{00}}\right)h_0 + \left(\pi\rho A_{\beta_0 h_1} + S_{\beta_{10}}\right)h_1 + \left(\pi\rho A_{\beta_0 h_2} + S_{\beta_{20}}\right)h_2$$
$$+\left(\pi\rho A_{\beta_0 h_3} + S_{\beta_{30}}\right)h_3 + \left(\pi\rho A_{\beta_0\alpha_0} + P_{\alpha_0\beta_0}\right)\alpha_0 + \left(\pi\rho A_{\beta_0\alpha_1} + P_{\alpha_1\beta_0}\right)\alpha_1 \qquad (276)$$
$$+\left[\pi\rho A_{\beta_0\beta_0} + I_{\beta_0} - I_{\beta_0}\left(1+ig_{\beta_0}\right)\left(\frac{\omega_{\beta_0}}{\omega}\right)^2\right]\beta_0 + \pi\rho A_{\beta_0\beta_1}\beta_1 = 0$$

$$\left(\pi\rho A_{\beta_1 h_0} + S_{\beta_{01}}\right)h_0 + \left(\pi\rho A_{\beta_1 h_1} + S_{\beta_{11}}\right)h_1 + \left(\pi\rho A_{\beta_1 h_2} + S_{\beta_{21}}\right)h_2$$
$$+\left(\pi\rho A_{\beta_1 h_3} + S_{\beta_{31}}\right)h_3 + \left(\pi\rho A_{\beta_1\alpha_0} + P_{\alpha_0\beta_1}\right)\alpha_0 + \left(\pi\rho A_{\beta_1\alpha_1} + P_{\alpha_1\beta_1}\right)\alpha_1 \qquad (277)$$
$$+\pi\rho A_{\beta_1\beta_0}\beta_0 + \left[\pi\rho A_{\beta_1\beta_1} + I_{\beta_1} - I_{\beta_1}\left(1+ig_{\beta_1}\right)\left(\frac{\omega_{\beta_1}}{\omega}\right)^2\right]\beta_1 = 0$$

These eight equations to the flutter problem given in equations (270) through (277) can be written in matrix form as

$$
\begin{bmatrix}
\begin{Bmatrix} \pi\rho A_{h_0h_0}+M_0 \\ -M_0\left(1+ig_{h_0}\right)\left(\dfrac{\omega_{h_0}}{\omega}\right)^2 \end{Bmatrix} & \pi\rho A_{h_0h_1} & \pi\rho A_{h_0h_2} & \pi\rho A_{h_0h_3} & \pi\rho A_{h_0\alpha_0}+S_{\alpha_{00}} & \pi\rho A_{h_0\alpha_1}+S_{\alpha_{01}} & \pi\rho A_{h_0\beta_0}+S_{\beta_{00}} & \pi\rho A_{h_0\beta_1}+S_{\beta_{01}} \\
\pi\rho A_{h_1h_0} & \begin{Bmatrix} \pi\rho A_{h_1h_1}+M_1 \\ -M_1\left(1+ig_{h_1}\right)\left(\dfrac{\omega_{h_1}}{\omega}\right)^2 \end{Bmatrix} & \pi\rho A_{h_1h_2} & \pi\rho A_{h_1h_3} & \pi\rho A_{h_1\alpha_0}+S_{\alpha_{10}} & \pi\rho A_{h_1\alpha_1}+S_{\alpha_{11}} & \pi\rho A_{h_1\beta_0}+S_{\beta_{10}} & \pi\rho A_{h_1\beta_1}+S_{\beta_{11}} \\
\pi\rho A_{h_2h_0} & \pi\rho A_{h_2h_1} & \begin{Bmatrix} \pi\rho A_{h_2h_2}+M_2 \\ -M_2\left(1+ig_{h_2}\right)\left(\dfrac{\omega_{h_2}}{\omega}\right)^2 \end{Bmatrix} & \pi\rho A_{h_2h_3} & \pi\rho A_{h_2\alpha_0}+S_{\alpha_{20}} & \pi\rho A_{h_2\alpha_1}+S_{\alpha_{21}} & \pi\rho A_{h_2\beta_0}+S_{\beta_{20}} & \pi\rho A_{h_2\beta_1}+S_{\beta_{21}} \\
\pi\rho A_{h_3h_0} & \pi\rho A_{h_3h_1} & \pi\rho A_{h_3h_1} & \begin{Bmatrix} \pi\rho A_{h_3h_3}+M_3 \\ -M_3\left(1+ig_{h_3}\right)\left(\dfrac{\omega_{h_3}}{\omega}\right)^2 \end{Bmatrix} & \pi\rho A_{h_3\alpha_0}+S_{\alpha_{30}} & \pi\rho A_{h_3\alpha_1}+S_{\alpha_{31}} & \pi\rho A_{h_3\beta_0}+S_{\beta_{30}} & \pi\rho A_{h_3\beta_1}+S_{\beta_{31}} \\
\pi\rho A_{\alpha_0h_0}+S_{\alpha_{00}} & \pi\rho A_{\alpha_0h_1}+S_{\alpha_{10}} & \pi\rho A_{\alpha_0h_2}+S_{\alpha_{20}} & \pi\rho A_{\alpha_0h_3}+S_{\alpha_{30}} & \begin{Bmatrix} \pi\rho A_{\alpha_0\alpha_0}+I_{\alpha_0} \\ -I_{\alpha_0}\left(1+ig_{\alpha_0}\right)\left(\dfrac{\omega_{\alpha_0}}{\omega}\right)^2 \end{Bmatrix} & \pi\rho A_{\alpha_0\alpha_1} & \pi\rho A_{\alpha_0\beta_0}+P_{\alpha_0\beta_0} & \pi\rho A_{\alpha_0\beta_1}+P_{\alpha_0\beta_1} \\
\pi\rho A_{\alpha_1h_0}+S_{\alpha_{01}} & \pi\rho A_{\alpha_1h_1}+S_{\alpha_{11}} & \pi\rho A_{\alpha_1h_2}+S_{\alpha_{21}} & \pi\rho A_{\alpha_1h_3}+S_{\alpha_{31}} & \pi\rho A_{\alpha_1\alpha_0} & \begin{Bmatrix} \pi\rho A_{\alpha_1\alpha_1}+I_{\alpha_1} \\ -I_{\alpha_1}\left(1+ig_{\alpha_1}\right)\left(\dfrac{\omega_{\alpha_1}}{\omega}\right)^2 \end{Bmatrix} & \pi\rho A_{\alpha_1\beta_0}+P_{\alpha_1\beta_0} & \pi\rho A_{\alpha_1\beta_1}+P_{\alpha_1\beta_1} \\
\pi\rho A_{\beta_0h_0}+S_{\beta_{00}} & \pi\rho A_{\beta_0h_1}+S_{\beta_{10}} & \pi\rho A_{\beta_0h_2}+S_{\beta_{20}} & \pi\rho A_{\beta_0h_3}+S_{\beta_{30}} & \pi\rho A_{\beta_0\alpha_0}+P_{\alpha_0\beta_0} & \pi\rho A_{\beta_0\alpha_1}+P_{\alpha_0\beta_0} & \begin{Bmatrix} \pi\rho A_{\beta_0\beta_0}+I_{\beta_0} \\ -I_{\beta_0}\left(1+ig_{\beta_0}\right)\left(\dfrac{\omega_{\beta_0}}{\omega}\right)^2 \end{Bmatrix} & \pi\rho A_{\beta_0\beta_1} \\
\pi\rho A_{\beta_1h_0}+S_{\beta_{01}} & \pi\rho A_{\beta_1h_1}+S_{\beta_{11}} & \pi\rho A_{\beta_1h_2}+S_{\beta_{21}} & \pi\rho A_{\beta_1h_3}+S_{\beta_{31}} & \pi\rho A_{\beta_1\alpha_0}+P_{\alpha_0\beta_1} & \pi\rho A_{\beta_1\alpha_1}+P_{\alpha_1\beta_1} & \pi\rho A_{\beta_1\beta_0} & \begin{Bmatrix} \pi\rho A_{\beta_1\beta_1}+I_{\beta_1} \\ -I_{\beta_1}\left(1+ig_{\beta_1}\right)\left(\dfrac{\omega_{\beta_1}}{\omega}\right)^2 \end{Bmatrix}
\end{bmatrix}
\begin{bmatrix} h_0 \\ h_1 \\ h_2 \\ h_3 \\ \alpha_0 \\ \alpha_1 \\ \beta_0 \\ \beta_1 \end{bmatrix} = 0
\tag{278}
$$

B. SOLVING THE EIGENVALUE PROBLEM

It can be seen that equation (278) is a set of complex homogenous equations where the primary variable is the flutter frequency (ω). Unfortunately, the blade structural damping coefficients in equation (278) are not easily obtained. To overcome this problem, Smilg and Wasserman [Ref. 45] suggest a method that effectively equates the damping coefficients, $g_{h_0} = g_{h_1} = g_{h_2} = g_{h_3} = g_{\alpha_0} = g_{\alpha_1} = g_{\beta_0} = g_{\beta_1} = g$. By examining equation (278) it can be seen that the flutter frequency and the structural damping always appear together. Therefore, arbitrarily defining a combined variable of frequency and damping as

$$Z = \left(\frac{\omega_{\alpha_1}}{\omega} \right)^2 \left(1 + ig\right), \tag{279}$$

then for a given value of the reduced frequency, *k*, equation (278) can be written in the form $\left(\overline{A} - IZ\right)X = 0$. The choice of the definition of the variable Z is somewhat arbitrary, but it is a complex quantity that has a ratio of a reference frequency to the flutter frequency in its real part and a product of the flutter frequency and the damping coefficient in the imaginary part. Since the first torsional frequency is used as the reference frequency for determining whether or not to include a mode, it becomes the most logical choice as the reference frequency for *Z*. Equation (278) can now be rewritten as

$$\begin{vmatrix}
\overline{A}_{h_0h_0} - Z & \overline{A}_{h_0h_1} & \overline{A}_{h_0h_2} & \overline{A}_{h_0h_3} & \overline{A}_{h_0\alpha_0} & \overline{A}_{h_0\alpha_1} & \overline{A}_{h_0\beta_0} & \overline{A}_{h_0\beta_1} \\
\overline{A}_{h_1h_0} & \overline{A}_{h_1h_1} - Z & \overline{A}_{h_1h_2} & \overline{A}_{h_1h_3} & \overline{A}_{h_1\alpha_0} & \overline{A}_{h_1\alpha_1} & \overline{A}_{h_1\beta_0} & \overline{A}_{h_1\beta_1} \\
\overline{A}_{h_2h_0} & \overline{A}_{h_2h_1} & \overline{A}_{h_2h_2} - Z & \overline{A}_{h_2h_3} & \overline{A}_{h_2\alpha_0} & \overline{A}_{h_2\alpha_1} & \overline{A}_{h_2\beta_0} & \overline{A}_{h_2\beta_1} \\
\overline{A}_{h_3h_0} & \overline{A}_{h_3h_1} & \overline{A}_{h_3h_2} & \overline{A}_{h_3h_3} - Z & \overline{A}_{h_3\alpha_0} & \overline{A}_{h_3\alpha_1} & \overline{A}_{h_3\beta_0} & \overline{A}_{h_3\beta_1} \\
\overline{A}_{\alpha_0h_0} & \overline{A}_{\alpha_0h_1} & \overline{A}_{\alpha_0h_2} & \overline{A}_{\alpha_0h_3} & \overline{A}_{\alpha_0\alpha_0} - Z & \overline{A}_{\alpha_0\alpha_1} & \overline{A}_{\alpha_0\beta_0} & \overline{A}_{\alpha_0\beta_1} \\
\overline{A}_{\alpha_1h_0} & \overline{A}_{\alpha_1h_1} & \overline{A}_{\alpha_1h_2} & \overline{A}_{\alpha_1h_3} & \overline{A}_{\alpha_1\alpha_0} & \overline{A}_{\alpha_1\alpha_1} - Z & \overline{A}_{\alpha_1\beta_0} & \overline{A}_{\alpha_1\beta_1} \\
\overline{A}_{\beta_0h_0} & \overline{A}_{\beta_0h_1} & \overline{A}_{\beta_0h_2} & \overline{A}_{\beta_0h_3} & \overline{A}_{\beta_0\alpha_0} & \overline{A}_{\beta_0\alpha_1} & \overline{A}_{\beta_0\beta_0} - Z & \overline{A}_{\beta_0\beta_1} \\
\overline{A}_{\beta_1h_0} & \overline{A}_{\beta_1h_1} & \overline{A}_{\beta_1h_2} & \overline{A}_{\beta_1h_3} & \overline{A}_{\beta_1\alpha_0} & \overline{A}_{\beta_1\alpha_1} & \overline{A}_{\beta_1\beta_0} & \overline{A}_{\beta_1\beta_1} - Z
\end{vmatrix} = 0 \tag{280}$$

where the determinant elements of equation (280) are defined as:

$$\bar{A}_{h_0h_0} = \left(\frac{\pi\rho A_{h_0h_0}}{M_0} + 1 \right) \left(\frac{\omega_{\alpha_1}}{\omega_{h_0}} \right)^2 \tag{281}$$

$$\bar{A}_{h_0h_1} = \left(\frac{\pi\rho A_{h_0h_1}}{M_0} \right) \left(\frac{\omega_{\alpha_1}}{\omega_{h_0}} \right)^2 \tag{282}$$

$$\bar{A}_{h_0h_2} = \left(\frac{\pi\rho A_{h_0h_2}}{M_0} \right) \left(\frac{\omega_{\alpha_1}}{\omega_{h_0}} \right)^2 \tag{283}$$

$$\bar{A}_{h_0h_3} = \left(\frac{\pi\rho A_{h_0h_3}}{M_0} \right) \left(\frac{\omega_{\alpha_1}}{\omega_{h_0}} \right)^2 \tag{284}$$

$$\bar{A}_{h_0\alpha_0} = \left(\frac{\pi\rho A_{h_0\alpha_0} + S_{\alpha_{00}}}{M_0} \right) \left(\frac{\omega_{\alpha_1}}{\omega_{h_0}} \right)^2 \tag{285}$$

$$\bar{A}_{h_0\alpha_1} = \left(\frac{\pi\rho A_{h_0\alpha_1} + S_{\alpha_{01}}}{M_0} \right) \left(\frac{\omega_{\alpha_1}}{\omega_{h_0}} \right)^2 \tag{286}$$

$$\bar{A}_{h_0\beta_0} = \left(\frac{\pi\rho A_{h_0\beta_0} + S_{\beta_{00}}}{M_0} \right) \left(\frac{\omega_{\alpha_1}}{\omega_{h_0}} \right)^2 \tag{287}$$

$$\bar{A}_{h_0\beta_1} = \left(\frac{\pi\rho A_{h_0\beta_1} + S_{\beta_{01}}}{M_0} \right) \left(\frac{\omega_{\alpha_1}}{\omega_{h_0}} \right)^2 \tag{288}$$

$$\bar{A}_{h_1h_0} = \left(\frac{\pi\rho A_{h_1h_0}}{M_1} \right) \left(\frac{\omega_{\alpha_1}}{\omega_{h_1}} \right)^2 \tag{289}$$

$$\bar{A}_{h_1h_1} = \left(\frac{\pi\rho A_{h_1h_1}}{M_1} + 1 \right) \left(\frac{\omega_{\alpha_1}}{\omega_{h_1}} \right)^2 \tag{290}$$

$$\bar{A}_{h_1h_2} = \left(\frac{\pi\rho A_{h_1h_2}}{M_1} \right) \left(\frac{\omega_{\alpha_1}}{\omega_{h_1}} \right)^2 \tag{291}$$

$$\bar{A}_{h_1h_3} = \left(\frac{\pi\rho A_{h_1h_3}}{M_1} \right) \left(\frac{\omega_{\alpha_1}}{\omega_{h_1}} \right)^2 \tag{292}$$

$$\bar{A}_{h_1\alpha_0} = \left(\frac{\pi\rho A_{h_1\alpha_0} + S_{\alpha_{10}}}{M_1} \right) \left(\frac{\omega_{\alpha_1}}{\omega_{h_1}} \right)^2 \tag{293}$$

$$\bar{A}_{h_1\alpha_1} = \left(\frac{\pi\rho A_{h_1\alpha_1} + S_{\alpha_{11}}}{M_1} \right) \left(\frac{\omega_{\alpha_1}}{\omega_{h_1}} \right)^2 \tag{294}$$

$$\bar{A}_{h_1\beta_0} = \left(\frac{\pi\rho A_{h_1\beta_0} + S_{\beta_{10}}}{M_1} \right) \left(\frac{\omega_{\alpha_1}}{\omega_{h_1}} \right)^2 \tag{295}$$

$$\bar{A}_{h_1\beta_1} = \left(\frac{\pi\rho A_{h_1\beta_1} + S_{\beta_{11}}}{M_1} \right) \left(\frac{\omega_{\alpha_1}}{\omega_{h_1}} \right)^2 \tag{296}$$

$$\bar{A}_{h_2h_0} = \left(\frac{\pi\rho A_{h_2h_0}}{M_2} \right) \left(\frac{\omega_{\alpha_1}}{\omega_{h_2}} \right)^2 \tag{297}$$

$$\bar{A}_{h_2h_1} = \left(\frac{\pi\rho A_{h_2h_1}}{M_2} \right) \left(\frac{\omega_{\alpha_1}}{\omega_{h_2}} \right)^2 \tag{298}$$

$$\bar{A}_{h_2h_2} = \left(\frac{\pi\rho A_{h_2h_2}}{M_2} + 1 \right) \left(\frac{\omega_{\alpha_1}}{\omega_{h_2}} \right)^2 \tag{299}$$

$$\bar{A}_{h_2h_3} = \left(\frac{\pi\rho A_{h_2h_3}}{M_2} \right) \left(\frac{\omega_{\alpha_1}}{\omega_{h_2}} \right)^2 \tag{300}$$

$$\bar{A}_{h_2\alpha_0} = \left(\frac{\pi\rho A_{h_2\alpha_0} + S_{\alpha_{20}}}{M_2} \right) \left(\frac{\omega_{\alpha_1}}{\omega_{h_2}} \right)^2 \tag{301}$$

$$\overline{A}_{h_2\alpha_1} = \left(\frac{\pi\rho A_{h_2\alpha_1} + S_{\alpha_{21}}}{M_2} \right) \left(\frac{\omega_{\alpha_1}}{\omega_{h_2}} \right)^2 \tag{302}$$

$$\overline{A}_{h_2\beta_0} = \left(\frac{\pi\rho A_{h_2\beta_0} + S_{\beta_{20}}}{M_2} \right) \left(\frac{\omega_{\alpha_1}}{\omega_{h_2}} \right)^2 \tag{303}$$

$$\overline{A}_{h_2\beta_1} = \left(\frac{\pi\rho A_{h_2\beta_1} + S_{\beta_{21}}}{M_2} \right) \left(\frac{\omega_{\alpha_1}}{\omega_{h_2}} \right)^2 \tag{304}$$

$$\overline{A}_{h_3h_0} = \left(\frac{\pi\rho A_{h_3h_0}}{M_3} \right) \left(\frac{\omega_{\alpha_1}}{\omega_{h_3}} \right)^2 \tag{305}$$

$$\overline{A}_{h_3h_1} = \left(\frac{\pi\rho A_{h_3h_1}}{M_3} \right) \left(\frac{\omega_{\alpha_1}}{\omega_{h_3}} \right)^2 \tag{306}$$

$$\overline{A}_{h_3h_2} = \left(\frac{\pi\rho A_{h_3h_2}}{M_3} \right) \left(\frac{\omega_{\alpha_1}}{\omega_{h_3}} \right)^2 \tag{307}$$

$$\overline{A}_{h_3h_3} = \left(\frac{\pi\rho A_{h_3h_3}}{M_3} + 1 \right) \left(\frac{\omega_{\alpha_1}}{\omega_{h_3}} \right)^2 \tag{308}$$

$$\overline{A}_{h_3\alpha_0} = \left(\frac{\pi\rho A_{h_3\alpha_0} + S_{\alpha_{30}}}{M_3} \right) \left(\frac{\omega_{\alpha_1}}{\omega_{h_3}} \right)^2 \tag{309}$$

$$\overline{A}_{h_3\alpha_1} = \left(\frac{\pi\rho A_{h_3\alpha_1} + S_{\alpha_{31}}}{M_3} \right) \left(\frac{\omega_{\alpha_1}}{\omega_{h_3}} \right)^2 \tag{310}$$

$$\overline{A}_{h_3\beta_0} = \left(\frac{\pi\rho A_{h_3\beta_0} + S_{\beta_{30}}}{M_3} \right) \left(\frac{\omega_{\alpha_1}}{\omega_{h_3}} \right)^2 \tag{311}$$

$$\overline{A}_{h_3\beta_1} = \left(\frac{\pi\rho A_{h_3\beta_1} + S_{\beta_{31}}}{M_3} \right) \left(\frac{\omega_{\alpha_1}}{\omega_{h_3}} \right)^2 \tag{312}$$

$$\overline{A}_{\alpha_0 h_0} = \left(\frac{\pi\rho A_{\alpha_0 h_0} + S_{\alpha_{00}}}{I_{\alpha_0}} \right) \left(\frac{\omega_{\alpha_1}}{\omega_{\alpha_0}} \right)^2 \tag{313}$$

$$\overline{A}_{\alpha_0 h_1} = \left(\frac{\pi\rho A_{\alpha_0 h_1} + S_{\alpha_{10}}}{I_{\alpha_0}} \right) \left(\frac{\omega_{\alpha_1}}{\omega_{\alpha_0}} \right)^2 \tag{314}$$

$$\overline{A}_{\alpha_0 h_2} = \left(\frac{\pi\rho A_{\alpha_0 h_2} + S_{\alpha_{20}}}{I_{\alpha_0}} \right) \left(\frac{\omega_{\alpha_1}}{\omega_{\alpha_0}} \right)^2 \tag{315}$$

$$\overline{A}_{\alpha_0 h_3} = \left(\frac{\pi\rho A_{\alpha_0 h_3} + S_{\alpha_{30}}}{I_{\alpha_0}} \right) \left(\frac{\omega_{\alpha_1}}{\omega_{\alpha_0}} \right)^2 \tag{316}$$

$$\overline{A}_{\alpha_0 \alpha_0} = \left(\frac{\pi\rho A_{\alpha_0 \alpha_0}}{I_{\alpha_0}} + 1 \right) \left(\frac{\omega_{\alpha_1}}{\omega_{\alpha_0}} \right)^2 \tag{317}$$

$$\overline{A}_{\alpha_0 \alpha_1} = \left(\frac{\pi\rho A_{\alpha_0 \alpha_1}}{I_{\alpha_0}} \right) \left(\frac{\omega_{\alpha_1}}{\omega_{\alpha_0}} \right)^2 \tag{318}$$

$$\overline{A}_{\alpha_0 \beta_0} = \left(\frac{\pi\rho A_{\alpha_0 \beta_0} + P_{\alpha_0 \beta_0}}{I_{\alpha_0}} \right) \left(\frac{\omega_{\alpha_1}}{\omega_{\alpha_0}} \right)^2 \tag{319}$$

$$\overline{A}_{\alpha_0 \beta_1} = \left(\frac{\pi\rho A_{\alpha_0 \beta_1} + P_{\alpha_0 \beta_1}}{I_{\alpha_0}} \right) \left(\frac{\omega_{\alpha_1}}{\omega_{\alpha_0}} \right)^2 \tag{320}$$

$$\overline{A}_{\alpha_1 h_0} = \left(\frac{\pi\rho A_{\alpha_1 h_0} + S_{\alpha_{01}}}{I_{\alpha_1}} \right) \tag{321}$$

$$\overline{A}_{\alpha_1 h_1} = \left(\frac{\pi\rho A_{\alpha_1 h_1} + S_{\alpha_{11}}}{I_{\alpha_1}} \right) \tag{322}$$

$$\overline{A}_{\alpha_1 h_2} = \left(\frac{\pi\rho A_{\alpha_1 h_2} + S_{\alpha_{21}}}{I_{\alpha_1}} \right) \tag{323}$$

$$\bar{A}_{\alpha_1 h_3} = \left(\frac{\pi\rho A_{\alpha_1 h_3} + S_{\alpha_{31}}}{I_{\alpha_1}} \right) \tag{324}$$

$$\bar{A}_{\alpha_1 \alpha_0} = \left(\frac{\pi\rho A_{\alpha_1 \alpha_0}}{I_{\alpha_1}} \right) \tag{325}$$

$$\bar{A}_{\alpha_1 \alpha_1} = \left(\frac{\pi\rho A_{\alpha_1 \alpha_1}}{I_{\alpha_1}} + 1 \right) \tag{326}$$

$$\bar{A}_{\alpha_1 \beta_0} = \left(\frac{\pi\rho A_{\alpha_1 \beta_0} + P_{\alpha_1 \beta_0}}{I_{\alpha_1}} \right) \tag{327}$$

$$\bar{A}_{\alpha_1 \beta_1} = \left(\frac{\pi\rho A_{\alpha_1 \beta_1} + P_{\alpha_1 \beta_1}}{I_{\alpha_1}} \right) \tag{328}$$

$$\bar{A}_{\beta_0 h_0} = \left(\frac{\pi\rho A_{\beta_0 h_0} + S_{\beta_{00}}}{I_{\beta_0}} \right) \left(\frac{\omega_{\alpha_1}}{\omega_{\beta_0}} \right)^2 \tag{329}$$

$$\bar{A}_{\beta_0 h_1} = \left(\frac{\pi\rho A_{\beta_0 h_1} + S_{\beta_{10}}}{I_{\beta_0}} \right) \left(\frac{\omega_{\alpha_1}}{\omega_{\beta_0}} \right)^2 \tag{330}$$

$$\bar{A}_{\beta_0 h_2} = \left(\frac{\pi\rho A_{\beta_0 h_2} + S_{\beta_{20}}}{I_{\beta_0}} \right) \left(\frac{\omega_{\alpha_1}}{\omega_{\beta_0}} \right)^2 \tag{331}$$

$$\bar{A}_{\beta_0 h_3} = \left(\frac{\pi\rho A_{\beta_0 h_3} + S_{\beta_{30}}}{I_{\beta_0}} \right) \left(\frac{\omega_{\alpha_1}}{\omega_{\beta_0}} \right)^2 \tag{332}$$

$$\bar{A}_{\beta_0 \alpha_0} = \left(\frac{\pi\rho A_{\beta_0 \alpha_0} + P_{\alpha_0 \beta_0}}{I_{\beta_0}} \right) \left(\frac{\omega_{\alpha_1}}{\omega_{\beta_0}} \right)^2 \tag{333}$$

$$\bar{A}_{\beta_0 \alpha_1} = \left(\frac{\pi\rho A_{\beta_0 \alpha_1} + P_{\alpha_1 \beta_0}}{I_{\beta_0}} \right) \left(\frac{\omega_{\alpha_1}}{\omega_{\beta_0}} \right)^2 \tag{334}$$

$$\bar{A}_{\beta_0\beta_0} = \left(\frac{\pi\rho A_{\beta_0\beta_0}}{I_{\beta_0}} + 1 \right) \left(\frac{\omega_{\alpha_1}}{\omega_{\beta_0}} \right)^2 \tag{335}$$

$$\bar{A}_{\beta_0\beta_1} = \left(\frac{\pi\rho A_{\beta_0\beta_1}}{I_{\beta_0}} \right) \left(\frac{\omega_{\alpha_1}}{\omega_{\beta_0}} \right)^2 \tag{336}$$

$$\bar{A}_{\beta_1 h_0} = \left(\frac{\pi\rho A_{\beta_1 h_0} + S_{\beta_{01}}}{I_{\beta_1}} \right) \left(\frac{\omega_{\alpha_1}}{\omega_{\beta_1}} \right)^2 \tag{337}$$

$$\bar{A}_{\beta_1 h_1} = \left(\frac{\pi\rho A_{\beta_1 h_1} + S_{\beta_{11}}}{I_{\beta_1}} \right) \left(\frac{\omega_{\alpha_1}}{\omega_{\beta_1}} \right)^2 \tag{338}$$

$$\bar{A}_{\beta_1 h_2} = \left(\frac{\pi\rho A_{\beta_1 h_2} + S_{\beta_{21}}}{I_{\beta_1}} \right) \left(\frac{\omega_{\alpha_1}}{\omega_{\beta_1}} \right)^2 \tag{339}$$

$$\bar{A}_{\beta_1 h_3} = \left(\frac{\pi\rho A_{\beta_1 h_3} + S_{\beta_{31}}}{I_{\beta_1}} \right) \left(\frac{\omega_{\alpha_1}}{\omega_{\beta_1}} \right)^2 \tag{340}$$

$$\bar{A}_{\beta_1\alpha_0} = \left(\frac{\pi\rho A_{\beta_1\alpha_0} + P_{\alpha_0\beta_1}}{I_{\beta_1}} \right) \left(\frac{\omega_{\alpha_1}}{\omega_{\beta_1}} \right)^2 \tag{341}$$

$$\bar{A}_{\beta_1\alpha_1} = \left(\frac{\pi\rho A_{\beta_1\alpha_1} + P_{\alpha_1\beta_1}}{I_{\beta_1}} \right) \left(\frac{\omega_{\alpha_1}}{\omega_{\beta_1}} \right)^2 \tag{342}$$

$$\bar{A}_{\beta_1\beta_0} = \left(\frac{\pi\rho A_{\beta_1\beta_0}}{I_{\beta_1}} \right) \left(\frac{\omega_{\alpha_1}}{\omega_{\beta_1}} \right)^2 \tag{343}$$

$$\bar{A}_{\beta_1\beta_1} = \left(\frac{\pi\rho A_{\beta_1\beta_1}}{I_{\beta_1}} + 1 \right) \left(\frac{\omega_{\alpha_1}}{\omega_{\beta_1}} \right)^2 , \tag{344}$$

and the $A_{h_0 h_0}$ through $A_{\beta_1\beta_1}$ terms are defined by equations (197) through (260).

It should be noted that the coefficients of the characteristic equation ($\bar{A}$ terms) of the $\left(\bar{A} - IZ\right)$ matrix (an 8th order polynomial in *Z*) are complex, due to the lift deficiency

function which is imbedded in the aerodynamic coefficients listed in equations (63) through (78). Therefore, the eigenvalues will be complex, and not necessarily complex conjugate pairs. Since the first torsional natural frequency is already known, the coupled frequency of oscillation (ω_i) for each eigenvalue can be found from the real part of Z given, or

$$\omega_i = \frac{\omega_{\alpha_1}}{\sqrt{\mathrm{Re}(Z)}} \tag{345}$$

The natural frequency must be positive and real, and therefore an eigenvalue with a negative real part is not permissible, otherwise there would be no physical significance to equation (345). For the example rotor blade it will be shown that all the eigenvalues have a positive real part.

Once the natural frequency is obtained for each eigenvalue (ω_i), the damping coefficient required for flutter to exist (g_i) for each eigenvalue can be found from the imaginary part of Z in equation (279), or

$$g_i = \mathrm{Im}(Z)\left(\frac{\omega_i}{\omega_{\alpha_1}}\right)^2 \tag{346}$$

If g is negative for the reduced frequency chosen, then damping must be decreased in order to obtain neutral stability. Negative values of g represent the stable, or non-flutter, condition. Thus, eigenvalues with a negative imaginary part are stable solutions. If g is positive, then damping must be increased to obtain neutral stability. Positive values of g represent the unstable, or flutter condition, and eigenvalues with a positive imaginary part are unstable solutions. When a plot of g is made against $1/k$ (k being reduce frequency), there will be curves corresponding to the variation of each eigenvalue as the reduced frequency varies. Some of these curves will have only values of g that are negative. These are the non-critical curves that represent stable coupled modes and do not influence the flutter solution. However in most cases, at least one curve will start with a negative value of g and then at some point cross the abscissa ($1/k$) to a positive value of

g. This curve is called the critical curve, and the value of $1/k$ where this curve crosses the abscissa represents the critical flutter speed, or flutter point. The critical flutter speed is found from the relationship:

$$v_{FL} = \frac{\omega_{crit} b}{k_{crit}} \tag{347}$$

where ω_{crit} is found from equation (345) for the critical curve evaluated at the reduced frequency that corresponds to the crossover point (k_{crit}). Results are commonly plotted as g vs. v instead of g vs. $1/k$ with the critical and noncritical curves identified in the same manner described above.

For fixed-wing aircraft, the velocity seen by the wing is constant along the span of the wing, and a g-v plot makes sense because the reduced frequency is also constant along the wing. However, for a rotor blade, the velocity is a function of the rotor span ($v = \Omega r$), and the reduced frequency, defined by equation (87), is also a function of rotor span. Therefore, to eliminate the rotor span dependency of the g-v plots, the rotational velocity ($\Omega = v/r$) will be used, and plots of g vs. Ω will be made.

C. STRIP THEORY AND LUMPED PARAMETER SYSTEM

Since the true structural properties of typical rotor blades often contain discontinuities, the integrals in the $A_{h_0 h_0}$ through $A_{\beta_1 \beta_1}$ terms defined in equations (197) through (260) and used in equations (281) through (344) may not have closed-form solutions. To overcome this problem, strip theory and a lumped-mass, transfer matrix method similar to that applied for the Holzer and Myklestad methods can be used by replacing the integrals in equations (197) through (260) with summations. The rotor blade can be divided into a convenient number of segments with the mass of each segment divided by two and concentrated at each end of the segment. A massless, flexible connection is made between the concentrated masses with structural elastic properties that are averaged over the segment length. The integrals from e_R to R in equations (197) through (260) have summations along all segments while the integrals from r_1 to r_2 are summed only along the segments that have the trailing-edge flap

incorporated. If it is assumed that there are N segments with the trailing-edge flap located from segments n_1 to n_2, equations (197) through (260) can be written as:

$$A_{h_0h_0} = \sum_{n=1}^{N} b_n^2 \left[f_0(y) \right]_n^2 (L_h)_n \tag{348}$$

$$A_{h_0h_1} = \sum_{n=1}^{N} b_n^2 f_0(y)_n \, f_1(y)_n (L_h)_n \tag{349}$$

$$A_{h_0h_2} = \sum_{n=1}^{N} b_n^2 f_0(y)_n \, f_2(y)_n (L_h)_n \tag{350}$$

$$A_{h_0h_3} = \sum_{n=1}^{N} b_n^2 f_0(y)_n \, f_3(y)_n (L_h)_n \tag{351}$$

$$A_{h_0\alpha_0} = \sum_{n=1}^{N} b_n^3 f_0(y)_n \, F_0(y)_n \left[(L_\alpha)_n - \left(\frac{1}{2} + a_n \right) (L_h)_n \right] \tag{352}$$

$$A_{h_0\alpha_1} = \sum_{n=1}^{N} b_n^3 f_0(y)_n \, F_1(y)_n \left[(L_\alpha)_n - \left(\frac{1}{2} + a_n \right) (L_h)_n \right] \tag{353}$$

$$A_{h_0\beta_0} = \sum_{n=n_1}^{n_2} b_n^3 f_0(y)_n \, G_0(y)_n \left[(L_\beta)_n - (c_n - e_n)(L_z)_n \right] \tag{354}$$

$$A_{h_0\beta_1} = \sum_{n=n_1}^{n_2} b_n^3 f_0(y)_n \, G_1(y)_n \left[(L_\beta)_n - (c_n - e_n)(L_z)_n \right] \tag{355}$$

$$A_{h_1h_0} = \sum_{n=1}^{N} b_n^2 f_1(y)_n \, f_0(y)_n (L_h)_n = A_{h_0h_1} \tag{356}$$

$$A_{h_1h_1} = \sum_{n=1}^{N} b_n^2 \left[f_1(y) \right]_n^2 (L_h)_n \tag{357}$$

$$A_{h_1h_2} = \sum_{n=1}^{N} b_n^2 f_1(y)_n \, f_2(y)_n (L_h)_n \tag{358}$$

$$A_{h_1h_3} = \sum_{n=1}^{N} b_n^2 f_1(y)_n \, f_3(y)_n \, (L_h)_n \tag{359}$$

$$A_{h_1\alpha_0} = \sum_{n=1}^{N} b_n^3 f_1(y)_n \, F_0(y)_n \left[(L_\alpha)_n - \left(\frac{1}{2} + a_n \right) (L_h)_n \right] \tag{360}$$

$$A_{h_1\alpha_1} = \sum_{n=1}^{N} b_n^3 f_1(y)_n \, F_1(y)_n \left[(L_\alpha)_n - \left(\frac{1}{2} + a_n \right) (L_h)_n \right] \tag{361}$$

$$A_{h_1\beta_0} = \sum_{n=n_1}^{n_2} b_n^3 f_1(y)_n \, G_0(y)_n \left[(L_\beta)_n - (c_n - e_n)(L_z)_n \right] \tag{362}$$

$$A_{h_1\beta_1} = \sum_{n=n_1}^{n_2} b_n^3 f_1(y)_n \, G_1(y)_n \left[(L_\beta)_n - (c_n - e_n)(L_z)_n \right] \tag{363}$$

$$A_{h_2h_0} = \sum_{n=1}^{N} b_n^2 f_2(y)_n \, f_0(y)_n \, (L_h)_n = A_{h_0h_2} \tag{364}$$

$$A_{h_2h_1} = \sum_{n=1}^{N} b_n^2 f_2(y)_n \, f_1(y)_n \, (L_h)_n = A_{h_1h_2} \tag{365}$$

$$A_{h_2h_2} = \sum_{n=1}^{N} b_n^2 \left[f_2(y) \right]_n^2 (L_h)_n \tag{366}$$

$$A_{h_2h_3} = \sum_{n=1}^{N} b_n^2 f_2(y)_n \, f_3(y)_n \, (L_h)_n \tag{367}$$

$$A_{h_2\alpha_0} = \sum_{n=1}^{N} b_n^3 f_2(y)_n \, F_0(y)_n \left[(L_\alpha)_n - \left(\frac{1}{2} + a_n \right) (L_h)_n \right] \tag{368}$$

$$A_{h_2\alpha_1} = \sum_{n=1}^{N} b_n^3 f_2(y)_n \, F_1(y)_n \left[(L_\alpha)_n - \left(\frac{1}{2} + a_n \right) (L_h)_n \right] \tag{369}$$

$$A_{h_2\beta_0} = \sum_{n=n_1}^{n_2} b_n^3 f_2(y)_n \, G_0(y)_n \left[(L_\beta)_n - (c_n - e_n)(L_z)_n \right] \tag{370}$$

$$A_{h_2\beta_1} = \sum_{n=n_1}^{n_2} b_n^3 f_2(y)_n \, G_1(y)_n \left[\left(L_\beta\right)_n - \left(c_n - e_n\right)\left(L_z\right)_n \right] \tag{371}$$

$$A_{h_3h_0} = \sum_{n=1}^{N} b_n^2 f_3(y)_n \, f_0(y)_n \left(L_h\right)_n = A_{h_0h_3} \tag{372}$$

$$A_{h_3h_1} = \sum_{n=1}^{N} b_n^2 f_3(y)_n \, f_1(y)_n \left(L_h\right)_n = A_{h_1h_3} \tag{373}$$

$$A_{h_3h_2} = \sum_{n=1}^{N} b_n^2 f_3(y)_n \, f_2(y)_n \left(L_h\right)_n = A_{h_2h_3} \tag{374}$$

$$A_{h_3h_3} = \sum_{n=1}^{N} b_n^2 \left[f_3(y) \right]_n^2 \left(L_h\right)_n \tag{375}$$

$$A_{h_3\alpha_0} = \sum_{n=1}^{N} b_n^3 f_3(y)_n \, F_0(y)_n \left[\left(L_\alpha\right)_n - \left(\frac{1}{2} + a_n\right)\left(L_h\right)_n \right] \tag{376}$$

$$A_{h_3\alpha_1} = \sum_{n=1}^{N} b_n^3 f_3(y)_n \, F_1(y)_n \left[\left(L_\alpha\right)_n - \left(\frac{1}{2} + a_n\right)\left(L_h\right)_n \right] \tag{377}$$

$$A_{h_3\beta_0} = \sum_{n=n_1}^{n_2} b_n^3 f_3(y)_n \, G_0(y)_n \left[\left(L_\beta\right)_n - \left(c_n - e_n\right)\left(L_z\right)_n \right] \tag{378}$$

$$A_{h_3\beta_1} = \sum_{n=n_1}^{n_2} b_n^3 f_3(y)_n \, G_1(y)_n \left[\left(L_\beta\right)_n - \left(c_n - e_n\right)\left(L_z\right)_n \right] \tag{379}$$

$$A_{\alpha_0h_0} = \sum_{n=1}^{N} b_n^3 F_0(y)_n \, f_0(y)_n \left[\left(M_h\right)_n - \left(\frac{1}{2} + a_n\right)\left(L_h\right)_n \right] \tag{380}$$

$$A_{\alpha_0h_1} = \sum_{n=1}^{N} b_n^3 F_0(y)_n \, f_1(y)_n \left[\left(M_h\right)_n - \left(\frac{1}{2} + a_n\right)\left(L_h\right)_n \right] \tag{381}$$

$$A_{\alpha_0h_2} = \sum_{n=1}^{N} b_n^3 F_0(y)_n \, f_2(y)_n \left[\left(M_h\right)_n - \left(\frac{1}{2} + a_n\right)\left(L_h\right)_n \right] \tag{382}$$

$$A_{\alpha_0 h_3} = \sum_{n=1}^{N} b_n^3 F_0(y)_n f_3(y)_n \left[(M_h)_n - \left(\frac{1}{2} + a_n \right) (L_h)_n \right] \tag{383}$$

$$A_{\alpha_0 \alpha_0} = \sum_{n=1}^{N} b_n^4 \left[F_0(y) \right]_n^2 \left[(M_\alpha)_n - \left(\frac{1}{2} + a_n \right) \left((L_\alpha)_n + (M_h)_n \right) + \left(\frac{1}{2} + a_n \right)^2 (L_h)_n \right] \tag{384}$$

$$A_{\alpha_0 \alpha_1} = \sum_{n=1}^{N} b_n^4 F_0(y)_n F_1(y)_n \left[(M_\alpha)_n - \left(\frac{1}{2} + a_n \right) \left((L_\alpha)_n + (M_h)_n \right) + \left(\frac{1}{2} + a_n \right)^2 (L_h)_n \right] \tag{385}$$

$$A_{\alpha_0 \beta_0} = \sum_{n=n_1}^{n_2} b_n^4 F_0(y)_n G_0(y)_n \left[(M_\beta)_n - \left(\frac{1}{2} + a_n \right) (L_\beta)_n - (c_n - e_n)(M_z)_n + (c_n - e_n) \left(\frac{1}{2} + a_n \right) (L_z)_n \right] \tag{386}$$

$$A_{\alpha_0 \beta_1} = \sum_{n=n_1}^{n_2} b_n^4 F_0(y)_n G_1(y)_n \left[(M_\beta)_n - \left(\frac{1}{2} + a_n \right) (L_\beta)_n - (c_n - e_n)(M_z)_n + (c_n - e_n) \left(\frac{1}{2} + a_n \right) (L_z)_n \right] \tag{387}$$

$$A_{\alpha_1 h_0} = \sum_{n=1}^{N} b_n^3 F_1(y)_n f_0(y)_n \left[(M_h)_n - \left(\frac{1}{2} + a_n \right) (L_h)_n \right] \tag{388}$$

$$A_{\alpha_1 h_1} = \sum_{n=1}^{N} b_n^3 F_1(y)_n f_1(y)_n \left[(M_h)_n - \left(\frac{1}{2} + a_n \right) (L_h)_n \right] \tag{389}$$

$$A_{\alpha_1 h_2} = \sum_{n=1}^{N} b_n^3 F_1(y)_n f_2(y)_n \left[(M_h)_n - \left(\frac{1}{2} + a_n \right) (L_h)_n \right] \tag{390}$$

$$A_{\alpha_1 h_3} = \sum_{n=1}^{N} b_n^3 F_1(y)_n f_3(y)_n \left[(M_h)_n - \left(\frac{1}{2} + a_n \right) (L_h)_n \right] \tag{391}$$

$$A_{\alpha_1\alpha_0}=\sum_{n=1}^{N}b_n^4F_1(y)_n\,F_0(y)_n\Big[(M_\alpha)_n-\Big(\frac{1}{2}+a_n\Big)\big((L_\alpha)_n+(M_h)_n\big)+\Big(\frac{1}{2}+a_n\Big)^2(L_h)_n\Big]=A_{\alpha_0\alpha_1} \tag{392}$$

$$A_{\alpha_1\alpha_1}=\sum_{n=1}^{N}b_n^4\big[F_1(y)\big]_n^2\Big[(M_\alpha)_n-\Big(\frac{1}{2}+a_n\Big)\big((L_\alpha)_n+(M_h)_n\big)+\Big(\frac{1}{2}+a_n\Big)^2(L_h)_n\Big] \tag{393}$$

$$A_{\alpha_1\beta_0}=\sum_{n=n_1}^{n_2}b_n^4F_1(y)_n\,G_0(y)_n\Big[(M_\beta)_n-\Big(\frac{1}{2}+a_n\Big)(L_\beta)_n-(c_n-e_n)(M_z)_n+(c_n-e_n)\Big(\frac{1}{2}+a_n\Big)(L_z)_n\Big] \tag{394}$$

$$A_{\alpha_1\beta_1}=\sum_{n=n_1}^{n_2}b_n^4F_1(y)_n\,G_1(y)_n\Big[(M_\beta)_n-\Big(\frac{1}{2}+a_n\Big)(L_\beta)_n-(c_n-e_n)(M_z)_n+(c_n-e_n)\Big(\frac{1}{2}+a_n\Big)(L_z)_n\Big] \tag{395}$$

$$A_{\beta_0h_0}=\sum_{n=n_1}^{n_2}b_n^3G_0(y)_n\,f_0(y)_n\big[(T_h)_n-(c_n-e_n)(P_h)_n\big] \tag{396}$$

$$A_{\beta_0h_1}=\sum_{n=n_1}^{n_2}b_n^3G_0(y)_n\,f_1(y)_n\big[(T_h)_n-(c_n-e_n)(P_h)_n\big] \tag{397}$$

$$A_{\beta_0h_2}=\sum_{n=n_1}^{n_2}b_n^3G_0(y)_n\,f_2(y)_n\big[(T_h)_n-(c_n-e_n)(P_h)_n\big] \tag{398}$$

$$A_{\beta_0h_3}=\sum_{n=n_1}^{n_2}b_n^3G_0(y)_n\,f_3(y)_n\big[(T_h)_n-(c_n-e_n)(P_h)_n\big] \tag{399}$$

$$A_{\beta_0\alpha_0}=\sum_{n=n_1}^{n_2}b_n^4G_0(y)_n\,F_0(y)_n\Big[(T_\alpha)_n-(c_n-e_n)(P_\alpha)_n+\Big(\frac{1}{2}+a_n\Big)(T_h)_n+\Big(\frac{1}{2}+a_n\Big)(c_n-e_n)(P_h)_n\Big] \tag{400}$$

$$A_{\beta_0\alpha_1} = \sum_{n=n_1}^{n_2} b_n^4 G_0(y)_n F_1(y)_n \Big[(T_\alpha)_n - (c_n - e_n)(P_\alpha)_n + \left(\frac{1}{2} + a_n\right)(T_h)_n + \left(\frac{1}{2} + a_n\right)(c_n - e_n)(P_h)_n \Big] \tag{401}$$

$$A_{\beta_0\beta_0} = \sum_{n=n_1}^{n_2} b_n^4 \left[G_0(y) \right]_n^2 \Big[(T_\beta)_n - (c_n - e_n)\big((P_\beta)_n + (T_z)_n\big) + (c_n - e_n)^2 (P_z)_n \Big] \tag{402}$$

$$A_{\beta_0\beta_1} = \sum_{n=n_1}^{n_2} b_n^4 G_0(y)_n G_1(y)_n \Big[(T_\beta)_n - (c_n - e_n)\big((P_\beta)_n + (T_z)_n\big) + (c_n - e_n)^2 (P_z)_n \Big] \tag{403}$$

$$A_{\beta_1 h_0} = \sum_{n=n_1}^{n_2} b_n^3 G_1(y)_n f_0(y)_n \Big[(T_h)_n - (c_n - e_n)(P_h)_n \Big] \tag{404}$$

$$A_{\beta_1 h_1} = \sum_{n=n_1}^{n_2} b_n^3 G_1(y)_n f_1(y)_n \Big[(T_h)_n - (c_n - e_n)(P_h)_n \Big] \tag{405}$$

$$A_{\beta_1 h_2} = \sum_{n=n_1}^{n_2} b_n^3 G_1(y)_n f_2(y)_n \Big[(T_h)_n - (c_n - e_n)(P_h)_n \Big] \tag{406}$$

$$A_{\beta_1 h_3} = \sum_{n=n_1}^{n_2} b_n^3 G_1(y)_n f_3(y)_n \Big[(T_h)_n - (c_n - e_n)(P_h)_n \Big] \tag{407}$$

$$A_{\beta_1\alpha_0} = \sum_{n=n_1}^{n_2} b_n^4 G_1(y)_n F_0(y)_n \Big[(T_\alpha)_n - (c_n - e_n)(P_\alpha)_n + \left(\frac{1}{2} + a_n\right)(T_h)_n + \left(\frac{1}{2} + a_n\right)(c_n - e_n)(P_h)_n \Big] \tag{408}$$

$$A_{\beta_1\alpha_1} = \sum_{n=n_1}^{n_2} b_n^4 G_1(y)_n F_1(y)_n \Big[(T_\alpha)_n - (c_n - e_n)(P_\alpha)_n + \left(\frac{1}{2} + a_n\right)(T_h)_n + \left(\frac{1}{2} + a_n\right)(c_n - e_n)(P_h)_n \Big] \tag{409}$$

$$A_{\beta_1\beta_0} = \sum_{n=n_1}^{n_2} b_n^4 G_1(y)_n \, G_0(y)_n \Big[\left(T_\beta\right)_n - \left(c_n - e_n\right)\left(\left(P_\beta\right)_n + \left(T_z\right)_n\right) + \left(c_n - e_n\right)^2 \left(P_z\right)_n \Big] = A_{\beta_0\beta_1} \tag{410}$$

$$A_{\beta_1\beta_1} = \sum_{n=n_1}^{n_2} b_n^4 \left[G_1(y)\right]_n^2 \Big[\left(T_\beta\right)_n - \left(c_n - e_n\right)\left(\left(P_\beta\right)_n + \left(T_z\right)_n\right) + \left(c_n - e_n\right)^2 \left(P_z\right)_n \Big] \tag{411}$$

The bending (f_i), blade torsional (F_i), and flap torsional (G_i) deflections are defined by equations (115), (116) and (117) and found by recursive application of equation (26) for the torsional modes and equation (50) for the bending modes.

IV. EXAMPLE ROTOR BLADE CHARACTERISTICS

Now that the coupled aeroelastic equations of motion have been developed to perform a flutter analysis for rotor blades with trailing-edge flaps in the frequency domain, application of this theory will be made to demonstrate its usefulness. Due to the proprietary rights of many of the current rotor blades under development, it became necessary to develop an example rotor blade that could be used in the analysis to demonstrate the robustness and applicability of the theory. The example rotor blade chosen is a hingeless design that is similar to the rotor blade described in Table B-17 of TRECOM Technical Report 64-15 [Ref. 56], which is modeled after the blade designed for the Sikorsky H-3 (S-61). This rotor blade has a length of 31 feet (R = 31 ft.) and is part of a five-bladed helicopter (N_b = 5) with a gross weight of 16,800 lbs. The primary differences between the TRECOM blade and the example blade is that a 25% chord, trailing-edge flap has been incorporated from station 279 to 334 on the rotor blade, the root end restraint has been modified from an articulated design to a hingeless design, and the mass of the blade has been redistributed to account for added weight of the flap but designed in such a manner that the overall mass of the blade remains the same. Additionally, the c.g. of the rotor blade where the flap has been incorporated has been shifted from 25% chord to 40% chord to show effects of c.g. displacement on the flutter speed. A summary of properties of this example rotor blade is given in Table 2.

Due to the hingeless design assumed for the modified H-3 (S-61) example rotor blade, the full 8DOF system is not needed. The hingeless design eliminates the h_0 and α_0 rigid body motions, and since the 1st torsional frequency of the flap is much greater than 1.2 times the 1st torsional frequency of the blade, the β_1 motion can be neglected. Thus, a 5DOF system will be used for the analyses (h_1, h_2, h_3, α_1 and β_0), and equation (280) can be reduced to

$$\begin{vmatrix} \overline{A}_{h_1h_1} - Z & \overline{A}_{h_1h_2} & \overline{A}_{h_1h_3} & \overline{A}_{h_1\alpha_1} & \overline{A}_{h_1\beta_0} \\ \overline{A}_{h_2h_1} & \overline{A}_{h_2h_2} - Z & \overline{A}_{h_2h_3} & \overline{A}_{h_2\alpha_1} & \overline{A}_{h_2\beta_0} \\ \overline{A}_{h_3h_1} & \overline{A}_{h_3h_2} & \overline{A}_{h_3h_3} - Z & \overline{A}_{h_3\alpha_1} & \overline{A}_{h_3\beta_0} \\ \overline{A}_{\alpha_1h_1} & \overline{A}_{\alpha_1h_2} & \overline{A}_{\alpha_1h_3} & \overline{A}_{\alpha_1\alpha_1} - Z & \overline{A}_{\alpha_1\beta_0} \\ \overline{A}_{\beta_0h_1} & \overline{A}_{\beta_0h_2} & \overline{A}_{\beta_0h_3} & \overline{A}_{\beta_0\alpha_1} & \overline{A}_{\beta_0\beta_0} - Z \end{vmatrix} = 0 \qquad (412)$$

where the determinant elements are defined the same as before in equations (281) through (344). All subsequent g-Ω plots will be based on the 5DOF determinant of equation (412).

Table 2. Example Rotor Blade Sectional Properties

Radius (r_n) (in)	Weight (W_n) (lb_m)	Chord ($2b$) (in)	Flapwise Moment of Inertia (I_{zz}) (in^4)	Flapwise Static Unbalance (S_{zz}) (in^3)	Chordwise Moment of Inertia (I_{xx}) (in^4)
12.63	20.46	8.1	5.0	5.0	26.0
18.6	84.17	8.1	5.0	5.0	26.0
37.2	55.21	8.1	5.0	5.0	26.0
55.8	10.51	8.1	4.4	3.6	35.0
74.4	8.53	8.1	3.04	2.7	30.5
93.0	9.06	18.25	2.91	2.6	29.8
111.6	8.78	18.25	2.8	2.5	29.3
130.2	9.73	18.25	2.71	2.4	28.5
148.8	10.01	18.25	2.6	2.36	28.0
167.4	9.94	18.25	2.51	2.3	27.3
186.0	9.91	18.25	2.45	2.25	27.0
204.6	9.37	18.25	2.35	2.2	24.8
223.2	9.45	18.25	2.29	2.1	24.3
241.8	9.14	18.25	2.19	2.0	24.0
260.4	9.03	18.25	2.1	1.95	23.7
279.0	9.93	18.25	2.04	1.9	20.9
297.6	9.94	18.25	2.0	1.9	20.8
316.2	9.95	18.25	1.99	1.84	20.6
334.8	9.96	18.25	1.95	1.82	20.5
353.4	9.96	18.25	1.93	1.8	20.3
372.0	2.56	18.25	0.97	0.9	10.1

Table 2. (Cont'd)

Radius (r_n) (in)	Chordwise Static Unbalance (S_{xx}) (in^3)	Polar Moment of Inertia (J) (in^4)	Blade Mass Moment of Inertia (I_α) about e.a. (slug-ft)	Flap Mass Moment of Inertia (I_β) about flap hinge (slug-ft)	Nondimensional c.g. position
12.63	6.0	100.0	0.6	–	-0.5
18.6	6.0	100.0	0.6	–	-0.5
37.2	6.0	50.0	0.3	–	-0.5
55.8	7.95	30.0	0.08	–	-0.5
74.4	6.92	14.0	0.075	–	-0.5
93.0	6.7	9.9	0.074	–	-0.5
111.6	6.58	9.0	0.073	–	-0.5
130.2	6.4	8.5	0.072	–	-0.5
148.8	6.27	8.2	0.07	–	-0.5
167.4	6.2	7.9	0.068	–	-0.5
186.0	6.13	7.6	0.065	–	-0.5
204.6	5.8	7.3	0.062	–	-0.5
223.2	5.5	7.0	0.059	–	-0.5
241.8	5.6	6.8	0.058	–	-0.5
260.4	5.5	6.6	0.055	–	-0.5
279.0	5.12	6.3	0.054	0.00044	-0.2
297.6	5.1	6.0	0.052	0.00042	-0.2
316.2	5.03	5.9	0.051	0.00041	-0.2
334.8	5.0	5.7	0.05	0.00040	-0.2
353.4	5.0	5.5	0.048	–	-0.5
372.0	2.5	2.8	0.025	–	-0.5

While the theory is capable of handling different materials along the span of the blade, for simplicity, the example blade is assumed to be made of aluminum, and both the modulus of elasticity (E) and the shear modulus (G) are constant over the span of the blade, where $E = 10 \times 10^6$ psi and $G = 3.76 \times 10^6$ psi.

THIS PAGE INTENTIONALLY LEFT BLANK

V. VALIDATION OF 3-D ROTARY WING FLUTTER THEORY

A. COMPARISON WITH CLASSIC FLUTTER THEORIES

Equation (278) represents the 8DOF flutter equation for a rotor blade with a trailing-edge flap. In order to determine if this equation has validity, several limiting cases should be considered and compared with the classic flutter equations. The first case will be single degree of freedom (1DOF) flutter associated with pure pitching of the airfoil. The second case will be two degree of freedom (2DOF) flutter associated with coupled pitch-plunge motion. The third case will be the three degree of freedom (3DOF) flutter associated with coupled motion of bending, torsion, and aileron (trailing-edge flap). In each case, the 8DOF system will be reduced to the corresponding classic flutter case giving some validity to this current theory.

1. Single Degree of Freedom Flutter

The 1DOF case can be developed by setting the bending motions, trailing-edge flap motions, and the rigid body blade torsional motion to zero. Using equation (275), the equation of motion for a single pitch degree of freedom becomes

$$\pi\rho A_{\alpha_1\alpha_1} + I_{\alpha_1} - I_{\alpha_1}\left(1+ig_{\alpha_1}\right)\left(\frac{\omega_{\alpha_1}}{\omega}\right)^2 = 0 \tag{413}$$

where $A_{\alpha_1\alpha_1}$ is defined by equation (393). In the development of equation (393) it was assumed that there were spanwise variations of the properties (3D effects). Classic flutter equations are normally written in 2D form with no spanwise variations included. To convert equation (393) to a 2D equivalent, the dependence on mode shape (and variations in blade section properties) is eliminated by setting $F_1(y)=1$. If only one section is assumed, equation (393) becomes

$$A_{\alpha_1\alpha_1} = b^4\left[M_\alpha - \left(\frac{1}{2}+a\right)\left(L_\alpha + M_\alpha\right) + \left(\frac{1}{2}+a\right)^2 L_h\right]. \tag{414}$$

Equation (414) has both a real and imaginary part, and when equations (63), (64), (67), and (68) are substituted into equation (414), the result is

$$A_{\alpha_1\alpha_1} = b^4\left\{\left[\frac{3}{8}-\left(\frac{1}{2}+a\right)\left(1+\frac{2G}{k}-\frac{2F}{k^2}\right)+\left(\frac{1}{2}+a\right)^2\left(1+\frac{2G}{k}\right)\right]\right.$$
$$\left.+\frac{i}{k}\left[-1+\left(\frac{1}{2}+a\right)\left(1+2F+\frac{2G}{k}\right)-\left(\frac{1}{2}+a\right)^2(2F)\right]\right\}, \tag{415}$$

where F is the real part of the chosen lift deficiency function (Theodorsen for the classic case), and G is the imaginary part. Substituting equation (415) into equation (413) yields

$$\pi\rho b^4\left\{\left[\frac{3}{8}-\left(\frac{1}{2}+a\right)\left(1+\frac{2G}{k}-\frac{2F}{k^2}\right)+\left(\frac{1}{2}+a\right)^2\left(1+\frac{2G}{k}\right)\right]\right.$$
$$\left.+\frac{i}{k}\left[-1+\left(\frac{1}{2}+a\right)\left(1+2F+\frac{2G}{k}\right)-\left(\frac{1}{2}+a\right)^2(2F)\right]\right\} \tag{416}$$
$$+I_{\alpha_1}-I_{\alpha_1}\left(1+ig_{\alpha_1}\right)\left(\frac{\omega_{\alpha_1}}{\omega}\right)^2=0.$$

In order to solve equation (416), both the real and imaginary parts must go to zero simultaneously. The imaginary part can be written as

$$\frac{\pi\rho b^4}{k}\left[-1+\left(\frac{1}{2}+a\right)\left(1+2F+\frac{2G}{k}\right)-\left(\frac{1}{2}+a\right)^2(2F)\right]-I_{\alpha_1}g_{\alpha_1}\left(\frac{\omega_{\alpha_1}}{\omega}\right)^2=0, \tag{417}$$

and the real part can be written as

$$\pi\rho b^4\left[\frac{3}{8}-\left(\frac{1}{2}+a\right)\left(1+\frac{2G}{k}-\frac{2F}{k^2}\right)+\left(\frac{1}{2}+a\right)^2\left(1+\frac{2G}{k}\right)\right]+I_{\alpha_1}\left[1-\left(\frac{\omega_{\alpha_1}}{\omega}\right)^2\right]=0. \tag{418}$$

Equation (417) cannot be solved explicitly for k because F and G are functions of k. However, the method of Smilg and Wasserman [Ref. 45] can be used whereby the damping coefficient (g_{α_1}) is plotted against (1/k), and the value of 1/k where $g_{\alpha_1}=0$ is a solution to equation (417) and can be used to find the flutter frequency from equation (418). A solution in this manner is identical to using equations (345) and (346). With a little algebra, it can be shown that equations (417) and (418) can be written as

$$\frac{1}{k}\left[-\left(\frac{1}{2}+a\right)\left(\frac{2G}{k}\right)-\left(\frac{1}{4}-a^2\right)(2F)+\left(\frac{1}{2}-a\right)\right]+\frac{I_{\alpha_1}g_{\alpha_1}}{\pi\rho b^4}\left(\frac{\omega_{\alpha_1}}{\omega}\right)^2=0 \tag{419}$$

and

$$\left(\frac{1}{8}+a^2\right)+\left(\frac{1}{4}-a^2\right)\left(\frac{2G}{k}\right)-\left(\frac{1}{2}+a\right)\left(\frac{2F}{k^2}\right)+\frac{I_{\alpha_1}}{\pi\rho b^4}\left[\left(\frac{\omega_{\alpha_1}}{\omega}\right)^2-1\right]=0 \tag{420}$$

which are the damping and frequency equations given by equations (3) and (4) in Runyan's report on single degree of freedom flutter [Ref. 57]. Therefore, it has been shown that the 8DOF theory can be reduced to the classic 1DOF case of torsional flutter.

2. Two Degree of Freedom Flutter

The classic 2DOF flutter case with coupled pitch-plunge motion can be obtained by setting the rigid body motions, and the higher modes of the bending and trailing-edge flap motion to zero. For the 2DOF case, equations (271) and (275) can be written as

$$\left[\pi\rho A_{h_1h_1}+M_1-M_1\left(1+ig_{h_1}\right)\left(\frac{\omega_{h_1}}{\omega}\right)^2\right]h_1+\left(\pi\rho A_{h_1\alpha_1}+S_{\alpha_{11}}\right)\alpha_1=0 \tag{421}$$

and

$$\left(\pi\rho A_{\alpha_1h_1}+S_{\alpha_{11}}\right)h_1+\left[\pi\rho A_{\alpha_1\alpha_1}+I_{\alpha_1}-I_{\alpha_1}\left(1+ig_{\alpha_1}\right)\left(\frac{\omega_{\alpha_1}}{\omega}\right)^2\right]\alpha_1=0\,. \tag{422}$$

The expressions for $A_{h_1h_1}$, $A_{h_1\alpha_1}$, $A_{\alpha_1h_1}$, and $A_{\alpha_1\alpha_1}$ can be written in 2D form as

$$A_{h_1h_1}=b^2L_h \tag{423}$$

$$A_{h_1\alpha_1}=b^3\left[L_\alpha-\left(\frac{1}{2}+a\right)L_h\right] \tag{424}$$

$$A_{\alpha_1h_1}=b^3\left[M_h-\left(\frac{1}{2}+a\right)L_h\right] \tag{425}$$

and

$$A_{\alpha_1\alpha_1}=b^4\left[M_\alpha-\left(\frac{1}{2}+a\right)\left(L_\alpha+M_h\right)+\left(\frac{1}{2}+a\right)^2L_h\right]. \tag{426}$$

Substituting equations (423) through (426) into equations (421) and (422) and writing the result in matrix format yields

$$\begin{bmatrix} L_h + \dfrac{M_1}{\pi\rho b^2} - \dfrac{M_1}{\pi\rho b^2}\left(1+ig_{h_1}\right)\left(\dfrac{\omega_{h_1}}{\omega}\right)^2 & L_\alpha - \left(\dfrac{1}{2}+a\right)L_h + \dfrac{S_{\alpha_{11}}}{\pi\rho b^3} \\ M_h - \left(\dfrac{1}{2}+a\right)L_h + \dfrac{S_{\alpha_{11}}}{\pi\rho b^3} & \left\{ \begin{array}{l} M_\alpha - \left(\dfrac{1}{2}+a\right)\left(L_\alpha + M_h\right) + \left(\dfrac{1}{2}+a\right)^2 L_h \\ \quad + \dfrac{I_{\alpha_1}}{\pi\rho b^4} - \dfrac{I_{\alpha_1}}{\pi\rho b^4}\left(1+ig_{\alpha_1}\right)\left(\dfrac{\omega_{\alpha_1}}{\omega}\right)^2 \end{array} \right\} \end{bmatrix} \begin{bmatrix} h_1 \\ \alpha_1 \end{bmatrix} = 0. \tag{427}$$

If structural damping is assumed to be zero ($g_{h_1} = g_{\alpha_1} = 0$) and the following parameters are used that were defined by Theodorsen [Ref. 46]:

$$\kappa = \frac{\pi\rho b^2}{M_1} = \text{ mass ratio}$$

$$r_\alpha^2 = \frac{I_{\alpha_1}}{M_1 b^2} = \text{ radius of gyration divided by } b$$

$$x_\alpha = \frac{S_{\alpha_{11}}}{M_1 b} = \text{ static unbalance divided by } b,$$

then equation (427) becomes

$$\begin{bmatrix} \dfrac{1}{\kappa}\left(1-\left(\dfrac{\omega_{h_1}}{\omega}\right)^2\right) + L_h & L_\alpha - \left(\dfrac{1}{2}+a\right)L_h + \dfrac{x_\alpha}{\kappa} \\ M_h - \left(\dfrac{1}{2}+a\right)L_h + \dfrac{x_\alpha}{\kappa} & \left\{ \begin{array}{l} M_\alpha - \left(\dfrac{1}{2}+a\right)\left(L_\alpha + M_h\right) \\ \quad + \left(\dfrac{1}{2}+a\right)^2 L_h + \dfrac{r_\alpha^2}{\kappa}\left(1-\left(\dfrac{\omega_{\alpha_1}}{\omega}\right)^2\right) \end{array} \right\} \end{bmatrix} \begin{bmatrix} h_1 \\ \alpha_1 \end{bmatrix} = 0 \tag{428}$$

Since equation (428) is an homogenous equation and h_1 and α_1 are not both zero, the flutter solution is an eigenvalue problem, and it is found by setting the determinant equal to zero, or

$$\Delta = \begin{vmatrix} \frac{1}{\kappa}\left(1-\left(\frac{\omega_{h_1}}{\omega}\right)^2\right)+L_h & L_\alpha-\left(\frac{1}{2}+a\right)L_h+\frac{x_\alpha}{\kappa} \\ M_h-\left(\frac{1}{2}+a\right)L_h+\frac{x_\alpha}{\kappa} & \left\{\begin{array}{l} M_\alpha-\left(\frac{1}{2}+a\right)\left(L_\alpha+M_h\right) \\ \quad +\left(\frac{1}{2}+a\right)^2 L_h+\frac{r_\alpha^2}{\kappa}\left(1-\left(\frac{\omega_{\alpha_1}}{\omega}\right)^2\right) \end{array}\right\} \end{vmatrix} = 0 \qquad (429)$$

Equation (429) is the same 2DOF flutter equation shown in equation 9-20 of Bisplinghoff, et al [Ref. 1]. To further illustrate that this 8DOF flutter theory has validity when reduced to the 2DOF case, a comparison of equation (429) will be made to classic 2DOF flutter work done by Theodorsen and Garrick [Ref. 58]. Defining the flutter parameter as

$$X = \frac{r_\alpha^2}{\kappa}\left(\frac{\omega_{\alpha_1}}{\omega}\right)^2, \qquad (430)$$

equation (429) can be written as

$$\Delta = \begin{vmatrix} r_\alpha^2\left(\frac{\omega_{\alpha_1}}{\omega_{h_1}}\right)^2\left(\frac{1}{\kappa}+L_h\right)-X & r_\alpha^2\left(\frac{\omega_{\alpha_1}}{\omega_{h_1}}\right)^2\left[L_\alpha-\left(\frac{1}{2}+a\right)L_h+\frac{x_\alpha}{\kappa}\right] \\ M_h-\left(\frac{1}{2}+a\right)L_h+\frac{x_\alpha}{\kappa} & M_\alpha-\left(\frac{1}{2}+a\right)\left(L_\alpha+M_h\right)+\left(\frac{1}{2}+a\right)^2 L_h+\frac{r_\alpha^2}{\kappa}-X \end{vmatrix} = 0. \qquad (431)$$

Since the parameters L_h, L_α and M_α are complex quantities and functions of reduced frequency (k), the characteristic equation of the determinant will also be complex and a function of reduced frequency. The method that Theodorsen and Garrick used to find the flutter solution was to separate the real and imaginary parts of the characteristic equation from the flutter determinant, and plot both parts as $\sqrt{X}$ against $1/k$. The value of $1/k$ where the real and imaginary curves intersect would be the reduced frequency for flutter, and the parameter $\sqrt{X}$ can be used to find the flutter frequency using equation (430). Using the same parameters for the numerical example in Ref. 58, equation (431) can be used to generate an equivalent plot of Figure 1 of Ref. 58, which is case 1, or the flexure-

torsion case considered by Theodorsen and Garrick. The equivalent plot is shown in Figure 25 below, and Appendix D contains the MATLAB® program used to generate the curves in Figure 25. It can be seen that the point of intersection between the real and imaginary curves occurs at $1/k = 2.46$, which is the same value determined by Theodorsen and Garrick. Therefore, it has been shown that the 8DOF theory can be reduced to the classic 2DOF case of torsional flutter.

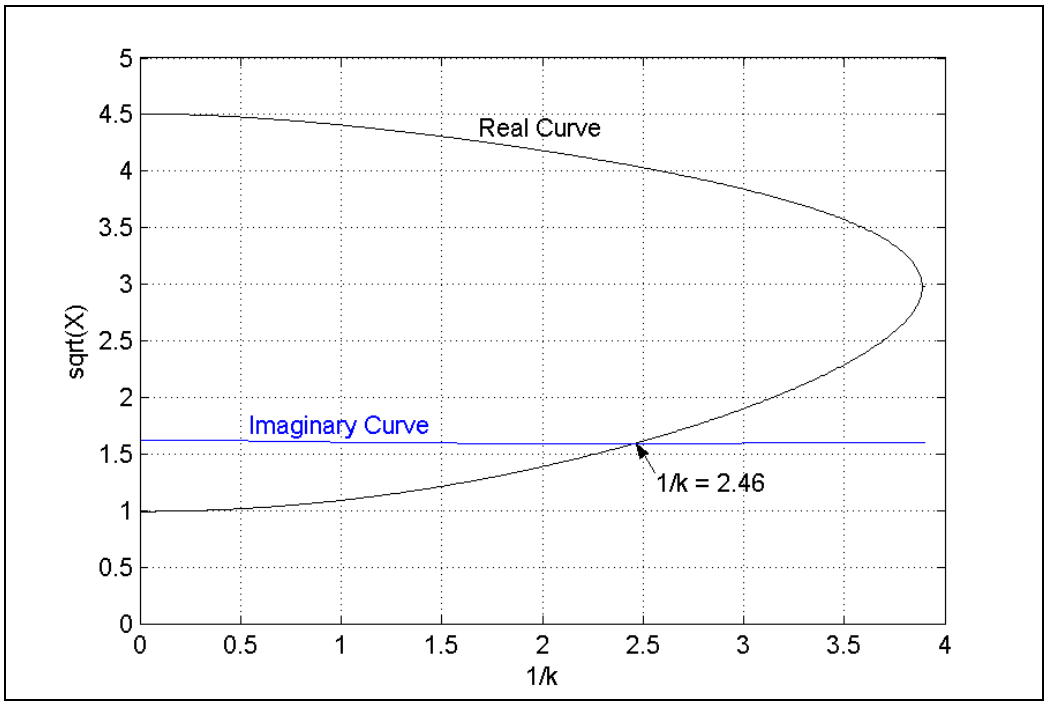

Figure 25. Real and imaginary roots of flutter determinant (Case 1) using data from Ref. 58.

3. Three Degree of Freedom Flutter

The development of the classic 3DOF, three-dimensional flutter theory, which is based on the 3DOF, two-dimensional flutter theory developed by Theodorsen [Ref. 46], can be found in Bisplinghoff, et al [Ref. 1] and Scanlan and Rosenbaum [Ref. 3]. It is normally assumed that the aileron (or trailing-edge flap) is very stiff structurally compared to the control system, and therefore the deflection of the aileron can be considered as a rigid body motion only. It is also assumed that the aileron has a slight twist proportional to the wing twist along its span. The 8DOF flutter theory presented

here can be reduced to the 3DOF theory by setting $h_0 = h_2 = h_3 = \alpha_0 = \beta_1 = 0$. The matrix equation (278) becomes

$$\begin{bmatrix} \begin{Bmatrix} \pi\rho A_{h_1 h_1} + M_1 \\ -M_1\left(1+ig_{h_1}\right)\left(\dfrac{\omega_{h_1}}{\omega}\right)^2 \end{Bmatrix} & \pi\rho A_{h_1\alpha_1} + S_{\alpha_{11}} & \pi\rho A_{h_1\beta_0} + S_{\beta_{10}} \\ \pi\rho A_{\alpha_1 h_1} + S_{\alpha_{11}} & \begin{Bmatrix} \pi\rho A_{\alpha_1\alpha_1} + I_{\alpha_1} \\ -I_{\alpha_1}\left(1+ig_{\alpha_1}\right)\left(\dfrac{\omega_{\alpha_1}}{\omega}\right)^2 \end{Bmatrix} & \pi\rho A_{\alpha_1\beta_0} + P_{\alpha_1\beta_0} \\ \pi\rho A_{\beta_0 h_1} + S_{\beta_{10}} & \pi\rho A_{\beta_0\alpha_1} + P_{\alpha_1\beta_0} & \begin{Bmatrix} \pi\rho A_{\beta_0\beta_0} + I_{\beta_0} \\ -I_{\beta_0}\left(1+ig_{\beta_0}\right)\left(\dfrac{\omega_{\beta_0}}{\omega}\right)^2 \end{Bmatrix} \end{bmatrix} \begin{bmatrix} h_1 \\ \alpha_1 \\ \beta_0 \end{bmatrix} = 0. \tag{432}$$

Equation (432) is exactly the same as equation 9.22 in Scanlan and Rosenbaum [Ref. 3], and if Theodorsen's lift deficiency function is used in the aerodynamic terms (A_{ij}), the results will be identical. The primary difference for rotary wing flutter is that Loewy's or the finite wake lift deficiency functions may be used, and the values of the aerodynamic coefficients, and hence the aerodynamic terms, will change. Therefore, the rotary wing 8DOF flutter equation (278) can be reduced to the classic 3DOF, three-dimensional flutter equation when Theodorsen's lift deficiency function is used.

B. AERODYNAMIC COEFFICIENTS

It is sometimes more convenient to write the equations of motion in the form that Theodorsen first presented them [Ref. 46]. Equations (60), (61), and (62) can be written as

$$\begin{aligned} L' = {} & \rho b^2 \left\{ v\pi\dot{\alpha} + \pi\ddot{h} - \pi b a\ddot{\alpha} - vT_4\dot{\beta} - T_1 b\ddot{\beta} \right\} \\ & -2\pi\rho v b C(k)\left\{ v\alpha + \dot{h} + b\left(\frac{1}{2}+a\right)\dot{\alpha} + \frac{1}{\pi}T_{10}v\beta + \frac{1}{2\pi}bT_{11}\dot{\beta} \right\} \end{aligned} \tag{433}$$

$$M' = -\rho b^2 \left\{ \pi\left(\frac{1}{2}+a\right) vb\dot{\alpha} + \pi b^2\left(\frac{1}{8}+a^2\right)\ddot{\alpha} + \left(T_4+T_{10}\right)v^2\beta \right.$$
$$+\left[T_1 - T_8 - \left(c-a\right)T_4 + \frac{1}{2}T_{11}\right] vb\dot{\beta} - \left[T_7 + \left(c-a\right)T_1\right] b^2\ddot{\beta} - a\pi b\ddot{h}\Big\} \qquad (434)$$
$$+2\pi\rho v b^2 C(k)\left(a+\frac{1}{2}\right)\left\{v\alpha + \dot{h} + b\left(\frac{1}{2}-a\right)\dot{\alpha} + \frac{1}{\pi}T_{10}v\beta + \frac{1}{2\pi}bT_{11}\dot{\beta}\right\}$$

and

$$T' = -\rho b^2 \left\{ \left[-2T_9 - T_1 + T_4\left(a-\frac{1}{2}\right)\right] vb\dot{\alpha} + 2T_{13}b^2\ddot{\alpha} \right.$$
$$+\frac{1}{\pi}\left(T_5 - T_4T_{10}\right)v^2\beta - \frac{1}{2\pi}T_4T_{11}vb\dot{\beta} - \frac{1}{\pi}T_3b^2\ddot{\beta} - T_1b\ddot{h}\Big\} \qquad (435)$$
$$-\rho v b^2 T_{12} C(k)\left\{v\alpha + \dot{h} + b\left(\frac{1}{2}-a\right)\dot{\alpha} + \frac{1}{\pi}T_{10}v\beta + \frac{1}{2\pi}bT_{11}\dot{\beta}\right\},$$

where the assumption of simple harmonic motion has not been introduced yet. The first sets of terms in braces in equations (433) through (435) are a result of the flow acceleration effects and are typically called non-circulatory, or apparent mass terms [Ref. 1 and 59]. The second sets of terms in braces (all preceded by $C(k)$) are a result of the circulation created about the airfoil and are called circulatory terms.

From equations (433) through (435) it can be seen that two main parameters that affect the rotary-wing flutter solution are the freestream velocity ($v = \Omega r$) and the choice of lift deficiency function, $C(k)$. (The T-functions and ϕ-functions depend only on the geometry of the airfoil, and thus once the airfoil's physical parameters are set, those functions become constant.) The freestream velocity seen by the rotor blade is a function of its radial position and rotational velocity, or $v = \Omega r$. The reduced frequency for rotary wing in a hover is defined by equation (87), and because of the change in velocity along the span of the blade, there is a different value of reduced frequency for each section of the blade. Thus, the value of k used in the aerodynamic terms given in equations (63) through (78) and the lift deficiency function change for each blade station, therefore causing the aerodynamic terms and the lift deficiency function to be functions of the radial position along the rotor blade.

Since aerodynamic terms will vary as reduced frequency and lift deficiency function varies, Table 3 shows a comparison of the value of the aerodynamic coefficients calculated by the flutter program listed in Appendix A, to the generally accepted values calculated by Smilg and Wasserman and listed in Appendix V of Ref. 45 for $e = c = 0.5$, and $k = 0.8$. For the Loewy and single wake lift deficiency functions, a wake spacing for the example helicopter hovering out of ground effect is used, where $\hat{h} = \hat{h}_0 = 1.14$. Note that in Table 3 with the exception of some rounding errors, the values of the aerodynamic coefficients using Theodorsen's lift deficiency function calculated with MATLAB® agree well with those reported by Smilg and Wasserman. Since MATLAB® can generate aerodynamic coefficients for any combination of e, c, k, $\hat{h}$, and m, it is unnecessary to generate tables of coefficients similar to those of Smilg and Wasserman. Appendix E contains a MATLAB® program that calculates just the aerodynamic coefficients.

It can also be seen that layers of shed vorticity beneath the rotor have a significant effect on aerodynamic coefficients. When comparing Loewy's lift deficiency function with an infinite number of previously shed wakes to the finite wake lift deficiency function with just a single previously shed wake, it can be seen that the number of wakes has a lesser effect than frequency ratio, which effectively is the phase relationship between the shed layers of vorticity. In other words, it is just as important (and maybe more so) to know the phase relationship between layers of shed vorticity as it is to know wake spacing and the number of wakes. Thus, it is expected that frequency ratio will have a significant effect on the flutter solution due to the larger changes to aerodynamic coefficients caused by changes in frequency ratio.

Table 3. Comparison of Aerodynamic Coefficients ($e = c = 0.5$, $k = 0.8$ and $\hat{h} = 1.14$)

Coefficient	Smilg and Wasserman	Theodorsen	Loewy			
			$m = 0$	$m = 0.25$	$m = 0.5$	$m = 0.75$
L_h	0.70880 -1.38530i	0.70874 -1.38537i	0.52031 -0.95194i	1.20891 -1.23500i	0.80296 -1.83605i	0.30485 -1.51864i
L_α	1.52280 -2.27119i	-1.52296 -2.27130i	-1.16961 -1.60233i	-0.83484 -2.74613i	-1.99210 -2.83975i	-2.09345 -1.89971i
L_β	-1.07467 -0.30907i	-1.07474 -0.30908i	-0.78375 -0.07603i	-0.85687 -0.65874i	-1.39834 -0.47398i	-1.25970 -0.02917i
L_z	0.01816 -0.84362i	0.01813 -0.84369i	-0.09663 -0.57973i	0.32272 -0.75211i	0.07550 -1.11815i	-0.22784 -0.92485i

M_h	0.5 +0i	0.5 +0i	0.5 +0i	0.5 +0i	0.5 +0i	0.5 +0i
M_α	0.375 -1.25i	0.375 -1.25i	0.375 -1.25i	0.375 -1.25i	0.375 -1.25i	0.375 -1.25i
M_β	-0.61022 -0.41665i	-0.61022 -0.41667i	-0.61022 -0.41667i	-0.61022 -0.41667i	-0.61022 -0.41667i	-0.61022 -0.41667i
M_z	0.16666 -0.51688i	0.16667 -0.51687i	0.16667 -0.51687i	0.16667 -0.51687i	0.16667 -0.51687i	0.16667 -0.51687i
T_h	0.03680 -0.01558i	0.03681 -0.01558i	0.03469 -0.01071i	0.04243 -0.01389i	0.03787 -0.02065i	0.03226 -0.01708i
T_α	0.01311 -0.09764i	0.013111 -0.09763i	0.017085 -0.09011i	0.02085 -0.10297i	0.00783 -0.10403i	0.00669 -0.09345i
T_β	-0.04440 -0.05125i	-0.04441 -0.05125i	-0.04113 -0.04863i	-0.04196 -0.05518i	-0.04805 -0.05311i	-0.04649 -0.04810i
T_z	0.01932 -0.03929i	0.01931 -0.03930i	0.01802 -0.03633i	0.02274 -0.03827i	0.01996 -0.04238i	0.01655 -0.04021i
P_h	0.17871 -0.07989i	0.17870 -0.07989i	0.16784 -0.05490i	0.20755 -0.07122i	0.18414 -0.10588i	0.15541 -0.08758i
P_α	0.05002 -0.47556i	0.05000 -0.47556i	0.07038 -0.43699i	0.08969 -0.50295i	0.02295 -0.50835i	0.01711 -0.45413i
P_β	-0.28045 -0.22767i	-0.28045 -0.22767i	-0.26367 -0.21423i	-0.26789 -0.24784i	-0.29911 -0.23718i	-0.29112 -0.21153i
P_z	0.08499 -0.23863i	0.08498 -0.23863i	0.07837 -0.22341i	0.10255 -0.23335i	0.08829 -0.25446i	0.07080 -0.24331i

Table 3. (Cont'd)

Coefficient	Theodorsen	Single Wake			
		$m = 0$	$m = 0.25$	$m = 0.5$	$m = 0.75$
L_h	0.70874 -1.38537i	0.58372 -1.07264i	1.07068 -1.07103i	0.81497 -2.13400i	0.30778 -1.37253i
L_α	-1.52296 -2.27130i	-1.25708 -1.80229i	-0.76811 -2.40939i	-2.35254 -3.15271i	-1.90788 -1.75725i
L_β	-1.07474 -0.30908i	-0.86253 -0.14925i	-0.76063 -0.51962i	-1.62268 -0.54472i	-1.14787 -0.00119i
L_z	0.01813 -0.84369i	-0.05801 -0.65324i	0.23855 -0.65226i	0.08282 -1.29960i	-0.22606 -0.83587i
M_h	0.5 +0i	0.5 +0i	0.5 +0i	0.5 +0i	0.5 +0i
M_α	0.375 -1.25i	0.375 -1.25i	0.375 -1.25i	0.375 -1.25i	0.375 -1.25i
M_β	-0.61022 -0.41667i	-0.61022 -0.41667i	-0.61022 -0.41667i	-0.61022 -0.41667i	-0.61022 -0.41667i
M_z	0.16667 -0.51687i	0.16667 -0.51687i	0.16667 -0.51687i	0.16667 -0.51687i	0.16667 -0.51687i
T_h	0.03681 -0.01558i	0.03540 -0.01206i	0.04088 -0.01205i	0.03800 -0.02400i	0.03230 -0.01544i
T_α	0.013111 -0.09763i	0.01610 -0.09236i	0.02160 -0.09919i	0.00378 -0.10755i	0.00878 -0.09185i
T_β	-0.04441 -0.05125i	-0.04202 -0.04945i	-0.04087 -0.05362i	-0.05057 -0.05390i	-0.04523 -0.04779i
T_z	0.01931 -0.03930i	0.01846 -0.03715i	0.02179 -0.03714i	0.02004 -0.04442i	0.01657 -0.03921i
P_h	0.17870 -0.07989i	0.17149 -0.06186i	0.19958 -0.06177i	0.18483 -0.12307i	0.15558 -0.07915i
P_α	0.05000 -0.47556i	0.06534 -0.44852i	0.09354 -0.48353i	0.00216 -0.52639i	0.02781 -0.44592i
P_β	-0.28045 -0.22767i	-0.26821 -0.21846i	-0.26234 -0.23981i	-0.31205 -0.24126i	-0.28467 -0.20992i
P_z	0.08498 -0.23863i	0.08059 -0.22765i	0.09770 -0.22759i	0.08872 -0.26492i	0.07090 -0.23818i

C. STRUCTURAL NATURAL FREQUENCIES

1. Uncoupled Natural Frequencies

In solving the eigenvalue problem for the flutter determinant given in equation (280), the $\overline{A}$ terms have uncoupled natural frequencies as one of the parameters. The uncoupled natural frequencies are calculated using the Holzer method described in section II.A.A. for torsional natural frequencies and the Myklestad method described in section II.A.B. for bending natural frequencies. Both these methods use the transfer

matrix method to find natural frequencies. While both methods take into account the centrifugal force associated with a rotating blade, the modes found are not coupled because the bending, blade torsional and trailing-edge flap torsional modes are calculated independently of other modes, and coupling effects such as those due to pitch and flap are not included. The coupling effects are introduced separately through the static unbalance and mechanical coupling terms. To illustrate this point, Figure 26 shows the effect of increased rpm (and thus increase centrifugal force) on the first three bending modes. It can be seen that the primary effect of increased centrifugal force is to gradually shift the nodes and antinodes of the mode shapes and to decrease amplitude of deflection for the antinodes. In other words, centrifugal force acts to stiffen the rotor blade.

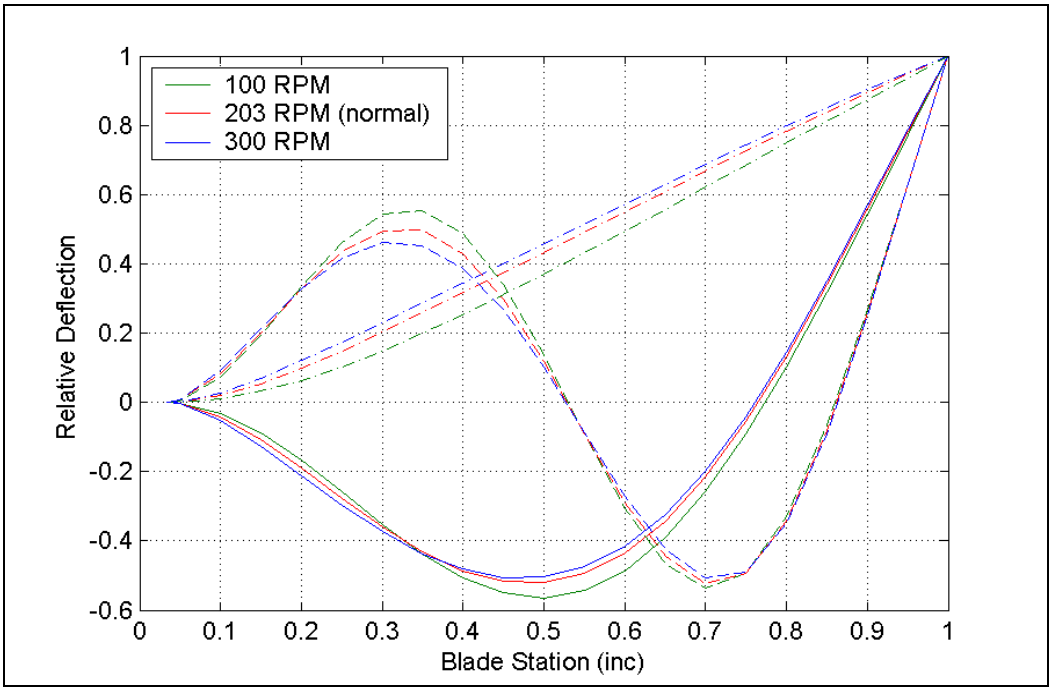

Figure 26. Vertical bending mode shapes at different rotational speeds

Table 4 shows the natural frequencies of the 1st, 2nd and 3rd bending modes and 1st and 2nd torsional modes for different rotational speeds for the example rotor blade. It is easily seen that the other effect of increased centrifugal force is to increase the natural frequency of each mode, with a greater effect seen on bending modes than on torsional modes. Accounting for the effect of centrifugal forces on the uncoupled bending natural frequencies has some practical limitations when the Myklestad method is used. Equation

(39) is the governing equation for the bending deflection and is a 4th order ordinary differential equation. Using the lumped-mass parameter method equation (39) becomes equation (48) when written in transfer matrix format. In order to solve equation (48), the $[\mathbf{K_n}]$ matrix must be inverted as shown in equation (50). Since the centrifugal force term only appears in two off-diagonal terms, there is a possibility that the $[\mathbf{K_n}]$ matrix may become singular if the number of significant figures carried through the calculations is inadequate. In fact, this does happen to the example rotor blade in the calculations carried out when the rpm exceeds 375, or about 1.85 times the normal operating rpm. Mathematically, the second term of equation (39) is becoming so large compared to the first term that in essence, the 4th order differential equation is reduced to a 2nd order differential equation thus reducing the rank of the $[\mathbf{K_n}]$ matrix and yielding a singularity in the solution above 375 rpm.

Table 4. Uncoupled Natural Frequencies (rad/s) at Different Rotational Speeds

Mode	100 RPM	203 RPM (normal)	300 RPM
1st Bending	12.77	23.95	34.50
2nd Bending	38.52	62.99	88.12
3rd Bending	84.27	115.84	151.68
1st Blade Torsion	138.59	139.81	141.70
2nd Blade Torsion	369.03	369.54	370.35

2. Coupled Natural Frequencies

While the uncoupled natural frequencies are used as inputs to equation (280), it is the coupled natural frequencies that result from the calculation that truly influence the flutter problem. The coupled natural frequencies are coupled in the sense that motion by more than one degree of freedom couples into another degree of freedom. The coupled natural frequencies are found by applying Lagrange's equation in the form shown in equation (261) with internal generalized forces set to zero, or

$$\frac{d}{dt}\left(\frac{\partial T}{\partial \dot{q}_n}\right)+\frac{\partial U}{\partial q_n}+\frac{\partial D}{\partial \dot{q}_n}=0 \tag{436}$$

Applying equation (436) to the 5DOF yields the following equations:

$$M_1\ddot{h}_1 + S_{\alpha_{10}}\ddot{\alpha}_0 + S_{\alpha_{11}}\ddot{\alpha}_1 + S_{\beta_{10}}\ddot{\beta}_0 + S_{\beta_{11}}\ddot{\beta}_1 + M_1\omega_{h_1}^2 h_1 + \frac{M_1\omega_{h_1}^2 g_{h_1}}{\omega}\dot{h}_1 = 0 \tag{437}$$

$$M_2\ddot{h}_2 + S_{\alpha_{20}}\ddot{\alpha}_0 + S_{\alpha_{21}}\ddot{\alpha}_1 + S_{\beta_{20}}\ddot{\beta}_0 + S_{\beta_{21}}\ddot{\beta}_1 + M_2\omega_{h_2}^2 h_2 + \frac{M_2\omega_{h_2}^2 g_{h_2}}{\omega}\dot{h}_2 = 0 \tag{438}$$

$$M_3\ddot{h}_3 + S_{\alpha_{30}}\ddot{\alpha}_0 + S_{\alpha_{31}}\ddot{\alpha}_1 + S_{\beta_{30}}\ddot{\beta}_0 + S_{\beta_{31}}\ddot{\beta}_1 + M_3\omega_{h_3}^2 h_3 + \frac{M_3\omega_{h_3}^2 g_{h_3}}{\omega}\dot{h}_3 = 0 \tag{439}$$

$$\begin{aligned} &I_{\alpha_1}\ddot{\alpha}_1 + S_{\alpha_{01}}\ddot{h}_0 + S_{\alpha_{11}}\ddot{h}_1 + S_{\alpha_{21}}\ddot{h}_2 + S_{\alpha_{31}}\ddot{h}_3 \\ &\quad + P_{\alpha_1\beta_0}\ddot{\beta}_0 + P_{\alpha_1\beta_1}\ddot{\beta}_1 + I_{\alpha_1}\omega_{\alpha_1}^2\alpha_1 + \frac{I_{\alpha_1}\omega_{\alpha_1}^2 g_{\alpha_1}}{\omega}\dot{\alpha}_1 = 0 \end{aligned} \tag{440}$$

$$\begin{aligned} &I_{\beta_0}\ddot{\beta}_0 + S_{\beta_{00}}\ddot{h}_0 + S_{\beta_{10}}\ddot{h}_1 + S_{\beta_{20}}\ddot{h}_2 + S_{\beta_{30}}\ddot{h}_3 \\ &\quad + P_{\alpha_0\beta_0}\ddot{\alpha}_0 + P_{\alpha_1\beta_0}\ddot{\alpha}_1 + I_{\beta_0}\omega_{\beta_0}^2\beta_0 + \frac{I_{\beta_0}\omega_{\beta_0}^2 g_{\beta_0}}{\omega}\dot{\beta}_0 = 0 \end{aligned} \tag{441}$$

If simple harmonic motion is assumed, equations (437) through (441) can be written in matrix format as:

$$\begin{bmatrix} M_1\left[1-\left(1+ig_{h_1}\right)\left(\frac{\omega_{h_1}}{\omega}\right)^2\right] & 0 & 0 & S_{\alpha_{11}} & S_{\beta_{10}} \\ 0 & M_2\left[1-\left(1+ig_{h_2}\right)\left(\frac{\omega_{h_2}}{\omega}\right)^2\right] & 0 & S_{\alpha_{21}} & S_{\beta_{20}} \\ 0 & 0 & M_3\left[1-\left(1+ig_{h_3}\right)\left(\frac{\omega_{h_3}}{\omega}\right)^2\right] & S_{\alpha_{31}} & S_{\beta_{30}} \\ S_{\alpha_{11}} & S_{\alpha_{21}} & S_{\alpha_{31}} & I_{\alpha_1}\left[1-\left(1+ig_{\alpha_1}\right)\left(\frac{\omega_{\alpha_1}}{\omega}\right)^2\right] & P_{\alpha_1\beta_0} \\ S_{\beta_{10}} & S_{\beta_{20}} & S_{\beta_{30}} & P_{\alpha_1\beta_0} & I_{\beta_0}\left[1-\left(1+ig_{\beta_0}\right)\left(\frac{\omega_{\beta_0}}{\omega}\right)^2\right] \end{bmatrix} \begin{bmatrix} h_1 \\ h_2 \\ h_3 \\ \alpha_1 \\ \beta_0 \end{bmatrix} = 0 \tag{442}$$

It can be seen that equation (442) is identical to equation (278) if all the terms that have density (ρ) are eliminated. Since ρ is never in the denominator of any term, those terms can be eliminated by simply by setting $\rho = 0$. A physical analogy would be that of running the rotor in a vacuum chamber. By eliminating the density terms, the effects of the air stream are no longer present, and flutter cannot exist. Thus, the solution to equation (442) will contain only the inertial and elastic forces, which is represented by the mechanical vibrations or structural dynamics problem shown in Figure 2. Applying the method of Smilg and Wasserman of effectively equating the damping coefficients and defining a new variable Z given in equation (279), the coupled natural frequencies can be obtained using equation (280) by setting $\rho = 0$. It should be noted that when equation (442) or equation (280) or (412) (with $\rho = 0$) is used, the eigenvalues will all become real and positive, and the damping coefficients (g) will be zero. This result is expected wince setting $\rho = 0$ effectively makes the blade motion occur in a vacuum, and hence no dissipation of the motion is present.

Figure 27 is a Southwell, or fan plot for the example rotor blade with the flap frequency set to zero ($\omega_\beta = 0$). At the normal operating rpm of 203, the coupled natural frequencies are 23.91, 62.92, 115.45, and 150.49 rad/s. A good structural design for rotor blades is to ensure that there are no natural frequencies at N_b and $N_b \pm 1$ times the rotational frequency at normal rpm. Additionally, natural frequencies at other integer multiples of the normal rotational frequency should be avoided to maximum extent practical. It can be seen from Figure 27 that the natural frequencies at normal operating rpm do not coincide with the 4P, 5P and 6P frequencies. The proximity of the 2nd bending frequency with the 3P frequency and the 1st blade torsion frequency with the 7P frequency would normally not present any problems. Figure 28 is a Southwell plot for the H-3 rotor blade [Ref. 60]. By comparing Figure 27 to Figure 28, it can be seen that the structural dynamics of the example rotor blade (with a trailing-edge flap) is reasonable when compare to the H-3 rotor blade (without the trailing-edge flap). The main differences between the two plots can be attributed to the c.g. shift from 25% chord to 40% chord due to inclusion of the trailing-edge flap.

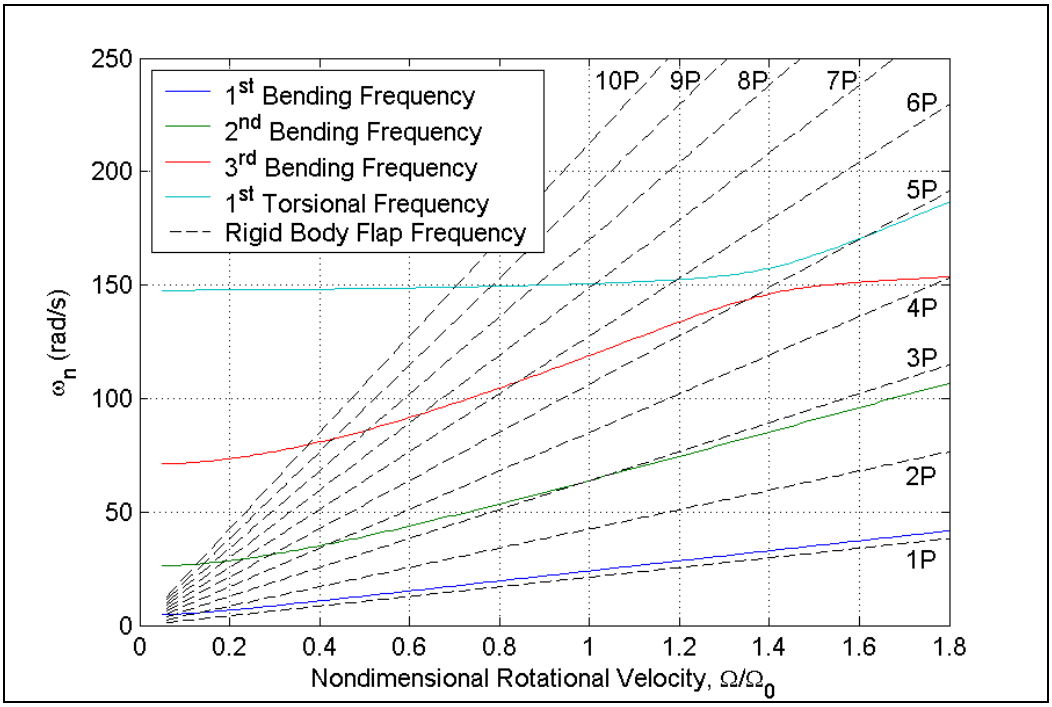

Figure 27. Southwell plot for example rotor blade (ω_β = 0P).

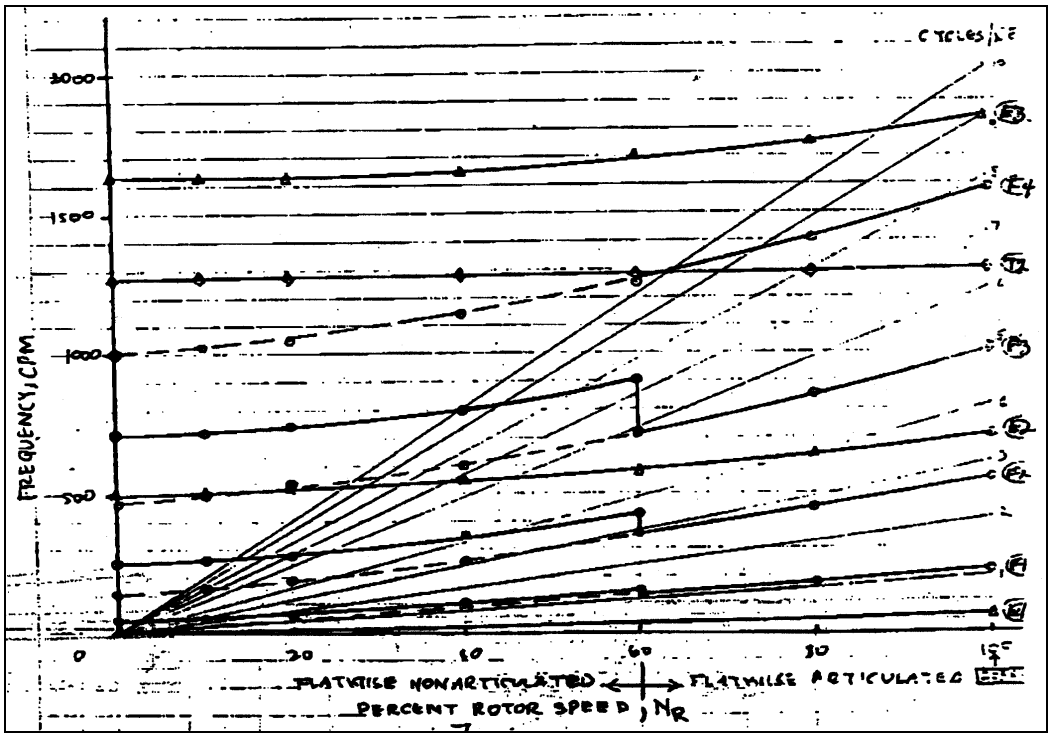

Figure 28. Southwell plot for H-3 rotor blade (from Ref. 60)

With the trailing-edge flap incorporated on the example rotor blade, the uncoupled natural frequency of the flap has the ability to influence the coupled natural frequencies, and hence structural dynamics of the rotor blade. Figure 29 through Figure 35 are the Southwell plots for flap frequencies of 1P through 7P. it can be seen from Figure 29 though Figure 32 that flap frequencies from 1P to 4P do not significantly affect the structural dynamics of the rotor blade. However, Figure 33 through Figure 35 show some interaction between the flap frequency and the 3rd bending and 1st blade torsional frequencies. Fortunately, the interaction between the modes occurs at a rotational frequency of 1.2 – 1.4 times the rotational frequency, which is well above the normal operating limits. Thus, from the viewpoint of structural dynamics alone, it may be concluded that the example rotor blade meets the criteria for a good structural design with the trailing-edge flap incorporated that includes a c.g. offset.

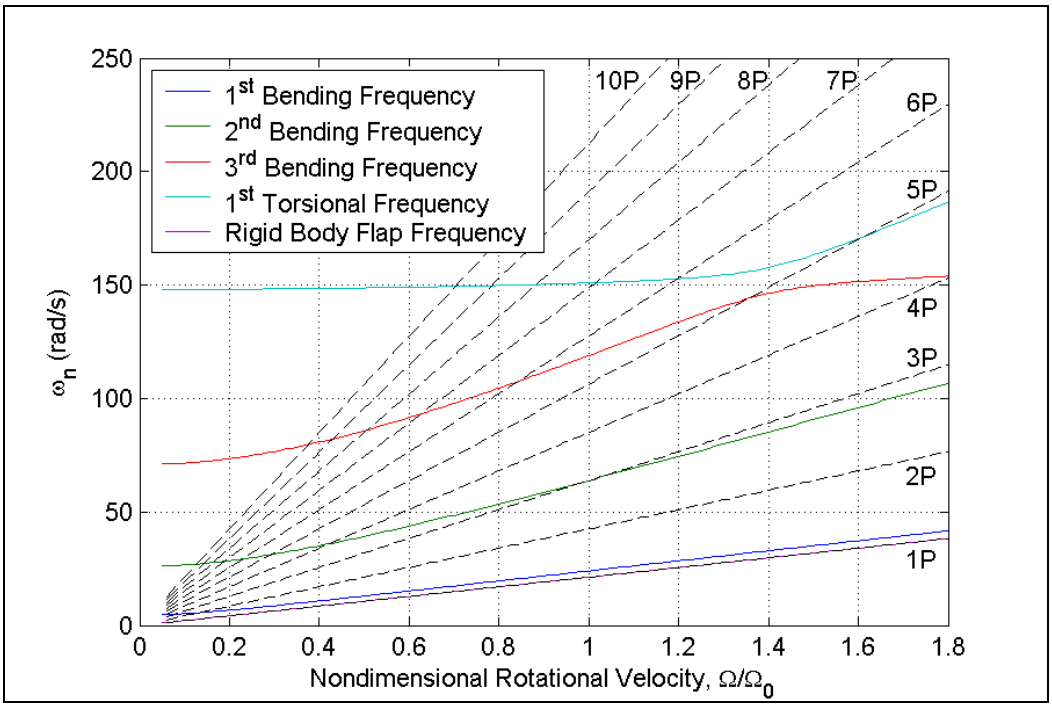

Figure 29. Southwell plot for example rotor blade (ω_β = 1P).

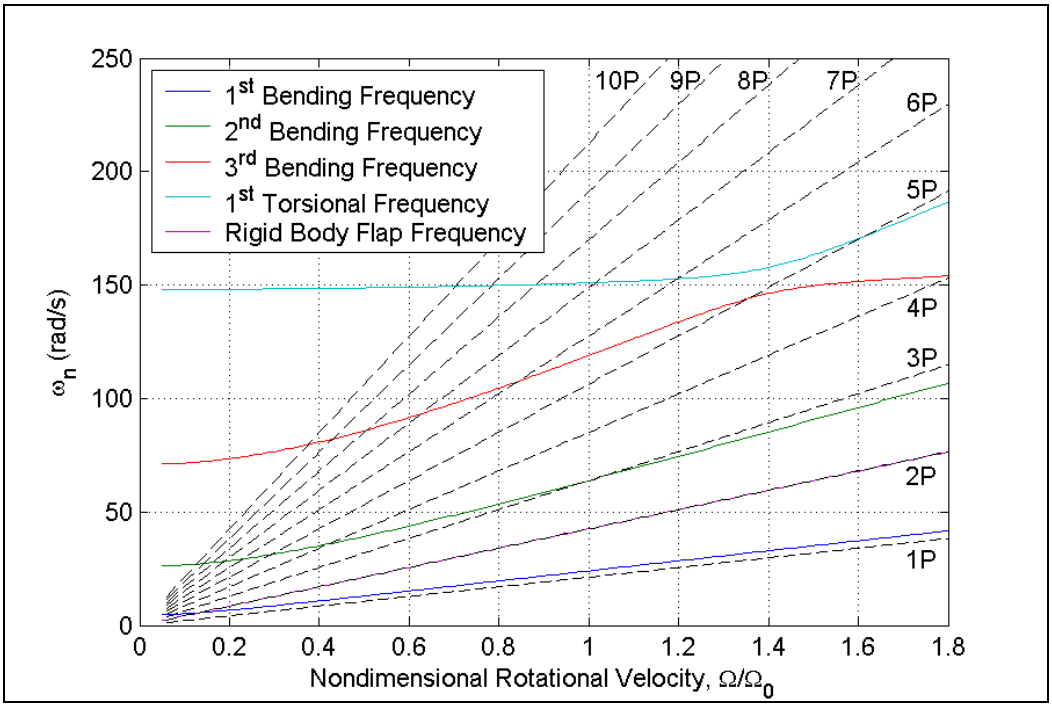

Figure 30. Southwell plot for example rotor blade (ω_β = 2P).

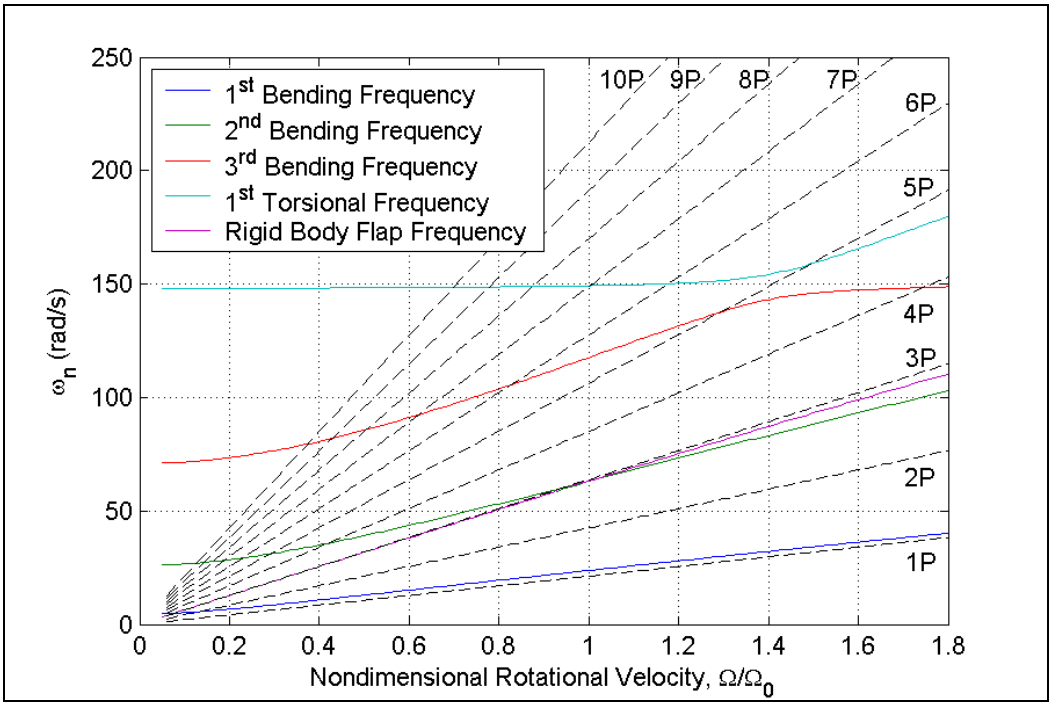

Figure 31. Southwell plot for example rotor blade (ω_β = 3P).

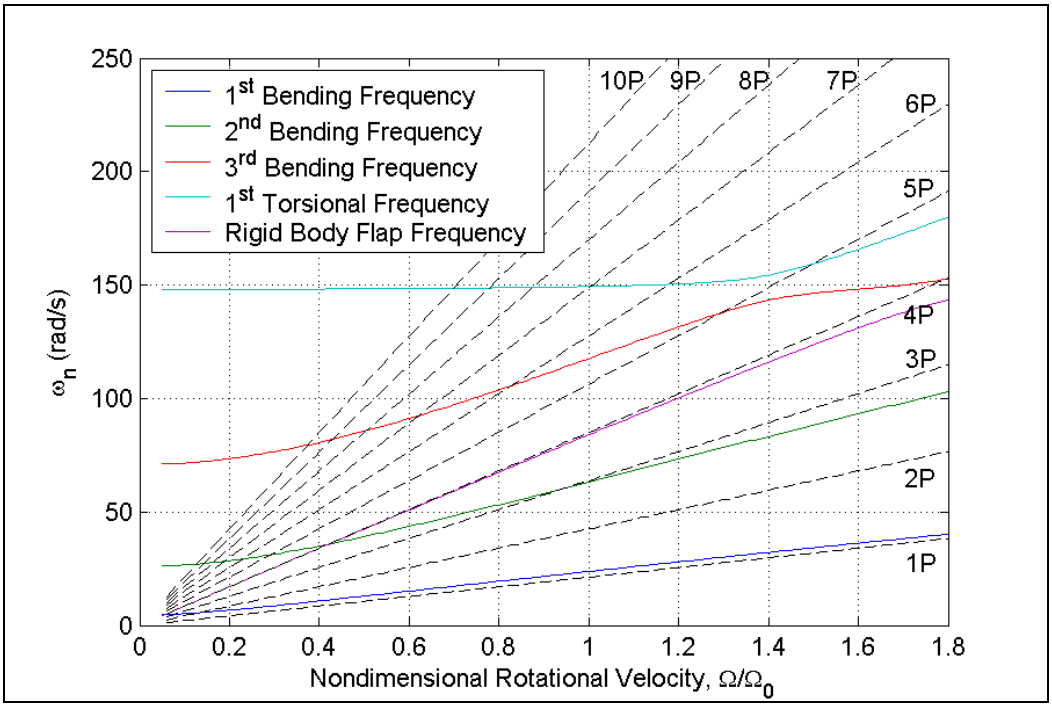

Figure 32. Southwell plot for example rotor blade (ω_β = 4P).

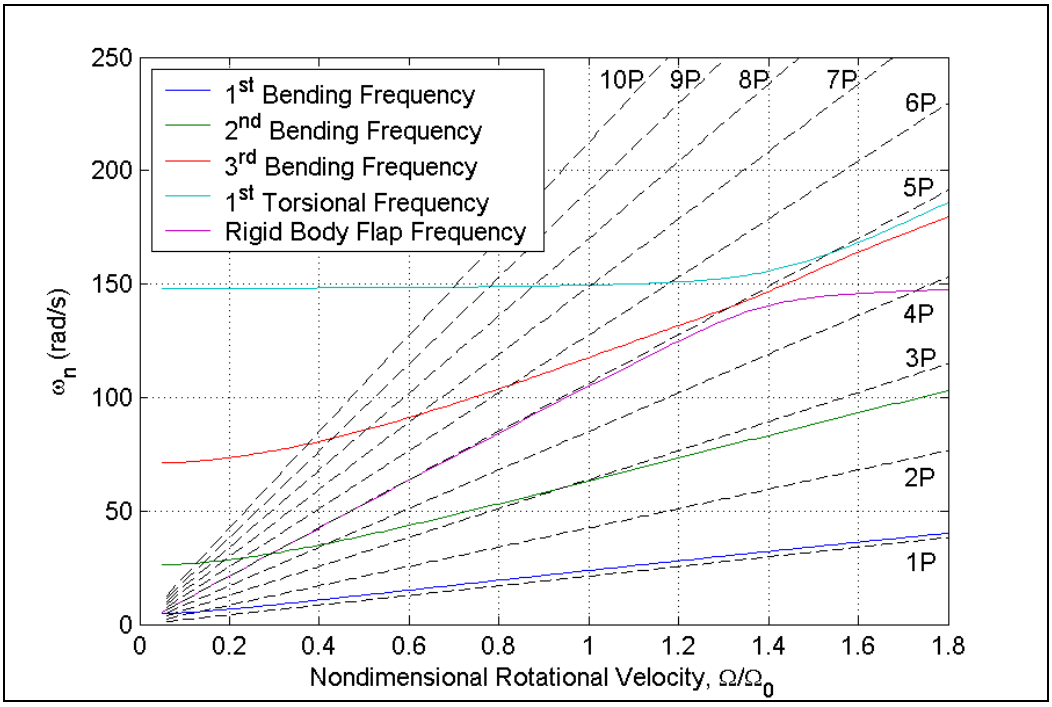

Figure 33. Southwell plot for example rotor blade (ω_β = 5P).

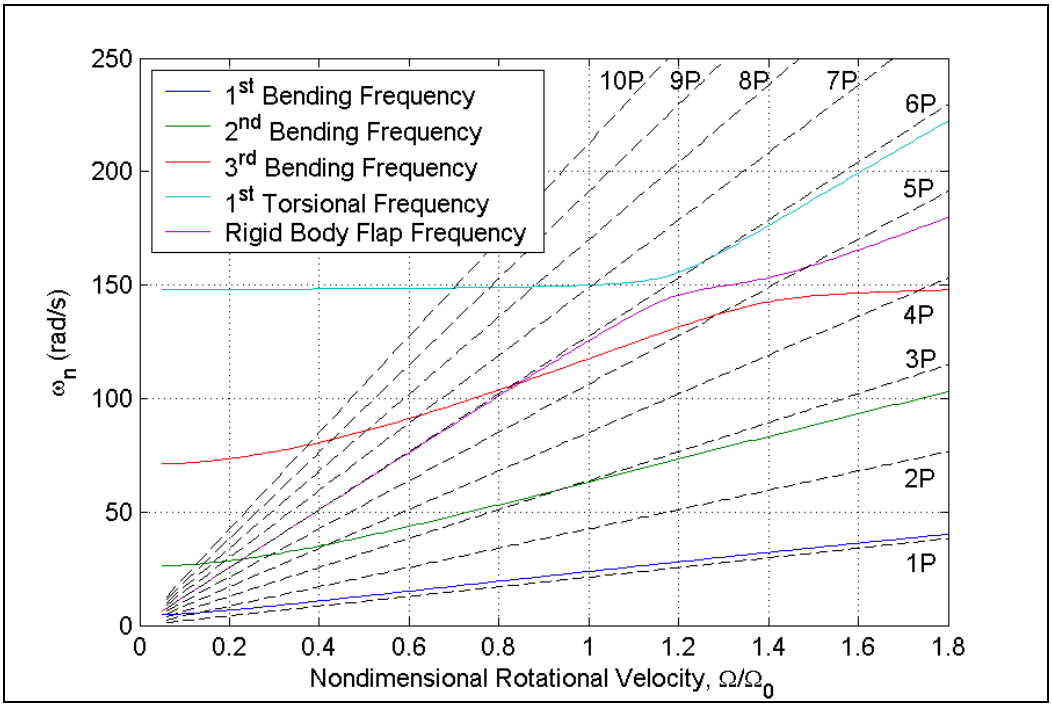

Figure 34. Southwell plot for example rotor blade (ω_β = 6P).

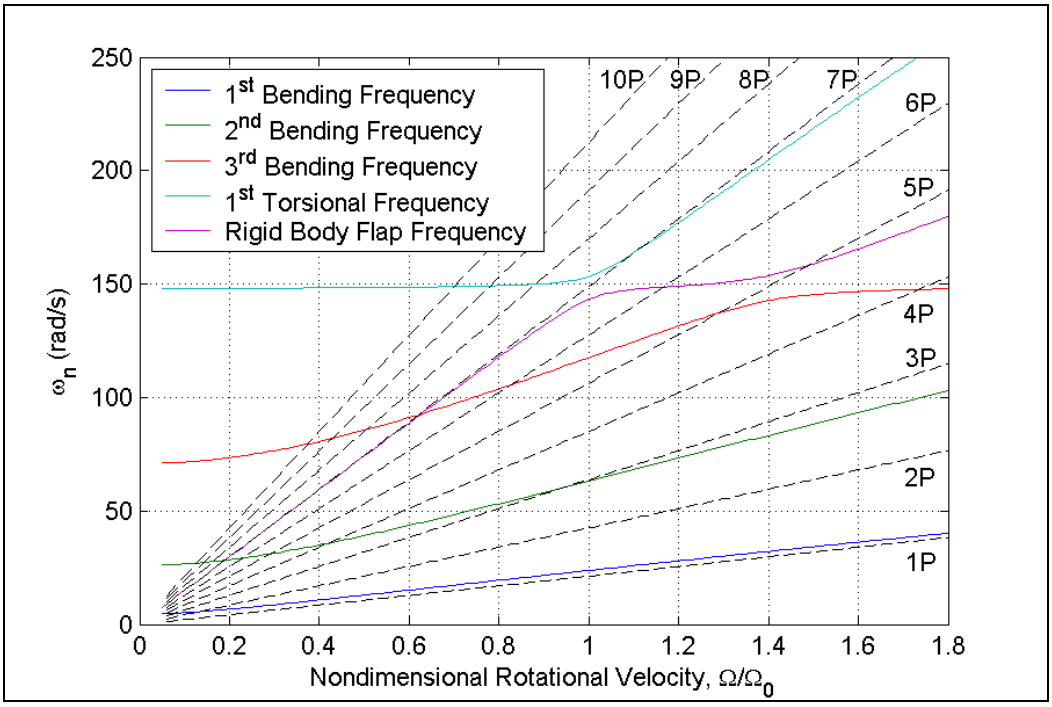

Figure 35. Southwell plot for example rotor blade (ω_β = 7P).

THIS PAGE INTENTIONALLY LEFT BLANK

VI. FLUTTER ANALYSIS FOR EXAMPLE ROTOR BLADE

To this point, both the structural dynamics and the unsteady aerodynamics have been examined independently to determine their individual contributions to the issue of rotor blade aeroelastic stability. In the previous section, it was shown that the example rotor blade has a good structural design even with the center of gravity moved aft in the portion with the trailing-edge flap incorporated, and that layers of shed vorticity beneath the reference blade can have a significant effect on the aerodynamic coefficients with the most notable parameter being the frequency ratio, or wake phasing relationship. Since flutter is a self-exited aeroelastic phenomenon, an analysis of the combined effects of structural dynamics and aerodynamics will provide a solution to the flutter problem.

Since there are several parameters that influence the flutter problem, the following parameters will be examined to determine how the variation of each parameter affects the flutter solution:

1. Flap frequencies of 0P, 4P, 5P and 6P
2. Choice of lift deficiency function
3. Frequency ratio for shed wakes
4. Center of gravity offset

While a trailing-edge flap can have any input frequency desired, the reason for limiting the scope of this study to the four inputs listed above are that 0P represents the condition of IBC turned off and 4P, 5P and 6P represent the $N_b - 1$, N_b (blade passage), and $N_b + 1$ vibration frequencies that are transmitted from rotating system to the fixed system. Therefore if it can be determined that flutter does not exist for these frequencies, it would be likely that flutter would not exist for other conditions.

A. 0P FLAP FREQUENCY

Since the 0P flap frequency corresponds to the condition of IBC turned off, it is the most critical case to be analyzed. If flutter exists for the 0P input frequency, then it will most likely exist with other flap frequencies. The first set of parameter to be analyzed will be the choice of lift deficiency function. Figure 36 is the g-Ω plot using the Theodorsen lift deficiency function for 0P flap frequency. The flutter speed is found by

noting the rotational velocity when the critical damping curve crosses the axis of the abscissa going from a negative to a positive value. The flutter speed of the example rotor blade using the Theodorsen lift deficiency function is $1.345\Omega_0$ (273 rpm). The overspeed limit for typical rotor systems ranges from $1.05\Omega_0$ to $1.2\Omega_0$ due to fatigue and reliability concerns [Ref. 12 and 25]. Thus, calculated flutter speeds above $1.2\Omega_0$ (or the maximum overspeed limit) would indicate via analysis that the rotor blade could be considered free from flutter in the normal operating environment and in compliance with FAA requirements [Ref. 4 and 5].

Figure 37 is the *g*-Ω plot for the example rotor blade with 0P flap frequency using Loewy's lift deficiency function with $m = 0$. The wake spacing has been set to the normal wake spacing in an out-of-ground-effect hover, or $\hat{h} = \hat{h}_0 = 1.14$. It can be seen that the effect of having the shed layers of vorticity exactly in phase with the layers above and below it is to raise the flutter speed to greater than $1.8\Omega_0$. Thus, the $m = 0$ case makes the rotor blade less susceptible to flutter. The effects of changes in frequency ratio using Loewy's lift deficiency function are shown in Figure 38 through Figure 40 for the cases of $m = 0.25$, $m = 0.5$, and $m = 0.75$, respectively. The case of $m = 0.25$ is interesting in that the flutter speed is $1.108\Omega_0$, which may be in the normal operating range of some rotor systems.

The large changes in flutter speed seen when frequency ratio is varied can be explained using Figure 41 in which Loewy [Ref. 49] plotted the pitch damping coefficient, defined by

$$C_{pitch-damping} = \frac{1}{k}\left[\left(\frac{1}{2}-a\right)-\left(\frac{1}{2}+a\right)\frac{2G'}{k}-\left(\frac{1}{4}-a^2\right)2F'\right],$$

against the frequency ratio for various wake spacings (inflow parameter). It can be seen that the pitch damping coefficient becomes negative (unstable) in the region where $m = 1.25$. Recall that the wake weighting function is periodic in *m*, and the $m = 0.25$ case shown in Figure 38 could correspond to any integer plus 0.25 case. Thus, this decreased pitch damping has a destabilizing effect on the flutter speed of the rotor blade.

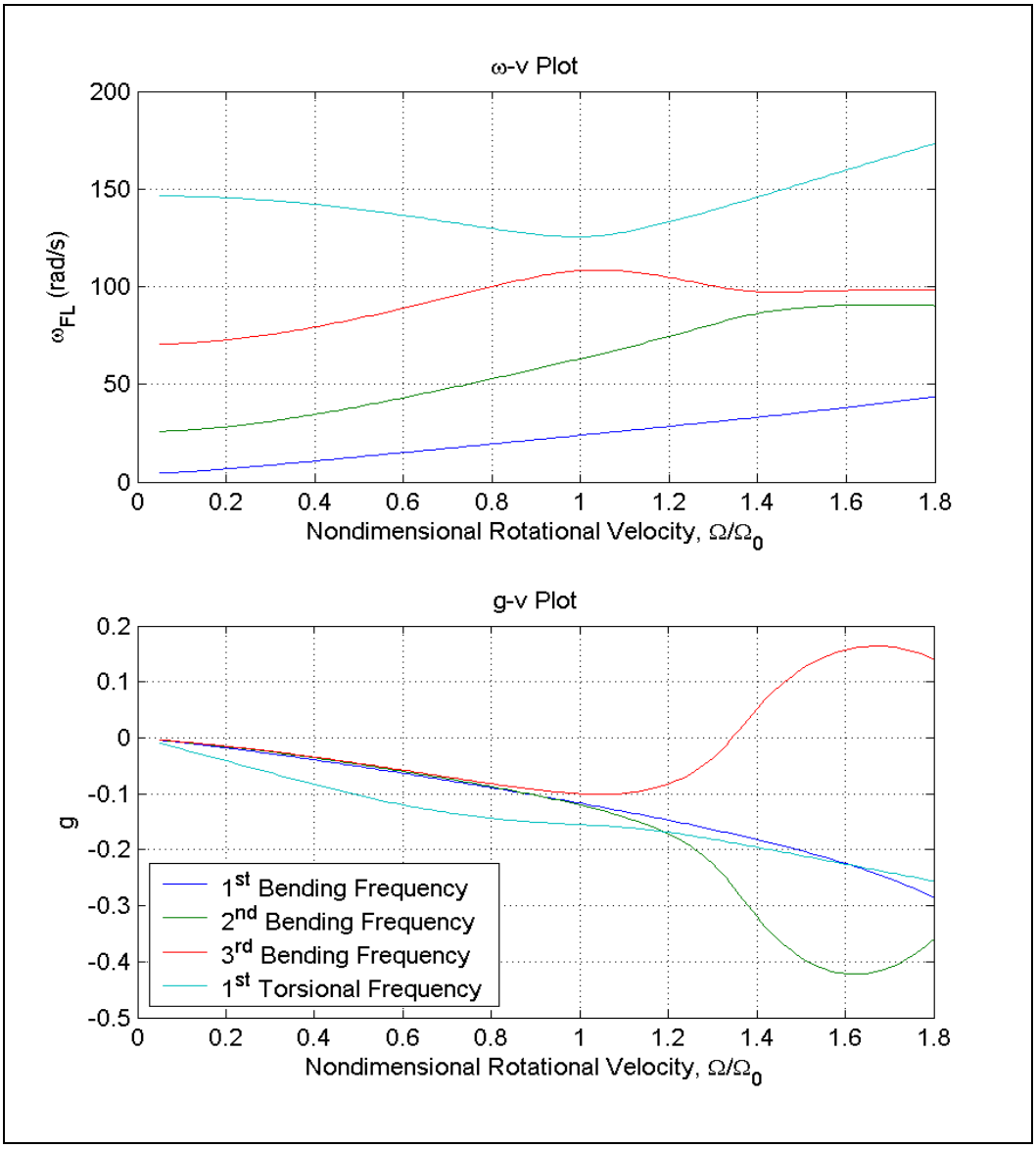

Figure 36. *g*-Ω plot for example rotor blade using Theodorsen's lift deficiency function (ω_β = 0P).

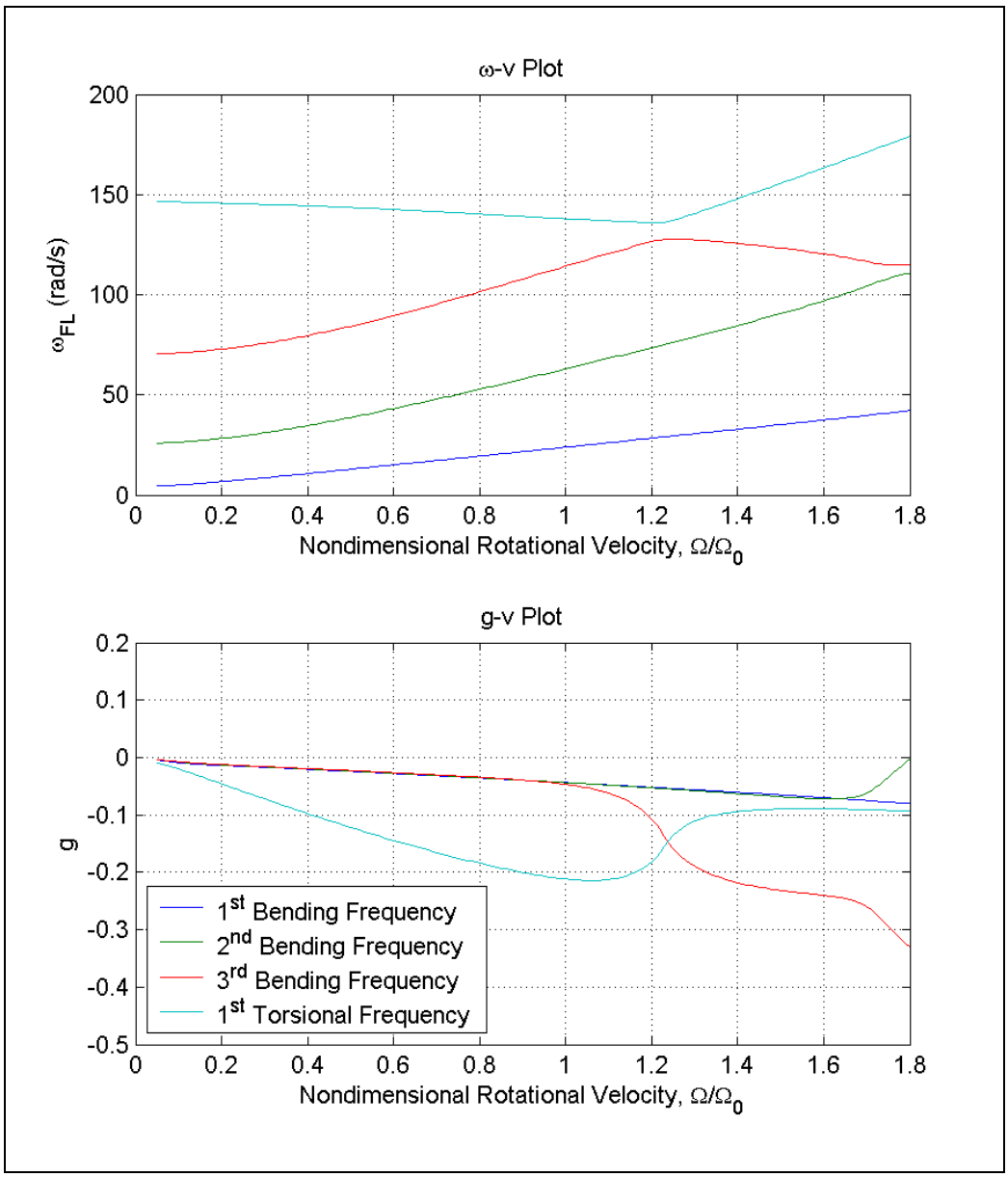

Figure 37. *g*-Ω plot for example rotor blade using Loewy's lift deficiency function, *m* = 0 (ω_β = 0P).

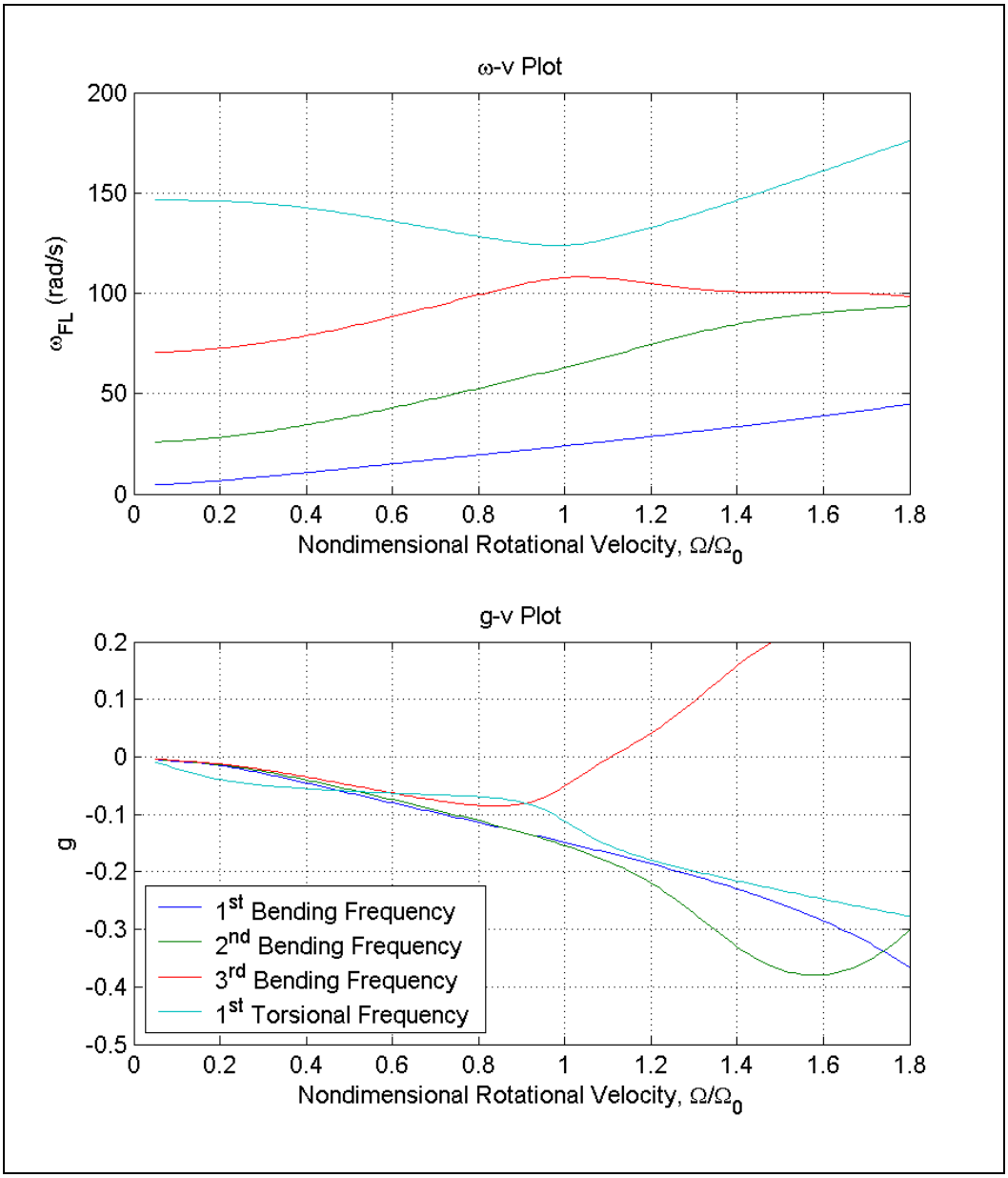

Figure 38. *g*-Ω plot for example rotor blade using Loewy's lift deficiency function, $m = 0.25$ ($\omega_\beta = 0P$).

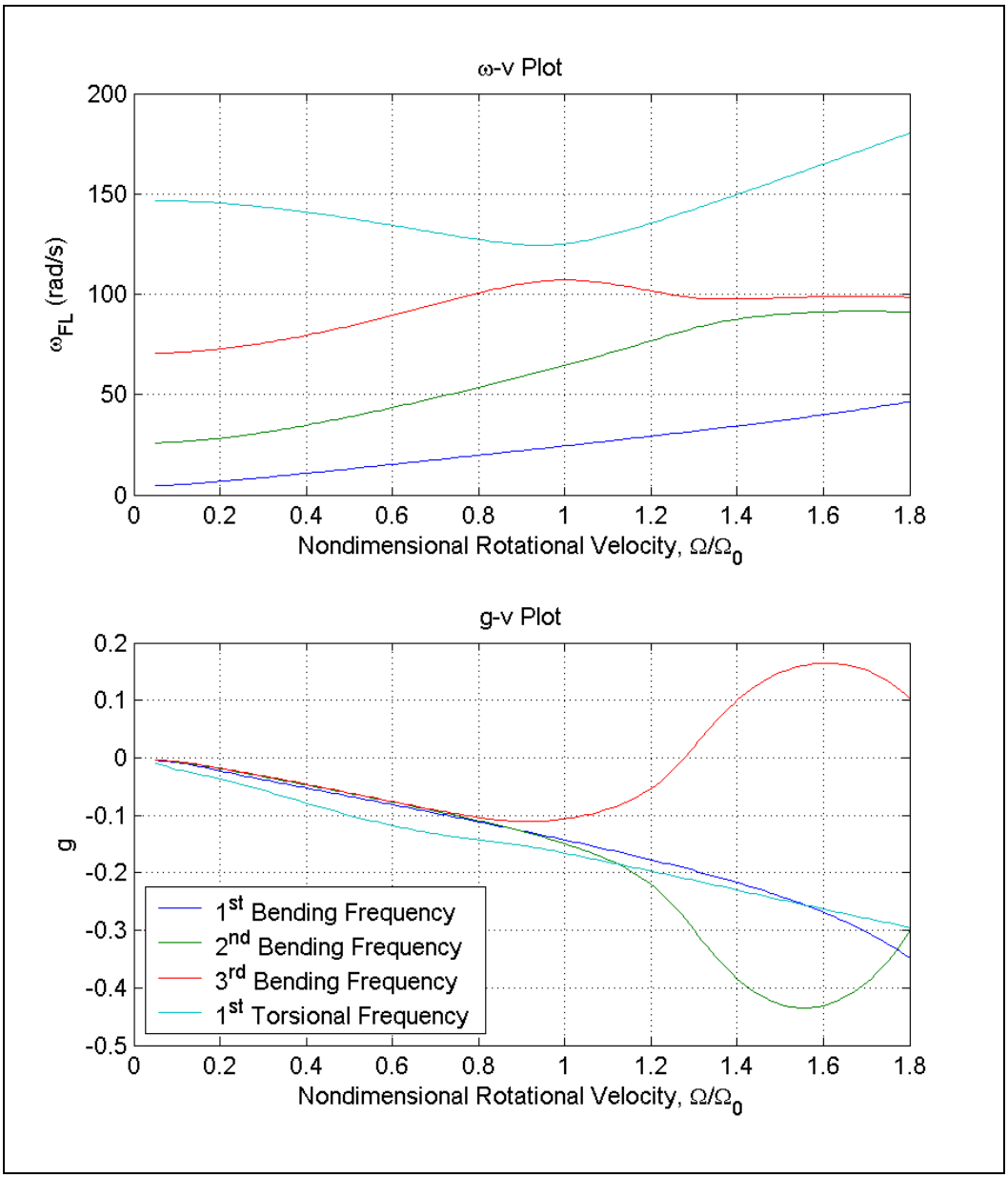

Figure 39. *g*-Ω plot for example rotor blade using Loewy's lift deficiency function, *m* = 0.5 (ω_β = 0P).

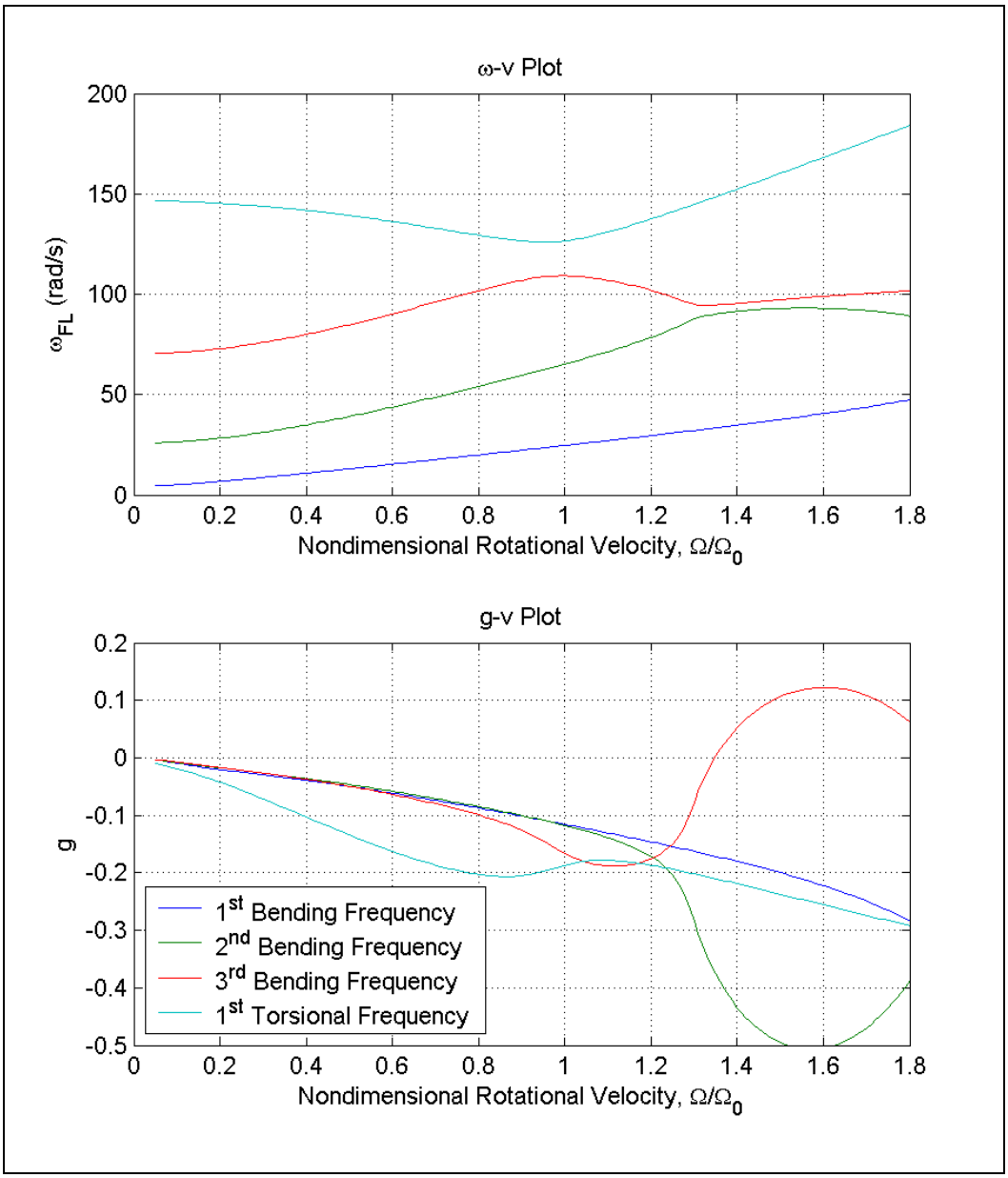

Figure 40. *g*-Ω plot for example rotor blade using Loewy's lift deficiency function, *m* = 0.75 (ω_β = 0P).

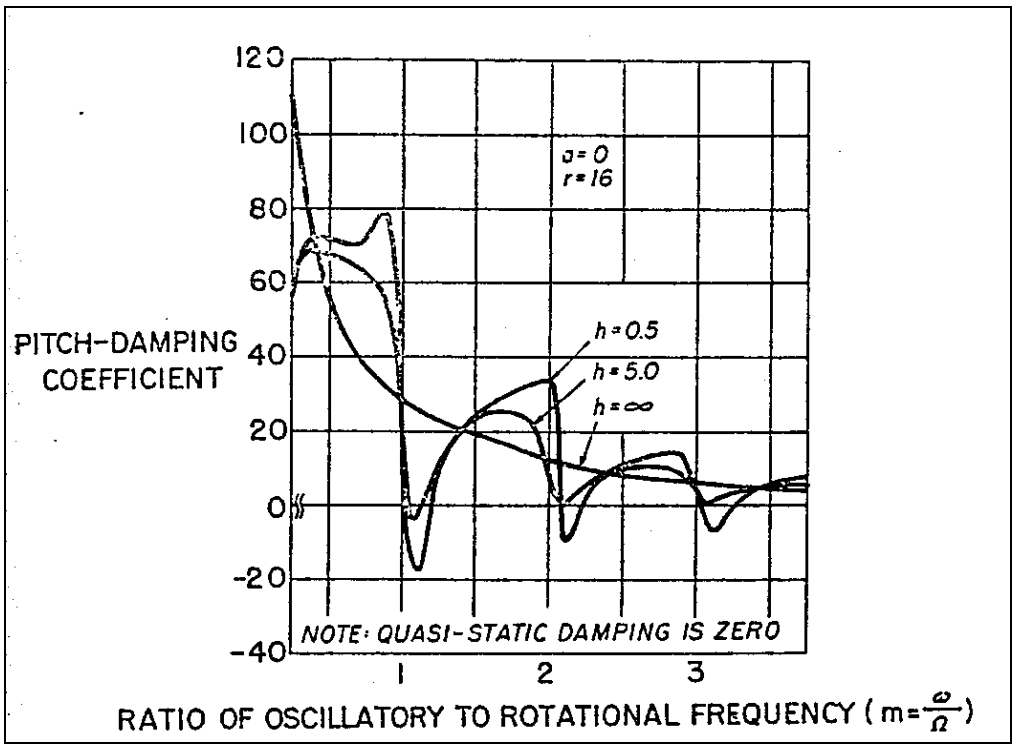

Figure 41. Pitch damping coefficient versus frequency ratio (a = 0) (from Ref. 49).

This destabilizing effect was also noted by Jones and Platzer [Ref. 61] and Turner [Ref. 62]. Jones and Platzer used a panel code to plot the time rate change of the pitch amplitude against frequency ratio for the case of a single wake beneath an airfoil that was oscillating in pure pitch about the leading edge (a = -1.0). Their results showed an instability for $1.52 \leq m \leq 1.84$, which is consistent with Figure 16 (a = -1.0) from Loewy [Ref. 49]. Since the example rotor blade had an aft c.g. offset in the sections with trailing-edge flaps, the effect on pitch damping would be similar to moving the elastic axis aft towards the midchord. Figure 41 above, which is a copy of Figure 18 (a = 0) from Loewy, shows the instability to be in the region of $1.0 < m < 1.25$ corresponding to the results seen for the example rotor blade.

Turner used a panel code to plot the imaginary part of the moment coefficient against the horizontal shift (X_{shift}, expressed in terms of chord lengths) of the lead airfoil in a two airfoil system where both airfoils were oscillating in pure pitch at the same frequency and amplitude. He noted that a positive value for the imaginary part of the moment coefficient corresponded to a negative pitch damping producing an instability.

This horizontal shift can be related to the noninteger portion of the frequency ratio by noting the phase shift between the two layers of vorticity. Since the two airfoils are oscillating at the same frequency and amplitude, the phase shift can be found by taking the ratio of the X_{shift} coordinate to the wavelength of the oscillating layers of vorticity. The wavelength of the layers of vorticity can be found by noting that the oscillating frequency is a circular frequency of oscillation with units of rad/s. This circular frequency can be converted into a frequency in Hz by dividing by 2π, or

$$f = \frac{\omega}{2\pi}. \tag{443}$$

The wavelength of the layers of vorticity can now be written as the ratio of the velocity to the frequency, *f*, or using equation (443)

$$\lambda_v = \frac{2\pi v}{\omega} \tag{444}$$

Therefore using equation (444), the noninteger portion of the frequency ratio can be written as

$$m_{noninteger} = \frac{X_{shift}(2b)\omega}{2\pi v} = \frac{X_{shift}k}{\pi} \tag{445}$$

using the definition of reduced frequency given in equation (80).

Loewy's lift deficiency function assumes that the strength of the previously shed vortices does not change over time or distance. In essence, the effects of viscosity have been neglected in order to obtain a solution via thin airfoil theory, which assumes an incompressible, inviscid fluid. Since the strength of the previously shed vortices would have most likely decayed to zero at a large distance, Peters and He [Ref. 63] developed a lift deficiency function that incorporated a decay function that allows the user to set the rate of decay of the vortices so that those vortices closest to the reference blade will have the greatest effect. While the method of Peters and He is very robust (working in both the frequency and time domain), the finite wake lift deficiency function may provide a simpler method to account for the large effects on the downwash of vortices near the blade while neglecting the diminished effects of vortices at a large distance. Based on wake spacing and the induced velocity of the rotor, the user may select the appropriate

number of wakes to include in the analysis, and in essence introduce some of the effects of viscosity into the thin airfoil theory by limiting the number of wakes that are considered.

Additionally, the finite wake method may be easier to use when making comparisons to computation fluid dynamics (CFD) codes. An example of this type of comparison is shown in Figure 42, in which an Euler code was modified to calculate the propulsive force coefficient, defined by in Ref. 64 as

$$
\begin{aligned}
C_{P_x} = \pi k^2 \Bigg\{ & \bar{h}_0^2 \left(F^2 + G^2\right) \\
& + \bar{\alpha}_0^2 \Bigg[\left(F^2 + G^2\right)\left(\frac{1}{k^2} + \left(\frac{1}{2} - a\right)^2\right) + \frac{1}{2}\left(\frac{1}{2} - a\right) \\
& \qquad - F\left(\frac{1}{2} - a + \frac{1}{k^2}\right) - \left(\frac{1}{2} + a\right)\frac{G}{k} \Bigg] \\
& + \bar{\alpha}_0 \bar{h}_0 \left[\left(\frac{1}{2} - a\right)\left(F^2 + G^2\right) + \frac{1}{2}\left(\frac{1}{2} - \frac{G}{k} - F\right) \right] \Bigg\},
\end{aligned}
$$

with a single wake beneath the reference airfoil and the results were compared to the propulsive force coefficient calculated by the finite wake lift deficiency function. This type of comparison would not be possible using Loewy's lift deficiency function since it would be impossible to model an infinite number of wakes in a CFD code. For this reason, *g*-Ω plots for the example rotor blade using the finite-wake lift deficiency function with a single wake are shown in Figure 43 through Figure 46 for 0P flap frequency. The results are very similar to the Loewy lift deficiency function, but the flutter speed tends not to deviate as much from that calculated using the Theodorsen lift deficiency function. A summary of all the flutter results for the example rotor blade with 0P flap frequency is given in Table 5.

Table 5. Flutter Frequencies and Speeds for Example Rotor Blade (ω_β = 0P).

ω_β	Lift Deficiency Function	m	h/h_0	Flutter Frequency ω_{FL}	Flutter Speed Ω/Ω_0
0P	Theodorsen	-	-	100.7	1.345
	Loewy	0.0	1.0	~110.8	>1.8
		0.25	1.0	107.2	1.108
		0.50	1.0	98.8	1.278
		0.75	1.0	94.7	1.348
	Single Wake	0.0	1.0	102.8	1.447
		0.25	1.0	111.6	1.117
		0.50	1.0	96.4	1.213
		0.75	1.0	93.5	1.410

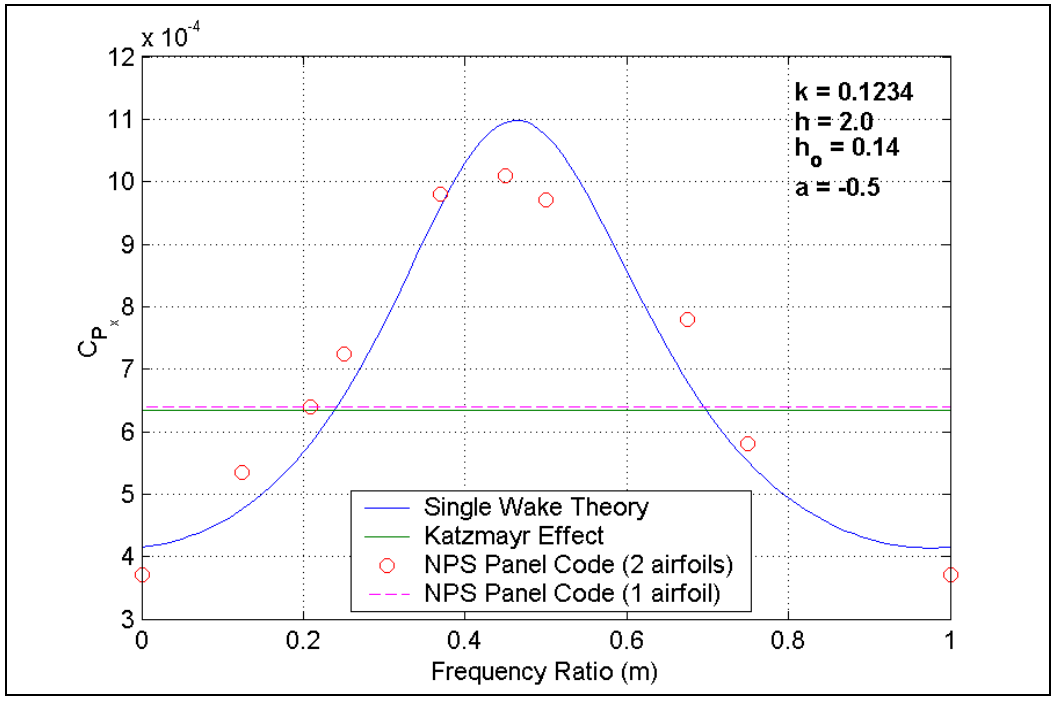

Figure 42. Comparison of single-wake propulsive force coefficient in plunge only to Euler code (from Ref. 14 and 15).

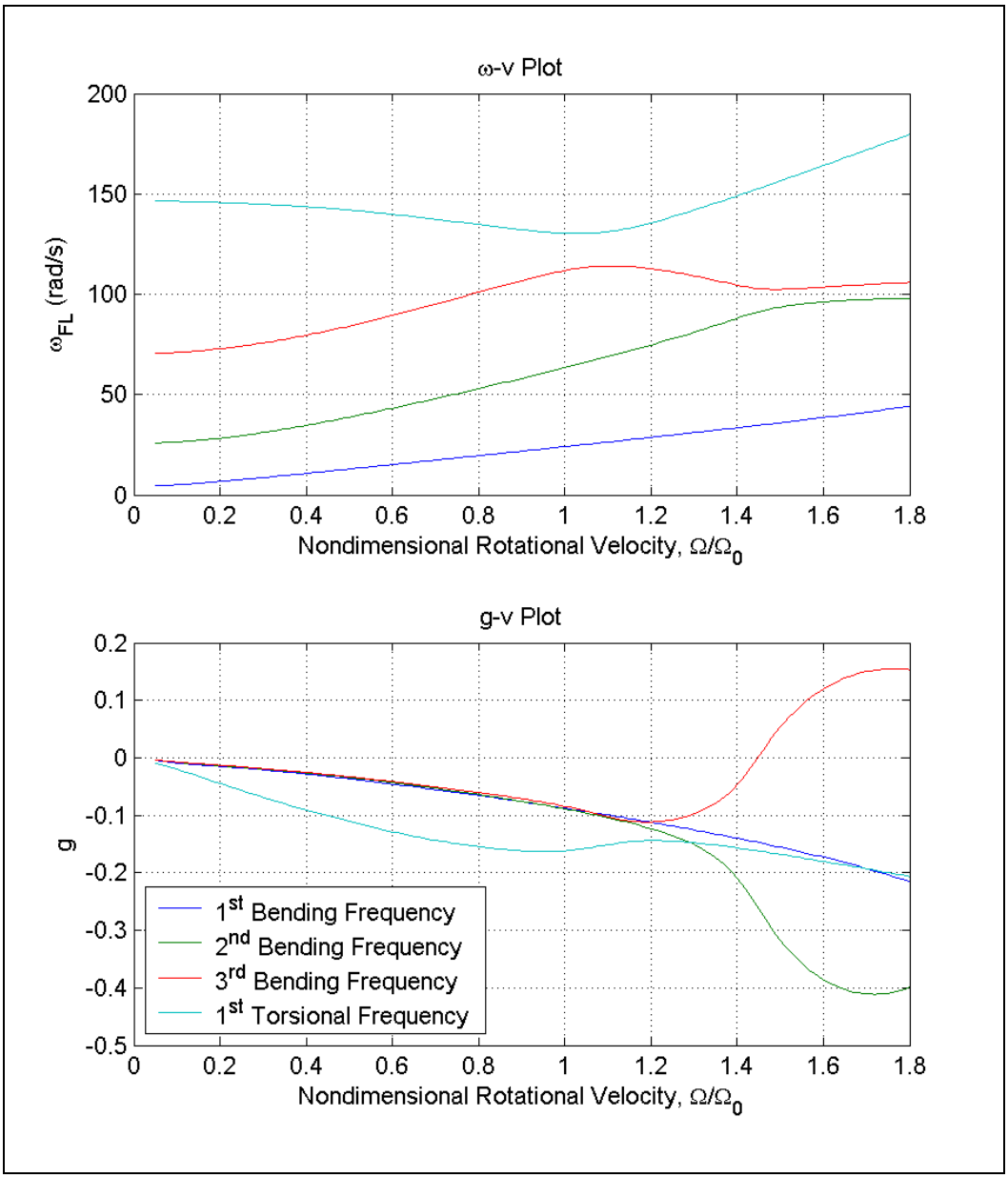

Figure 43. *g*-Ω plot for example rotor blade using finite wake lift deficiency function with a single wake, $m = 0$ ($\omega_\beta = 0P$).

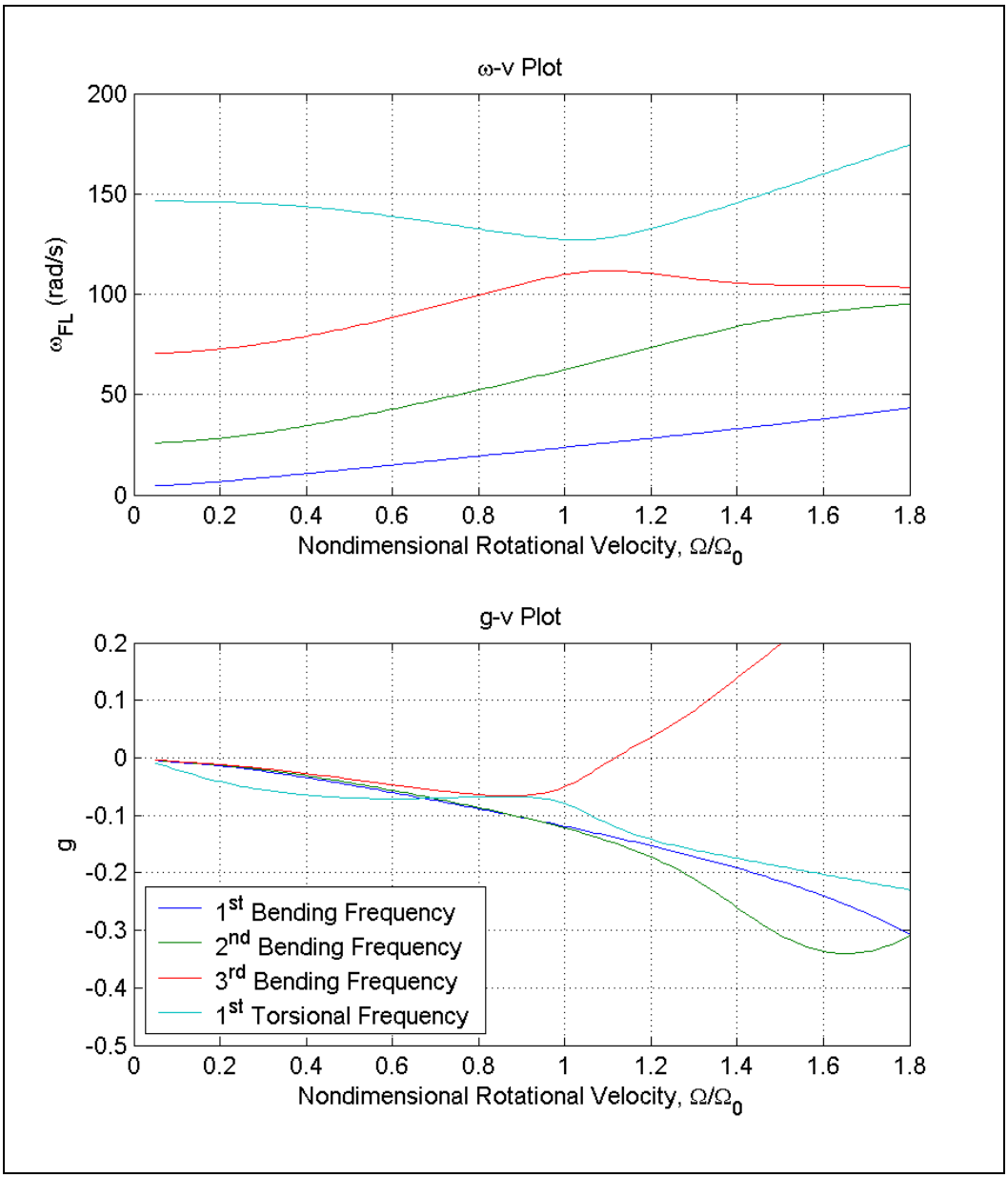

Figure 44. *g*-Ω plot for example rotor blade using finite wake lift deficiency function with a single wake, $m = 0.25$ ($\omega_\beta = 0P$).

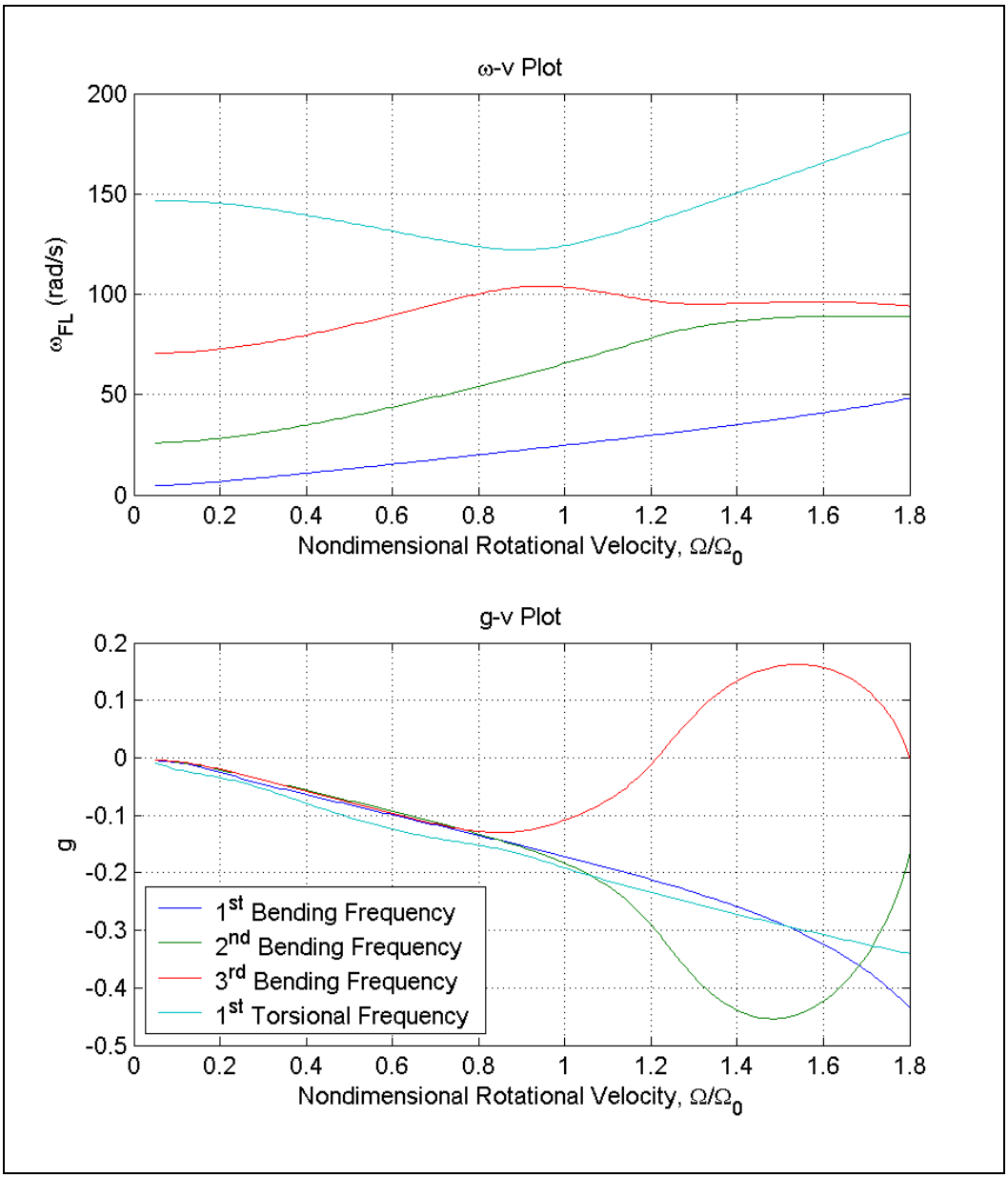

Figure 45. *g*-Ω plot for example rotor blade using finite wake lift deficiency function with a single wake, $m = 0.5$ ($\omega_\beta = 0P$).

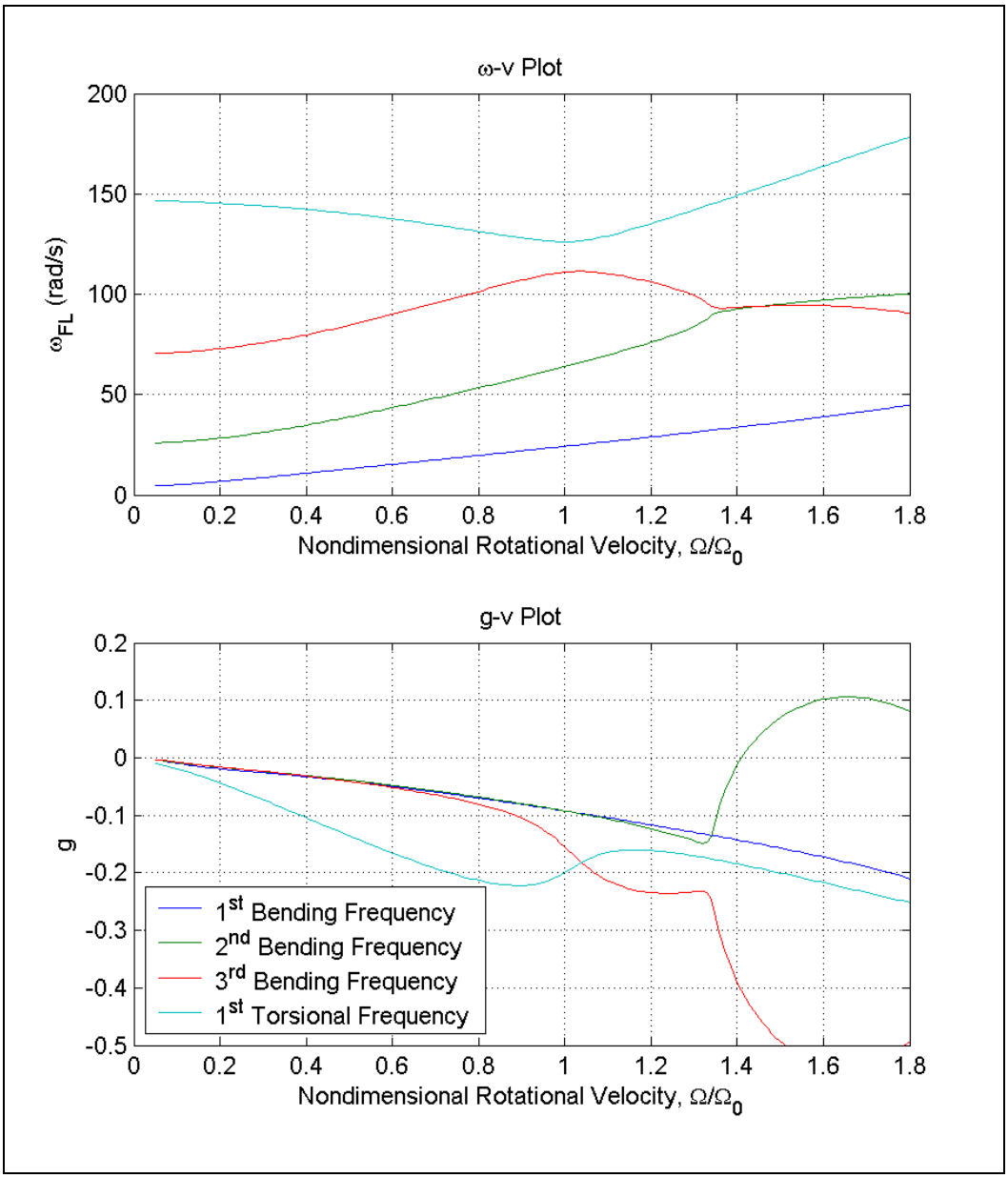

Figure 46. *g*-Ω plot for example rotor blade using finite wake lift deficiency function with a single wake, $m = 0.75$ ($\omega_\beta = 0P$).

Since it would be difficult in practice to maintain an exact frequency ratio as the shed layers of vorticity will move with the mass of air due to wind and begin to dissipate as the vortices interact with one another, it is worthwhile to have another look at the structural characteristics of example rotor blade because of the large changes in flutter speed as the frequency ratio is varied. Recall the quote from the 1960 Sikorsky Report No. 50131 for the Advanced Tactical Helicopter (A.T.H.) [Ref. 6] that to be free of flutter, the "main and tail rotor blades of the A.T.H. have been designed so that center of gravity, elastic axis, and aerodynamic center are coincident." In the example rotor blade, the center of gravity in the sections with the trailing-edge flap was moved aft from the 25% chord to the 40% chord. The purpose of this feature was to see if the c.g./e.a./a.c. design constraints used on the A.T.H., and currently used on many helicopters, are necessary given this new flutter analysis method. Figure 47 through Figure 55 are *g*-Ω plots of the example rotor blade, in which the c.g. in the sections with the trailing-edge flap was made to remain at the 25% chord (no c.g. offset cases). It can be seen from the figures that the rotor blade is aeroelastically stable for all lift deficiency functions and frequency ratios therefore giving additional credibility to the statement about the A.T.H. main and tail rotor blades being free from flutter. Therefore, while some amount of c.g. offset may be permissible, it still has a large effect on the stability of the rotor blade and care must be used when moving the c.g. off the 25% chord position, even if it is only along a small section of the rotor blade where the trailing-edge flap is incorporated.

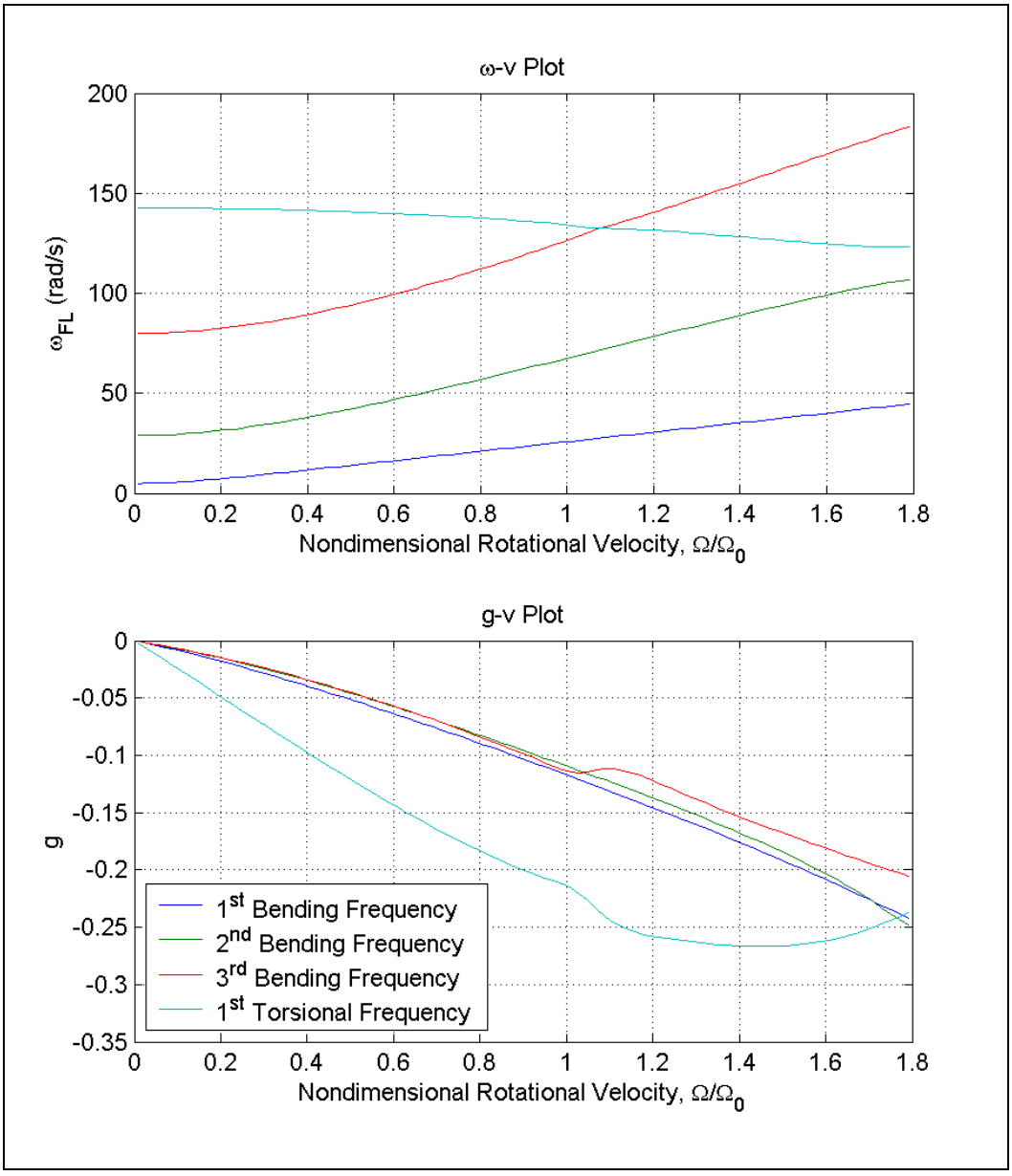

Figure 47. *g*-Ω plot for example rotor blade with no c.g. offset using Theodorsen's lift deficiency function (ω_β = 0P).

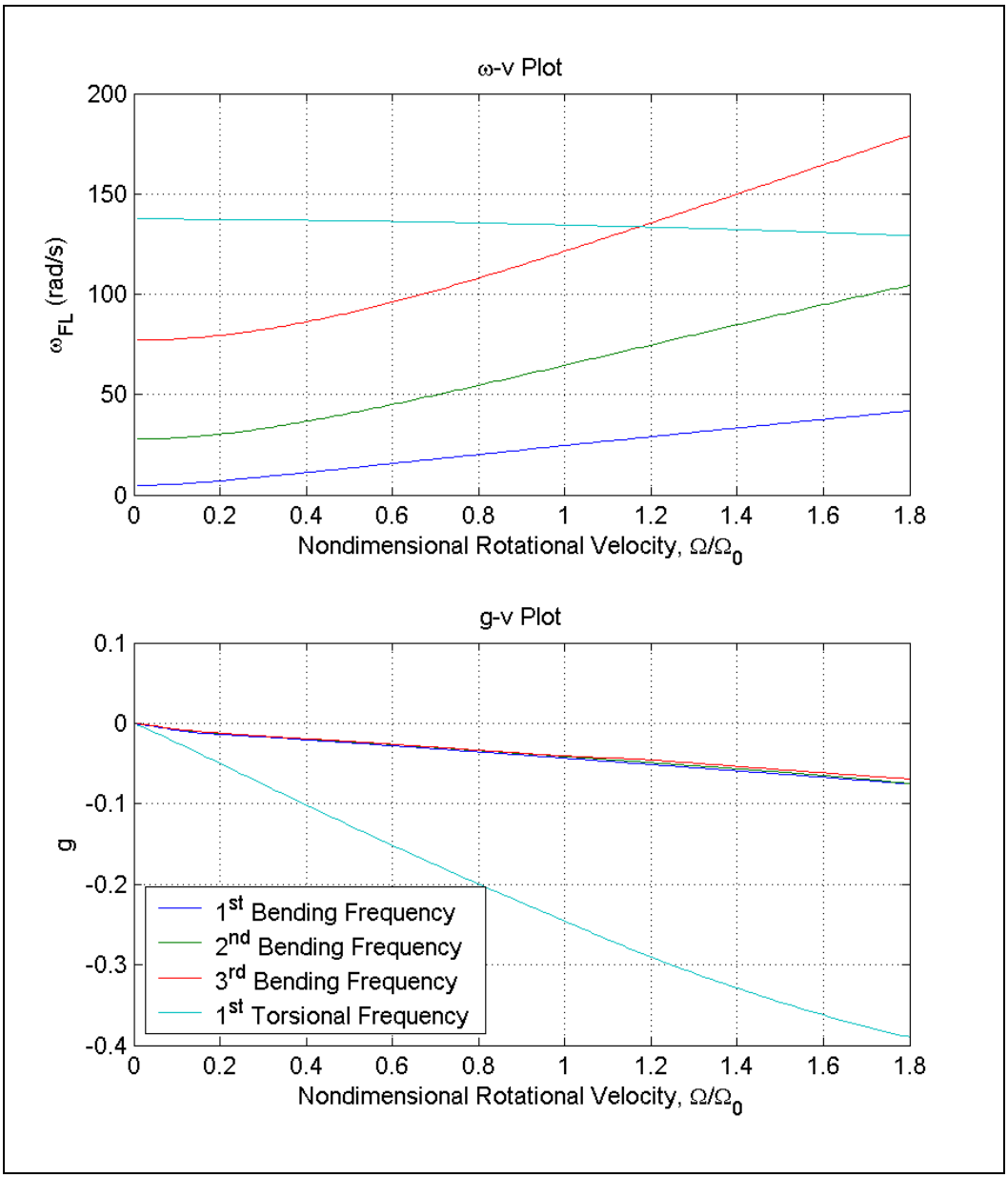

Figure 48. *g*-Ω plot for example rotor blade with no c.g. offset using Loewy's lift deficiency function, $m = 0$ ($\omega_\beta = 0$P).

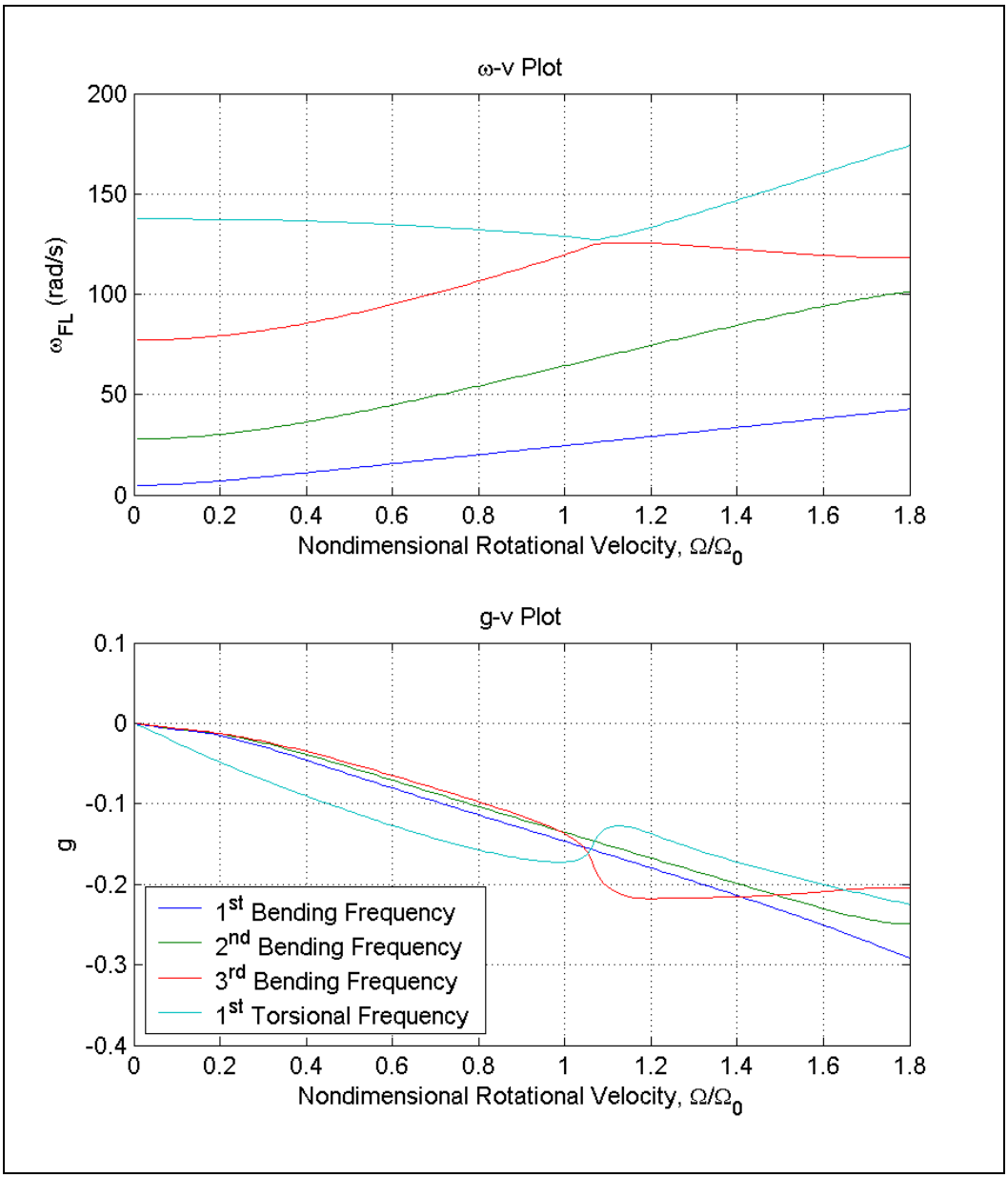

Figure 49. *g*-Ω plot for example rotor blade with no c.g. offset using Loewy's lift deficiency function, $m = 0.25$ ($\omega_\beta = 0$P).

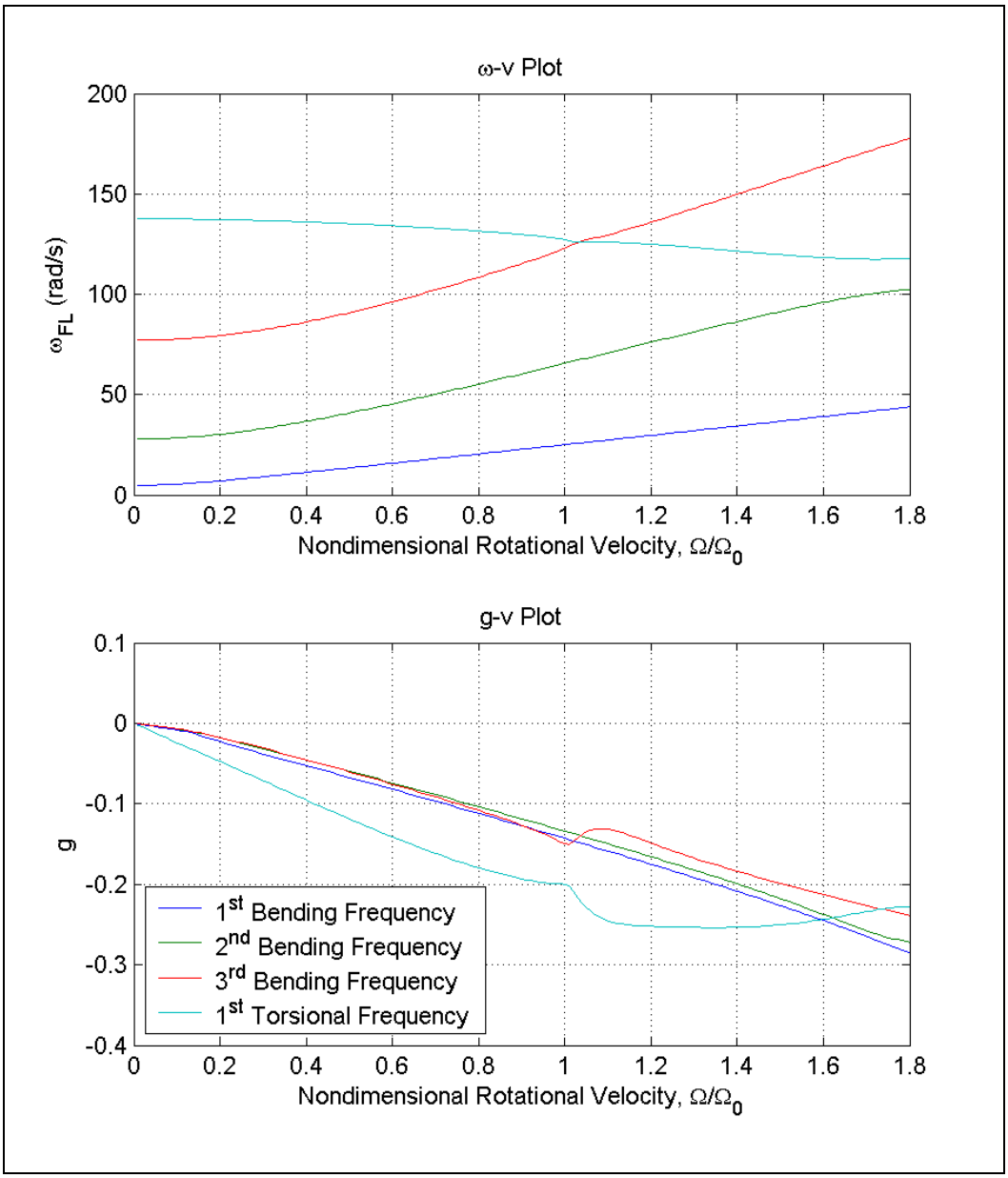

Figure 50. *g*-Ω plot for example rotor blade with no c.g. offset using Loewy's lift deficiency function, $m = 0.5$ ($\omega_\beta = 0$P).

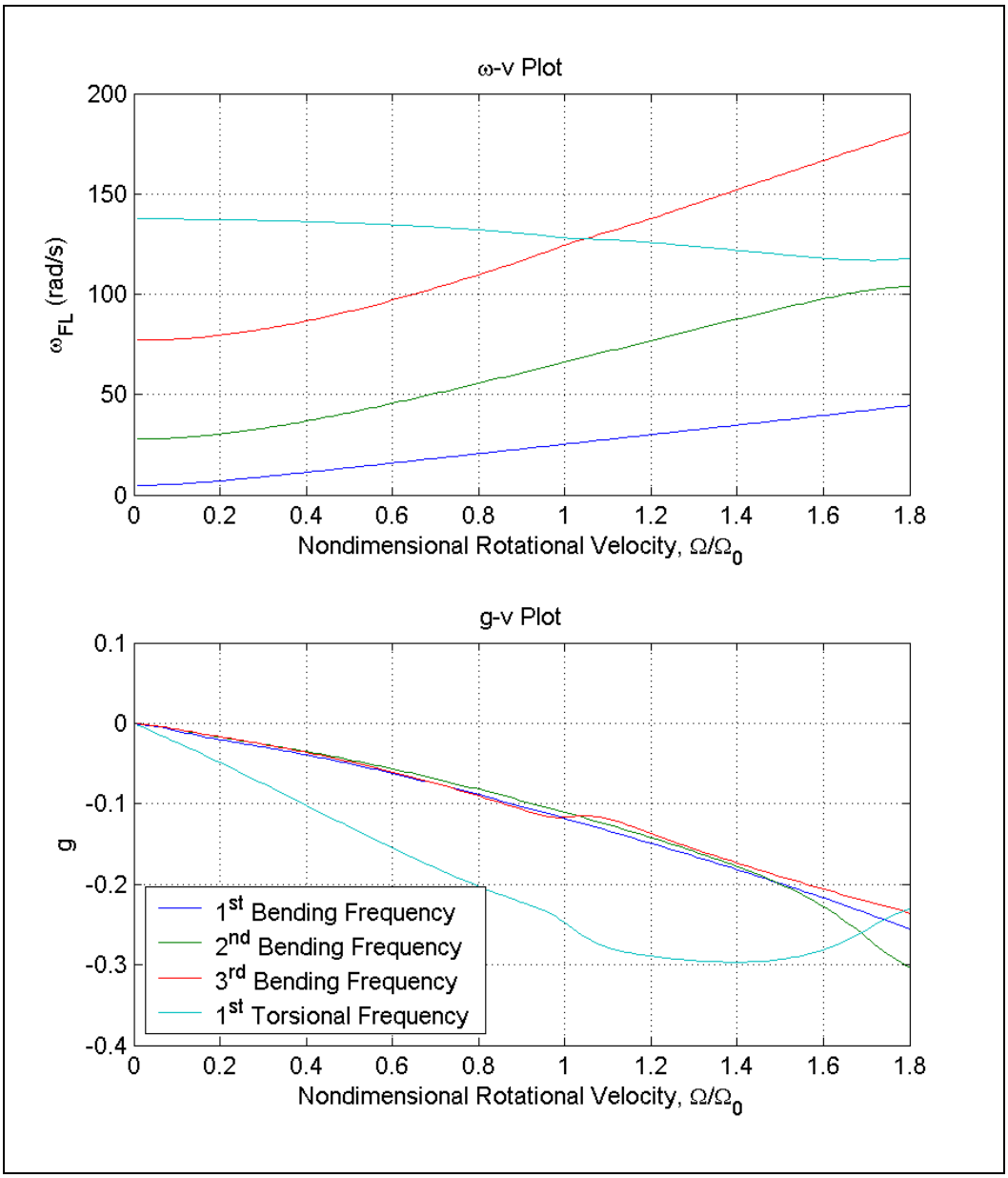

Figure 51. *g*-Ω plot for example rotor blade with no c.g. offset using Loewy's lift deficiency function, $m = 0.75$ ($\omega_\beta = 0P$).

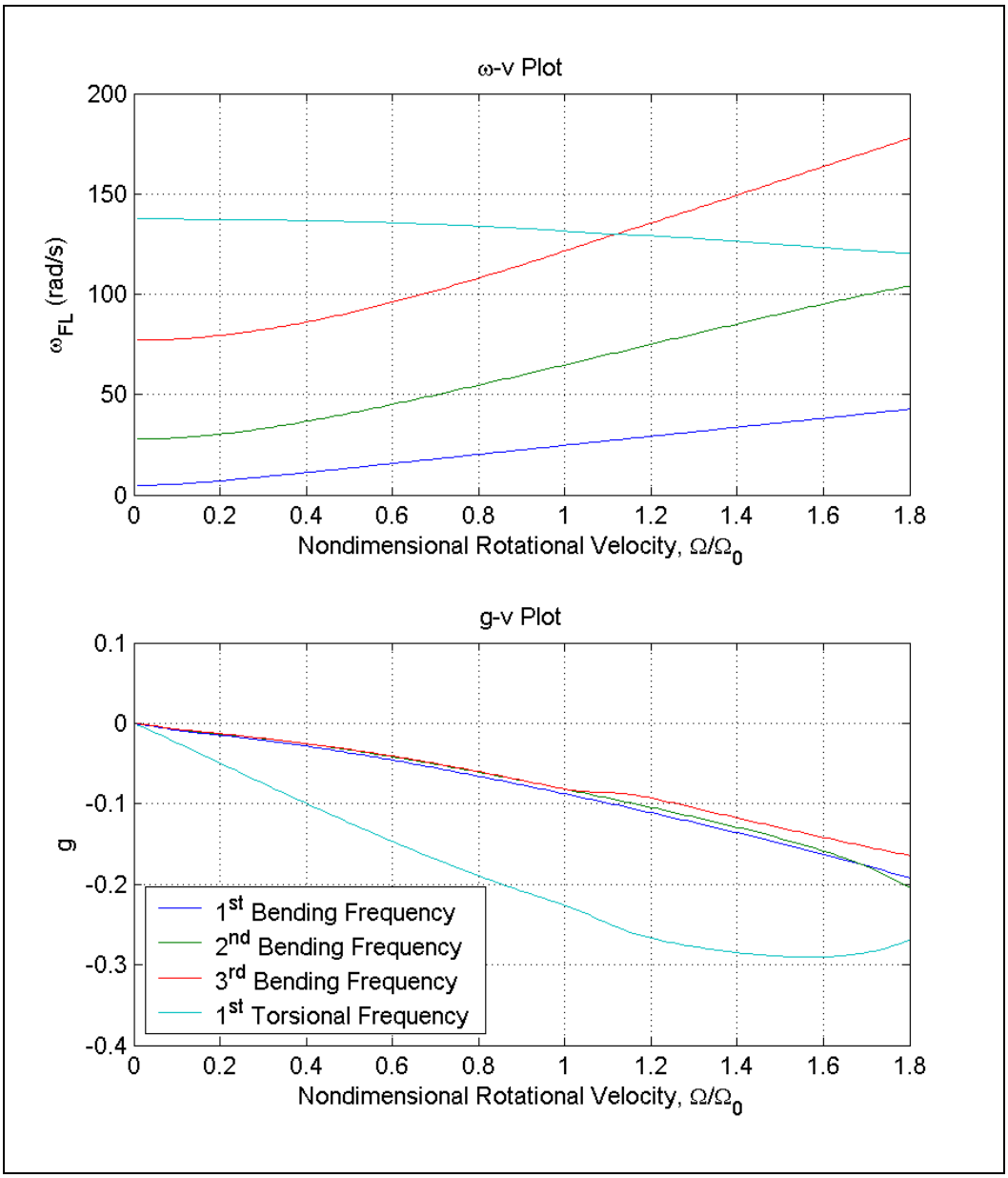

Figure 52. *g*-Ω plot for example rotor blade with no c.g. offset using finite wake lift deficiency function with a single wake, $m = 0$ ($\omega_\beta = 0P$).

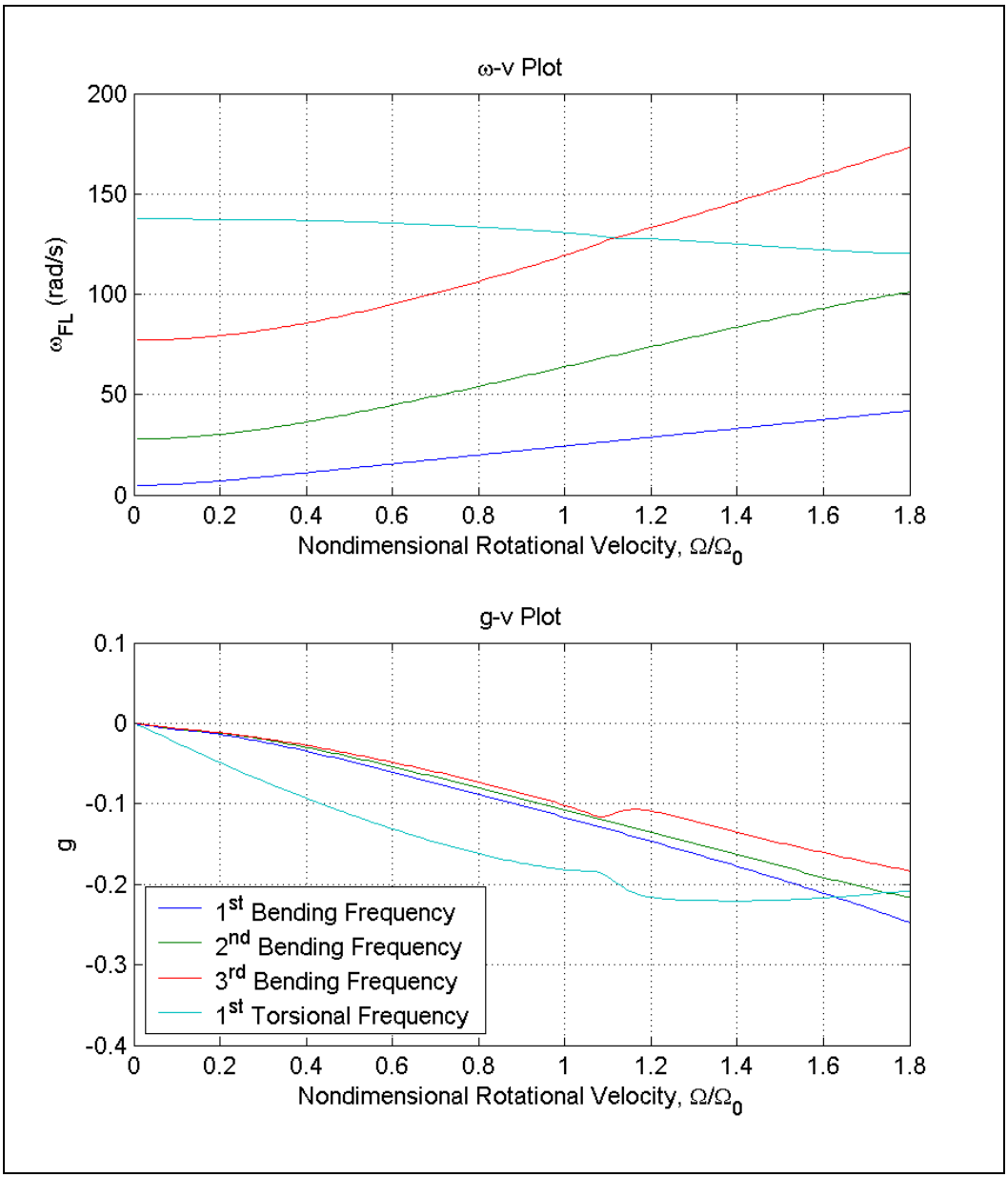

Figure 53. *g*-Ω plot for example rotor blade with no c.g. offset using finite wake lift deficiency function with a single wake, $m = 0.25$ ($\omega_\beta = 0P$).

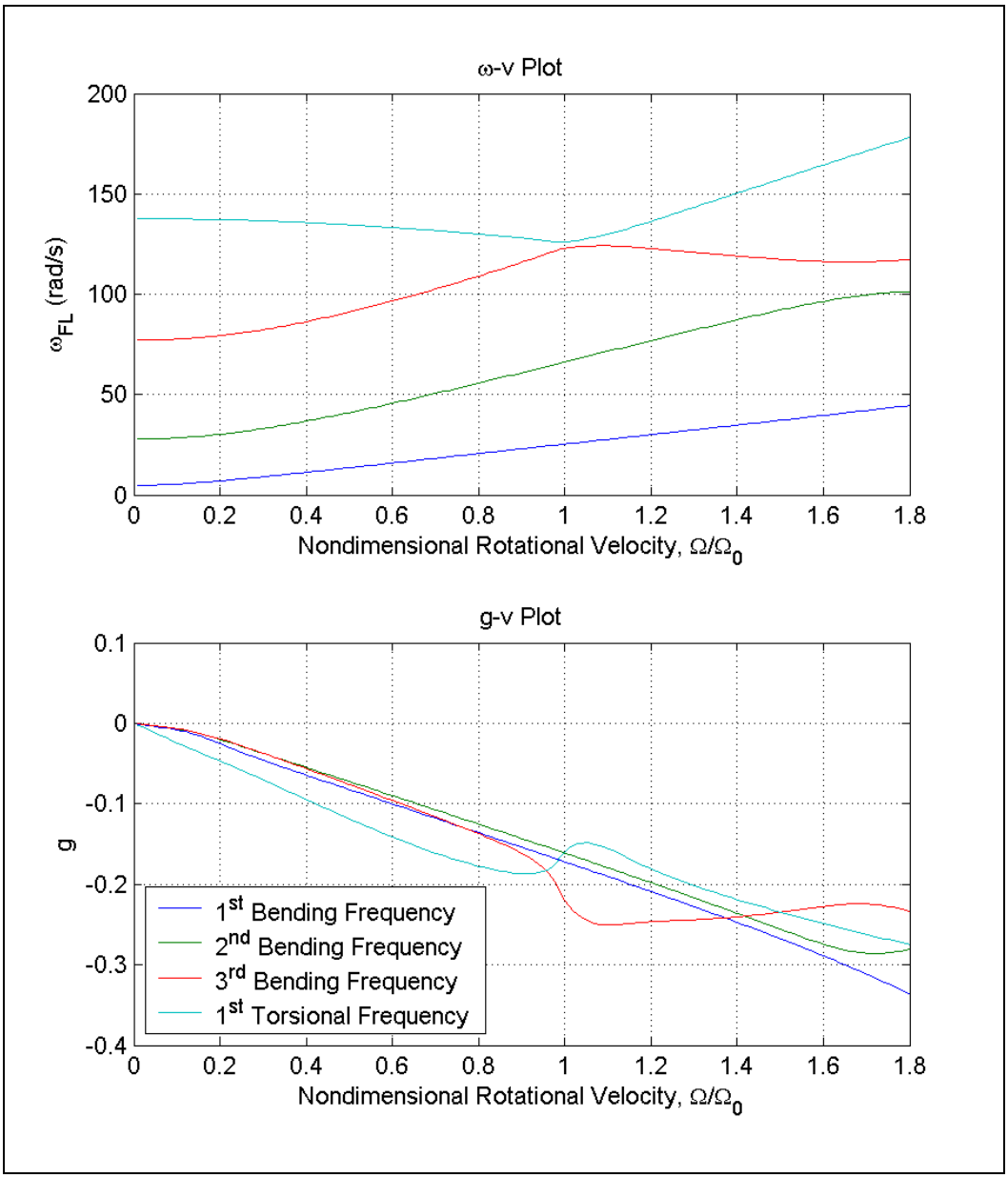

Figure 54. *g*-Ω plot for example rotor blade with no c.g. offset using finite wake lift deficiency function with a single wake, $m = 0.5$ ($\omega_\beta = 0P$).

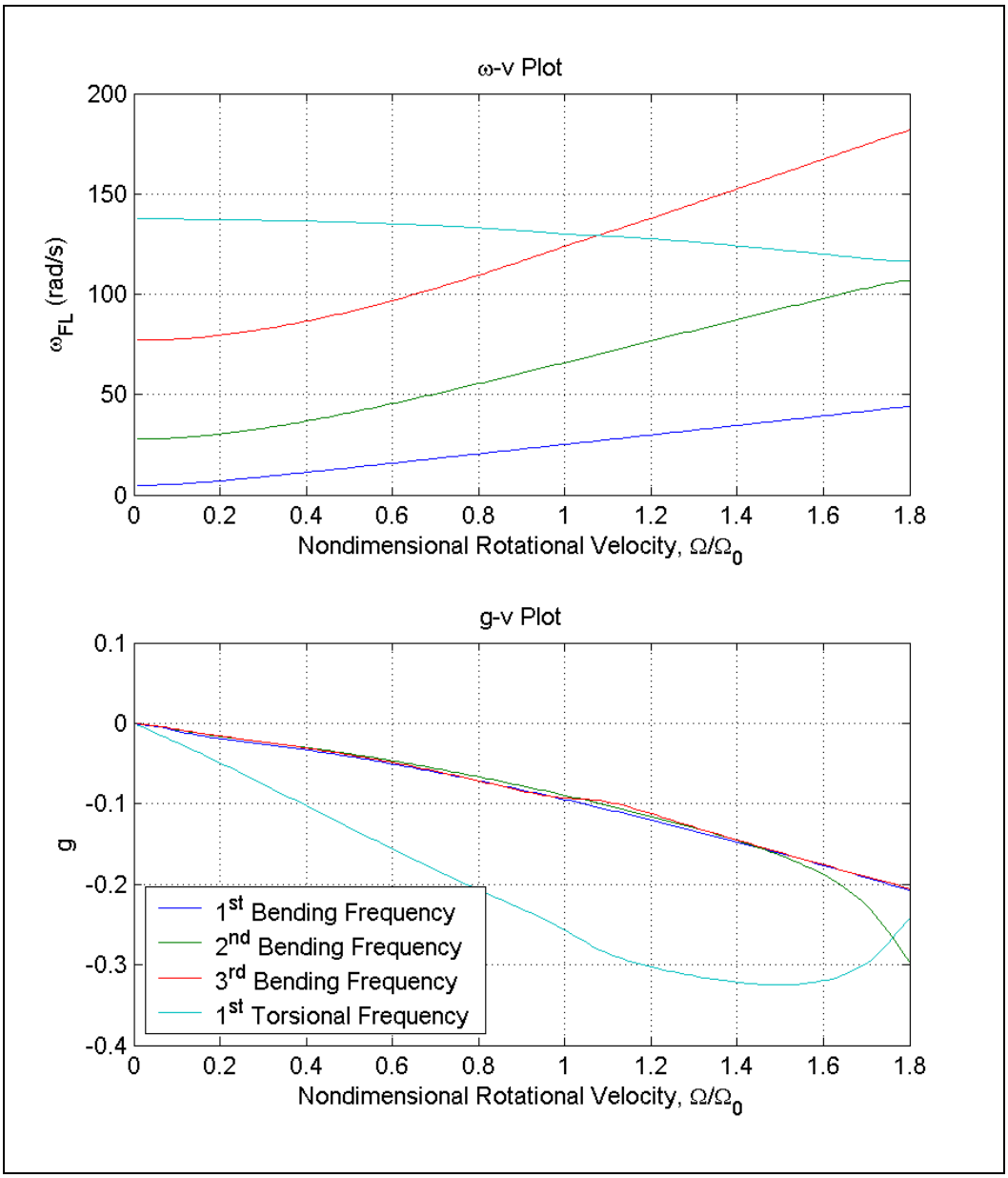

Figure 55. *g*-Ω plot for example rotor blade with no c.g. offset using finite wake lift deficiency function with a single wake, *m* = 0.75 (ω_β = 0P).

B. 4P FLAP FREQUENCY

In comparing the Southwell plot for the 4P flap frequency in Figure 32 to that of the 0P plot in Figure 27, the interaction between the various coupled modes is about the same with the noted exception of the flap frequency. Figure 56 through Figure 64 are the *g*-Ω plots for the example rotor blade with c.g. offset, and these plots look very similar to

the 0P plots with c.g. offset. Arguments similar to those for the 0P flap frequency can be made for the 4P frequency for the changes seen as the frequency ratio is varied. A summary of the flutter frequencies and speeds for the 4P flap frequency is contained in Table 6. When the c.g. offset is removed, the blade becomes stable with all lift deficiency functions and all frequency ratios. Plots of the 4P flap frequency without c.g. offset have not been included since they are similar to the 0P plots.

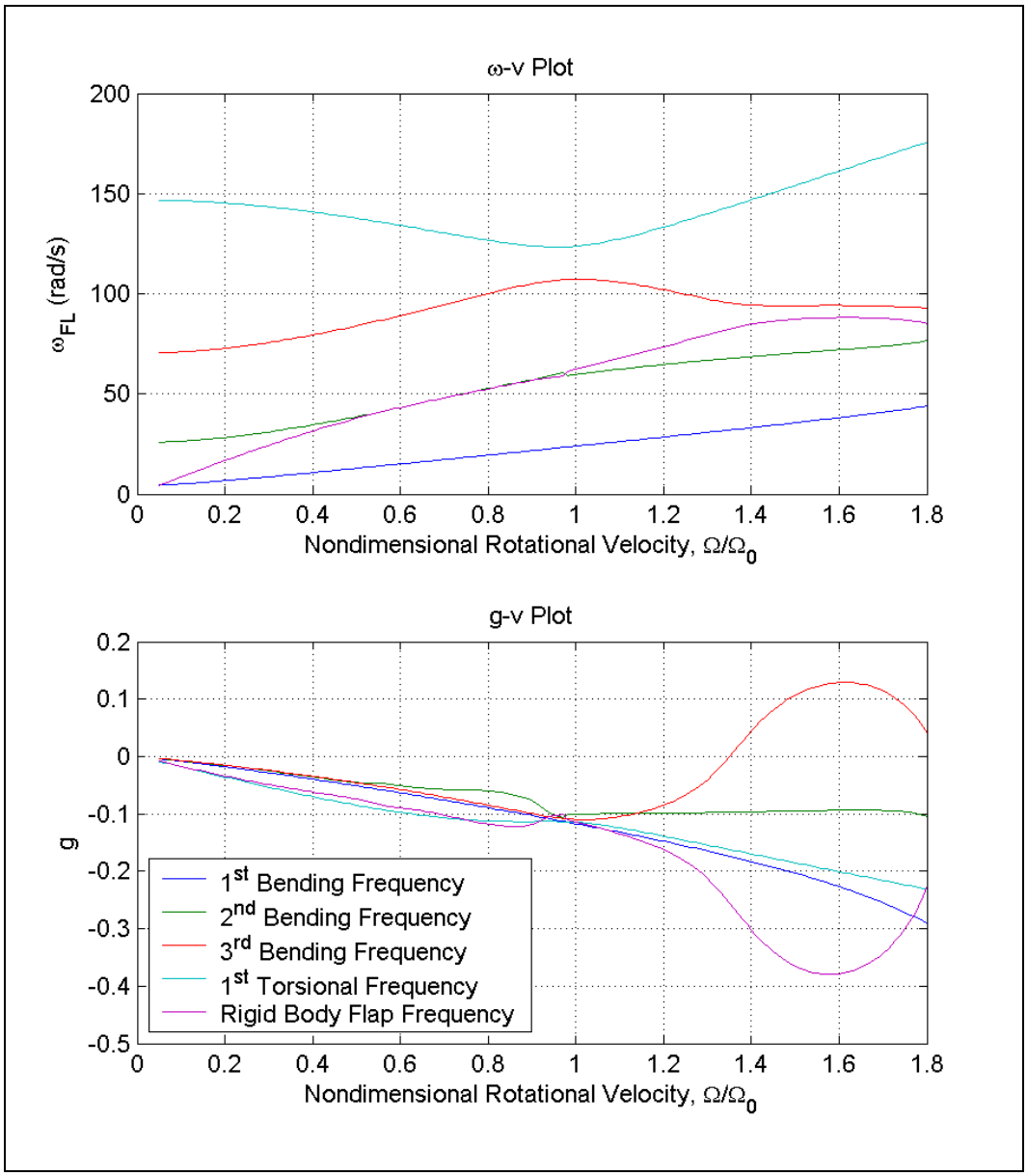

Figure 56. *g*-Ω plot for example rotor blade using Theodorsen's lift deficiency function (ω_β = 4P).

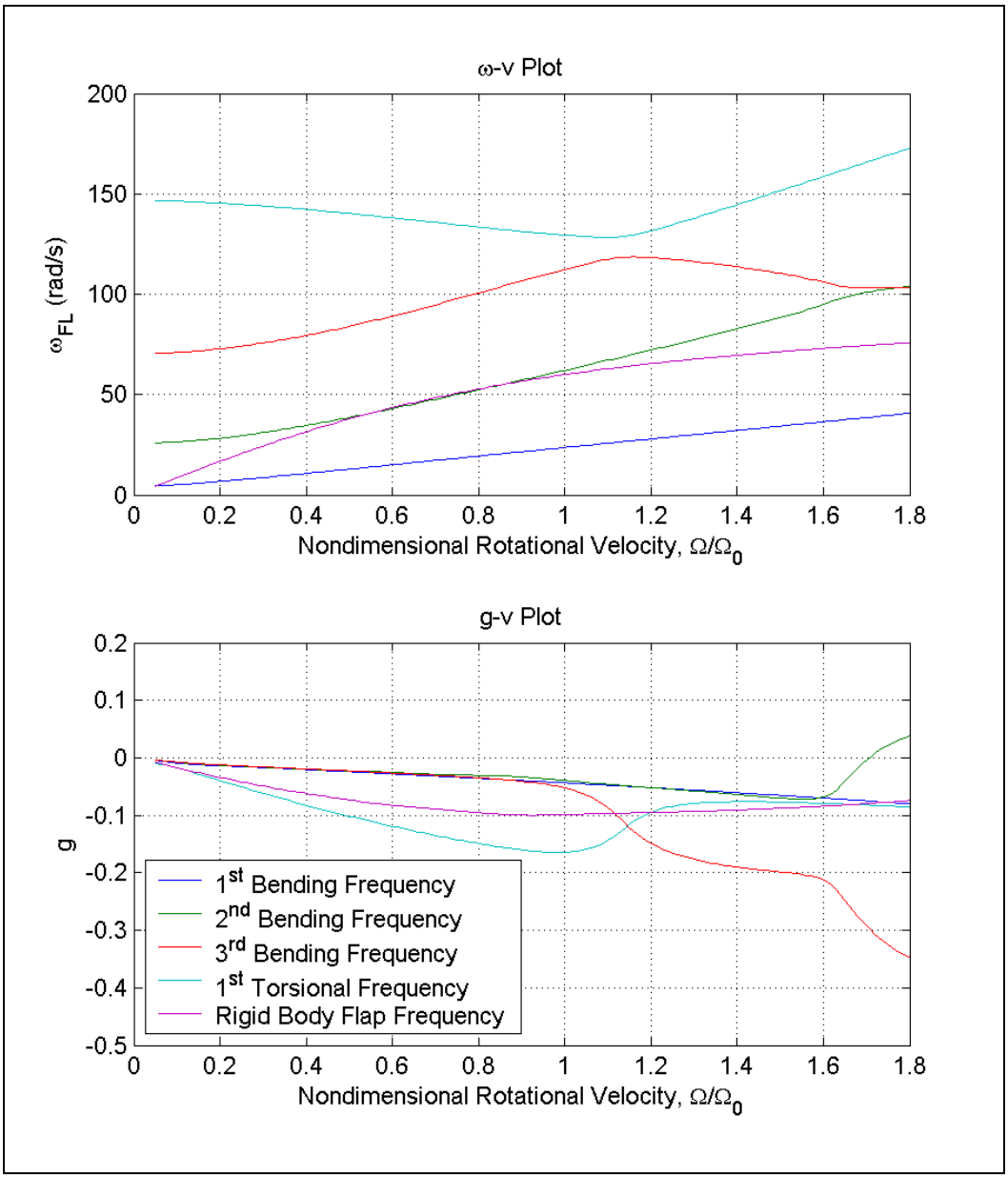

Figure 57. *g*-Ω plot for example rotor blade using Loewy's lift deficiency function, $m = 0$ ($\omega_\beta = 4P$).

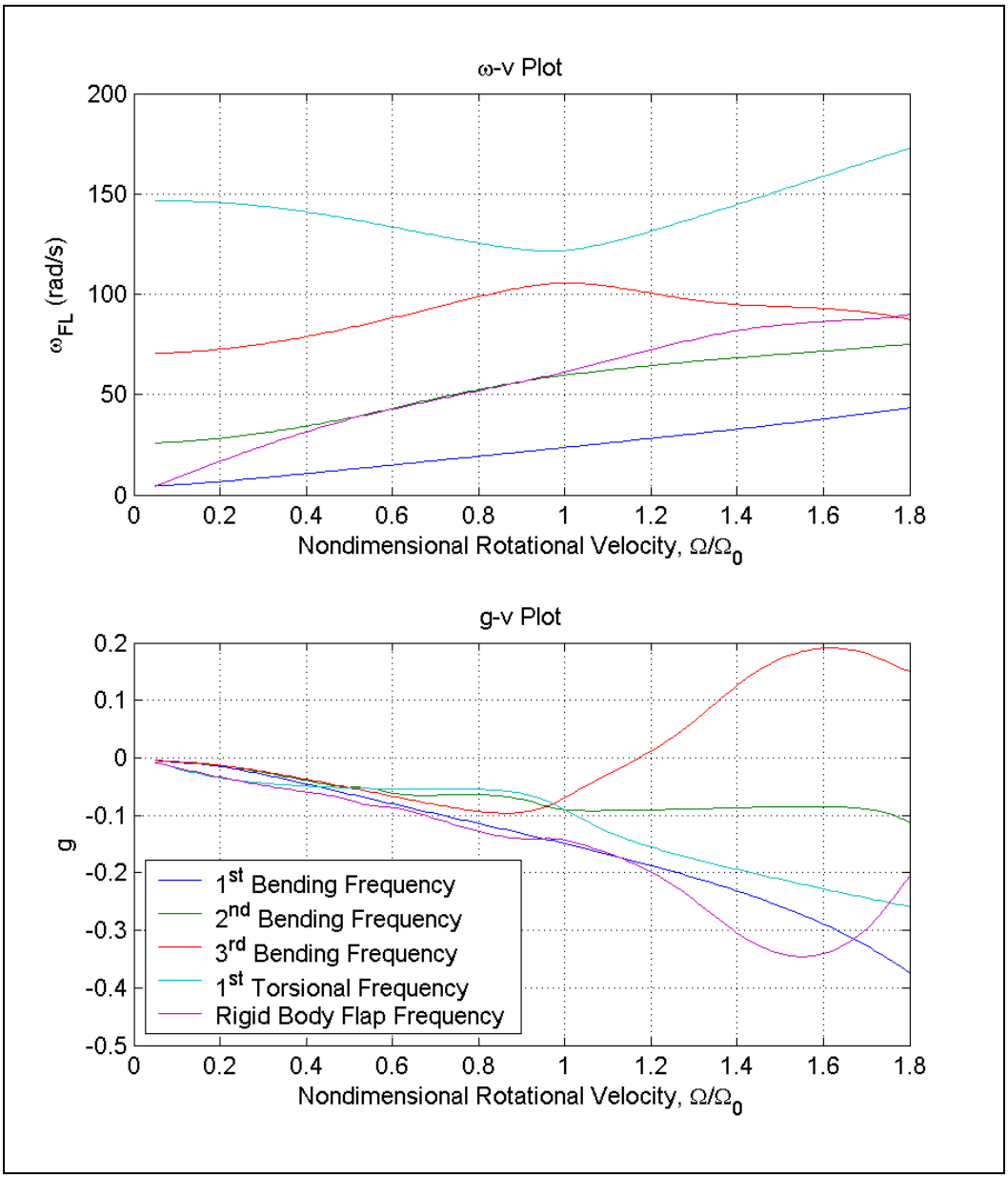

Figure 58. *g*-Ω plot for example rotor blade using Loewy's lift deficiency function, $m = 0.25$ ($\omega_\beta = 4P$).

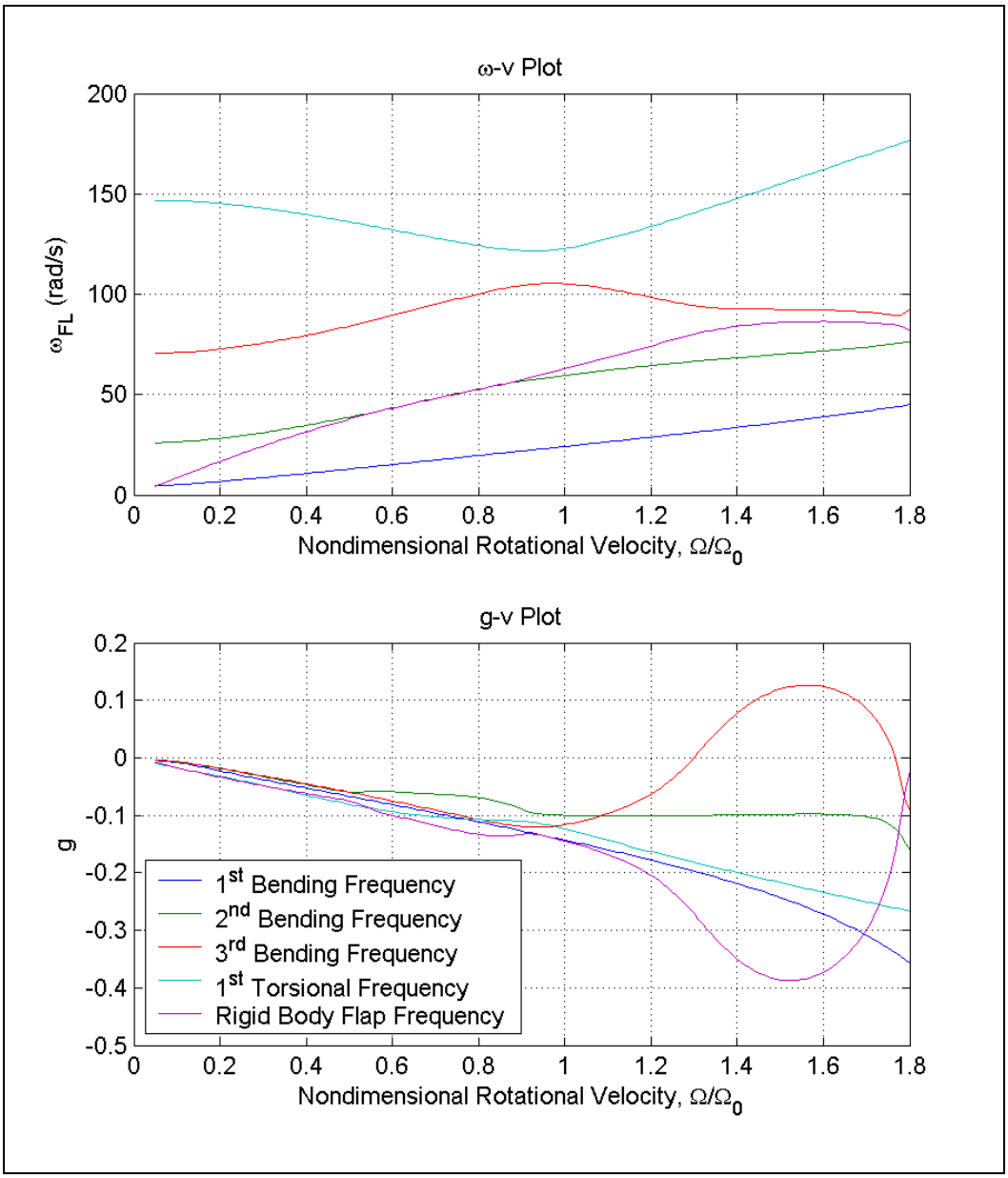

Figure 59. *g*-Ω plot for example rotor blade using Loewy's lift deficiency function, $m = 0.5$ ($\omega_\beta = 4P$).

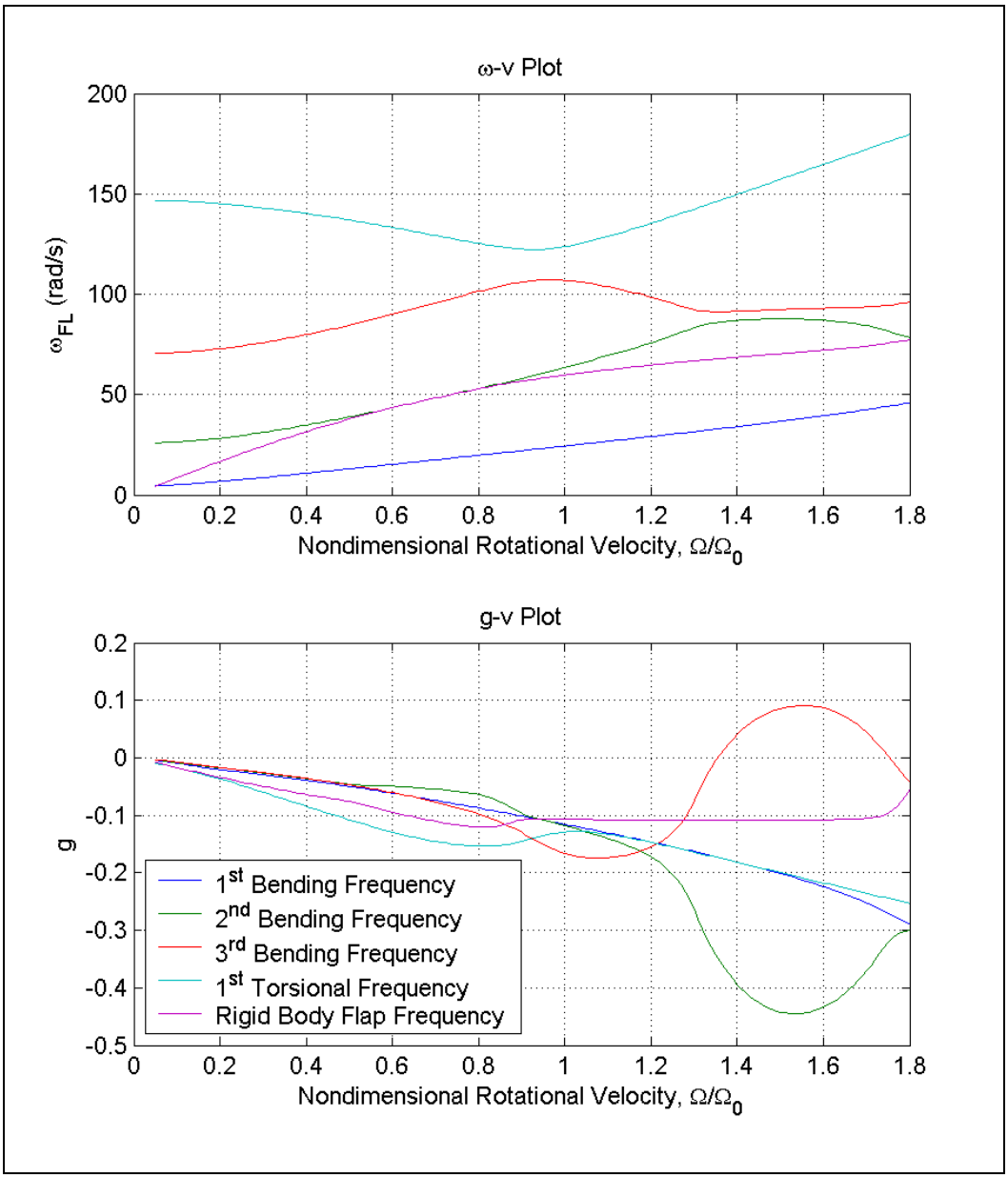

Figure 60. *g*-Ω plot for example rotor blade using Loewy's lift deficiency function, $m = 0.75$ ($\omega_\beta = 4P$).

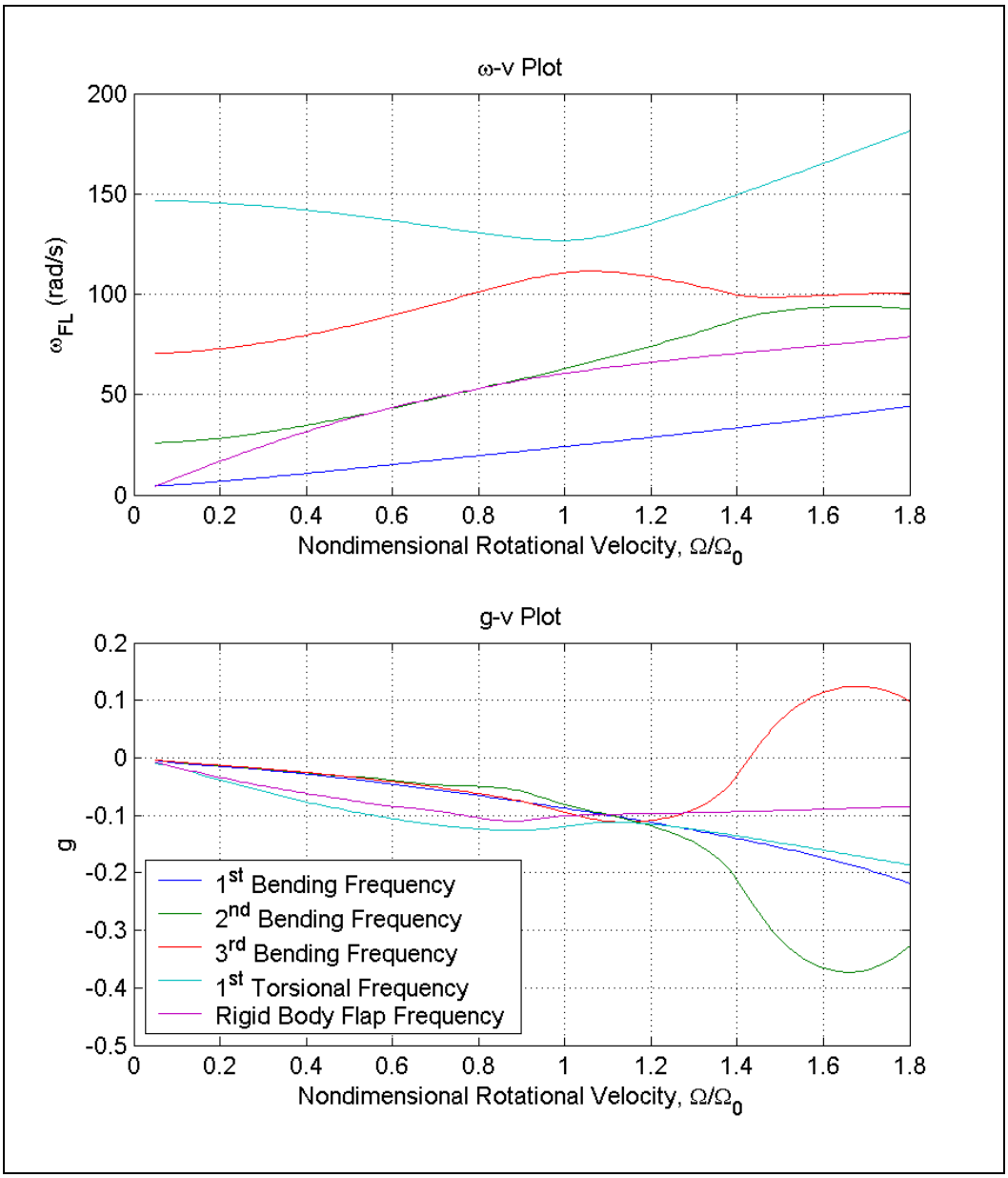

Figure 61. *g*-Ω plot for example rotor blade using finite wake lift deficiency function with a single wake, $m = 0$ ($\omega_\beta = 4P$).

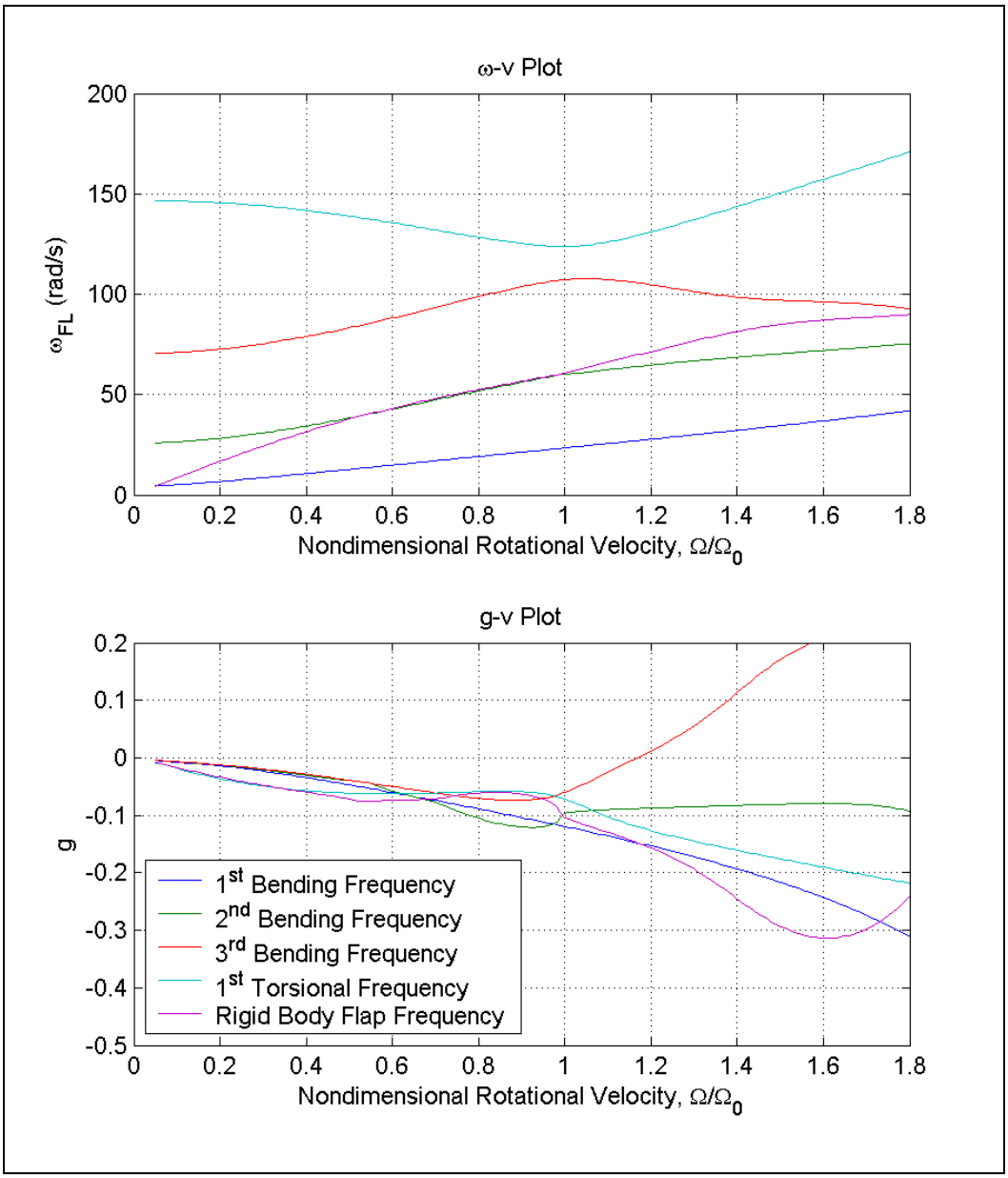

Figure 62. *g*-Ω plot for example rotor blade using finite wake lift deficiency function with a single wake, $m = 0.25$ ($\omega_\beta = 4P$).

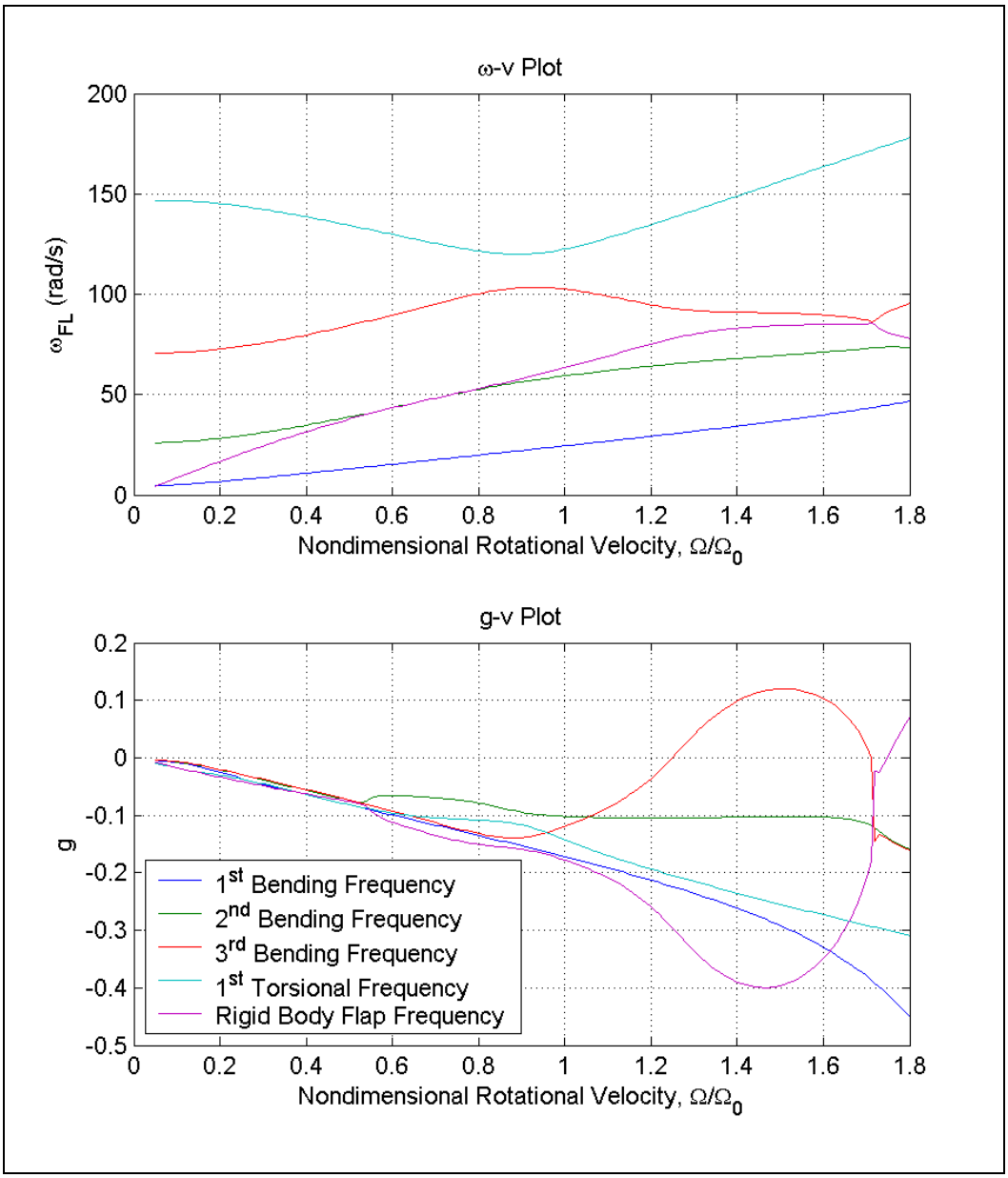

Figure 63. *g*-Ω plot for example rotor blade using finite wake lift deficiency function with a single wake, $m = 0.5$ ($\omega_\beta = 4P$).

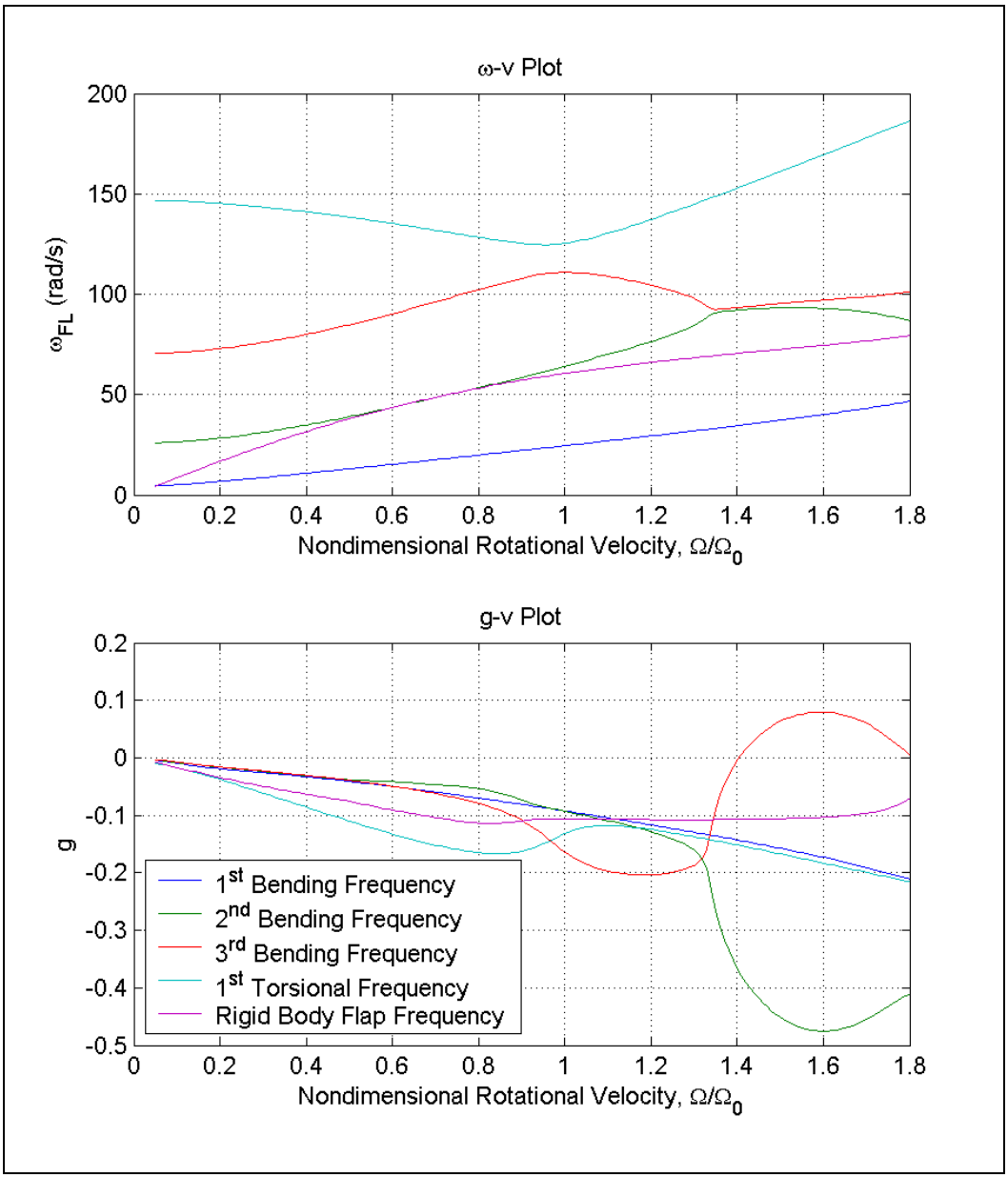

Figure 64. *g*-Ω plot for example rotor blade using finite wake lift deficiency function with a single wake, $m = 0.75$ ($\omega_\beta = 4P$).

Table 6. Flutter Frequencies and Speeds for Example Rotor Blade (ω_β = 4P).

ω_β	Lift Deficiency Function	m	h/h_0	Flutter Frequency ω_{FL}	Flutter Speed Ω/Ω_0
4P	Theodorsen	-	-	95.4	1.350
	Loewy	0.0	1.0	103.2	1.706
		0.25	1.0	101.6	1.173
		0.50	1.0	94.4	1.299
		0.75	1.0	91.3	1.354
	Single Wake	0.0	1.0	98.9	1.429
		0.25	1.0	105.6	1.169
		0.50	1.0	93.0	1.249
		0.75	1.0	93.4	1.404

C. 5P FLAP FREQUENCY AND EFFECTS OF WAKE SPACING

For the example rotor blade, the 5P frequency is the blade passage frequency. Inputs at the blade passage frequency are significant because these inputs will be transferred from the rotating system to the fixed system as either 5P vibrations for collective inputs, or 4P and 6P vibrations for cyclic inputs. A *g*-Ω plot using Theodorsen's lift deficiency function for the 5P flap frequency is shown in Figure 65. The flutter speed is $1.304\Omega_0$ (265 rpm), which is above the normal operating range, but lower than the flutter speeds calculated using 0P and 4P flap frequencies. Figure 66 through Figure 69 are *g*-Ω plots using Loewy's lift deficiency function for the 5P flap frequency. The flutter speed for the case of $m = 0$ is still above that using Theodorsen, but for the cases of $m = 0.25$, $m = 0.5$, and $m = 0.75$, the flutter speeds are below the Theodorsen case. It can be noted that the large variation in flutter speeds between the Loewy cases and the Theodorsen cases seen in the 0P and 4P flap frequencies is becoming smaller for the 5P flap frequency. Figure 70 through Figure 73 are *g*-Ω plots using the finite wake lift deficiency with a single wake. Again, the variations in flutter speeds for the 5P flap frequency are smaller than the 0P and 4P input frequencies. A possible reason for this apparent decrease in the variation is that there is more interaction between the coupled modes with a 5P flap frequency as can be seen in Figure 33. Primarily, it is the flap input, 1st blade torsion, and 3rd bending modes that are interacting more causing two natural frequencies to coincide at the blade passage frequency when

the rotational frequency is $1.2\Omega_0$ – $1.3\Omega_0$. Recall from the previous discussion on the Southwell plot for the 5P input frequency that from structural dynamics alone, the example blade was a good blade design because the modes were interacting well above the normal operating range. While this is still the case, it can be seen that the structural dynamics is the driving force on the flutter solution. When natural frequencies begin to coincide, the choice of lift deficiency functions becomes less of an issue.

For the Loewy and finite wake lift deficiency functions, wake spacing is also a parameter that can be varied. Because the 5P flap frequency corresponded to the blade passage frequency, it was decided to investigate the effect of wake spacing on the flutter speed. Table 7 contains a summary of the flutter frequencies and speeds for a 5P flap frequency for different frequency ratios and wake spacings. The wake spacings that are less than $1.0\,\hat{h}_0$ represent the partial power cases and correspond to the rotor in a descent or on the ground with partial power applied, while the wake spacings that is greater than 1.0. $\hat{h}_0$ correspond to the rotor in a climb. The primary effect of an increase in wake spacing is that the flutter speed moves closer to the Theodorsen case. This can be explained mathematically by noting that as $\hat{h} \to \infty$, $C'\left(k, \hat{h}, m\right)$ and $C'_N\left(k, \hat{h}, m\right) \to C\left(k\right)$, and the flutter speed would converge to the Theodorsen solution. Except for large changes in the wake spacing, Table 7 shows small changes in the flutter frequencies and speeds.

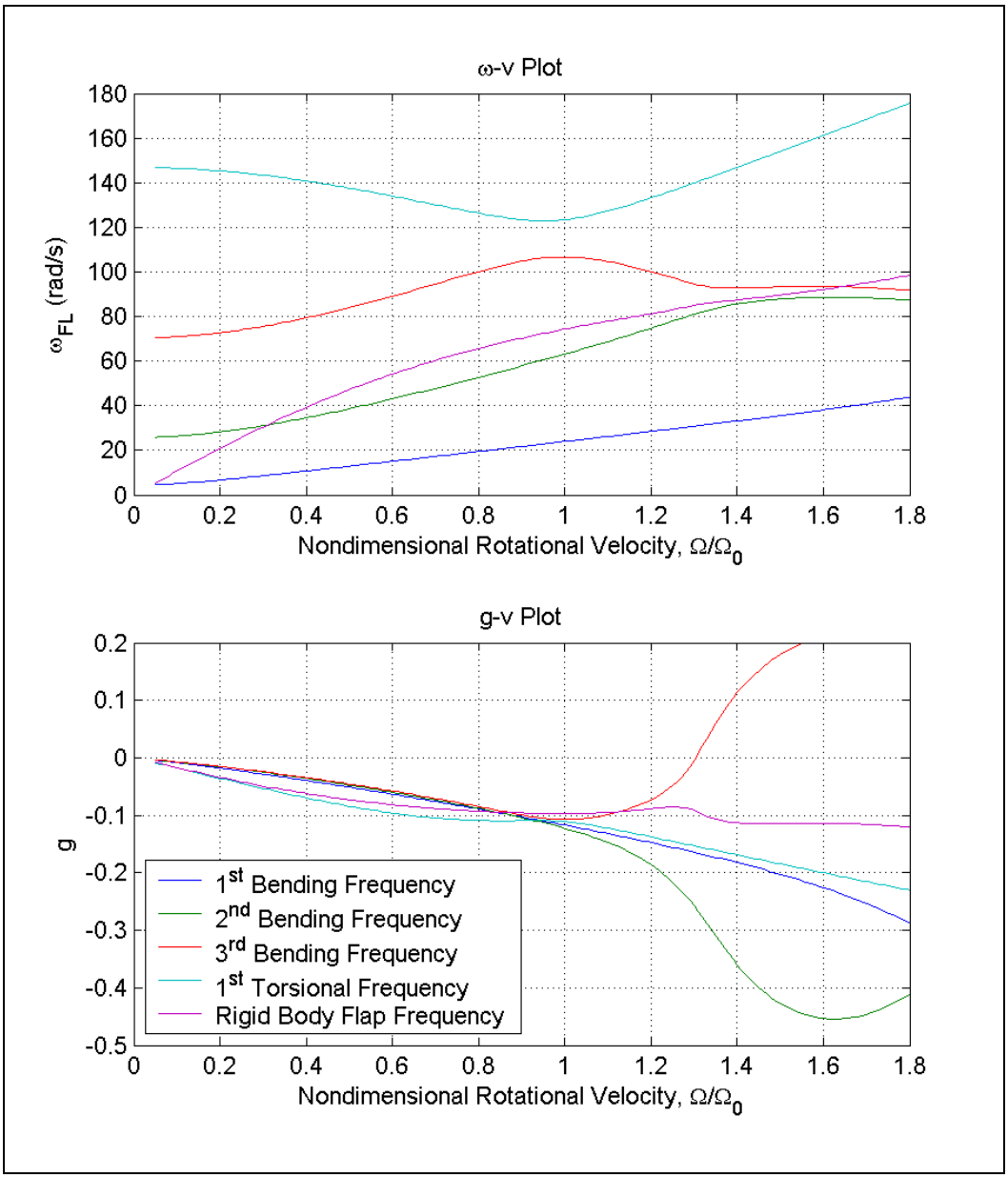

Figure 65. *g*-Ω plot for example rotor blade using Theodorsen's lift deficiency function (ω_β = 5P).

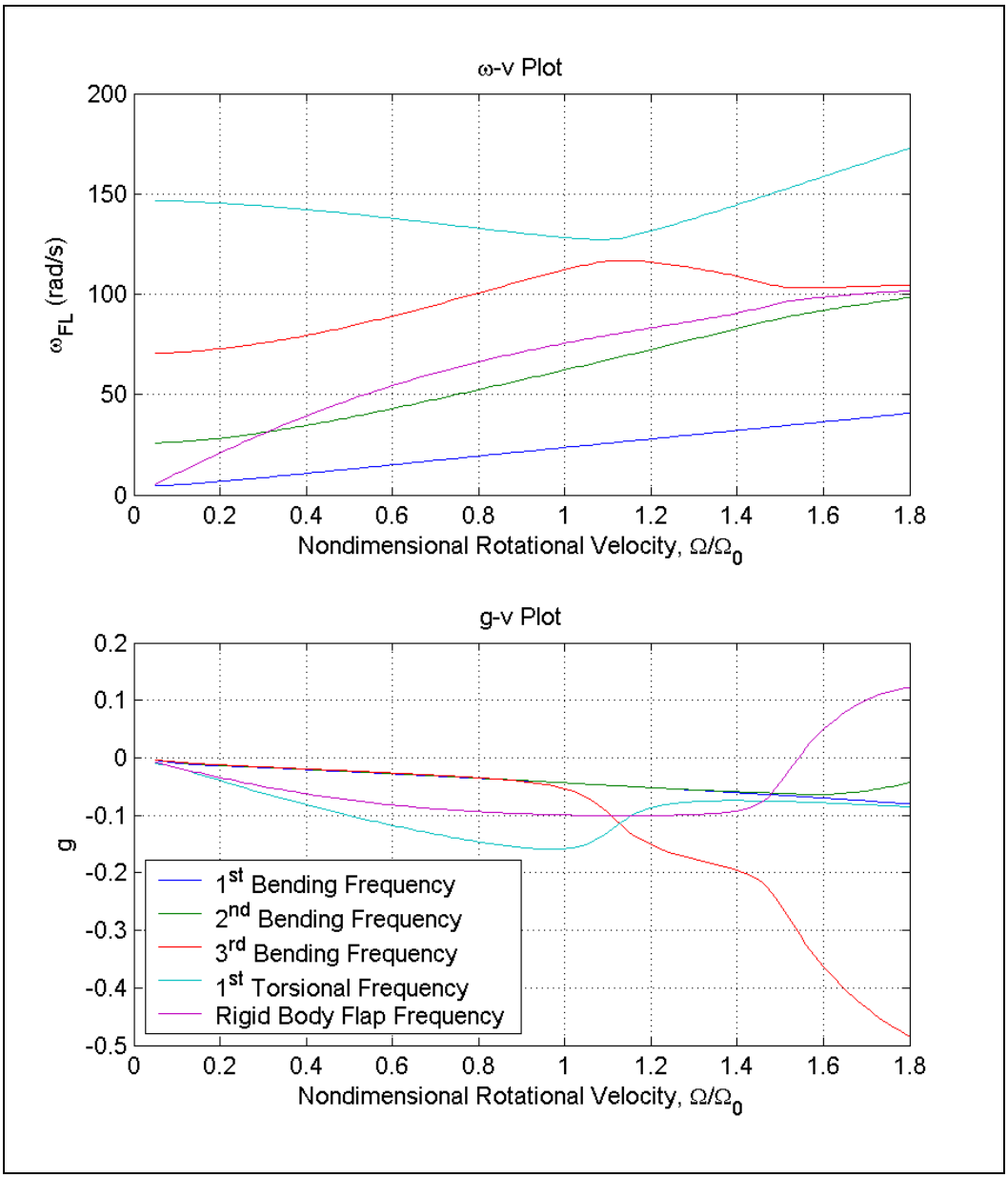

Figure 66. *g*-Ω plot for example rotor blade using Loewy's lift deficiency function, $m = 0$ ($\omega_\beta = 5P$).

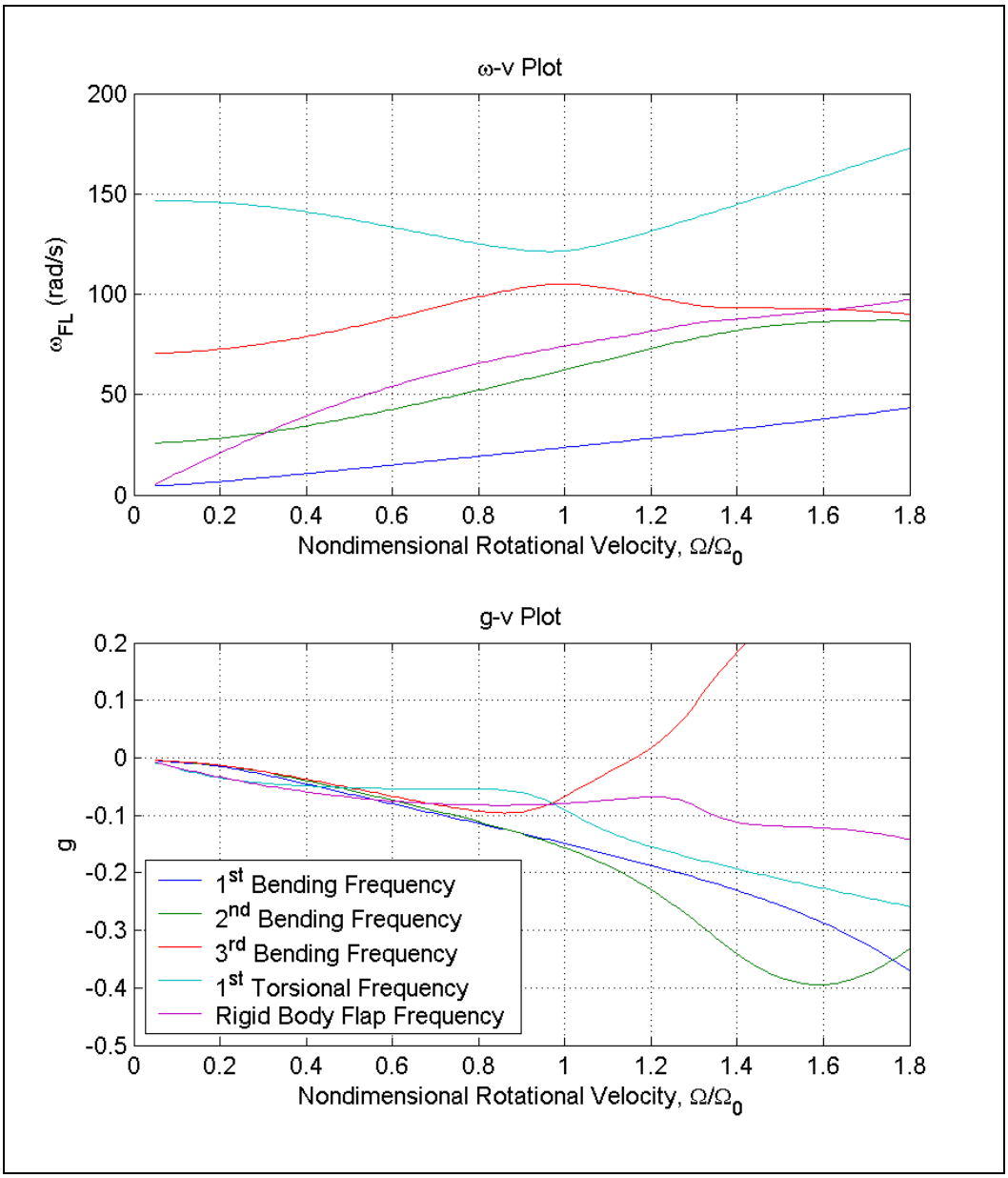

Figure 67. *g*-Ω plot for example rotor blade using Loewy's lift deficiency function, $m = 0.25$ ($\omega_\beta = 5P$).

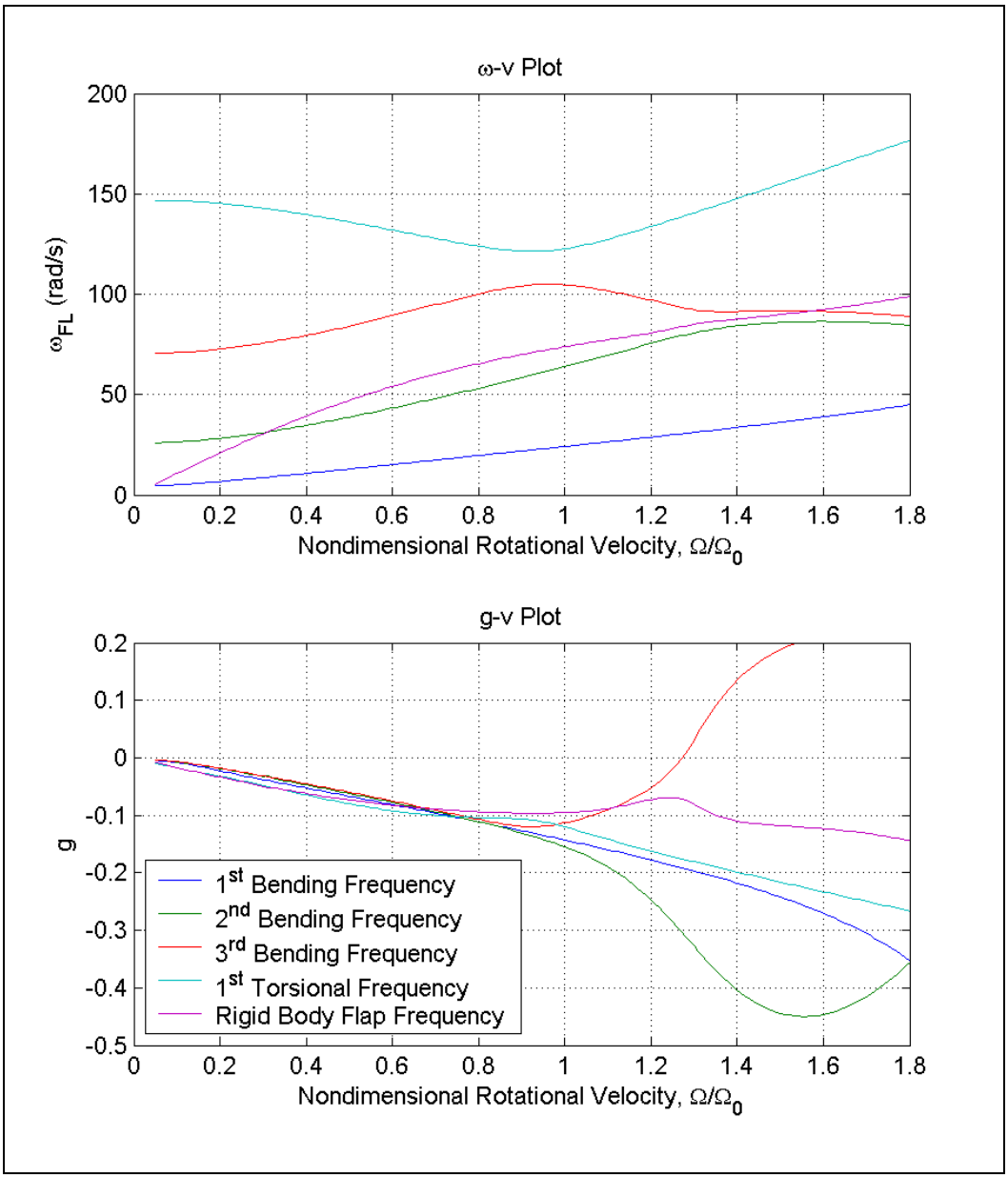

Figure 68. *g*-Ω plot for example rotor blade using Loewy's lift deficiency function, $m = 0.5$ ($\omega_\beta = 5P$).

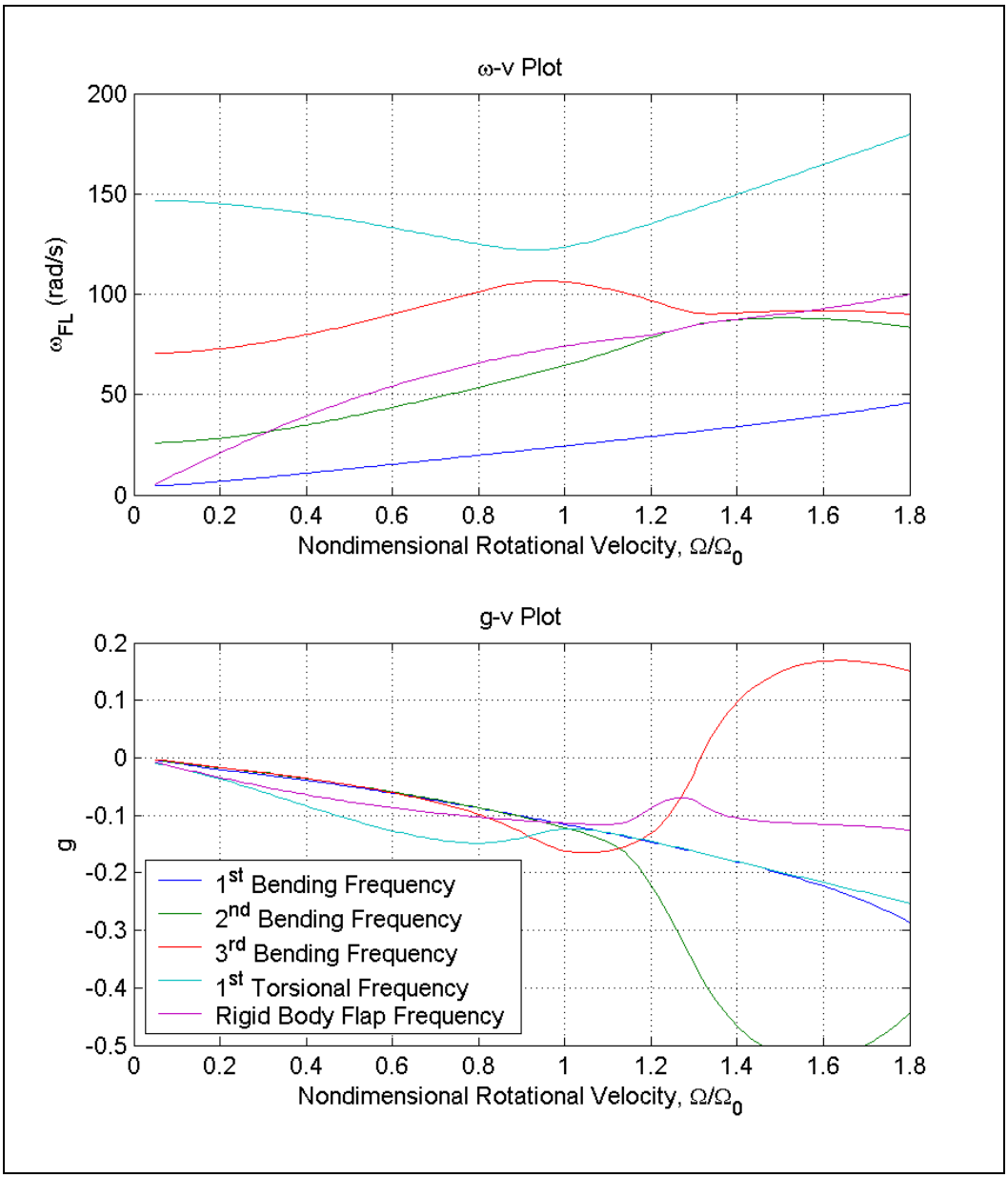

Figure 69. *g*-Ω plot for example rotor blade using Loewy's lift deficiency function, $m = 0.75$ ($\omega_\beta = 5P$).

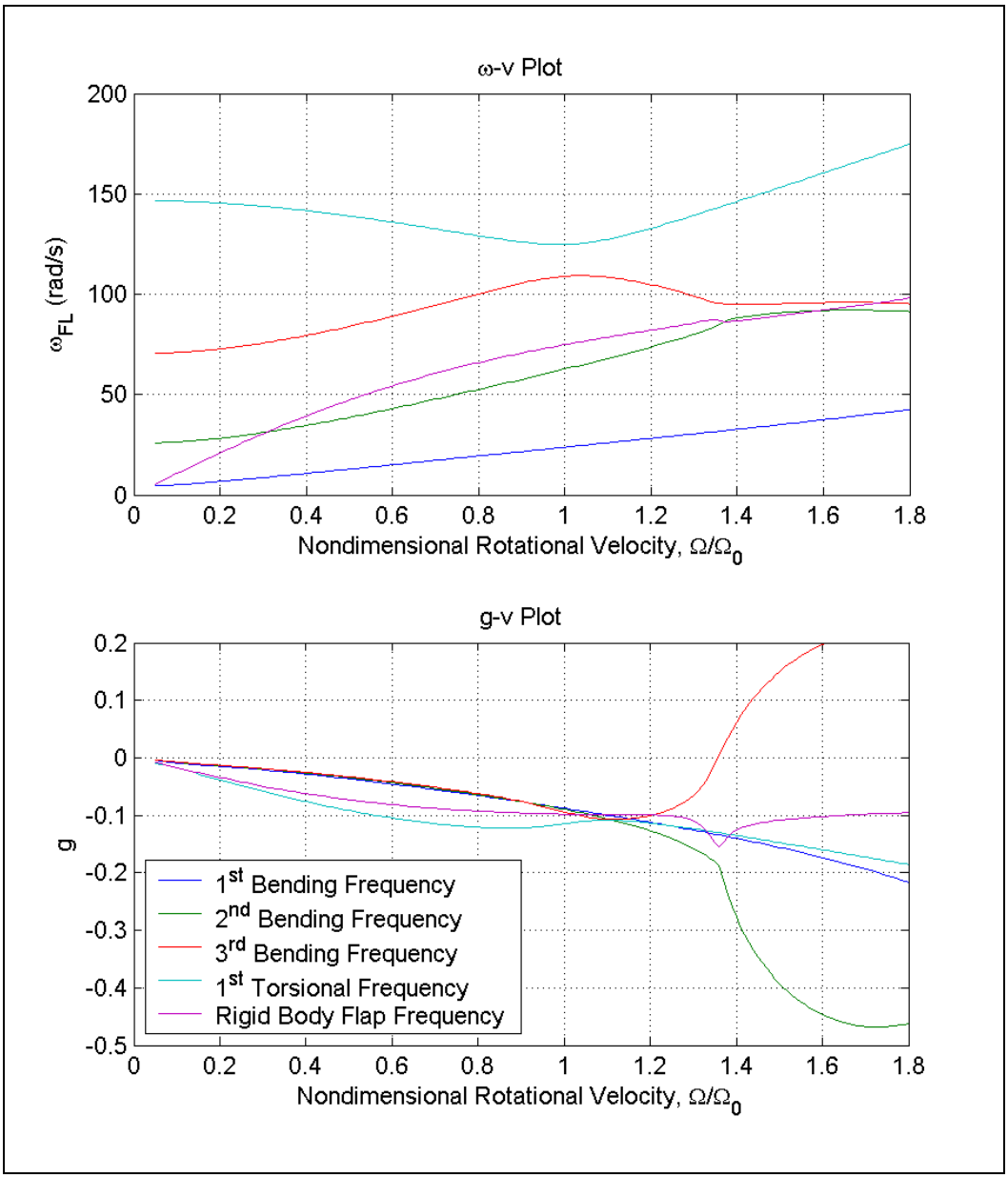

Figure 70. *g*-Ω plot for example rotor blade using finite wake lift deficiency function with a single wake, $m = 0$ ($\omega_\beta = 5P$).

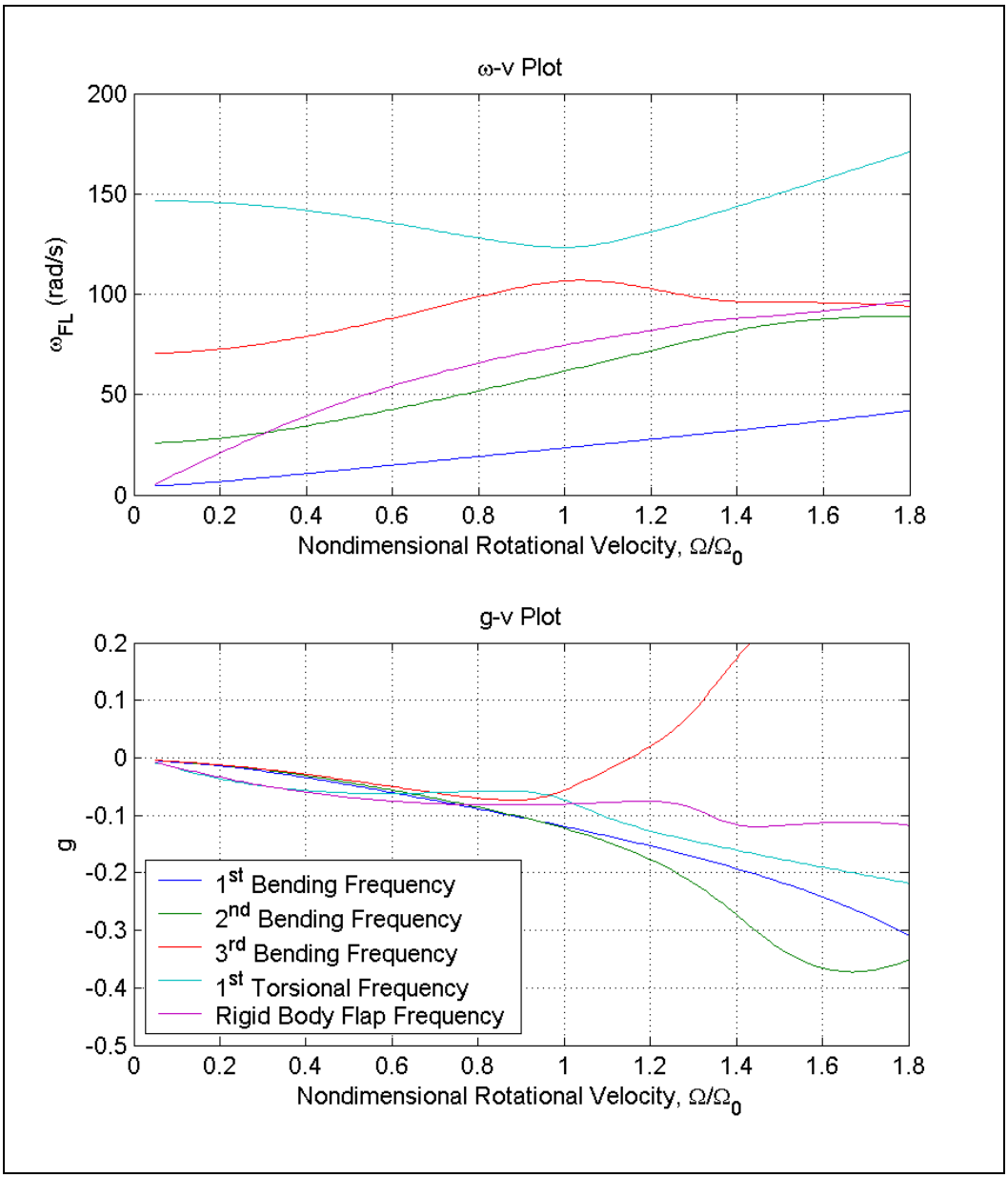

Figure 71. *g*-Ω plot for example rotor blade using finite wake lift deficiency function with a single wake, $m = 0.25$ ($\omega_\beta = 5P$).

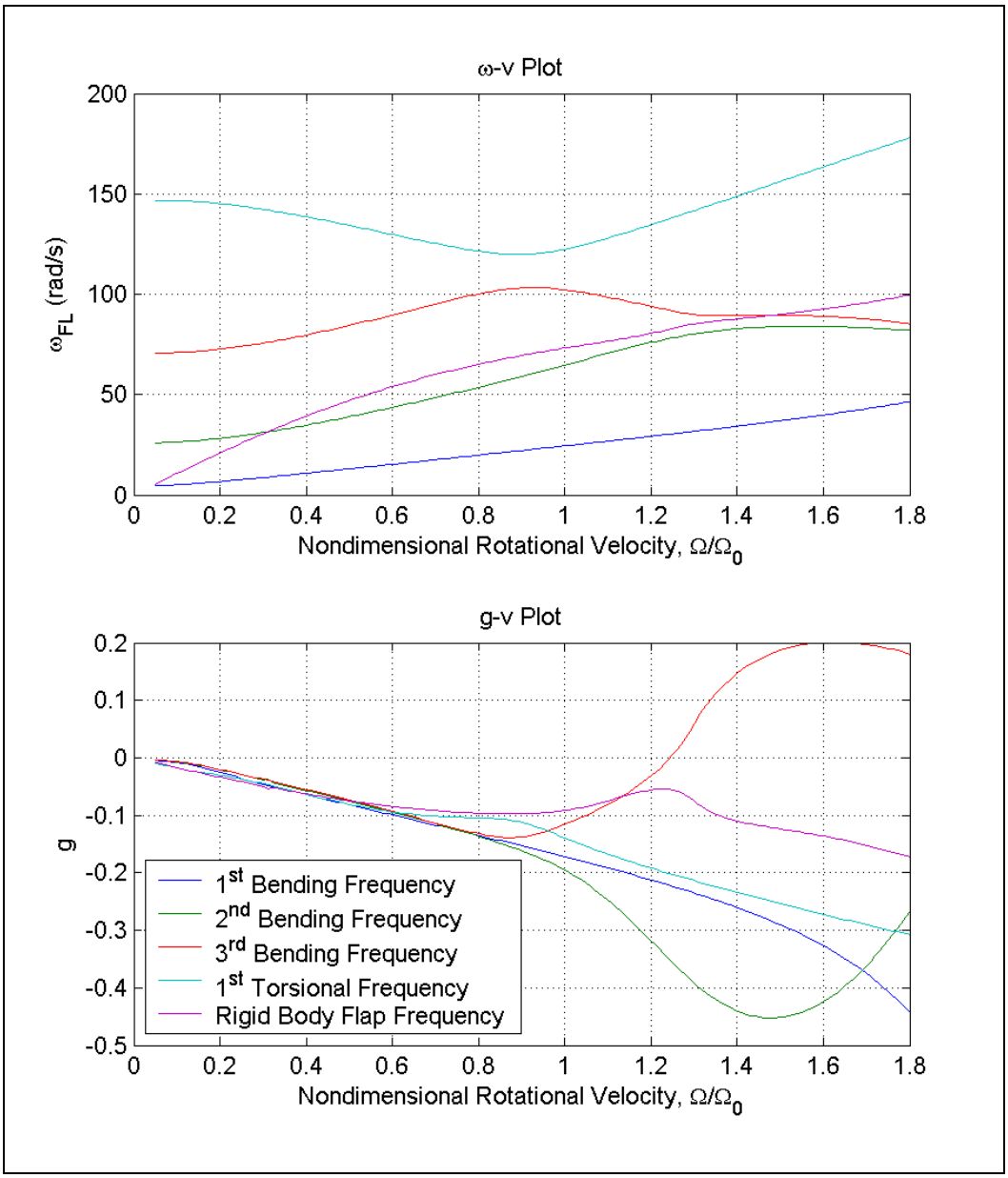

Figure 72. *g*-Ω plot for example rotor blade using finite wake lift deficiency function with a single wake, $m = 0.5$ ($\omega_\beta = 5P$).

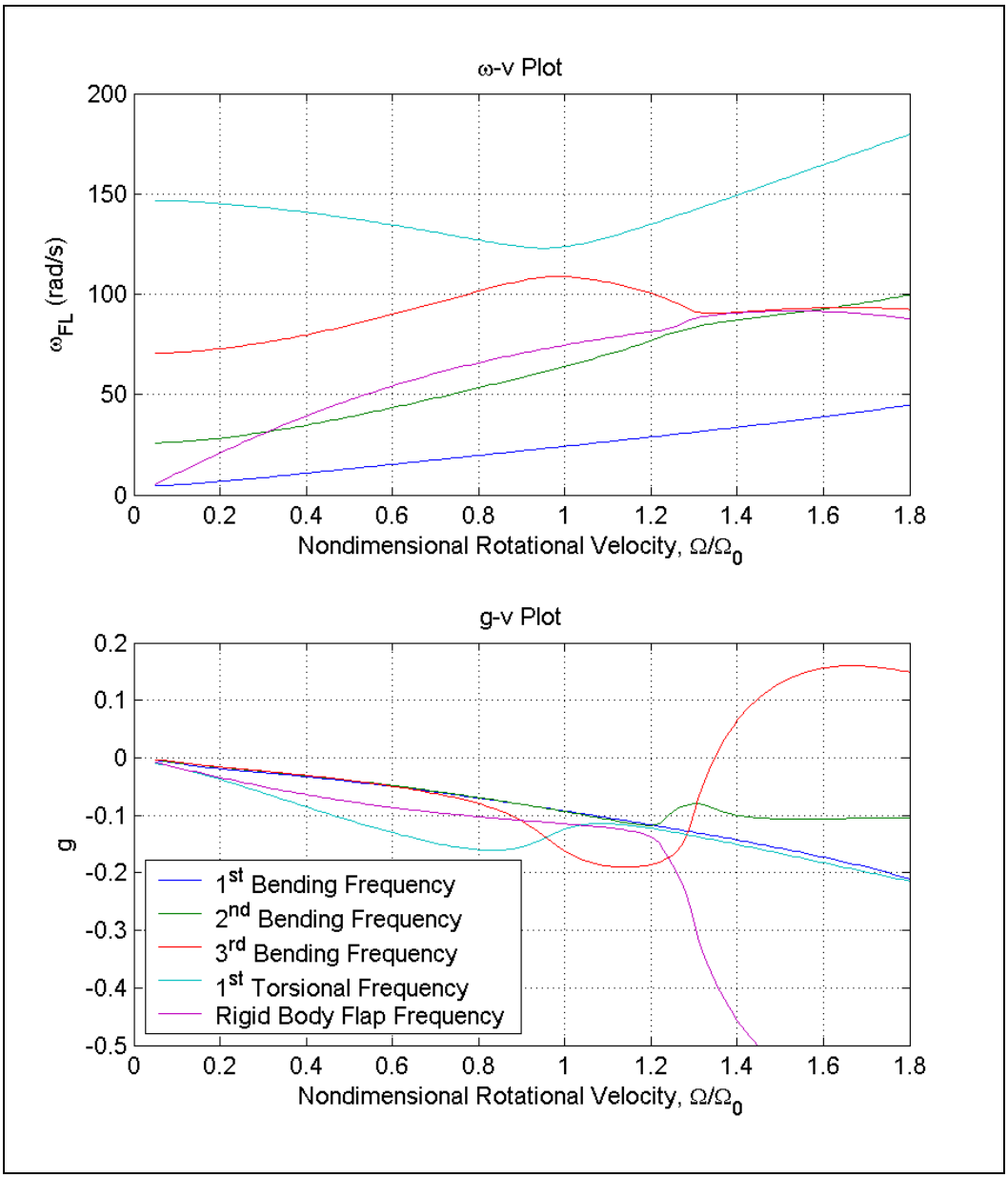

Figure 73. *g*-Ω plot for example rotor blade using finite wake lift deficiency function with a single wake, $m = 0.75$ ($\omega_\beta = 5P$).

Table 7. Flutter Frequencies and Speeds for Example Rotor Blade (ω_β = 5P).

ω_β	Lift Deficiency Function	m	h/h_0	Flutter Frequency ω_{FL}	Flutter Speed Ω/Ω_0
5P	Theodorsen	-	-	94.4	1.304
	Loewy	0.0	0.25	102.0	1.784
			0.50	98.1	1.634
			0.75	97.5	1.579
			1.0	97.2	1.541
			2.0	96.3	1.454
		0.25	0.25	100.6	1.150
			0.50	100.6	1.154
			0.75	100.5	1.159
			1.0	100.4	1.164
			2.0	100.0	1.184
		0.50	0.25	93.2	1.271
			0.50	93.2	1.271
			0.75	93.3	1.271
			1.0	93.3	1.272
			2.0	93.5	1.274
		0.75	0.25	90.2	1.314
			0.50	90.3	1.315
			0.75	90.4	1.315
			1.0	90.4	1.315
			2.0	90.7	1.317
	Single Wake	0.0	0.25	95.6	1.362
			0.50	95.5	1.360
			0.75	95.5	1.358
			1.0	95.5	1.357
			2.0	95.3	1.351
		0.25	0.25	105.8	1.130
			0.50	105.3	1.138
			0.75	104.9	1.146
			1.0	104.5	1.154
			2.0	102.9	1.184
		0.50	0.25	91.2	1.243
			0.50	91.5	1.243
			0.75	91.7	1.243
			1.0	91.9	1.244
			2.0	92.5	1.250
		0.75	0.25	90.3	1.351
			0.50	90.4	1.350
			0.75	90.4	1.349
			1.0	90.5	1.348
			2.0	90.7	1.344

Removing the effect of c.g. offset for the 5P flap frequency does not show the same aeroelastic stability as it did with the 0P and 4P input frequencies. Even with no c.g. offset, Figure 74 indicates a flutter speed at $1.59\Omega_0$ when using Theodorsen's lift deficiency function, which is an apparent contradiction to the classic design criteria stating that the rotor blade would be free from flutter when the c.g., e.a., and a.c. are coincident at the 25% chord. There are two reasons why this is not a contradiction but rather a case where the design criteria is no longer valid. The first is that coinciding the c.g., e.a., and a.c. at the 25% chord to be free from flutter is only valid for 1P inputs. For most conventional rotor blades (those without flaps), the pilot, or automatic flight control system, can only input a 1P frequency because of the design of the swashplate. The swashplate is typically designed with a rotating section and a stationary section connected by means of a race of bearing assembly. Inputs are always made to the stationary section which is then tilted to provide input to the rotating section. Because the rotating section is tilted as a whole, the input frequency would always be 1P, and the design criteria would be valid. With the development of HHC and IBC devices that can provide inputs at frequencies besides 1P, the design criteria should be reconsidered. The second reason is that the design criteria were based on conventional rotor blades without trailing-edge flaps. The inclusion of the moment coefficients about the flap hinge (T_α, T_β, T_h, and T_z) and the force coefficients on the flap (P_α, P_β, P_h, and P_z) for rotor blades with trailing-edge flaps make the design criteria invalid since the location of the flap hinge must be taken into consideration. Thus, flutter can now exist for rotor blades with trailing-edge flaps even if the c.g., e.a., and a.c. are coincident at the 25% chord, and the choice of lift deficiency function only changes the flutter speed slightly as the instability is being driven primarily by the structural dynamics.

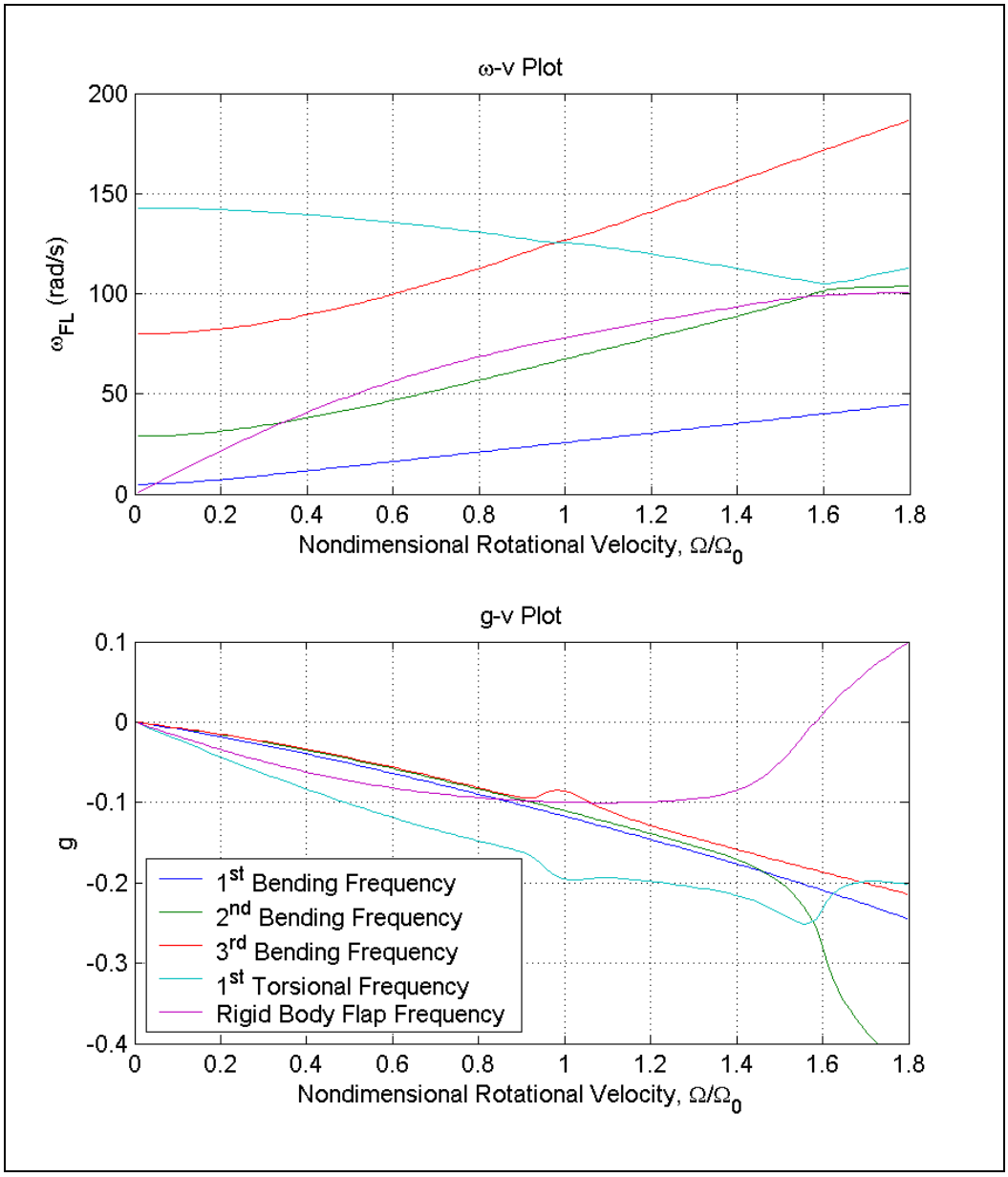

Figure 74. *g*-Ω plot for example rotor blade with no c.g. offset using Theodorsen's lift deficiency function (ω_β = 5P).

D. 6P FLAP FREQUENCY

Figure 34 is the Southwell plot for the 6P flap frequency. It can be seen that the rigid body flap mode and the 1st blade torsional modes interact along the 6P fan line near $1.2\Omega_0$. Figure 75 is a g-Ω plot for the example rotor blade with a 6P flap frequency using Theodorsen's lift deficiency function, and it can be seen that when the aerodynamic forces and moments are included, the interaction is between the 3rd bending and rigid body flap modes with the flutter speed occurring at $1.106\Omega_0$. Since 6P is the frequency that is (N_b + 1) times the rotational frequency, the fact that the flutter speed may be below the overspeed limit of the rotor is of great concern. Large, divergent motions caused by flutter induced by a 6P flap frequency will be transmitted from the rotating system to the fixed system, possibly yielding large vibrations and motion in the fixed system. Removing the c.g. offset does little to change the flutter speed as shown in Figure 76. The primary cause of this aeroelastic instability is the coupling of the rigid body flap mode with the 1st blade torsional mode and the 3rd bending mode. When the structural dynamics of the rotor blade is such that two or three coupled natural frequencies coincide, the aerodynamic damping forces are insufficient to prevent flutter. Table 8 contains a summary of the flutter frequencies and speeds for different choices of the lift deficiency function and frequency ratio, all of which yield about the same result.

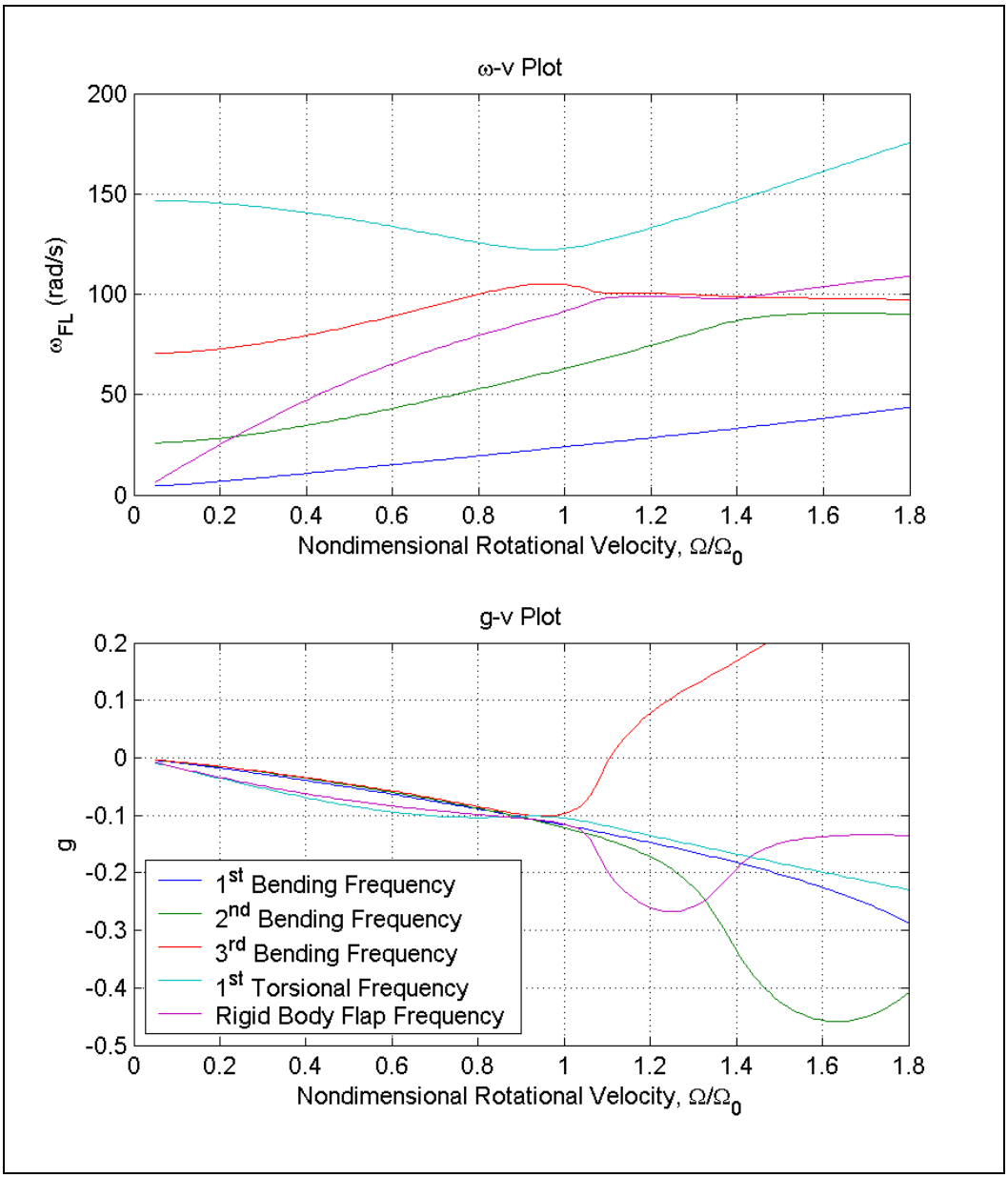

Figure 75. *g*-Ω plot for example rotor blade using Theodorsen's lift deficiency function (ω_β = 6P).

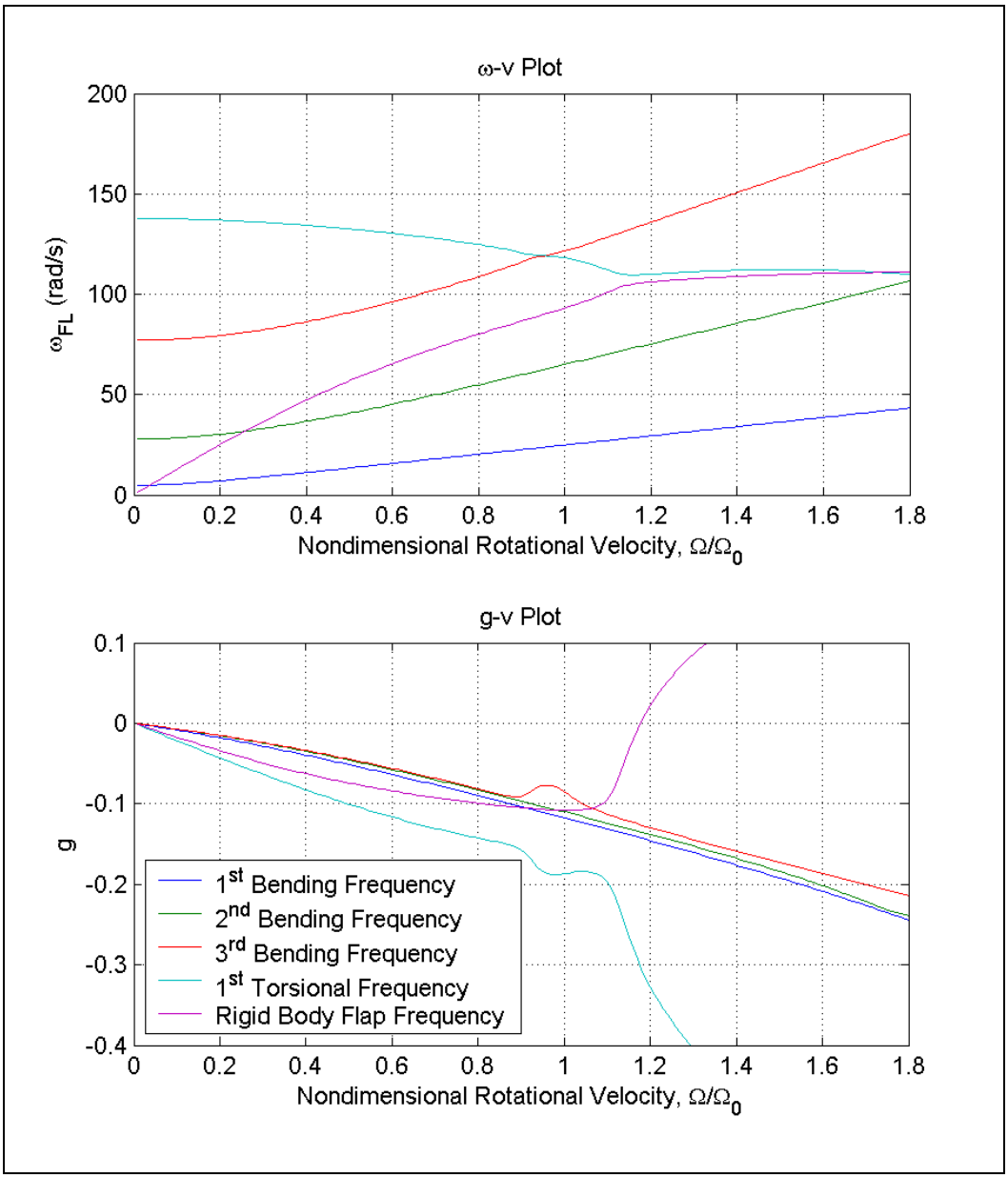

Figure 76. *g*-Ω plot for example rotor blade with no c.g. offset using Theodorsen's lift deficiency function (ω_β = 6P).

Table 8. Flutter Frequencies and Speeds for Example Rotor Blade (ω_β = 6P).

ω_β	Lift Deficiency Function	m	h/h_0	Flutter Frequency ω_{FL}	Flutter Speed Ω/Ω_0
6P	Theodorsen	-	-	100.5	1.106
	Loewy	0.0	1.0	109.7	1.193
		0.25	1.0	100.4	1.065
		0.50	1.0	98.8	1.104
		0.75	1.0	99.4	1.143
	Single Wake	0.0	1.0	102.6	1.122
		0.25	1.0	103.5	1.059
		0.50	1.0	98.0	1.120
		0.75	1.0	100.7	1.153

E. OTHER FLAP FREQUENCIES

With the freedom to apply any input frequency to the trailing-edge flap, including non-integer multiples of the rotational frequency, the breadth of possible flutter analyses may seem to be limitless. However, the rotor acts as a filter and allows primarily integer multiples of the rotational frequency to pass from the rotating system to the fixed system. The predominant frequencies that are transmitted from the rotating to fixed systems are the blade passage frequency (N_b or 5P) and the $N_b \pm 1$, or the 4P and 6P frequencies for the example rotor system. Flap inputs at these frequencies were studied in the previous sections because of their capability to be transmitted directly from the rotating system to the fixed system. In other words, if the rotor system would experience flutter at one of these input frequencies, there is a possibility that the divergent motion of the rotor blades could be transmitted into large vibrations and/or motion in the fixed system.

Other frequencies typically studied as the sources of vibrations are the low frequency vibrations. Table 9 through Table 11 show the results of the flutter analyses for 1P, 2P and 3P flap frequencies. It can be seen that these flap frequencies show similar results when compared to the 0P and 4P flap frequencies. These similarities might be expected when looking at the Southwell plots of Figure 29 through Figure 31, where there is little interaction between the coupled modes, especially near the blade passage frequency. Therefore is can be concluded that flap frequencies at low integer values of the rotational speed will yield flutter speeds at approximately the same values as if there were no flap at all.

Table 9. Flutter Frequencies and Speeds for Example Rotor Blade (ω_β = 1P).

ω_β	Lift Deficiency Function	m	h/h_0	Flutter Frequency ω_{FL}	Flutter Speed Ω/Ω_0
1P	Theodorsen	-	-	96.4	1.361
	Loewy	0.0	1.0	107.4	1.753
		0.25	1.0	104.2	1.173
		0.50	1.0	97.0	1.304
		0.75	1.0	93.9	1.362
	Single Wake	0.0	1.0	100.3	1.447
		0.25	1.0	108.4	1.174
		0.50	1.0	93.5	1.248
		0.75	1.0	94.3	1.416

Table 10. Flutter Frequencies and Speeds for Example Rotor Blade (ω_β = 2P).

ω_β	Lift Deficiency Function	m	h/h_0	Flutter Frequency ω_{FL}	Flutter Speed Ω/Ω_0
2P	Theodorsen	-	-	98.4	1.360
	Loewy	0.0	1.0	107.0	1.748
		0.25	1.0	104.0	1.173
		0.50	1.0	95.1	1.303
		0.75	1.0	93.9	1.361
	Single Wake	0.0	1.0	100.1	1.446
		0.25	1.0	108.2	1.173
		0.50	1.0	93.5	1.248
		0.75	1.0	94.2	1.415

Table 11. Flutter Frequencies and Speeds for Example Rotor Blade (ω_β = 3P).

ω_β	Lift Deficiency Function	m	h/h_0	Flutter Frequency ω_{FL}	Flutter Speed Ω/Ω_0
3P	Theodorsen	-	-	98.1	1.357
	Loewy	0.0	1.0	102.7	1.736
		0.25	1.0	103.7	1.173
		0.50	1.0	94.8	1.302
		0.75	1.0	93.7	1.359
	Single Wake	0.0	1.0	99.7	1.441
		0.25	1.0	107.9	1.172
		0.50	1.0	93.3	1.249
		0.75	1.0	94.0	1.412

The 7P flap frequency is interesting in that the flutter speed in below normal operating rpm as shown in Table 12. Even if the c.g. offset is removed, the flutter speed

is still below Ω_0. The reason for the aeroelastic instability at such low rpm can be seen by looking at the Southwell plot for the 7P flap frequency shown in Figure 35. The rigid body flap mode and the 1st blade torsional modes interact along the 7P fan line near Ω_0. This interaction can be seen better by looking at the *g*-Ω plot using Theodorsen's lift deficiency function for the 7P flap frequency shown in Figure 77, and noting that the interaction is actually between the rigid body flap, 3rd bending and 1st blade torsional modes when the aerodynamic forces are included. Using the Loewy and finite wake lift deficiency functions give similar results to Figure 77, and the flutter speeds are listed in Table 12.

Normally, the integer multiple frequencies that are not N_b or $N_b \pm 1$ of rotor speed are less of a concern since they are not the primary frequencies that are filtered through the rotor system. However, when the rigid body flap frequency is set at these other frequencies, modes which typically might be ignored may become more troublesome, especially if the amplitude of deflection of the flap is significant. Therefore, it can be concluded that care must be used when setting the flap frequency to integer multiples other than N_b or $N_b \pm 1$.

Table 12. Flutter Frequencies and Speeds for Example Rotor Blade (ω_β = 7P).

ω_β	Lift Deficiency Function	m	h/h_0	Flutter Frequency ω_{FL}	Flutter Speed Ω/Ω_0
7P	Theodorsen	-	-	105.0	0.938
	Loewy	0.0	1.0	107.0	0.924
		0.25	1.0	101.9	0.903
		0.50	1.0	105.7	0.957
		0.75	1.0	108.2	0.990
	Single Wake	0.0	1.0	105.6	0.928
		0.25	1.0	103.1	0.887
		0.50	1.0	104.4	1.024
		0.75	1.0	108.7	0.976

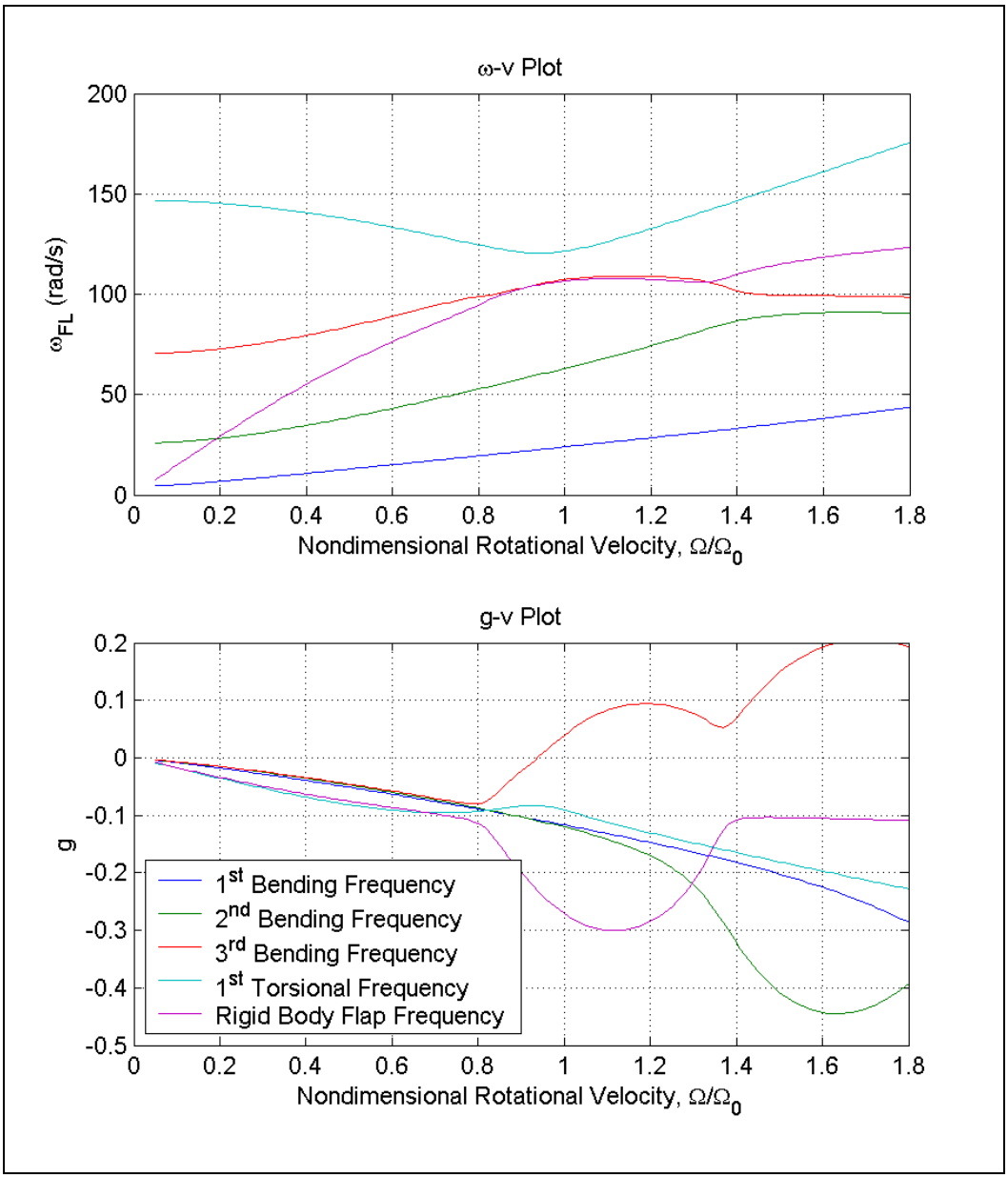

Figure 77. *g*-Ω plot for example rotor blade using Theodorsen's lift deficiency function (ω_β = 7P).

THIS PAGE INTENTIONALLY LEFT BLANK

VII. CONCLUSIONS AND RECOMMENDATIONS

The solution to the flutter problem for rotary-wing aircraft is inherently more complicated than the fixed-wing counterpart, especially for rotor blades with trailing-edge flaps. The frequency-domain approach is used here to develop the flutter equations of motion that could be used quickly and easily without the need to learn all the ins and outs of one of the rotor dynamics computational codes. The method may be easily programmed in any language that has access to an eigenvalue subroutine that can handle complex coefficients. In this dissertation, the equations of motion were programmed in MATLAB®, and copies of the codes are contained in Appendices A through D.

Using the method of lumped-mass parameters, the rotor blade can be divided into a sufficient number of segments to approximate the continuous system. This method has been used very successfully in the past to find the uncoupled natural frequencies for blade torsion and bending via the Holzer and Myklestad-Prohl methods. An extension of this method was made that determined the reduced frequency for each segment of the blade so that each segment's contribution to the unsteady aerodynamic forces and moments can be calculated. Lagrange's equation was then applied to develop the flutter equations of motion and to set up the flutter determinant. The solution to the flutter determinant is a complex eigenvalue problem that yields the coupled natural frequencies from the real part of the eigenvalues and the damping from the imaginary part. Plots were made of the coupled natural frequencies and the damping versus the rotational velocity (or the reciprocal of the reduced frequency), and the point where the damping crosses the velocity axis is the flutter speed. The point on the frequency curve that corresponds to the crossing point of the unstable damping curve is the flutter frequency.

Flutter analyses were performed on an example rotor blade with a trailing-edge flap in order to see the effects of the variation of parameters and demonstrate the robustness of the methodology. The primary parameter that was varied was the rigid body flap frequency. It was shown that flap frequencies at low integer multiples of the rotational speed were stable as long as the rotor blade was stable without any flap incorporated ($\omega_\beta = 0$). Flap frequencies at higher integer multiples of the rotational frequency must be used with caution since there may be some interaction between the

higher order coupled modes and the input frequency that could produce a lower flutter speed. *Additionally, it was shown that current design practice of collocating the c.g. and e.a. at the 25% chord to remove the possibilities of flutter is not valid when a trailing-edge flap is incorporated.* The reason is that additional forces and moments created by movement of the trailing-edge flap can couple with the higher order bending and torsional modes of the blade to create flutter.

Another parameter that was varied was the choice of lift deficiency function. Theodorsen's lift deficiency function, while applicable to the fixed-wing case, may not be as valid for rotary-wing aircraft where the effects of previously shed layers of vorticity should be considered. Theodorsen's lift deficiency function was used primarily to set a baseline for the flutter calculations so that comparisons with the other lift deficiency functions can be made. The other lift deficiency functions chosen were Loewy's lift deficiency function and the finite wake lift deficiency function. It was seen that the frequency ratio (m), which effectively measures the phase relationship between shed layers of vorticity, was the parameter in these other lift deficiency functions that affected the results the most. The case of $m = 0$ (wakes completely in phase) always yielded a the highest flutter speed, and the case of $m = 0.25$ yielded the lowest flutter speed. The reason for this phenomenon can be seen from the plot of the pitch damping coefficient versus frequency ratio found in Loewy [Ref. 49]. The finite wake lift deficiency function was used to show the effects of just a single layer of vorticity beneath the rotor. The results were similar to the Loewy lift deficiency function, but the single wake function would be a more likely candidate for future comparison to Euler computational fluid dynamics codes.

The methodology to perform a flutter analysis presented in this dissertation is very robust and capable of handling variations in many different parameters. However, it was never intended to be all encompassing, and there are several recommendations for future work.

1. Apply this methodology to current research on the new rotor blade with the trailing-edge flap on the MD-900 [Ref. 2] to predict the flutter speeds prior to wind tunnel testing.

2. Conduct wind tunnel tests of rotor blades with trailing edge flaps to validate this methodology for predicting the flutter speed.
3. Explore the issue of c.g. offset to determine how much latitude there is in the design constraint of collocating the c.g., e.a., and a.c. at the 25% chord.
4. Compare this methodology to panel codes and other rotor dynamics codes such as UPOT, CAMRAD, 2GCHAS, and UMARC.
5. Expand the choice of lift deficiency functions to include those capable of being used in forward flight. Choices should include those of Peters and He [Ref. 63] and Shipman and Wood [Ref. 65].
6. Add compressibility effects via the method described by Hammond [Ref. 66].
7. Redevelop the equations of motion so that the actual deflections of the flap could be provided as an input and a forced response calculated similar to the method of Gerstenberger and Wood [Ref. 34].
8. Develop a new lift deficiency function that includes the effects of viscosity and perform a flutter analysis.
9. Use a finite element model of the rotor blade to obtain better estimates of the uncoupled natural frequencies.

THIS PAGE INTENTIONALLY LEFT BLANK

APPENDIX A. ROTOR BLADE FLUTTER PROGRAM

The MATLAB® program for calculating the flutter frequency and velocity is listed below.

```
% This program runs a flutter analysis for rotor blades with a flap
% incorporated.  The output will be a g-v plot that determines the flutter
% frequency and flutter speed.
clear
%clf
%clc
global Kappa k_root R
type=menu('Type of rotor system','Articulated', 'Hingeless (infinite stiffness at root)','Hingeless
(finite stiffness at root)');
switch type
   case 1       % Articulated Boundary Conditions
      disp('Articulated rotor chosen.')
   case 2       % Hingeless (infinite stiffness at root) Boundary Conditions
      disp('Hingeless rotor with infinite stiffness at root chosen.')
   case 3       % Hingeless (finite stiffness at root) Boundary Conditions
      disp('Hingeless rotor with flexible restraint at root chosen.')
end

%
% Calculate density
%altitude=input('What is the altitude of the rotorcraft (in feet)? ')
altitude=1000          % 1000 ft altitude chosen for all test cases.
if altitude>36100
   disp('Please select an altitude below 36,100 feet.')
   altitude=input('What is the altitude of the rotorcraft (in feet)? ')
end
std_lapse_rate=0.003565;      % (deg R/ft)
T_ref=518.67;                 % (deg R)
rho_ref=0.0023769;              % (slug/ft^3)
g_o=32.1740485;               % (ft/s^2)
g_c=32.1740485;               % (ft-lbm/lbf-s^2)
R_gas=1545/28.97;             % (ft-lbf/lbm-deg R)
p_ref=2116.22;                % (lbf/ft^2)
Temp=T_ref-std_lapse_rate*altitude;      %Atmospheric temperature (deg R) using standard
adiabatic lapse rate
press=p_ref*(1-std_lapse_rate*altitude/T_ref)^(g_o/(R_gas*std_lapse_rate*g_c));     %
Atmospheric pressure (lb/ft^2)
rho=press/(R_gas*g_c*Temp);               % Atmospheric density (slug/ft^3)

% Blade section properites for H-1R Blade
R=372/12;          % H-3 blade
r1=279/12;         % distance from root of blade to beginning of trailing edge flap (in)
r2=334.8/12;         % distance from root of blade to end of trailing edge flap (in)
```

```
twist=-10;       % built-in linear blade twist from root to tip (deg) **NOTE:  flap has same twist as
blade**
Omega_rpm=203;     % numerical instabilities in taking inverse of matrix occur if Omega_rpm >
375
Omega=Omega_rpm*2*pi/60;    % rotor speed (rad/s)
N_b=5;          % Number of rotor blades
GW=16800;
A=pi*R^2;
v_i=sqrt(GW/(2*rho*A));

% Find the vertical bending mode shapes

% Radial stations (in) from root to tip
rn=[12.63; 18.6; 37.2; 55.8; 74.4; 93.0; 111.6; 130.2; 148.8; 167.4; 186.0;
   204.6; 223.2; 241.8; 260.4; 279.0; 297.6; 316.2; 334.8; 353.4; 372.0];
rn=rn/12;         % convert radial station from in to ft

% Flapwise Area Moment of Inertia (in^4) from root to tip
Izzn=[5.0; 5.0; 5.0; 4.4; 3.04; 2.91; 2.8; 2.71; 2.6; 2.51; 2.45;
   2.35; 2.29; 2.19; 2.1; 2.04; 2.0; 1.99; 1.95; 1.93; 0.97];
Izzn=Izzn/12^4;         % Converting area moment of inertia from in^4 to ft^4

% Edgewise Area Moment of Inertia (in^4) from root to tip
Ixxn=[26.0; 26.0; 26.0; 35.0; 30.5; 29.8; 29.3; 28.5; 28.0; 27.3;
   27.0; 24.8; 24.3; 24.0; 23.7; 20.9; 20.8; 20.6; 20.5; 20.3; 10.1];
Ixxn=Ixxn/12^4;         % Converting area moment of inertia from in^4 to ft^4

% Flapwise static unbalance (in^3) from root to tip
Szzn=[5.0; 5.0; 5.0; 3.6; 2.7; 2.6; 2.5; 2.4; 2.36; 2.3; 2.25;
   2.2; 2.1; 2.0; 1.95; 1.9; 1.9; 1.84; 1.82; 1.8; 0.9];
Szzn=Szzn/12^3;        % Converting static unbalance from in^3 to ft^3

% Edgewise static unbalance (in^3) from root to tip
Sxxn=[6.0; 6.0; 6.0; 7.95; 6.92; 6.70; 6.58; 6.4; 6.27; 6.2; 6.13;
   5.8; 5.5; 5.6; 5.5; 5.12; 5.10; 5.03; 5.0; 5.0; 2.5];
Sxxn=Sxxn/12^3;

% Torsional polar moment of inertia, J (in^4) from root to tip
Jn=[100.0; 100.0; 50.0; 30.0; 14.0; 9.9; 9.0; 8.5; 8.2; 7.9;
   7.6; 7.3; 7.0; 6.8; 6.6; 6.3; 6.0; 5.9; 5.7; 5.5; 2.8];
Jn=Jn/12^4;             % Converting polar moment of inertia from in^4 to ft^4

% Area of midline of each section (in^2) from root to tip
Arean=[100.0; 100.0; 50.0; 14.1; 13.68; 13.58; 13.52; 13.47; 13.4; 13.38;
   13.35; 13.25; 13.2; 13.13; 13.1; 13.0; 12.98; 12.96; 12.94; 12.92; 6.46];
Arean=Arean/12^2;     % Converting area from in^2 to ft^2

% Mass moment of inertia per unit span of rotor blade about the elastic axis (slug-ft)
Ialpha=[0.5; 0.5; 0.5; 0.07; 0.065; 0.064; 0.063; 0.062; 0.06; 0.058;
   0.055; 0.052; 0.049; 0.048; 0.045; 0.044; 0.042; 0.041; 0.040; 0.038; 0.015];
```

```
% Weight (lb_m) of each radial station from root to tip
Wn=[20.46; 84.17; 55.21; 10.51; 8.53; 9.06; 8.78; 9.73; 10.01; 9.94;
   9.91; 9.37; 9.45; 9.14; 9.03; 9.93; 9.94; 9.95; 9.96; 9.96; 2.56];

mn=Wn/(32.1740485564);     % mass of each radial station (slugs)

% semichord at each section from root to tip
b_sect=[8.1; 8.1; 8.1; 8.1; 8.1; 18.25; 18.25; 18.25; 18.25; 18.25; 18.25;
   18.25; 18.25; 18.25; 18.25; 18.25; 18.25; 18.25; 18.25; 18.25; 18.25]/2;
b_sect=b_sect/12;              % convert semichord from in to ft

En=10e6;             % blade made of aluminum (lb_f/in^2, or psi)
En=En*12^2;          % Converting modulus of elasticity from psi to psf
Kappa=9e6;           % Root end bearing stiffness for bending (in-lb_f/rad)
Kappa=Kappa/12;   % convert from in-lb_f/rad to ft-lb_f/rad
k_root=1e6;          % Pitch bearing stiffness (ft-lb_f/rad)
bendmodeshp=4;

% Find the blade torsional mode shapes via Holzer function
torsmodeshp=3;
Al_rho=5.4;               % slug/ft^3
%k_root=1;                  % root stiffness in pitch
%e_pitch=12.63/R;            % effective pitch offset
nu=0.33;
G_n=En/(2*(1+nu));              % psf

% Everything below this line goes into the flutter function
i=sqrt(-1);
e=0.3;
c=0.5;
a=-0.5;
p=-1/3*(sqrt(1-c^2))^3;

% find mass moment of inertial about c.g.
lsn=diff(rn);          % determine length of each segment
N=length(lsn);       % number of radial stations
for n=1:length(rn),
   if rn(n)>=r1 & rn(n)<=r2
      Ibeta(n)=0.01*Ialpha(n);
      G0(n)=1;
      cg(n)=-0.2;
   else
      Ibeta(n)=0;
      G0(n)=0;
      cg(n)=-0.5;
   end
end
Ibeta=Ibeta';                      % slug-ft
Sbeta=zeros(size(Ibeta));       % c.g. of flap is at the hinge
```

```
G0=G0';
cg=cg';
xbar=Szzn./Arean;
zbar=Sxxn./Arean;
nP=6                    % Flap frequency x Omega
if nP==-1
   % Adjust cgea to account for lack of trailing edge flap
   cgea=sqrt(xbar.^2+zbar.^2);     % Reference axis is blade centerline for z and 1/4-chord for x
   Salpha=mn.*cgea;                % c.g. is aft of e.a.
else
   %Adjust cgea to account for trailing edge flap
   xbar=xbar+(cg-a).*b_sect;
   cgea=sqrt(xbar.^2+zbar.^2);     % Reference axis is blade centerline for z and 1/4-chord for x
   Salpha=mn.*cgea;                % c.g. is aft of e.a.
end

% Make choice of lift deficiency function
liftdef=menu('Choice of Lift Deficiency Function', 'Theodorsen', 'Loewy', 'Single-Wake');
switch liftdef
   case 1       % Theodorsen lift deficiency function
      disp('Theodorsen lift deficiency function chosen.')
   case 2       % Hingeless (infinite stiffness at root) Boundary Conditions
      disp('Loewy lift deficiency function chosen.')
   case 3       % Hingeless (finite stiffness at root) Boundary Conditions
      disp('Single Wake lift deficiency function chosen.')
end

h=2*pi*v_i/(18.25/12*N_b*Omega)     %Wake spacing
%h=2*h              % Adjust the wake spacing for partial collective loading
m=0.0;               % Set the frequency ratio

% Define the T and phi functions
T1=-1/3*sqrt(1-c.^2)*(2+c.^2)+c.*acos(c);
T3=-(1/8+c.^2).*(acos(c)).^2+1/4*c.*sqrt(1-c.^2).*acos(c)*(7+2*c.^2)
                                                        -1/8*(1-c.^2).*(5*c.^2+4);
T4=-acos(c)+c.*sqrt(1-c.^2);
T5=-(1-c.^2)-(acos(c)).^2+2*c.*sqrt(1-c.^2).*acos(c);
T7=-(1/8+c.^2).*acos(c)+1/8*c.*sqrt(1-c.^2).*(7+2*c.^2);
T10=sqrt(1-c.^2)+acos(c);
T11=acos(c).*(1-2*c)+sqrt(1-c.^2).*(2-c);
T12=sqrt(1-c.^2).*(2+c)-acos(c).*(2*c+1);
phi1=T10;
phi2=T11;
phi3=-T4;
phi31=acos(c)-sqrt(1-c.^2);
phi32=acos(c)+sqrt(1-c.^2).*(1-2*c);
phi35=2*(1-c.^2);
phi36=phi32*phi3+2*(1-c.^2).^2;
phi37=phi3*(phi2-phi3);
phi5=T4+T10;
```

```
phi6=2*acos(c)+2/3*sqrt(1-c.^2).*(2+c).*(1-2*c);
phi8=T12;
phi10=phi31*phi5;
phi17=phi3.^2+(1-c.^2).^2;
for loop=2:2
   if loop==1
      rho=0          % Use rho=0 to check structural dynamics only.  (Zeros out the areodynamics)
   else
      rho=press/(R_gas*g_c*Temp);              % Atmospheric density (slug/ft^3)
   end
   fknt=1;
   for Omega1=0.05*Omega:Omega/100:1.8*Omega,
      OMEGA(fknt)=Omega1;
      Omega_fan(fknt,:)=[1,2,3,4,5,6,7,8,9,10]*Omega1;
      disp('The rotational frequency is')
      disp(Omega1)
      omega_b(fknt)=nP*Omega1;              % Flap frequency

      % Find bending mode shapes for given Omega1
      [deflection,omega_bend]=myklestad(rn, Izzn, En, mn, Omega1, bendmodeshp,type);
      f0=rn/R;
      f1(:,fknt)=deflection(1,:)';
      f2(:,fknt)=deflection(2,:)';
      f3(:,fknt)=deflection(3,:)';
      f4(:,fknt)=deflection(4,:)';
      omega_h(fknt,:)=omega_bend;

      % Find torsional mode shapes for given Omega1
      [alpha_rotation,omega_tor]=holzer_blade(rn, Jn, Arean, Ialpha, G_n, Al_rho, mn,
                                                          Omega1, twist, torsmodeshp,type);
      F0=rn/R';
      F1(:,fknt)=alpha_rotation(1,:)';
      F2(:,fknt)=alpha_rotation(2,:)';
      F3(:,fknt)=alpha_rotation(3,:)';
      omega_a(fknt,:)=omega_tor;

      if fknt==1
         omega_start=[omega_h(1,1), omega_h(1,2), omega_h(1,3), omega_a(1,1), omega_b(1)];
      end

      k=b_sect*omega_a(fknt,1)./(Omega1*rn);
      k_07(fknt)=k(15);       % The reduced frequency at 0.7R is index 15 on the blade
      j0=besselj(0,k);
      y0=bessely(0,k);
      j1=besselj(1,k);
      y1=bessely(1,k);
      H2_0=besselh(0,2,k);
      H2_1=besselh(1,2,k);
      switch liftdef
         case 1
```

```
    % Theodorsen lift deficiency function
    Ck=H2_1./(H2_1+i*H2_0);

  case 2
    % Loewy lift deficiency function
    %W_Loewy=1 ./ (exp(k .* h) * exp(i*2*pi*m) -1);
    %alfhat_L=real(W_Loewy);
    %bethat_L=imag(W_Loewy);
    %A_L=(j1 .* (1+2*alfhat_L)) + y0 - (2*j0 .*bethat_L);
    %B_L=-y1 + (2*j1 .* bethat_L) + (j0 .* (1+2*alfhat_L));
    %den_L=A_L .^2 + B_L.^ 2;
    %F_L=((j1.*(1+2*alfhat_L).*A_L)-((y1 - 2*j1.*bethat_L).*B_L))./den_L;
    %G_L=-(((y1- 2*j1.* bethat_L).* A_L)+(j1 .*(1+2*alfhat_L).* B_L))./den_L;
    %Ck=F_L+i.*G_L;          % Loewy lift defiency function

    % Estimate to Loewy lift defiency function
    W1=exp(-( i*2*pi*m+k .* h));
    W_Loewy2=W1;
    for n=2:100
      W_Loewy2=W_Loewy2 + exp(-( i*2*pi*m*n+n*k .* h));    %finite wakes
    end
    alfhat=real(W_Loewy2);
    bethat=imag(W_Loewy2);
    A=(j1 .* (1+2*alfhat)) + y0 - (2*j0 .*bethat);
    B=-y1 + (2*j1 .* bethat) + (j0 .* (1+2*alfhat));
    den=A .^2 + B.^ 2;
    F_Loewy2=((j1.*(1+2*alfhat).*A)-((y1 - 2*j1.*bethat).*B))./den;
    G_Loewy2=-(((y1- 2*j1.* bethat).* A)+(j1 .*(1+2*alfhat).* B))./den;
    Ck=F_Loewy2+i.*G_Loewy2;  % Estimate to Loewy lift deficiency function

  case 3
    % Single wake lift deficiency function
    W_Single=exp(-i*2*pi*m) .* exp(-k.*h);
    alfhat_S=real(W_Single);
    bethat_S=imag(W_Single);
    A_S=(j1 .* (1+2*alfhat_S)) + y0 - (2*j0 .*bethat_S);
    B_S=-y1 + (2*j1 .* bethat_S) + (j0 .* (1+2*alfhat_S));
    den_S=A_S .^2 + B_S.^ 2;
    F_S=((j1.*(1+2*alfhat_S).*A_S)-((y1 - 2*j1.*bethat_S).*B_S))./den_S;
    G_S=-(((y1- 2*j1.* bethat_S).* A_S)+(j1 .*(1+2*alfhat_S).* B_S))./den_S;
    Ck=F_S+i.*G_S;          % Single wake lift deficiency function
end
% L, M, T and P terms using chosen lift deficiency function
Lh=1-2*(i./k).*Ck;
La=1/2-(i./k).*(1+2*Ck)-2.*Ck./(k.^2);
Lb=-T1/pi+i./(pi*k).*(T4-T11.*Ck)-2.*(T10/pi).*Ck./(k.^2);
Lz=-2*(i./k).*(phi1/pi).*Ck+phi3/pi;
Mh=1/2;
Ma=3/8-(i./k);
Mb=-T7/pi-(e+1/2).*T1/pi+(i./k).*(2*p+T4)/pi-(1./k.^2).*((T4+T10)/pi);
```

```
Mz=-(i./k).*phi5/pi+1/4*phi6/pi;
Th=-T1/pi-(i./k).*(T12/pi).*Ck;
Ta=-(1/pi)*(T7+(e+1/2).*T1)-(i./k).*((2*p-2*T1-T4)/(2*pi)+T12/pi.*Ck)
                                                    -(1./k.^2).*(T12/pi).*Ck;
Tb=-T3/(pi^2)+(i./k).*(T4.*T11-T11.*T12.*Ck)./(2*(pi^2))
                                -(1./k.^2).*(T5-T4.*T10+T10.*T12.*Ck)/(pi^2);
Tz=-(i./k).*(phi1.*phi8.*Ck+phi10)/(pi^2)+1/2*phi37/(pi^2);
Ph=-2*(i./k).*phi31.*Ck/pi+phi3/pi;
Pa=-2*(1./(k.^2)+(i./k)).*phi31.*Ck/pi-(i./k).*phi32/pi+phi6/(4*pi);
Pb=-(2/pi)*(phi1./(k.^2)+i*phi2./(2*k)).*phi31.*Ck/pi-phi35./((k.^2)*(pi^2))
                                                -(i./k).*phi36/(pi^2)+phi37/(2*pi^2);
Pz=-2*(i./k).*phi1.*phi31/(pi^2).*Ck-(i./k).*phi35/(pi^2)+phi17/(pi^2);

% Calculating the generalized masses
M1=sum(mn.*f1(:,fknt).^2);
M2=sum(mn.*f2(:,fknt).^2);
M3=sum(mn.*f3(:,fknt).^2);
Ia1=sum(Ialpha.*F1(:,fknt).^2);
Ib0=sum(Ibeta.*G0.^2);
Sa11=sum(Salpha.*f1(:,fknt).*F1(:,fknt));
Sa21=sum(Salpha.*f2(:,fknt).*F1(:,fknt));
Sa31=sum(Salpha.*f3(:,fknt).*F1(:,fknt));
Sb10=sum(Sbeta.*f1(:,fknt).*G0);
Sb20=sum(Sbeta.*f2(:,fknt).*G0);
Sb30=sum(Sbeta.*f3(:,fknt).*G0);
Pa1b0=sum((Sbeta.*(c-a).*b_sect + Ibeta).*F1(:,fknt).*G0);

% Aerodynamics terms (A) using Theodorsen's lift deficiency function
Ah1h1=sum(b_sect.^2.*f1(:,fknt).^2.*Lh);
Ah1h2=sum(b_sect.^2.*f1(:,fknt).*f2(:,fknt).*Lh);
Ah1h3=sum(b_sect.^2.*f1(:,fknt).*f3(:,fknt).*Lh);
Ah1a1=sum(b_sect.^3.*f1(:,fknt).*F1(:,fknt).*(La-(1/2+a).*Lh));
Ah1b0=sum(b_sect.^3.*f1(:,fknt).*G0.*(Lb-(c-e).*Lz));
Ah2h1=sum(b_sect.^2.*f2(:,fknt).*f1(:,fknt).*Lh);
Ah2h2=sum(b_sect.^2.*f2(:,fknt).^2.*Lh);
Ah2h3=sum(b_sect.^2.*f2(:,fknt).*f3(:,fknt).*Lh);
Ah2a1=sum(b_sect.^3.*f2(:,fknt).*F1(:,fknt).*(La-(1/2+a).*Lh));
Ah2b0=sum(b_sect.^3.*f2(:,fknt).*G0.*(Lb-(c-e).*Lz));
Ah3h1=sum(b_sect.^2.*f3(:,fknt).*f1(:,fknt).*Lh);
Ah3h2=sum(b_sect.^2.*f3(:,fknt).*f2(:,fknt).*Lh);
Ah3h3=sum(b_sect.^2.*f3(:,fknt).^2.*Lh);
Ah3a1=sum(b_sect.^3.*f3(:,fknt).*F1(:,fknt).*(La-(1/2+a).*Lh));
Ah3b0=sum(b_sect.^3.*f3(:,fknt).*G0.*(Lb-(c-e).*Lz));
Aa1h1=sum(b_sect.^3.*F1(:,fknt).*f1(:,fknt).*(Mh-(1/2+a).*Lh));
Aa1h2=sum(b_sect.^3.*F1(:,fknt).*f2(:,fknt).*(Mh-(1/2+a).*Lh));
Aa1h3=sum(b_sect.^3.*F1(:,fknt).*f3(:,fknt).*(Mh-(1/2+a).*Lh));
Aa1a1=sum(b_sect.^4.*F1(:,fknt).^2.*(Ma-(1/2+a).*(La+Mh)+(1/2+a).^2.*Lh));
Aa1b0=sum(b_sect.^4.*F1(:,fknt).*G0.*(Mb-(1/2+a).*Lb-(c-e).*Mz+(c-e).*(1/2+a).*Lz));
Ab0h1=sum(b_sect.^3.*G0.*f1(:,fknt).*(Th-(c-e).*Ph));
Ab0h2=sum(b_sect.^3.*G0.*f2(:,fknt).*(Th-(c-e).*Ph));
```

```
Ab0h3=sum(b_sect.^3.*G0.*f3(:,fknt).*(Th-(c-e).*Ph));
Ab0a1=sum(b_sect.^4.*G0.*F1(:,fknt).*(Ta-(c-e).*Pa+(1/2+a).*Th+(1/2+a).*(c-e).*Ph));
Ab0b0=sum(b_sect.^4.*G0.^2.*(Tb-(c-e).*(Pb+Tz)+(c-e).^2.*Pz));

% Solving the flutter determinant
%Check to see if the flap frequency is zero
if omega_b(fknt)==0
   dim=4;
   % Developing the Abar terms for flutter determinant
   Abarh1h1=(pi*rho*Ah1h1/M1+1)*(omega_a(fknt,1)/omega_h(fknt,1))^2;
   Abarh1h2=(pi*rho*Ah1h2/M1)*(omega_a(fknt,1)/omega_h(fknt,1))^2;
   Abarh1h3=(pi*rho*Ah1h3/M1)*(omega_a(fknt,1)/omega_h(fknt,1))^2;
   Abarh1a1=((pi*rho*Ah1a1+Sa11)/M1)*(omega_a(fknt,1)/omega_h(fknt,1))^2;
   Abarh2h1=(pi*rho*Ah2h1/M2)*(omega_a(fknt,1)/omega_h(fknt,2))^2;
   Abarh2h2=(pi*rho*Ah2h2/M2+1)*(omega_a(fknt,1)/omega_h(fknt,2))^2;
   Abarh2h3=(pi*rho*Ah2h3/M2)*(omega_a(fknt,1)/omega_h(fknt,2))^2;
   Abarh2a1=((pi*rho*Ah2a1+Sa21)/M2)*(omega_a(fknt,1)/omega_h(fknt,2))^2;
   Abarh3h1=(pi*rho*Ah3h1/M3)*(omega_a(fknt,1)/omega_h(fknt,3))^2;
   Abarh3h2=(pi*rho*Ah3h2/M3)*(omega_a(fknt,1)/omega_h(fknt,3))^2;
   Abarh3h3=(pi*rho*Ah3h3/M3+1)*(omega_a(fknt,1)/omega_h(fknt,3))^2;
   Abarh3a1=((pi*rho*Ah3a1+Sa31)/M3)*(omega_a(fknt,1)/omega_h(fknt,3))^2;
   Abara1h1=(pi*rho*Aa1h1+Sa11)/Ia1;
   Abara1h2=(pi*rho*Aa1h2+Sa21)/Ia1;
   Abara1h3=(pi*rho*Aa1h3+Sa31)/Ia1;
   Abara1a1=(pi*rho*Aa1a1/Ia1)+1;
   FlutMat(:,:,fknt)=[Abarh1h1, Abarh1h2, Abarh1h3, Abarh1a1;
      Abarh2h1, Abarh2h2, Abarh2h3, Abarh2a1;
      Abarh3h1, Abarh2h3, Abarh3h3, Abarh3a1;
      Abara1h1, Abara1h2, Abara1h3, Abara1a1];
else
   dim=5;
   Abarh1h1=(pi*rho*Ah1h1/M1+1)*(omega_a(fknt,1)/omega_h(fknt,1))^2;
   Abarh1h2=(pi*rho*Ah1h2/M1)*(omega_a(fknt,1)/omega_h(fknt,1))^2;
   Abarh1h3=(pi*rho*Ah1h3/M1)*(omega_a(fknt,1)/omega_h(fknt,1))^2;
   Abarh1a1=((pi*rho*Ah1a1+Sa11)/M1)*(omega_a(fknt,1)/omega_h(fknt,1))^2;
   Abarh1b0=((pi*rho*Ah1b0+Sb10)/M1)*(omega_a(fknt,1)/omega_h(fknt,1))^2;
   Abarh2h1=(pi*rho*Ah2h1/M2)*(omega_a(fknt,1)/omega_h(fknt,2))^2;
   Abarh2h2=(pi*rho*Ah2h2/M2+1)*(omega_a(fknt,1)/omega_h(fknt,2))^2;
   Abarh2h3=(pi*rho*Ah2h3/M2)*(omega_a(fknt,1)/omega_h(fknt,2))^2;
   Abarh2a1=((pi*rho*Ah2a1+Sa21)/M2)*(omega_a(fknt,1)/omega_h(fknt,2))^2;
   Abarh2b0=((pi*rho*Ah2b0+Sb20)/M2)*(omega_a(fknt,1)/omega_h(fknt,2))^2;
   Abarh3h1=(pi*rho*Ah3h1/M3)*(omega_a(fknt,1)/omega_h(fknt,3))^2;
   Abarh3h2=(pi*rho*Ah3h2/M3)*(omega_a(fknt,1)/omega_h(fknt,3))^2;
   Abarh3h3=(pi*rho*Ah3h3/M3+1)*(omega_a(fknt,1)/omega_h(fknt,3))^2;
   Abarh3a1=((pi*rho*Ah3a1+Sa31)/M3)*(omega_a(fknt,1)/omega_h(fknt,3))^2;
   Abarh3b0=((pi*rho*Ah3b0+Sb30)/M3)*(omega_a(fknt,1)/omega_h(fknt,3))^2;
   Abara1h1=(pi*rho*Aa1h1+Sa11)/Ia1;
   Abara1h2=(pi*rho*Aa1h2+Sa21)/Ia1;
   Abara1h3=(pi*rho*Aa1h3+Sa31)/Ia1;
   Abara1a1=(pi*rho*Aa1a1/Ia1)+1;
```

```
      Abara1b0=(pi*rho*Aa1b0+Pa1b0)/Ia1;
      Abarb0h1=((pi*rho*Ab0h1+Sb10)/Ib0)*(omega_a(fknt,1)/omega_b(fknt))^2;
      Abarb0h2=((pi*rho*Ab0h2+Sb20)/Ib0)*(omega_a(fknt,1)/omega_b(fknt))^2;
      Abarb0h3=((pi*rho*Ab0h3+Sb30)/Ib0)*(omega_a(fknt,1)/omega_b(fknt))^2;
      Abarb0a1=((pi*rho*Ab0a1+Pa1b0)/Ib0)*(omega_a(fknt,1)/omega_b(fknt))^2;
      Abarb0b0=((pi*rho*Ab0b0/Ib0)+1)*(omega_a(fknt,1)/omega_b(fknt))^2;
      FlutMat(:,:,fknt)=[Abarh1h1, Abarh1h2, Abarh1h3, Abarh1a1, Abarh1b0;
         Abarh2h1, Abarh2h2, Abarh2h3, Abarh2a1, Abarh2b0;
         Abarh3h1, Abarh3h2, Abarh3h3, Abarh3a1, Abarh3b0;
         Abara1h1, Abara1h2, Abara1h3, Abara1a1, Abara1b0;
         Abarb0h1, Abarb0h2, Abarb0h3, Abarb0a1, Abarb0b0];
   end

   disp('Calculating the rotor blade flutter frequency and speed')
   disp(' ')

   Joe(:,fknt)=eig(FlutMat(:,:,fknt));
   %[Joe_sort(:,fknt),ind]=sort(abs(Joe(:,fknt)));
   Joe=joesort2(Joe,dim,fknt,omega_a,omega_start,rho);
   %Joe(:,fknt)=Joe(ind,fknt);
   FlutFreq(:,fknt)=omega_a(fknt,1)./sqrt(real(Joe(:,fknt)));
   V_Flut(fknt)=Omega1*R;
   FlutDamp(:,fknt)=imag(Joe(:,fknt)).*(FlutFreq(:,fknt)/omega_a(fknt,1)).^2;
   fknt=fknt+1;
end
OMEGA=OMEGA';
Joe=Joe.';
FlutFreq=FlutFreq.';
V_Flut=V_Flut.';
FlutDamp=FlutDamp.';
if loop==1
   Joe_1=Joe;
   FlutFreq_1=FlutFreq;
   figure(1)
   plot(V_Flut/(Omega*R),FlutFreq_1,V_Flut/(Omega*R),Omega_fan,'k--')
   %title('Coupled Natural Frequencies (Without Aerodynamic Terms)')
   xlabel('Nondimensional Rotational Velocity, {\Omega}/{\Omega}_0')
   ylabel('{\omega}_n (rad/s)')
   grid
   axis([0,1.8,0,250])
   %legend('1^{st} Bending Frequency','2^{nd} Bending Frequency','3^{rd} Bending
                        Frequency','1^{st} Torsional Frequency',2)
   legend('1^{st} Bending Frequency','2^{nd} Bending Frequency','3^{rd} Bending
                        Frequency','1^{st} Torsional Frequency','Rigid Body Flap Frequency',2)

   figure(2)
   plot(V_Flut/(Omega*R),FlutFreq_1*30/pi,V_Flut/(Omega*R),Omega_fan*30/pi,'k--')
   %title('Coupled Natural Frequencies (Without Aerodynamic Terms)')
   xlabel('Nondimensional Rotational Velocity, {\Omega}/{\Omega}_0')
   ylabel('{\omega}_n (cpm)')
```

```
        grid
        axis([0,1.8,0,2500])
        %legend('1^{st} Bending Frequency','2^{nd} Bending Frequency','3^{rd} Bending
                        Frequency','1^{st} Torsional Frequency',2)
        legend('1^{st} Bending Frequency','2^{nd} Bending Frequency','3^{rd} Bending
                        Frequency','1^{st} Torsional Frequency','Rigid Body Flap Frequency',2)

        clear Joe FlutFreq FlutDamp
    else
        Joe_2=Joe;
        figure(3)
        subplot(2,1,1)
        plot(V_Flut/(Omega*R),FlutFreq);
        title('{\omega}-v Plot')
        xlabel('Nondimensional Rotational Velocity, {\Omega}/{\Omega}_0')
        ylabel('{\omega}_{FL} (rad/s)')
        grid
        subplot(2,1,2)
        plot(V_Flut/(Omega*R), FlutDamp);
        title('g-v Plot')
        xlabel('Nondimensional Rotational Velocity, {\Omega}/{\Omega}_0')
        ylabel('g')
        grid
        axis([0,1.8,-0.5,0.2000001])
        %legend('1^{st} Bending Frequency','2^{nd} Bending Frequency','3^{rd} Bending
                        Frequency','1^{st} Torsional Frequency',3)
        legend('1^{st} Bending Frequency','2^{nd} Bending Frequency','3^{rd} Bending
                        Frequency','1^{st} Torsional Frequency','Rigid Body Flap Frequency',3)
    end
end
```

APPENDIX B. THE HOLZER FUNCTION

The MATLAB® function for calculating the torsional natural frequencies and mode shapes is listed below.

```
function [rotation,omega_n]=holzer_blade(rn, Jn, Arean, Ialpha, G_n, Al_rho, mn, OpRv, twist,
                                modeshp, type)
% This function runs a Holzer analysis for rotating beams to calculate
% the torsional mode shapes and frequencies for the rotor blade.
% The purpose of this program is to provide input to the flutter program.
% disp('Calculating the torsional mode shapes for the rotor blade.')
% disp(' ')
%
global k_root R
lsn=diff(rn);          % determine length of each segment
N=length(lsn);       % number of radial stations
GJ=G_n*Jn;          % find torsional stiffness (lb_f-ft^2)
% Determine the centrifugal force (lb_f)
Gn(N+1)=mn(N+1) * rn(N+1) * OpRv^2;          % lb_f
for n=N:-1:1,
   Gn(n)=Gn(n+1) + mn(n) * rn(n) * OpRv^2;     % lb_f
end;
Gn=Gn';
% find mass moment of inertial about c.g.
theta_o=14.6*(pi/180);            % collective pitch (rad)
twist=twist*(pi/180);            % convert twist from degrees to radians
theta=theta_o+twist*(rn/R);   % determine theta for each segment
ka=sqrt(Jn./Arean);               % ft
Gnka2=Gn.*ka.^2;                % lb_f-ft^2
% Determining the natural frequencies
knt1=1;        % knt1 is the counting variable for omega1 (frequency)
for omega1=0:2:800,
   omega(knt1)=omega1;
   X1_n=[1;0];
   for n=N:-1:1,
      Kn=[1,                                                    0;
         -Ialpha(n+1)*lsn(n)*(omega1^2-OpRv^2*cos(2*theta(n+1))),     1];

      An=[1,      -lsn(n)/(GJ(n+1)+Gnka2(n+1));
         0,                        1];

      Fn=inv(Kn)*An;
      X1_n=Fn*X1_n;
   end;
   switch type
      case 1       % Articulated Boundary Conditions (free-free B.C.)
         Bc(knt1)=X1_n(2);
      case 2       % Hingeless (infinite stiffness at root) Boundary Conditions
```

```
        Bc(knt1)=X1_n(1);
    case 3      % Hingeless (finite stiffness at root) Boundary Conditions
        Bc(knt1)=k_root*X1_n(1)-X1_n(2);
  end
  knt1=knt1+1;
end;
Bc=Bc';omega=omega';

% Find the zeros of the determinant
slp=sign(Bc(1));
tol=1e-10;
knt2=2;
for mode=1:modeshp,
  while sign(Bc(knt2))==slp & knt2<length(Bc)
    knt2=knt2+1;
  end
  omega_low=omega(knt2-1);
  Bc_low=Bc(knt2-1);
  omega_high=omega(knt2);
  Bc_high=Bc(knt2);
  k=0;
  while abs(omega_high-omega_low)>tol & k<500
    omega_mid=(omega_low+omega_high)/2;
    X1=[1;0];
    for n=N:-1:1,
      Kn=[1,                                                    0;
        -Ialpha(n+1)*lsn(n)*(omega_mid^2-OpRv^2*cos(2*theta(n+1))),     1];

      An=[1,     -lsn(n)/(GJ(n+1)+Gnka2(n+1));
        0,                      1];

      Fn=inv(Kn)*An;
      X1=Fn*X1;
    end;
    switch type
      case 1      % Articulated Boundary Conditions
        Bc_mid=X1(2);
      case 2      % Hingeless (infinite stiffness at root) Boundary Conditions
        Bc_mid=X1(1);
      case 3      % Hingeless (finite stiffness at root) Boundary Conditions
        Bc_mid=k_root*X1(1)-X1(2);
    end
    if sign(Bc_low*Bc_mid)==-1
      omega_high=omega_mid;
      Bc_high=Bc_mid;
    else
      omega_low=omega_mid;
      Bc_low=Bc_mid;
    end
    k=k+1;
```

```
   end
   slp=sign(Bc(knt2));
   Bc_n(mode)=Bc_mid;
   omega_n(mode)=omega_mid;              % convert from rad/sec to cpm
end

for mode=1:modeshp,
   % Arbitrarily setting phi_N = 1, beta_n is found by
   phi_N=1;
   % set boundary condition at tip
   X_N=[phi_N;0];
   F1=eye(2);
   X_n(:,N+1,mode)=F1*X_N;
   for n=N:-1:1,
      Kn=[1,                                                    0;
         -Ialpha(n+1)*lsn(n)*(omega_n(mode)^2-OpRv^2*cos(2*theta(n+1))),     1];

      An=[1,      -lsn(n)/(GJ(n+1)+Gnka2(n+1));
         0,                        1];

      Fn=inv(Kn)*An;
      F1=Fn*F1;
      X_n(:,n,mode)=F1*X_N;
   end
   % determine deflections
   rotation(mode,:)=X_n(1,:,mode);
end
% Display the natural frequencies in cpm for the given operational rpm
omega_cpm=omega_n*30/pi;              % convert from rad/sec to cpm
disp('The torsional natural frequencies in rad/sec are: ')
disp(omega_n)
%disp('The torsional natural frequencies in cpm are: ')
%disp(omega_cpm)
%disp('The ratios of torsional natural frequencies to the rotational frequency are: ')
%disp(omega_n/OpRv)
```

THIS PAGE INTENTIONALLY LEFT BLANK

APPENDIX C. THE MYKELSTAD FUNCTION

The MATLAB® function for calculating the bending natural frequencies and mode shapes is listed below.

```
function [deflection,omega_n]=myklestad(rn, Izzn, En, mn, OpRv, modeshp, type)
% This function runs a Myklestad analysis for rotating beams to calculate
% the flapwise bending mode shapes and frequencies  The purpose of this
% program is to provide input to the flutter program.
disp('Calculating the flapwise bending mode shapes for the rotor blade.')
disp(' ')
%
global Kappa R
EI=En*Izzn;          % determine stiffness of blade (lb_f-ft^2)
lsn=diff(rn);        % determine length of each segment
N=length(lsn);       % number of radial stations

% Determine the centrifugal force (lb_f)
Gn(N+1)=mn(N+1) * rn(N+1) * OpRv^2;
for n=N:-1:1,
   Gn(n)=Gn(n+1) + mn(n) * rn(n) * OpRv^2;
end;

% Determining the natural frequencies
knt1=1;        % knt1 is the counting variable for omega1 (frequency)
for omega1=0:2:300,
   omega(knt1)=omega1;
   F(:,:,knt1)=eye(4);
   for n=1:N,
      Kn=[1,      0,         0,     -mn(n)*omega1^2;
          0,      1,         0,          -Gn(n+1);
          0,      0,         1,             0;
          0,      0,       lsn(n),          1];

      An=[1,                                  0,                                  0,                          0;
          lsn(n),                             1,                                  0,                   -Gn(n+1);
          -(lsn(n)^2)/(2*EI(n+1)),  -lsn(n)/EI(n+1),      1+lsn(n)^2*Gn(n+1)/(2*EI(n+1)),        0;
          -(lsn(n)^3)/(3*EI(n+1)), -(lsn(n)^2)/(2*EI(n+1)),   lsn(n)^3*Gn(n+1)/(3*EI(n+1)),     1];

      Fn=inv(Kn)*An;
      F(:,:,knt1)=F(:,:,knt1)*Fn;
   end;
   switch type
      case 1       % Articulated Boundary Conditions
         Bc(:,:,knt1)=[F(2,3,knt1), F(2,4,knt1); F(4,3,knt1), F(4,4,knt1)];
      case 2       % Hingeless (infinite stiffness at root) Boundary Conditions
         Bc(:,:,knt1)=[F(3,3,knt1), F(3,4,knt1);F(4,3,knt1),F(4,4,knt1)];
      case 3       % Hingeless (finite stiffness at root) Boundary Conditions
```

```
        Bc(:,:,knt1)=[F(2,3,knt1)+Kappa*F(3,3,knt1),F(2,4,knt1)+Kappa*F(3,4,knt1);
                                                    F(4,3,knt1),F(4,4,knt1)];
    end
    detbc(knt1)=det(Bc(:,:,knt1));
    knt1=knt1+1;
end;
detbc=detbc';omega=omega';

% Find the zeros of the determinant
slp=sign(detbc(1));
tol=1e-10;
knt2=2;
for mode=1:modeshp,
    while sign(detbc(knt2))==slp & knt2<length(detbc)
        knt2=knt2+1;
    end
    omega_low=omega(knt2-1);
    detbc_low=detbc(knt2-1);
    omega_high=omega(knt2);
    detbc_high=detbc(knt2);
    k=0;
    while abs(omega_high-omega_low)>tol & k<500
        omega_mid=(omega_low+omega_high)/2;
        F1=eye(4);
        for n=1:N,
            Kn=[1,      0,         0,     -mn(n)*omega_mid^2;
                0,      1,         0,         -Gn(n+1);
                0,      0,         1,             0;
                0,      0,       lsn(n),        1];

            An=[1,                                  0,                                  0,                          0;
                lsn(n),                             1,                                  0,                      -Gn(n+1);
                -(lsn(n)^2)/(2*EI(n+1)),    -lsn(n)/EI(n+1),   1+lsn(n)^2*Gn(n+1)/(2*EI(n+1)),     0;
                -(lsn(n)^3)/(3*EI(n+1)), -(lsn(n)^2)/(2*EI(n+1)), lsn(n)^3*Gn(n+1)/(3*EI(n+1)),  1];

            Fn=inv(Kn)*An;
            F1=F1*Fn;
        end;
        switch type
            case 1      % Articulated Boundary Conditions
                Bc_mid=[F1(2,3), F1(2,4); F1(4,3), F1(4,4)];
            case 2      % Hingeless (infinite stiffness at root) Boundary Conditions
                Bc_mid=[F1(3,3), F1(3,4);F1(4,3),F1(4,4)];
            case 3      % Hingeless (finite stiffness at root) Boundary Conditions
                Bc_mid=[F1(2,3)+Kappa*F1(3,3),F1(2,4)+Kappa*F1(3,4);F1(4,3),F1(4,4)];
        end
        detbc_mid=det(Bc_mid);
        if sign(detbc_low*detbc_mid)==-1
            omega_high=omega_mid;
            detbc_high=detbc_mid;
```

```
      else
         omega_low=omega_mid;
         detbc_low=detbc_mid;
      end
      k=k+1;
   end
   slp=sign(detbc(knt2));
   Bc_n(:,:,mode)=Bc_mid;
   omega_n(mode)=omega_mid;              % convert from rad/sec to cpm
end
for mode=1:modeshp,
   % Arbitrarily setting Z_N = 1, beta_n is found by
   Z_N=1;
   beta_n(mode)=-Bc_n(2,2,mode)/Bc_n(2,1,mode);
   X_N(:,mode)=[0;0;beta_n(mode);Z_N];
   F1=eye(4);
   X_n(:,N+1,mode)=F1*X_N(:,mode);
   for n=N:-1:1,
      Kn=[1,      0,         0,     -mn(n)*omega_n(mode)^2;
         0,       1,         0,          -Gn(n+1);
         0,       0,         1,             0;
         0,       0,       lsn(n),         1];

      An=[1,                                  0,                                  0,                          0;
         lsn(n),                              1,                                  0,                      -Gn(n+1);
         -(lsn(n)^2)/(2*EI(n+1)),    -lsn(n)/EI(n+1),    1+lsn(n)^2*Gn(n+1)/(2*EI(n+1)),        0;
         -(lsn(n)^3)/(3*EI(n+1)), -(lsn(n)^2)/(2*EI(n+1)),  lsn(n)^3*Gn(n+1)/(3*EI(n+1)),    1];

      Fn=inv(Kn)*An;
      F1=Fn*F1;
      X_n(:,n,mode)=F1*X_N(:,mode);
   end
   % determine deflections
   deflection(mode,:)=X_n(4,:,mode);
end
% Display the natural frequencies in cpm for the given operational rpm
omega_cpm=omega_n*30/pi;              % convert from rad/sec to cpm
%disp('The bending natural frequencies in rad/sec are: ')
%disp(omega_n)
%disp('The bending natural frequencies in cpm are: ')
%disp(omega_cpm)
%disp('The ratios of bending natural frequencies to the rotational frequency are: ')
%disp(omega_n/OpRv)
```

THIS PAGE INTENTIONALLY LEFT BLANK

APPENDIX D. PROGRAM FOR CALCULATING REAL AND IMAGINARY CURVES FOR FLUTTER DETERMINANT

The MATLAB® program for calculating the aerodynamic coefficients is listed below.

```
% This program calculates the terms for the 2DOF flutter determinant with
% no structural damping and makes a plot of the real and imaginary curves
% (Ref. NACA TR 685)
clear
ra2=0.25;
wa2wh2=16;
kappa=0.25;
a=-0.4;
xa=0.2;
c=0.6
n=1;
for kinv=0.01:0.01:3.9,
   k=1./kinv;
   H2_0=besselh(0,2,k);
   H2_1=besselh(1,2,k);
   Ck=H2_1./(H2_1+i*H2_0);
   Lh=1-2*(i./k).*Ck;
   La=1/2-(i./k).*(1+2*Ck)-2.*Ck./(k.^2);
   Mh=1/2;
   Ma=3/8-(i./k);
   term11=ra2*wa2wh2*(1/kappa+Lh);
   term12=ra2*wa2wh2*(La-(0.5+a)*Lh+xa/kappa);
   term21=Mh-(0.5+a)*Lh+xa/kappa;
   term22=Ma-(0.5+a)*(La+Mh)+(0.5+a)^2*Lh+ra2/kappa;
   A=[term11,term12;term21,term22];
   coeffs(n,:)=poly(A);
   realroots(:,n)=sqrt(roots(real(coeffs(n,:))));
   imagroots(:,n)=sqrt(roots(imag(coeffs(n,:))));
   n=n+1;
end
kinv=0.01:0.01:3.9;
plot(kinv,realroots,'k',kinv,imagroots,'b')
grid
axis([0,4,0,5])
xlabel('1/k')
ylabel('sqrt(X)')
```

THIS PAGE INTENTIONALLY LEFT BLANK

APPENDIX E. PROGRAM FOR CALCULATING AERODYNAMIC COEFFICIENTS

The MATLAB® program for calculating the aerodynamic coefficients is listed below.

```
% This program calculates the aerodynamic coefficients for a given reduced
% frequency, wake spacing and frequency ratio.  User can choose the lift
% deficiency function
liftdef=menu('Choice of Lift Deficiency Function', 'Theodorsen', 'Loewy', 'Single-Wake');
altitude=1000
std_lapse_rate=0.003565;      % (deg R/ft)
T_ref=518.67;                 % (deg R)
rho_ref=0.0023769;            % (slug/ft^3)
g_o=32.1740485;               % (ft/s^2)
g_c=32.1740485;               % (ft-lbm/lbf-s^2)
R_gas=1545/28.97;             % (ft-lbf/lbm-deg R)
p_ref=2116.22;                % (lbf/ft^2)
Temp=T_ref-std_lapse_rate*altitude;      %Atmospheric temperature (deg R) using standard
adiabatic lapse rate
press=p_ref*(1-std_lapse_rate*altitude/T_ref)^(g_o/(R_gas*std_lapse_rate*g_c));
                                                % Atmospheric pressure (lb/ft^2)
rho=press/(R_gas*g_c*Temp);                % Atmospheric density (slug/ft^3)

R=372/12;          % H-3 blade
N_b=5;         % Number of rotor blades
GW=12000;
A=pi*R^2;
v_i=sqrt(GW/(2*rho*A));
Omega_rpm=203;     % numerical instabilities in taking inverse of matrix occur if
                   % Omega_rpm > 375
Omega=Omega_rpm*2*pi/60;    % rotor speed (rad/s)
h=2*pi*v_i/(18.25/12*N_b*Omega)
kinv=1.25
k=1/kinv
e=0.5;
c=0.5;
a=-0.5;
p=-1/3*(sqrt(1-c^2))^3;

% Define the T and phi functions
T1=-1/3*sqrt(1-c.^2)*(2+c.^2)+c.*acos(c);
T3=-(1/8+c.^2).*(acos(c)).^2+1/4*c.*sqrt(1-c.^2).*acos(c)*(7+2*c.^2)
                                                    -1/8*(1-c.^2).*(5*c.^2+4);
T4=-acos(c)+c.*sqrt(1-c.^2);
T5=-(1-c.^2)-(acos(c)).^2+2*c.*sqrt(1-c.^2).*acos(c);
T7=-(1/8+c.^2).*acos(c)+1/8*c.*sqrt(1-c.^2).*(7+2*c.^2);
T10=sqrt(1-c.^2)+acos(c);
```

```
T11=acos(c).*(1-2*c)+sqrt(1-c.^2).*(2-c);
T12=sqrt(1-c.^2).*(2+c)-acos(c).*(2*c+1);
phi1=T10;
phi2=T11;
phi3=-T4;
phi31=acos(c)-sqrt(1-c.^2);
phi32=acos(c)+sqrt(1-c.^2).*(1-2*c);
phi35=2*(1-c.^2);
phi36=phi32*phi3+2*(1-c.^2).^2;
phi37=phi3*(phi2-phi3);
phi5=T4+T10;
phi6=2*acos(c)+2/3*sqrt(1-c.^2).*(2+c).*(1-2*c);
phi8=T12;
phi10=phi31*phi5;
phi17=phi3.^2+(1-c.^2).^2;

m=0:0.25:0.75;
j0=besselj(0,k);
y0=bessely(0,k);
j1=besselj(1,k);
y1=bessely(1,k);
H2_0=besselh(0,2,k);
H2_1=besselh(1,2,k);
switch liftdef
   case 1
      % Theodorsen lift deficiency function
      Ck=H2_1./(H2_1+i*H2_0);
      Mh=1/2;
      Ma=3/8-(i./k);
      Mb=-T7/pi-(e+1/2).*T1/pi+(i./k).*(2*p+T4)/pi-(1./k.^2).*((T4+T10)/pi);
      Mz=-(i./k).*phi5/pi+1/4*phi6/pi;
   case 2
      % Loewy lift deficiency function
      W_Loewy=1 ./ (exp(k .* h) * exp(i*2*pi*m) -1);
      alfhat_L=real(W_Loewy);
      bethat_L=imag(W_Loewy);
      A_L=(j1 .* (1+2*alfhat_L)) + y0 - (2*j0 .*bethat_L);
      B_L=-y1 + (2*j1 .* bethat_L) + (j0 .* (1+2*alfhat_L));
      den_L=A_L .^2 + B_L.^ 2;
      F_L=((j1.*(1+2*alfhat_L).*A_L)-((y1 - 2*j1.*bethat_L).*B_L))./den_L;
      G_L=-(((y1- 2*j1.* bethat_L).* A_L)+(j1 .*(1+2*alfhat_L).* B_L))./den_L;
      Ck=F_L+i.*G_L;          % Loewy lift defiency function
      Mh=(1/2)*ones(1,4);
      Ma=(3/8-(i./k))*ones(1,4);
      Mb=(-T7/pi-(e+1/2).*T1/pi+(i./k).*(2*p+T4)/pi-(1./k.^2).*((T4+T10)/pi))*ones(1,4);
      Mz=(-(i./k).*phi5/pi+1/4*phi6/pi)*ones(1,4);
   case 3
      % Single wake lift deficiency function
      W_Single=exp(-i*2*pi*m) .* exp(-k.*h);
      alfhat_S=real(W_Single);
```

```
        bethat_S=imag(W_Single);
        A_S=(j1 .* (1+2*alfhat_S)) + y0 - (2*j0 .*bethat_S);
        B_S=-y1 + (2*j1 .* bethat_S) + (j0 .* (1+2*alfhat_S));
        den_S=A_S .^2 + B_S.^ 2;
        F_S=((j1.*(1+2*alfhat_S).*A_S)-((y1 - 2*j1.*bethat_S).*B_S))./den_S;
        G_S=-(((y1- 2*j1.* bethat_S).* A_S)+(j1 .*(1+2*alfhat_S).* B_S))./den_S;
        Ck=F_S+i.*G_S;          % Single wake lift deficiency function
        Mh=(1/2)*ones(1,4);
        Ma=(3/8-(i./k))*ones(1,4);
        Mb=(-T7/pi-(e+1/2).*T1/pi+(i./k).*(2*p+T4)/pi-(1./k.^2).*((T4+T10)/pi))*ones(1,4);
        Mz=(-(i./k).*phi5/pi+1/4*phi6/pi)*ones(1,4);
end
% L, M, T and P terms using chosen lift deficiency function
Lh=1-2*(i./k).*Ck;
La=1/2-(i./k).*(1+2*Ck)-2.*Ck./(k.^2);
Lb=-T1/pi+i./(pi*k).*(T4-T11.*Ck)-2.*(T10/pi).*Ck./(k.^2);
Lz=-2*(i./k).*(phi1/pi).*Ck+phi3/pi;
Th=-T1/pi-(i./k).*(T12/pi).*Ck;
Ta=-(1/pi)*(T7+(e+1/2).*T1)-(i./k).*((2*p-2*T1-T4)/(2*pi)+T12/pi.*Ck)
                                                    -(1./k.^2).*(T12/pi).*Ck;
Tb=-T3/(pi^2)+(i./k).*(T4.*T11-T11.*T12.*Ck)./(2*(pi^2))
                                    -(1./k.^2).*(T5-T4.*T10+T10.*T12.*Ck)/(pi^2);
Tz=-(i./k).*(phi1.*phi8.*Ck+phi10)/(pi^2)+1/2*phi37/(pi^2);
Ph=-2*(i./k).*phi31.*Ck/pi+phi3/pi;
Pa=-2*(1./(k.^2)+(i./k)).*phi31.*Ck/pi-(i./k).*phi32/pi+phi6/(4*pi);
Pb=-(2/pi)*(phi1./(k.^2)+i*phi2./(2*k)).*phi31.*Ck/pi-phi35./((k.^2)*(pi^2))
                                                -(i./k).*phi36/(pi^2)+phi37/(2*pi^2);
Pz=-2*(i./k).*phi1.*phi31/(pi^2).*Ck-(i./k).*phi35/(pi^2)+phi17/(pi^2);
aerocoeff=[Lh;La;Lb;Lz;Mh;Ma;Mb;Mz;Th;Ta;Tb;Tz;Ph;Pa;Pb;Pz];
```

THIS PAGE INTENTIONALLY LEFT BLANK

APPENDIX F. THEODORSEN AND KÜSSNER FUNCTIONS

Theodorsen's *T*-functions are defined in Ref. 46 and are reproduced here for the convenience of the reader. The variable c is the non-dimensional distance from the mid-chord to the flap hinge (positive measured aft). The *T*-functions are functions of geometry only.

$$T_1 = -\frac{1}{3}\sqrt{1-c^2}\left(2+c^2\right)+c\cos^{-1}c$$

$$T_2 = c\left(1-c^2\right)-\left(\sqrt{1-c^2}\right)\left(1+c^2\right)\cos^{-1}c+c\left(\cos^{-1}c\right)^2$$

$$T_3 = -\left(\frac{1}{8}+c^2\right)\left(\cos^{-1}c\right)^2+\frac{1}{4}c\sqrt{1-c^2}\left(\cos^{-1}c\right)\left(7+2c^2\right)-\frac{1}{8}\left(1-c^2\right)\left(5c^2+4\right)$$

$$T_4 = -\cos^{-1}c+c\sqrt{1-c^2}$$

$$T_5 = -\left(1-c^2\right)-\left(\cos^{-1}c\right)^2+2c\sqrt{1-c^2}\left(\cos^{-1}c\right)$$

$$T_6 = T_2$$

$$T_7 = -\left(\frac{1}{8}+c^2\right)\left(\cos^{-1}c\right)+\frac{1}{8}c\sqrt{1-c^2}\left(7+2c^2\right)$$

$$T_8 = -\frac{1}{3}\left(\sqrt{1-c^2}\right)\left(2c^2+1\right)+c\cos^{-1}c$$

$$T_9 = \frac{1}{2}\left[\frac{1}{3}\left(\sqrt{1-c^2}\right)^3+aT_4\right]=\frac{1}{2}\left(-p+aT_4\right)$$

where $p = -\frac{1}{3}\left(\sqrt{1-c^2}\right)^3$

$$T_{10} = \sqrt{1-c^2}+\cos^{-1}c$$

$$T_{11} = \left(\cos^{-1}c\right)\left(1-2c\right)+\sqrt{1-c^2}\left(2-c\right)$$

$$T_{12} = \sqrt{1-c^2}\left(2+c\right)-\left(\cos^{-1}c\right)\left(2c+1\right)$$

$$T_{13} = \frac{1}{2}\left[-T_7-\left(c-a\right)T_1\right]$$

$$T_{14} = \frac{1}{16} + \frac{1}{2}ac$$

Küssner's ϕ-functions are defined in Ref. 47 and are reproduced here for the convenience of the reader. The ϕ-functions are functions of geometry only. The functions ϕ_1 to ϕ_{12} were developed by Küssner [Ref. 67], and the functions ϕ_{13} to ϕ_{21} were added by Dietze. The functions ϕ_{31} to ϕ_{37} were developed by Küssner and Schwartz [Ref. 47].

$$\phi_1 = \pi - \varphi + \sin\varphi$$

$$\phi_2 = (\pi - \varphi)(1 + 2\cos\varphi) + \sin\varphi(2 + \cos\varphi)$$

$$\phi_3 = \pi - \varphi + \sin\varphi\cos\varphi$$

$$\phi_4 = 2(\pi - \varphi)\cos\varphi + \frac{2}{3}(2 + \cos^2\varphi)\sin\varphi$$

$$\phi_5 = \sin\varphi(1 - \cos\varphi)$$

$$\phi_6 = 2(\pi - \varphi) + \frac{2}{3}\sin\varphi(2 - \cos\varphi)(1 + 2\cos\varphi)$$

$$\phi_7 = (\pi - \varphi)\left(\frac{1}{2} + 2\cos\varphi\right) + \frac{1}{6}(8 + 5\cos\varphi + 4\cos^2\varphi - 2\cos^3\varphi)\sin\varphi$$

$$\phi_8 = (\pi - \varphi)(-1 + 2\cos\varphi) + \sin\varphi(2 - \cos\varphi)$$

$$\phi_9 = (\pi - \varphi)(1 + 2\cos\varphi) + \frac{1}{3}(2 + 3\cos\varphi + 4\cos^2\varphi)\sin\varphi$$

$$\phi_{10} = \phi_{31}\phi_5$$

$$\phi_{11} = \phi_2\phi_3$$

$$\phi_{12} = (\pi - \varphi)^2\left(\frac{1}{2} + 4\cos^2\varphi\right) + (\pi - \varphi)(7 + 2\cos^2\varphi)\sin\varphi\cos\varphi + \left(2 + \frac{5}{2}\cos^2\varphi\right)\sin\varphi$$

$$\phi_{13} = \tan\frac{\varphi}{2} = \frac{1 - \cos\varphi}{\sin\varphi} = \frac{\sin\varphi}{1 + \cos\varphi}$$

$$\phi_{14} = 2\sin\varphi$$

$$\phi_{15} = \phi_{13} - \phi_{14}$$

$$\phi_{16} = \phi_1\phi_{14} = 2\phi_1\sin\varphi$$

$$\phi_{17} = \left(\phi_3\right)^2 + \sin^4\varphi$$

$$\phi_{18} = -\phi_{13}\left[\left(\pi-\varphi\right)\left(1+2\cos\varphi\right)-\sin\varphi\cos\varphi\right]$$

$$\phi_{19} = \frac{1}{2}\phi_3\phi_{14} = \phi_3\sin\varphi$$

$$\phi_{20} = \left(1+\cos\varphi\right)\sin\varphi$$

$$\phi_{21} = -2\left(\cos\varphi+\ln\sin^2\varphi\right)$$

$$\phi_{31} = \pi-\varphi-\sin\varphi$$

$$\phi_{32} = \pi-\varphi+\sin\varphi\left(1+2\cos\varphi\right)$$

$$\phi_{35} = 2\sin^2\varphi$$

$$\phi_{36} = \phi_{32}\phi_3 + 2\sin^4\varphi$$

$$\phi_{37} = \phi_3\left(\phi_2-\phi_3\right)$$

Noting that the flap hinge position, c, is mapped to the unit circle as $-\cos\varphi$ [Ref. 47], the relations $-\cos\varphi = c$, $\sin\varphi = \sqrt{1-c^2}$, $\sin\varphi\cos\varphi = c\sqrt{1-c^2}$, and $\pi-\varphi = \cos^{-1}c$ can be applied to the ϕ-functions yielding:

$$\phi_1 = \cos^{-1}c + \sqrt{1-c^2} = T_{10}$$

$$\phi_2 = \left(1-2c\right)\cos^{-1}c + \left(2-c\right)\sqrt{1-c^2} = T_{11}$$

$$\phi_3 = \cos^{-1}c - c\sqrt{1-c^2} = -T_4$$

$$\phi_4 = -2c\cos^{-1}c + \frac{2}{3}\left(2+c^2\right)\sqrt{1-c^2} = -2T_1$$

$$\phi_5 = \sqrt{1-c^2}\left(1+c\right) = T_4 + T_{10}$$

$$\phi_6 = 2\cos^{-1}c + \frac{2}{3}\sqrt{1-c^2}\left(2+c\right)\left(1-2c\right)$$

$$\phi_7 = \left(\frac{1}{2}-2c\right)\cos^{-1}c + \frac{1}{6}\left(\sqrt{1-c^2}\right)\left(8-5c+4c^2+2c^3\right) = -4\left[T_7 + \left(c+\frac{1}{2}\right)T_1\right] = 8T_{13}$$

$$\phi_8 = -\left(\cos^{-1}c\right)\left(1+2c\right) + \sqrt{1-c^2}\left(2+c\right) = T_{12}$$

$$\phi_{10} = \phi_{31}\phi_5 = \left(\cos^{-1} c - \sqrt{1-c^2}\right)(1+c)\sqrt{1-c^2}$$

$$\phi_{11} = \phi_2\phi_3 = -T_{11}T_4 = \left[(1-2c)\cos^{-1} c + (2-c)\sqrt{1-c^2}\right]\left[\cos^{-1} c - c\sqrt{1-c^2}\right]$$

$$\phi_{12} = -4\left\{-\left(\frac{1}{8}+c^2\right)\left(\cos^{-1} c\right)^2 + \frac{1}{4}c\sqrt{1-c^2}\left(\cos^{-1} c\right)\left(7+2c^2\right) - \frac{1}{8}\left(1-c^2\right)\left(5c^2+4\right)\right\}$$
$$= -4T_3$$

$$\phi_{13} = \frac{\sqrt{1-c^2}}{1-c}$$

$$\phi_{14} = 2\sqrt{1-c^2}$$

$$\phi_{15} = \frac{2c-1}{1-c}\sqrt{1-c^2} = \phi_{13} - \phi_{14}$$

$$\phi_{16} = 2\sqrt{1-c^2}\left[\cos^{-1} c + \sqrt{1-c^2}\right] = \phi_1\phi_{14}$$

$$\phi_{17} = \left(\phi_3\right)^2 + \left(1-c^2\right)^2 = \left[\cos^{-1} c - c\sqrt{1-c^2}\right]^2 + \left(1-c^2\right)^2$$

$$\phi_{18} = \frac{\sqrt{1-c^2}}{1-c}\left[(1-2c)\cos^{-1} c - c\sqrt{1-c^2}\right]$$

$$\phi_{19} = \left[\cos^{-1} c - c\sqrt{1-c^2}\right]\sqrt{1-c^2}$$

$$\phi_{20} = (1-c)\sqrt{1-c^2}$$

$$\phi_{21} = 2c - 2\ln\left(1-c^2\right)$$

$$\phi_{31} = \cos^{-1} c - \sqrt{1-c^2}$$

$$\phi_{32} = \cos^{-1} c + \sqrt{1-c^2}\,(1-2c)$$

$$\phi_{35} = 2\left(1-c^2\right)$$

$$\phi_{36} = \phi_{32}\phi_3 + 2\left(1-c^2\right)^2 = \left[\cos^{-1} c + \sqrt{1-c^2}\,(1-2c)\right]\left[\cos^{-1} c - c\sqrt{1-c^2}\right] + 2\left(1-c^2\right)^2$$

$$\phi_{37} = \phi_3\left(\phi_2 - \phi_3\right) = -2\left[\cos^{-1} c - c\sqrt{1-c^2}\right]\left[c\cos^{-1} c - \sqrt{1-c^2}\right]$$

LIST OF REFERENCES

1. Bisplinghoff, R. L., Ashley, H., and Halfman, R. L., *Aeroelasticity*, Addison-Wesley Publishing Company, Inc., Cambridge, Massachusetts, 1955.

2. Straub, F. K. and Charles, B. D., "Comprehensive Modeling of Rotor Blades with Trailing Edge Flaps," Proceedings of the 55th Annual Form of the American Helicopter Society, Montreal, Quebec, Canada, May 1999.

3. Scanlan, R. H. and Rosenbaum, R., *Introduction to the Study of Aircraft Vibration and Flutter*, The MacMillan Company, New York, 1951.

4. "Certification of Normal Category Rotorcraft," Federal Aviation Administration Aircraft Circular 27-1B, September 30, 1999.

5. "Certification of Transport Category Rotorcraft," Federal Aviation Administration Aircraft Circular 29-2C, September 30, 1999.

6. Wood, E. R., "Vibration and Flutter Report for Advanced Tactical Helicopter," *Sikorsky Aircraft Report* 50131, Stratford, Connecticut, 1960.

7. Wood, E. R., Couch, Mark A., and Canright, D., "On the Flutter Speed of a Rotor Blade in Forward Flight," Proceedings from the 28th European Rotorcraft Forum, Bristol, England, September 2002.

8. Rauchenstein, W. J., Jr., "A 3D Theodorsen-Based Rotor Blade Flutter Model Using Normal Modes," Master's Thesis, Naval Postgraduate School, Monterey, California, September 2002.

9. Gerstenberger, W., Wagner, R. A., Kelley, B., Ellis, C. W., Doman, G. S., and Leone, P. F., "The Rotary Round Table: How Can Helicopter Vibrations Be Minimized?," *Journal of the American Helicopter Society*, Vol. 2, No. 3, July 1957.

10. Loewy, R. G., "Helicopter Vibrations: A Technological Perspective," Alexander A. Nikolsky Honorary Lecture, *Journal of the American Helicopter Society*, Vol. 29, No. 4, October 1984.

11. Bousman, W. G., "Putting the Aero Back Into Aeroelasticity," Proceedings of the Eighth Annual ARO Workshop on Aeroelasticity of Rotorcraft Systems, University Park, Pennsylvania, October 1999.

12. "NATOPS Flight Manual Navy Model SH-60B Aircraft", Department of the Navy, NAVAIR A1-H60BB-NFM-000, May 1, 2000.

13. Wood, E. R., Powers, R. W., Cline, J. H., and Hammond, C.E., "On Developing and Flight Testing a Higher Harmonic Control System," *Journal of the American Helicopter Society*, Vol. 30, No. 2, January 1985.

14. Wood, E. R., Platzer, M. F., Abourahma, A., and Couch, M. A., "On the Unsteady Aerodynamics of Higher Harmonic Control," Proceedings of the Nineteenth European Rotorcraft Forum, No. C17, Cernobbio, Italy, September 1993.

15. Couch, M. A. and Wood, E. R., "A 2-D Unsteady Aerodynamic Application to HHC Test Data Show Performance Improvements," AIAA 2002-6017, Proceedings of the 2002 Biennial International Powered Lift Conference, Williamsburg, Virginia, November 2002.

16. Shaw, J., Hanker, E. J., and Teal, R. S., "Higher Harmonic Control: Wind Tunnel Demonstration of Fully Effective Vibratory Hub Force Suppression," Proceedings of the 41st Annual Form of the American Helicopter Society, Forth Worth, Texas, May 1985.

17. Miao, W., Kottapalli, S. B. R., and Frye, H. M., "Flight Demonstration of Higher Harmonic Control (HHC) on S-76," Proceedings of the 42nd Annual Forum of the American Helicopter Society, Washington, D.C., June 1986.

18. Walsh, D. M., "Flight Tests of an Open Loop Higher Harmonic Control System on an S-76A Helicopter," Proceedings of the 42nd Annual Forum of the American Helicopter Society, Washington D.C., June 1986.

19. Polychroniadis, M. and Achache, M., "Higher Harmonic Control: Flight Tests of an Experimental System on SA-349 Research Gazelle," Proceedings of the 42nd Annual Forum of the American Helicopter Society, Washington, D.C., June 1986.

20. Friedmann, P. P., "Rotary-Wing Aeroelasticity – Current Status and Future Trends," AIAA 2001-0427, Proceedings of the 39th AIAA Aerospace Sciences Meeting & Exhibit, Reno, Nevada, January 2001.

21. Jacklin, S. A., Haber, A., de Simone, G., Norman, T. R., and Shinoda, P., "Full-Scale Wind Tunnel Test of an Individual Blade Control System for a UH-60 Helicopter," Proceedings of the 58th Annual Forum of the American Helicopter Society, Montreal, Canada, June 2002.

22. Rodgers, J. P. and Hagood, N. W., "Hover Testing of a 1/6th Mach-Scale CH-47D Blade with Integral Twist Actuation," Proceedings of the 9th International Conference on Adaptive Structures and Technology, Cambridge, Massachusetts, October 1998.

23. Cesnik, C. E. S., Shin, S. J., and Wilbur, M. L., "Dynamic Response of Active Twist Rotor Blades," *Journal of Smart Materials and Structures*, Vol. 10, No. 1, February 2001, pp. 62-76.

24. Bernhard, A. P. F., O'Neill, J., Kohlhepp, F, Welsh, W., and Lorber, P., "Active Rotor Control (ARC) of a Mach-Scaled Trailing Edge Flap Rotor," Proceedings of the 57th Annual Forum of the American Helicopter Society, Washington, D.C., May 2001.

25. "NATOPS Flight Manual Navy Model SH-2G Aircraft", Department of the Navy, NAVAIR 01-260HCG-1, May 1, 1995.

26. Fulton, M. V., "Design of the Active Elevon Rotor for Low Vibration," Proceedings of the American Helicopter Society Aeromechanics Specialists' Meeting, Atlanta, Georgia, November 2000.

27. Milliot, T. A. and Friedmann, P. P., "Vibration Reduction in Helicopter Rotors Using an Actively Controlled Partial Span Trailing Edge Flap Located on the Blade," NASA Contractor Report 4611, June 1994.

28. Milgram, J. and Chopra, I., "Helicopter Vibration Reduction with Trailing Edge Flaps," Proceedings of the 36th AIAA/ASME/ASCE/AHS/ACS Structures, Structural Dynamics, and Materials Conference, New Orleans, Louisiana, April 1995.

29. Jänker, P., Klöppel, V., Hermle, F., *et al*, "Development and Evaluation of a Hybrid Piezoelectric Actuator for Advanced Flap Control Technology," Proceedings of the 25th European Rotorcraft Forum, Paper G-21, Rome, Italy, September 1999.

30. Johnson, W., "Rotorcraft Dynamics Models for a Comprehensive Analysis." Proceedings of the 54th Annual Forum of the American Helicopter Society, Washington, D.C., May 1998.

31. Milgram, J., Chopra, I., and Straub, F., "A Comprehensive Rotorcraft Aeroelastic Analysis with Trailing Edge Flap Model: Validation with Experimental Data," Proceedings of the 52nd Annual Forum of the American Helicopter Society, Washington, D.C., June 1996.

32. Yntema, R. T., "Simplified Procedures and Charts for the Rapid Estimation of Bending Frequencies of Rotating Beams", NACA Technical Note 3459, 1955.

33. Wood, E. R. and Hilzinger, K. D., "A Method for Determining the Fully Coupled Aeroelastic Response of Helicopter Rotor Blades," Proceedings of the 19th Annual Forum of the American Helicopter Society, Washington, D.C., May 1963.

34. Gerstenberger, W. and Wood, E. R., "Analysis of Helicopter Aeroelastic Characteristics in High-Speed Flight," *AIAA Journal*, Vol. 1, No. 10, October 1963.

35. Myklestad, N. O., "A New Method of Calculating Natural Modes of Uncoupled Bending Vibrations of Airplane Wings and Other Types of Beams," *Journal of the Aeronautical Sciences*, Vol. 11, No. 4, April 1944, pp. 153-162

36. Prohl, M. A., "A General Method for Calculating Critical Speeds of Flexible Rotors," *Journal of Applied Mechanics*, Vol. 12, No. 3, September 1945, pp. 142-148.

37. Houbolt, J. C. and Brooks, G. W., "Differential Equations of Motion for Combined Flapwise Bending, Chordwise Bending, and Torsion of Twisted Nonuniform Rotor Blades," NACA Technical Report 1346, 1958.

38. Hodges, D. H. and Dowell, E. H., "Nonlinear Equations of Motion for the Elastic Bending and Torsion of Twisted Nonuniform Rotor Blades," NASA Technical Note D-7818, December 1974.

39. Timoshenko, S. and Goodier, J. N., *Theory of Elasticity*, 2nd Edition, McGraw-Hill Book Company, New York, 1951.

40. Craig, R. R., Jr., *Mechanics of Materials*, 2nd Edition, John Wiley and Sons, New York, 2000.

41. Bielawa, R. L., *Rotary Wing Structural Dynamics and Aeroelasticity*, American Institute of Aeronautics and Astronautics, Reston, Virginia, 1992.

42. Volkin, R. S., "Estimation of Rotor Blade Torsional Deformations from Measured Blade Torsion Moments," Master's Thesis, Naval Postgraduate School, Monterey, California, March 2002.

43. Bramwell, A. R. S., Done, G. and Balmford, D., *Bramwell's Helicopter Dynamics*, American Institute of Aeronautics and Astronautics, Reston, Virginia, 2001.

44. Den Hartog, J. P., *Mechanical Vibrations*, 4th Edition, McGraw-Hill Book Company, New York, 1954.

45. Smilg, B. and Wasserman, L. S., "Application of Three-Dimensional Flutter Theory to Aircraft Structures (With Corrections for the Effects of Control Surface Aerodynamic Balance and Geared Tabs)," *Army Air Corps Technical Report* (*AAFTR*) 4798, Dayton, Ohio, July 1942.

46. Theordorsen, T., "General Theory of Aerodynamic Instability and the Mechanism of Flutter," NACA Technical Report No. 496, 1935.

47. Küssner, H. G. and Schwarz, L., "The Oscillating Wing with Aerodynamically Balanced Elevator," NACA Technical Memorandum No. 991, October 1941.

48. Couch, M. A., "A Finite Wake Theory for Two-Dimensional Rotary Wing Unsteady Aerodynamics," Master's Thesis, Naval Postgraduate School, September 1993.

49. Loewy, R. G., "A Two-Dimensional Approach to the Unsteady Aerodynamics of Rotary Wings," *Journal of the Aeronautical Sciences*, Vol. 24, No. 2, pp. 81-92, February 1957.

50. Aaron, R. D., Gutierrez, J. J., and Wood, E. R., "JSF Lift-Fan Approach for Design of a STOVL Heavy Lift Transport for Expeditionary Warfare," Proceedings of the 59th Annual Forum of the American Helicopter Society, Phoenix, Arizona, May 2003.

51. Söhngen, H., "Die Losungen der Interalgleichlung und deren Anwendung in der Tragflugeltheorie," *Mathematische Zeitschrift*, Band 45, 1935.

52. Daughaday, H., DuWaldt, F, and Gates, C., "Investigation of Helicopter Blade Flutter and Load Amplification Problems," *Journal of the American Helicopter Society*, Vol. 2, No. 3, pp. 27-45, July 1957.

53. Von Karman, T. and Biot, M., *Mathematical Methods in Engineering*, McGraw-Hill Book Company, New York, 1940

54. Prouty, R. W., *Helicopter performance, Stability, and Control*, Robert E. Krieger Publishing Company, Malabar, Florida, 1990.

55. Padfield, G. D., *Helicopter Flight Dynamics: The Theory and Application of Flying Qualities and Simulation Modeling*, American Institute of Aeronautics and Astronautics, Reston, Virginia, 1996.

56. Wood, E. R. and Buffalano, A. C., "Parametric Investigation of the Aerodynamic and Aeroelastic Characteristics of Articulated and Rigid (Hingeless) Helicopter Rotor Systems," TRECOM Technical Report 64-15, April 1964.

57. Runyan, H. L., "Single-Degree-of-Freedom-Flutter Calculations for a Wing in Subsonic Potential Flow and Comparison with an Experiment," NACA Technical Report No. 1089, 1951.

58. Theodorsen, T. and Garrick, I. E., "Mechanism of Flutter – A Theoretical and Experimental Investigation of the Flutter Problem," NACA Technical Report No. 685, 1938.

59. Leishman, J. G., *Principles of Helicopter Aerodynamics*, Cambridge University Press, New York, 2000.

60. Cassarino, S., "Investigation of the S-61L Main Rotor Blade Flatwise Bending Moments for a Slowed/Stopped Rotor in Wind Gust Conditions," *Sikorsky Technical Memorandum* TEM-G2-0982, Stratford, Connecticut, November 1978.

61. Jones, K. D. and Platzer, M. F., "Time-Domain Analysis of Low-Speed Airfoil Flutter," *AIAA Journal*, Vol. 34, No. 5, pp.1027-1033.

62. Turner, M. A., "A Computational Investigation of Wake-Induced Airfoil Flutter in Incompressible Flow and Active Flutter Control," Master's Thesis, Naval Postgraduate School, March 1994.

63. Peters, D. A. and He, C. J., "A Closed-Form Unsteady Aerodynamic Theory for Lifting Rotors in Hover and Forward Flight," Proceedings of the 43rd Annual Forum of the American Helicopter Society, St. Louis, Missouri, May 1987.

64. Garrick, I. E., "Propulsion of a Flapping and Oscillating Airfoil," *NACA T. R. No. 567*, 1936.

65. Shipman, K. W., and Wood, E. R., "A Two-Dimensional Theory for Rotor Blade Flutter in Forward Flight," *Journal of Aircraft*, Vol. 8, No. 12 pp. 1008-1015, December 1971.

66. Hammond, C. E., "Compressibility Effects in Helicopter Rotor Blade Flutter," Ph. D. Thesis, Georgia Institute of Technology, Atlanta, Georgia, December 1969.

67. Küssner, H. G., "Zuzammenfassender Bericht uber den instation Aren Auftrieb von Flugeln," *Luftfahrt-Forsch.*, 13, 412-424, 1936.

INITIAL DISTRIBUTION LIST

1. Defense Technical Information Center
   Ft. Belvoir, Virginia

2. Dudley Knox Library
   Naval Postgraduate School
   Monterey, California

3. Dr. E. Roberts Wood
   Naval Postgraduate School
   Monterey, California

4. Dr. Max F. Platzer
   Naval Postgraduate School
   Monterey, California

5. Dr. Donald A. Danielson
   Naval Postgraduate School
   Monterey, California

6. Dr. Garth V. Hobson
   Naval Postgraduate School
   Monterey, California

7. Dr. Russ W. Duren
   Naval Postgraduate School
   Monterey, California

8. CDR Mark A. Couch
   Naval Postgraduate School
   Monterey, California

9. Dr. James Mar
   Naval Postgraduate School
   Monterey, California

10. Dr. Robert E. Ball
    Naval Postgraduate School
    Monterey, California

11. Dr. Conrad Newberry
    Naval Postgraduate School
    Monterey, California

12. Dr. Robert G. Loewy
Georgia Institute of Technology
Atlanta, Georgia

13. Dr. Dewey Hodges
Georgia Institute of Technology
Atlanta, Georgia

14. Dr. Peretz Friedmann
University of Michigan
Ann Arbor, Michigan

15. Dr. Carlos Cesnik
University of Michigan
Ann Arbor, Michigan

16. Dr. Inderjit Chopra
University of Maryland
College Park, Maryland

17. Dr. J. Gordon Leishman
University of Maryland
College Park, Maryland

18. Dr. David A. Peters
Washington University
St. Louis, Missouri

19. Dr. Robert L. King
Mississippi State University
Mississippi State, Mississippi

20. Dr. Robert Calico
Air Force Institute of Technology
Wright Patterson Air Force Base, Ohio

21. Dr. Bradley Liebts
Air Force Institute of Technology
Wright Patterson Air Force Base, Ohio

22. Dr. Paul King
Air Force Institute of Technology
Wright Patterson Air Force Base, Ohio

23. Dr. Friedrich Straub
The Boeing Company
Mesa, Arizona

24. Mr. Lou Silverthorn
The Boeing Company
Mesa, Arizona

25. Dr. William Bousman
NASA Ames Research Center
Mountain View, California

26. Dr. Robert A. Ormiston
Aeroflightdynamics Directorate
U.S. Army Aviation and Missile Command

27. Dr. William Warmbrodt
Aeroflightdynamics Directorate
U.S. Army Aviation and Missile Command

28. Dr. Holt Ashley
Massachusetts Institute of Technology
Cambridge, Massachusetts

29. Dr. C. Eugene Hammond
Lockheed-Martin Corporation
Maitland, Florida

30. Mr. Robert Blackwell
Sikorsky Aircraft
Stratford, Connecticut

31. Mr. William D. Anderson
Lockheed-Martin Corporation
Marietta, Georgia

32. Dr. Judah Milgram
David-Taylor Laboratories